

ORIENTATIONAL PHENOMENA
AT NEMATIC LIQUID CRYSTAL SURFACES
AND
THEIR APPLICATIONS

— A PHENOMENOLOGY OF
ANISOTROPIC FLUID SURFACES —

Hiroshi Yokoyama

Electrotechnical Laboratory

PREFACE

The liquid crystal is often referred to as a fourth state of matter in that it appears in between the solid and the liquid states as a thermodynamically distinct phase. This somewhat self-contradicting name "liquid crystal" was indeed coined after the fact that due to this intermediate nature, the liquid crystals can exhibit at the same time the anisotropic properties, which are characteristic to solid state, and the fluidity to the liquid state. This marvelous state of matter is relatively a new comer to our recognition, having been known for only about a century. During this short history, however, more than 10,000 liquid crystalline substances have been found or synthesized, more than 10 different liquid crystalline phases identified, and a number of their fundamental physical and chemical properties explained. Most surprisingly, liquid crystals have become an indispensable ingredient of modern industry during the last two decades, mainly as a material for electro-optic displays, and, today, their use is expanding at an even more rapid pace.

It has been known from the very early days of liquid crystals that the surface or interface of liquid crystals plays a significant role in determining their appearance when viewed with polarized light. In liquid crystals, indeed, the state of a surface can affect the molecular arrangement over, say, 1 mm! away from their surfaces. This is undoubtedly one of the unique features of a liquid crystalline phase; in solids, molecules are too strongly correlated with each other to be appreciably influenced by the surface state, while in the isotropic liquids, molecules are not correlated at all over a macroscopic distance. The intermediate strength of the molecular correlations in liquid crystals is making their surface properties that remarkable.

The fact that the molecular arrangement, in particular the alignment within a liquid crystal can be controlled to a large extent by the boundary conditions has found wide applications for both scientific and industrial purposes to obtain liquid crystal preparations with a prescribed alignment property; a well-defined alignment is a prerequisite for reliable measurements of physical parameters and for operation of liquid crystal displays. So, liquid crystal scientists have, intentionally or unintentionally, always had to be exceptionally familiar and concerned with the phenomena occurring at their surfaces. Despite these encouraging circumstances, the understanding of liquid crystal surfaces has been unduly impeded, when compared with the level of understanding of their bulk counterparts. In recent years, however, witnessing the certain maturation of the field of liquid crystals, on the one hand, and the rise of interest in other fields into surfaces and thin film processes, on the other, an increasing number of theoretical and experimental studies have begun to be directed to serious exploration of the liquid crystal surfaces. Those range from the characterization, both macroscopic and microscopic, of the surface-induced alignment of liquid crystals to the investigation of novel phase transitions and critical phenomena at surfaces and in thin liquid crystalline films. And their connections with the findings in other fields are also being extensively exploited. Furthermore, the growing interest into the use of ferroelectric liquid crystals and more generally into aligned organic films is requiring to open up a new frontier in the practical applications of surface-alignment phenomena.

In his famous text book, The Physics of Liquid Crystals, P.G. de Gennes notes "...yet many experiments which could have been done thirty years ago are only now being performed," in

connection with the state of the whole field of liquid crystals. This statement even now applies to most of the current studies on liquid crystal surfaces. I am not, however, to imply that the consequences of those studies should be out of date, rather I understand, just as in the days when de Gennes wrote the book, that fundamental concepts and facts are now emerging in this intriguing field of research. In this article, I wish to give a comprehensive account of this emergent field, mainly following the works of the author performed in the last seven years in the Electrotechnical Laboratory. My intention here is primarily to figure out physical principles behind the alignment of liquid crystals at their surfaces. Consequently, a substantial emphasis of this thesis will be placed on the theoretical aspects of the interfaces of nematics. In the course of expositions, however, emphasis will also be laid on experimental techniques in use for liquid crystal surfaces, because, in my opinion, the development of such techniques has always been and is playing a decisive role in making up the current status of the field, and vice versa.

As made clear from time to time through the history of science, an ab initio understanding of any macroscopic phenomenon is realized only after an appropriate phenomenological description becomes available; and it may be even more so, as the system in question becomes more and more complex. Unfortunately, however, there has ever been no systematic effort to develop a phenomenology of the nematic interface, neither in theory nor in experiments. It is my ambition of writing this thesis to make a contribution in this direction. This is the reason why I included the term "phenomenology" in the title. As a matter of course, I am not necessarily satisfied with the result, and much is certainly left to be done. But I am convinced that at least a direction of future researches could be presented.

The preferential orientation of organic molecules at an interface is quite a universal phenomenon which manifests itself in various ordered structures in nature such as biological membranes, soap films, micelles and vesicles of amphiphilic molecules, Langmuir-Blodgett films, epitaxially grown layers, etc. Today, there is not so much distinction between basic and applied works in these field. The outcome of basic researches are soon reflected in applied area, and applied works are feeding the thought of basic researchers. The understanding of the surface alignment of nematic liquid crystals is of course important in its own right, but it will be even more significant in other fields in the long run. It is my great pleasure if this thesis is of some value to those who are working in these fields.

My sincere thanks are due to Professors T. Moriizumi, T. Hino, A. Fukuda, M. Iwamoto, and K. Takahashi of Tokyo Institute of Technology for their constant encouragement and considerations. I must also express my hearty gratitude to H. Kamei, S. Kobayashi, U. Itoh (now with Kodak), and all other members of Electronic Chemistry Section, Electrotechnical Laboratory, for their helpful, stimulating, and lasting discussions and positive critiques. Especially, I would like to thank H. Kamei, as it would be entirely impossible for me to complete this thesis without his patience. Finally, I want to thank my wife Hiroko for her devoted cooperations.

H. Yokoyama

April, 1987

CONTENTS

Chapter 1. INTRODUCTION	1-1
1.1 Motivation	1-1
1.2 Summary and Layout	1-4
1.3 Surface-induced alignment of nematic liquid crystals: Historical overview	1-10
1.4 Application of aligned liquid crystals	
Chapter 2. PHYSICAL PROPERTIES AND STRUCTURE OF NEMATIC LIQUID CRYSTALS	2-1
2.1 Fluid with uniaxial anisotropy: Nematic liquid crystal	2-2
2.2 Curvature elasticity	2-9
2.3 Landau-de Gennes theory of the isotropic to nematic phase transition	2-15
Chapter 3. CONCEPTS IN THE SURFACE-INDUCED ALIGNMENT OF NEMATICS	3-1
3.1 Pretilt angle, anchoring strength, and surface order	3-3
3.2 Methods of surface-induced alignment and proposed mechanisms of alignment	3-6
Chapter 4. THERMODYNAMICS OF THE NEMATIC LIQUID CRYSTAL INTERFACE	4-1
4.1 Gibbs' thermodynamics of fluid interfaces	4-3
4.2 The equilibrium shape of a nematic interface	4-19
4.3 Orientational thermodynamic variables and thermodynamics of bulk nematics	4-25
4.4 Thermodynamic formulation of a nematic interface	4-43

4.5	The surface of tension and the surface of extrapolation	4-57
4.6	Geometrical properties of the point of extrapolation and the connection with the Rapini-Papoular formalism	4-68
4.7	Generalized Gibbs equation in the near planar regime and the thermodynamic definition of the anchoring strength	4-81
4.8	Thermodynamic relations	4-96
4.9	Alignment transition at nematic interfaces: Thermodynamic inequalities for critical exponents	4-109
Chapter 5. STATISTICAL MECHANICAL THEORIES		5-1
5.1	Statistical mechanical theory of the interfacial tension of nematics	5-3
5.2	Density functional theory of the anchoring strength	5-24
5.3	The Landau-de Gennes theory of the nematic interface	5-47
5.4	Wall-induced pretransitional birefringence: Orientational wetting transition	5-54
5.5	Contact-angle phenomena at the clearing point	5-65
5.6	Anchoring strength in the Landau-de Gennes' model	5-70
Chapter 6. ORDER - DISORDER PHENOMENA AT NEMATIC INTERFACES		6-1
6.1	Contact angle phenomena at the clearing point: Equilibrium shape of a nematic drop at the isotropic-substrate interface	6-4
6.2	Wall-induced pretransitional birefringence	6-25
6.3	Nematic-isotropic transition in thin bounded films	6-32

Chapter 7. STABILITY OF THE SURFACE-INDUCED ALIGNMENT	7-1
7.1 Techniques for measuring the anchoring strength	7-3
7.2 The high electric field technique	7-22
7.3 Experimental determination of $\gamma(\Theta_0)$	7-31
7.4 Temperature-dependence of the anchoring strength	7-37

Chapter 8. CONCLUSION

APPENDIX 1.

Precision temperature controlled microscope	A-1
---	-----

APPENDIX 2.

Equilibrium shape of a nematic drop	A-7
-------------------------------------	-----

REFERENCES

Chapter 1

INTRODUCTION

1.1 Motivation

The surface or interface of matter is a geometrically marginal region wherein its, otherwise uniform, physical and chemical properties vary almost abruptly. Despite this geometrical limitation, it is not at all literally marginal; but known are a number of phenomena which are essentially connected with the presence of an interface: wetting, adhesion, lubrication, emulsification, adsorption, catalysis, crystallization and vaporization, vacuum deposition, biological processes at membranes, and further to name but a few, electrode processes and electron transport across semiconductor contacts.

Since the days of Young in early 19th century who, for the first time, recognized the significance of a surface for establishing mechanical equilibrium in liquid systems, the study of surface and interface has constituted a large branch of materials science. Today, because of that wide range of relevant phenomena, as listed above, and their technological and scientific import, we are experiencing even greater impetus for understanding the physics and chemistry underlying the interfacial processes.

The surface of nematic liquid crystals occupies an especially impressing position in the map of all the surfaces and interfaces found in nature. This is in almost the same sense that a liquid crystal is of interest as a phase in between the crystalline solid and the liquid states. More specifically, the nematic surface or interface is, on the one hand, flexible enough to assure easy access to thermodynamic equilibrium, yet on the other, hard enough to impose preferential orientation on constituent molecules,

thereby producing structural anisotropy which propagates far into the bulk medium.

This long known phenomenon, called the "surface-induced alignment" in liquid crystal parlance, is now of tremendous technological significance in the production of liquid crystal displays, playing in a sense as essential a role as that of the electro-optic effect itself in liquid crystals. Furthermore, the current need for high speed, large area, and high information density displays is opening up the introduction of novel operation mechanisms as well as the use of new materials, for instance, ferroelectric liquid crystals, which is then making the requirement even more intense and wide ranged for the alignment of liquid crystals on substrate surfaces. Along with this technological facet, it appears worth pointing out that the surfaces or thin films of liquid crystals offer an ideal sample to test the theoretical predictions made in connection with the phase transitions in lower dimensional and bounded systems.

From the surface scientific point of view, the origin of the alignment of nematics at their surfaces is no different from that of characteristic orientational states adopted generally by asymmetric molecules on liquid or solid surfaces; for example, that occurring in Langmuir films on water. But what probably makes it truly distinctive is the fact that this "microscopic" anisotropy in molecular orientation is brought into a "macroscopic" anisotropy by way of long-range orientational order existing in nematics. So that the understanding of nematic surfaces requires, among others, the understanding of their orientational properties.

The nematic surfaces are a kind of liquid surface; hence, it is not at all surprising even though they lack microscopic characterizations, as is today the case for ordinary liquids to which modern techniques such as electron microscopy, LEED, etc.

requiring ultra-high vacuum are largely inapplicable. However, most regrettable about the nematic surfaces is the fact that they are far from being adequately characterized even on the macroscopic (phenomenological) level, when compared with their ordinary liquid counterparts. Especially, in terms of their orientational properties, even an appropriate theoretical framework is not necessarily clear, on which such macroscopic characterizations may be correctly done.

Till the advent of liquid crystal displays in late 1960's, the orientational phenomena at nematic surfaces were the subject of only some sporadic studies. But in the last two decades, quite a few studies have been carried out, figuring out some fundamental concepts and features of the surface-induced alignment. It must at the same time be admitted, however, that a large part of them were either too descriptive or too speculative to give a coherent picture of the nematic surfaces on the macroscopic level. In the present thesis, I wish to set forth one possible scenario of how to draw a phenomenological picture of the nematic surfaces, starting from the thermodynamic basis of the alignment at surfaces to some specific observations which appear to be particularly illuminating the orientational properties of the nematic surfaces.

As well known, the direction of alignment (called the "director") and the orientational order are the key quantities specifying the orientational state of nematics. Consequently, our primary goal (as far as nematic sample is concerned) is to elucidate "How" and "Why" the director and the order are influenced by surfaces. To ultimately answer the question of "Why," on the one hand, one must take account of the detailed molecular interactions and predict their macroscopic consequences to such an extent to be compared with experiments. This is nothing but the aim of the condensed matter physics and chemistry as a

whole, and as far as structure formation in condensed phases is concerned, we know at present few successful examples. But, on the other, an answer to the former question may be greatly varying in its accuracy, ranging from a mere description of single observations to a presentation of a highly intercorrelated set of observations which are unified to be consistent with each other. What I try in this article is to answer the question of "How" in the last sense as deeply as possible. I believe only such an endeavor will be a real asset for answering some day the question of "Why."

1.2 Summary and Layout

Some chapters of this thesis are solely theoretical aiming at creating a phenomenological framework for nematic interfaces, and some are largely experimental devoted to the description of specific observations and the experimental techniques needed. Both are treated with equal emphasis as an indispensable and complimentary ingredient for the present goal. In experimental section, in particular, I have tried to select only such topics that are thought to "primarily" reflect the orientational property of the nematic surface: namely, the order-disorder phenomena and the stability of the orientation. Moreover, in order not to obscure the point, the experimental results presented are mostly those for a single nematic substance placed on two commonly used aligning substrates, which are shown a posteriori to be embodying oppositely extreme cases of surface-induced alignment.

In the rest of Chapter 1, a historical overview is given on the surface-induced alignment phenomenon, followed by the description of the current status of their applications.

Chapter 2 is a preparatory part, in which fundamental properties of nematic liquid crystals are compiled. In view of the fact that the surface-induced alignment is a phenomenon which

can be manifested and probed via the spatial configuration of the director in the bulk phase, the Frank theory of curvature elasticity is expounded in detail to facilitate self-contained expositions in later chapters. The nematic liquid crystal is one of few examples whose phase transition can be rather adequately treated by a phenomenological theory. In view of the importance of phenomenological description of nematics in later chapters, we shall briefly review the Landau-de Gennes phenomenological theory of the nematic-isotropic transition.

In Chapter 3, the fundamental concepts such as the pre-tilt (the alignment direction), the anchoring strength (a measure of the stability of alignment), etc. are introduced, which are needed for quantitative discussion of the alignment at nematic surfaces. Furthermore, in order to show up the current status of this field, the models and conjectures of the mechanism of alignment so far proposed, though none of them has concrete experimental support, are summarized.

Chapters 4 through 8 are the main part of this thesis; Chapters 4 and 5 are theoretical, in which the nematic interfaces are in turn treated thermodynamically and statistical mechanically with a view to giving a basis for the phenomenological unification of the interfacial properties of nematics. In Chapter 4, the Gibbs surface thermodynamics is extended to encompass nematic interfaces by taking into account the orientational degrees of freedom of a nematic based on the Oseen-Frank theory of curvature elasticity. In so doing, the Gibbs equation is generalized to a form which is obviously related to the pre-tilt angle and the anchoring strength. From this generalized Gibbs equation follow several thermodynamic relations which are to be used in later statistical mechanical treatments and are to provide important insights into the thermodynamic significance of the temperature-, pressure- or composition-

dependence of the pre-tilt angle and the anchoring strength. Especially, a quasi-thermodynamic condition is derived for the critical exponent when the pre-tilt or the anchoring strength exhibits some critical behavior in response to changes in those environmental conditions.

Chapter 5 is in essence divided into two parts. The former half is devoted to the derivation of some rigorous statistical mechanical formulas for the interface boundary tension and the anchoring strength at a hard wall-nematic interface. And in the latter half, an approximate theory is developed based on the (Landau-de Gennes type) van der Waals picture of the nematic interface, resulting in some explicit expressions for the interfacial tension, the contact angle, the anchoring strength, etc. involving a few phenomenological parameters. As often the case with rigorous statistical theories, the formulas obtained in the former part are not convenient for quantitative calculations. However, they serve as a conceptual basis for approximate theories. At present, especially, we are allowed by virtue of a variational property of the anchoring strength to observe a good parallelism to exist throughout the thermodynamics, the rigorous and the approximate statistical theories.

In Chapters 6 and 7, which are respectively concerned with the "microscopic" and the "macroscopic" aspects of the orientations at nematic interfaces, some typical experimental observations of the orientational phenomena are presented and discussed on the basis of theoretical ground founded in former chapters. As mentioned already, those experiments were mostly done with respect to an interface between a single material, 4-n-pentyl-4'-cyanobiphenyl (5CB), a typical room-temperature nematic liquid crystal, and a substrate which was treated either by the rubbing or by the oblique evaporation technique. These surface treatments are known as the commonest techniques which are currently enjoying wide

industrial and laboratory applications to achieve uniform planar alignment for use in liquid crystal devices. Through the exposition of the experimental results and their theoretical analyses in Chapters 6 and 7, it will be made clear that those alignment techniques are orienting nematic molecules based on very different mechanisms, being in sharp contrast to the fact that both techniques give rise to an apparently indistinguishable alignment of good quality for very wide range of nematic substances.

Chapter 6 deals with the orientational order-disorder phenomena associated with the nematic interface. Firstly, the contact angle phenomena occurring at the line of contact of the three phases, substrate, nematic, and isotropic, are considered. As well known in surface science, the contact angle gives a direct measure of the relative stability of the interfaces that meet at the line, in terms of the interfacial tensions. At present, in particular, it offers an estimate of the relative affinity of the ordered and the disordered states to the substrate, which governs the order-disorder phenomena at their surfaces. Secondly, the results of the wall-induced pretransitional birefringence experiments are presented, which give a measure of the strength of the molecular orientation induced by the substrates by measuring the local optical anisotropy in the nematic medium remaining near the substrate at temperatures above the nematic-isotropic transition point T_c . Finally examined is how the nematic-isotropic transition should be modified as the thickness of the nematic layer is decreased in between treated substrates; if the substrate favors (disfavors) the nematic order, the transition temperature will be enhanced (reduced) as the nematic thins.

All the results of those experiments done on the interface between 5CB and a substrate treated either by the rubbing or the oblique evaporation technique point in one common direction as to

the state of orientational ordering at these interfaces: The rubbed substrate tends to enhance the orientational order of the nematic in the vicinity of substrate, while the obliquely evaporated substrate does tend to destroy the ordering. It is furthermore indicated that the microscopic ordering induced by the rubbed substrate goes hand in hand with the macroscopic alignment of the nematic director on the substrate, while the disordering due to the obliquely evaporated substrate occurs quite independent of whether or not the substrate aligns the nematic over macroscopic distance.

Chapter 7 is concerned with the following macroscopic question: how stable is the alignment of a nematic at an interface? At first, the conventional techniques for measuring the anchoring strength are reviewed with an emphasis on the reliability and precision of these techniques. Next, the "high electric-field technique (HEFT)" developed by the present author is described in detail and the factors affecting its results discussed. The HEFT is not only an easy-to-use but a rather reliable technique, in comparison with the conventional ones, and is also useful to explore the complete functional dependence of the nematic-substrate interfacial tension on the director orientation.

The results of applications of the HEFT are presented, including the temperature- and the director angle-dependences of the anchoring strength, which were first obtained with this technique. The temperature-dependences, especially the quasi-critical weakening of the anchoring strength at the 5CB-obliquely evaporated SiO substrate interface, are discussed based on the thermodynamics and the Landau-de Gennes type theory of the nematic interface developed, respectively, in Chapters 4 and 5.

Chapter 8 is devoted to summary and conclusion with some comments on the future perspective of the field and its

implications of the orientational phenomena at nematic surfaces into the production of oriented, or more generally ordered thin films of organic molecules.

The alignment mechanisms of nematics on the rubbed and the obliquely evaporated substrates have always received much attention, and some "conjectures" have indeed been proposed. And today, it is unhappily often believed without reflection that (semi-)microscopic grooves, in a broad sense, brought about by the rubbing or the oblique evaporation process is responsible for both cases. As will be shown throughout this article, the alignment of nematics on these substrates are not this simple, but has a number of clear features which make them quite distinct. On the rubbed (polyvinylalcohol) substrate, the nematic assumes a higher orientational order, a small contact angle, and a large anchoring strength with negligible temperature-dependence, but on the obliquely evaporated (SiO) substrate, it takes oppositely a lower orientational order, a large contact angle, and a relatively small anchoring strength with marked temperature-dependence. These are properties that can not be easily reconciled on a simple mechanistic view based on the groove model. If it is understood through this thesis how crucial and useful is to collect such information that clearly signifies the difference of one alignment from the other, I would say that at least a part of the present goal should be reached.

1.3 Surface-induced alignment of nematic liquid crystals:

Historical overview

It is now well accepted that any sterically and/or functionally asymmetric molecules tend to more or less align in a preferred direction when placed at an interface between two distinct media. It was independently theorized long ago by Langmuir [1] and Harkins [2] based on close examination of large number of surface tension data that, at the free surface of pure organic (ordinary) liquids, there is a tendency for the hydrocarbon ends of molecules to be oriented outward when one end of the molecule is hydrocarbon and the other end has an extra affinity to the liquid. The concept of the "preferential surface orientation" of molecules successfully accounted for, semi-quantitatively at least, the various experimental observations. Langmuir [1] also directed his attention to molecular orientations in insoluble monomolecular films of saturated fatty acids and alcohols spread on water. And, based on the fact that the area of the water surface occupied by a single molecule (estimated from the number of molecules employed and the total area occupied) did not change as the length of hydrocarbon chains was varied from 14 to 34, he could correctly conclude that these rather elongated molecules assume an upright orientation with the hydrocarbon pointing outward from the water surface. Furthermore, Langmuir [1] attempted to interpret Traube's rule [3] concerning the surface tension of solutions as a manifestation of a planar orientation of hydrocarbon chains.

All of these pioneering works on the orientation of molecules at an interface were based on indirect evidence drawn from the measurements of various macroscopic quantities of a liquid interface. Though some more evidence has been accumulated by way of surface potential and optical experiments, etc. since then, the orientation of organic molecules at an interface still stands out

as a difficult subject to explore, both from an experimental and from a theoretical [4] view points.

The orientation of nematic liquid crystals at their interfaces has an even longer history of investigations. However, it has been approached from a direction, very different from that adopted for an ordinary liquid interface. Since 1888 in which Reinitzer first discovered the liquid crystalline state, the observation with a polarizing microscope has been the most fundamental and powerful procedure for studying liquid crystals. Indeed, it was Lehmann, a German physicist specialized in microscopic crystal analysis, who coined the names such as "flowing crystals," "crystalline liquid," and "liquid crystal" on the basis of his microscopic observations of the double refraction or birefringence in his liquid-like preparations. In Fig.1.1 shown is a typical patterns, now called the schlieren texture, exhibited by a thin film of a nematic liquid crystal held between glass plates when viewed under a polarizing microscope with crossed polars. Though the nematic sample flows like an oil, we can see bright regions indicating the presence of birefringence.

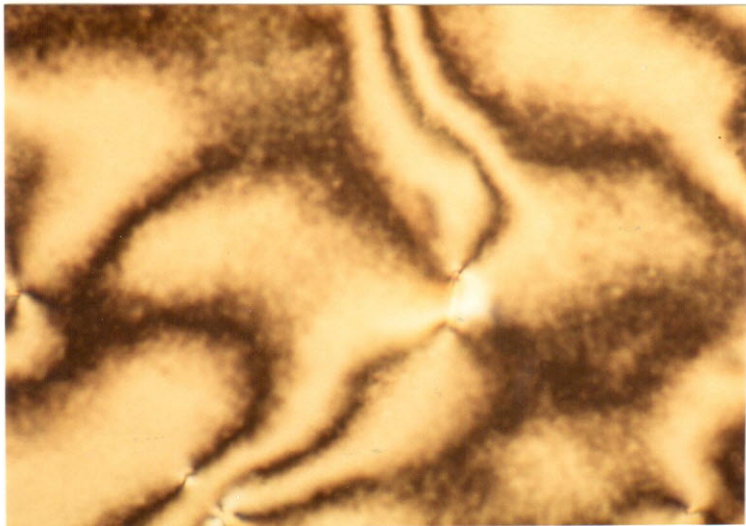


FIG.1.1. Schlieren texture of a thin nematic film confined between glass plates. Viewed under a polarizaing microscope with crossed polarizers.

In this figure, we can also see some alternating dark brushes, which is an indication that the optic axis is changing

from one point to the other in the specimen, and at the dark bands, it coincides with the axis of polarizers. We now know that such spatial variations of the optic axis is brought about by the action of the glass plates with which the nematic is in contact. And, this orientation of the optic axis is a manifestation of the microscopic orientation of the nematic molecules at the glass-nematic interface.

In contrast to the case of the molecular orientation at an ordinary-liquid interface, one can "directly" observe the surface-induced alignment of molecules in liquid crystals. Though it is not the microscopic orientation at the interface itself, liquid crystal scientists have been unfortunately satisfied with this advantage for more than half a century, and have paid little attention to the physical and chemical aspects of nematic interfaces even in the manner as Langmuir and Harkins did for ordinary-liquid interfaces. Nevertheless, it was certainly in this period leading to the advent of liquid crystal displays in late 60's that some notable observations of the phenomena were described and important progress in the surface-induced alignment methods was made [5]. Below, we shall briefly review such topics.

1.3.1 Pseudo-isotropy: the first uniform surface-induced alignment

Though the textures of liquid crystal preparations are seriously affected by their boundaries, it took more than ten years to lead the eyes of workers to surface effects. In 1906, 18 years after the discovery of the liquid crystal, Wallerant [6] and Lehmann [7] described "pseudo-isotropy" or "forced homeotropy"; the liquid crystal specimen appeared completely dark between crossed polars, regardless of the orientation of the polars, as if it was an isotropic substance.

Concerning this observation, Lehmann confidently stated [5]:

Pseudo-isotropy can be caused by the adsorptive(!) action of the glass; the optical axis is everywhere perpendicular to the surface....Thin layers adsorbed on the glass govern the orientation of the remaining molecules. They can be altered to such a degree like soft crystals by means of rubbing, that the entire mass obtains a uniform structure. The transformation temperature of the layers adsorbed by the glass is raised, so that they are maintained even when heated considerably to above the clarification point.

Furthermore, Lehmann [8] correctly pointed out the role of the vertical position of lecithin molecules in promoting the pseudo-isotropic or homeotropic alignment. The adsorption of long chain surface active agents such as lecithin is still in wide use for obtaining homeotropically aligned samples [9].

1.3.2 Rubbing method

In 1911, Mauguin [10] produced a uniformly aligned sample of a nematic liquid crystal, p-azoxyanisole, with its optic axis parallel to the glass plate whose surface had been rubbed in one direction with a piece of paper. In this case, the optic axis was parallel to the substrate, not perpendicular as in homeotropic alignment, and this type of alignment is called "planar" or sometimes "homogeneous." It is interesting to note that by using this technique, he obtained a twisted-nematic structure, which is just the configuration almost invariably used in current electro-optic displays, and closely investigated its optical properties. The rubbing method was also recognized to be effective by Zocher and Coper [11].

The rubbing method of the surface-induced alignment was also extensively used by Chatelain [12], probably independent of Mauguin, for the sake of the studies on optical properties of

nematics. Furthermore, he speculated that the planar orientation on a rubbed surface resulted from deposition of an adsorbed layer of fatty impurities which aligned the nematic molecules via dipole interactions. However, he did not rule out the possibility of physical alteration of the glass surface by the rubbing action.

The rubbing method is still one of the most important techniques for producing uniformly aligned layers of liquid crystals for use in display devices. Though much elaboration has been made on the rubbing procedure and materials since the days of Chatelain, the mechanism and the state of the alignment is far from clear cut. As a result, quite a few conjectures have been proposed; as opposed to the adsorbed impurity mechanism due to Chatelain, the rearrangement of the substrate material [13] and the grooves brought about during the rubbing process [14] have been suggested to be responsible for the alignment. One of the questions to be addressed and answered in this article is in fact concerned with the origin of the alignment on rubbed surfaces.

1.3.3 Epitaxy on crystalline surfaces

An important observation of the surface-induced alignment is the epitaxial orientation of nematic molecules on crystalline surfaces. Though it has so far found no practical application, it serves as clear experimental evidence showing that the alignment of a nematic liquid crystal is indeed governed by the microscopic interaction across the interface.

The orientation of liquid crystals on cleavage surfaces of crystals were investigated by Grandjean [15] in as early as 1916 for over 80 instances. He observed that, on a cleavage surface of a single crystal, a nematic liquid crystal formed several distinct regions in each of which the optic axis of the nematic was uniformly oriented in a direction clearly related to the symmetry of the basal crystal.

1.4 Application of aligned liquid crystals

Uniformly aligned layers of liquid crystals, often referred to as "single crystalline liquid crystal layers", play a critical role in the liquid crystal-based electro-optic displays. Though the alignment techniques of nematics had been pursued, as described in the previous section, primarily for the purpose of precise experimental studies of various anisotropic properties in early days, the proposal of "dynamic scattering type" liquid crystal displays due to Heilmeyer [16] in 1968 and especially the advent of "twisted nematic" (TN) displays by Schadt and Helfrich [17] in 1971 sparked a great deal of practical interest into the surface-induced alignment of nematics.

In this section, we shall describe the basic principle of liquid crystal displays with a view to illustrating the practical significance of the interfacial orientation of nematic liquid crystals. We will focus our attention on TN displays, as more than 99% of the commercial liquid crystal displays are of TN type, today [18,19]. However, since the orientational property of an interface has serious influence on the multiplex operation of liquid crystal displays, we will shortly discuss the point together with future perspective of the application of surface-induced alignment.

1.4.1 Basic structure of liquid crystal displays

In Fig.1.2 shown is the schematic illustration of the basic structure of a field-effect liquid crystal displays. The nematic liquid crystal is confined in between a couple of substrates to a thickness of about 10 μm . The substrates are usually glass plates (with the thickness of about 1 mm) coated with a transparent electrode made of Indium tin oxide (ITO), and the electrode is further covered with a layer of polymer or an

inorganic film which are then treated so as to align the liquid crystal in the desired manner. The separation between the substrate is maintained by means of a spacer such as small glass spheres or fibers, and the liquid crystal cell is hermetically sealed with frit glass or more commonly with polymeric resin.

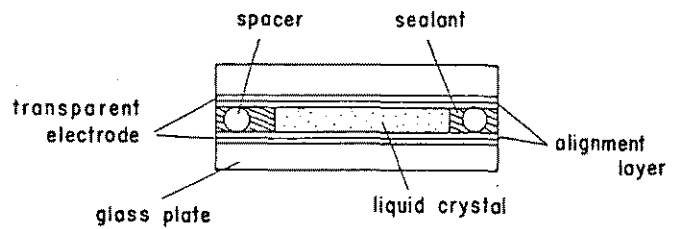


FIG.1.2. Cross-sectional view of a typical field-effect liquid crystal display cell.

1.4.2 Operation principle of TN displays

Field-effect liquid crystal displays are based on the reorientation of liquid crystal molecules upon the application of electric field. When we see this process between crossed polarizers, we can observe a change of brightness, i.e. from clear to dark or from dark to clear, depending on how the reorientation occurs. In any event, such a change is thought to be most efficiently brought about when the initial alignment is uniform rather than irregular as in Fig.1.1.

In TN display cells, the nematic molecules are forced to align parallel to the substrate, but the alignment directions at the upper and lower substrates are set to be perpendicular to each other (Fig.1.3). In the absence of electric field, this configuration results in a planar twisted profile of the nematic molecules (Twisted Nematic structure), and when a linearly polarized light travels along the axis of the twist, the plane of polarization rotates following the optic axis of the nematic. Then, after passing through the cell, the polarization is perpendicular to the initial direction [Fig.1.3(a)]. So that, in

the absence of electric field, TN cell appears clear between crossed polarizers.

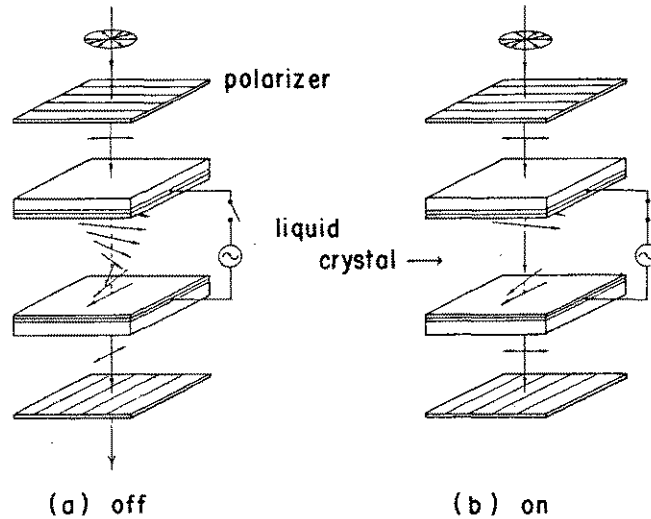


FIG.1.3. Principle of the twisted-nematic liquid crystal display. The arrows between the substrates denote the optic axis of the nematic liquid crystal. In the off state (a), the cell is transparent between crossed polarizers. In the on state (b), the cell appears dark.

The nematic liquid crystal to be used in TN displays is such that, in an electric field, the molecule, or equivalently the optic axis tends to orient along the field direction. Thus, on application of sufficiently high voltage to the TN cell, the optic axis reorients in the middle of the cell almost perpendicular to the substrate. In this case, the pseudo-isotropy condition obtains except in the vicinity of the substrate surfaces where the nematic molecules are strongly aligned. So, under this condition, the TN cell appears dark between crossed polarizers. We can therefore switch between the clear and the dark states by an application of voltage. Obviously, the TN cell can be used both in transmission and in reflection modes.

1.4.3 Requirements on the surface-induced alignment and a future trend

As appreciable from the above, the good initial alignment of nematic molecules is a prerequisite for the operation of the display. This situation is much the same in other type of displays. In contrast to a surface-induced alignment in scientific laboratory, the alignment in a display device should resist repeated operations over the years. In particular, it should be stable to decomposition products of the liquid crystal as well as to other impurities coming from the sealant, etc. Because the surface is extremely sensitive to small amount of impurities, these requirement has been a serious challenge to workers who have been in charge of developing the alignment techniques [20]. As will be described in Chapter 3, quite a few methods are now known, and some of them can indeed meet the above requirements to a satisfactory level as far as the conventional TN displays are concerned.

Recently, the application of liquid crystals has been expanded to encompass TV displays and various character terminals [21]. In these applications, the information content should be dramatically increased compared with the seven-segment displays in wrist watches. Consequently, a multiplexing operation becomes inevitable, which is in turn presenting problems of the deterioration of visibility and the reduction of the operation speed. Although a substantial progress has been made by the introduction of "active matrix" [22], a drastic improvement of the multiplexibility has been theoretically foreseen by way of a detailed control of the interfacial orientations [23-28].

In order to secure the visibility loss in TN structure, Scheffer and Nehring [29] proposed a "super-twisted nematic" display in which the optic axis is twisted more than 90 degrees. In order to achieve the required initial configuration of nematic

molecules, the surface of the substrate must be so treated that the molecules be aligned in a direction inclined by about 30 degrees from the substrate surface. Although the working principle of the display is no different from that of conventional TN displays, the lack of good alignment technique is impeding its commercial applications. The development of an appropriate method for such an alignment condition is now the subject of intense researches.

To overcome the limitation on the operation speed in TN cells, quite a few studies have been concentrated on the use of ferroelectric liquid crystals, which have been first synthesized in 1975 [30]. Because of the permanent dipole, the coupling with an electric field is several orders stronger than in the usual nematic liquid crystal. Moreover, by making use of a well aligned thin layer of ferroelectric liquid crystal, one can achieve a bistable operation with a response time on the order of micro seconds [31]. In this case, too, the hazard that is preventing it from commercial realization is the lack of technique to facilitate the alignment as required [32].

In view of these circumstances, it appears to be the high time to start intensive systematic and basic studies on the interfacial orientational phenomena of liquid crystals to bring over the surface-induced alignment techniques from the hands of artists to engineers.

Chapter 2

PHYSICAL PROPERTIES AND STRUCTURE OF NEMATIC LIQUID CRYSTALS

This chapter is devoted to the description of the fundamental properties of the nematic liquid crystal [1-6] so as to found a minimum necessary basis for investigating the nematic interface in later chapters. We focus our attention here on the symmetry and long range order in nematics as well as on the elastic properties. However, the treatment is extensive only for the Frank theory of curvature elasticity [7], since it plays an especially important role in formulating the principal concepts of the orientation at nematic interface. The symmetry and orientational order will be touched upon very briefly, mostly in relation to the phase transition between the nematic and the isotropic states, employing the treatments due to de Gennes [8].

In connection with the curvature elasticity, we shall be, at present, concerned only with uniformly aligned samples in the absence and presence of external field. As we are exclusively interested in the quantitative aspect of the interfacial orientation of nematics, we shall largely neglect such important topics as the "textures" and "disclinations" in thin nematic samples [9,10], although they are closely connected with the curvature elasticity as well as the surface properties.

2.1 Fluid with uniaxial anisotropy: Nematic liquid crystals

Liquid crystals are states of matter with partial order as regards the orientation of their constituent molecules, while translational order is entirely or partially lost. As mentioned in the previous chapter, the liquid crystalline state was first found about a century ago by Reinitzer and Lehmann in an organic substance.

Liquid crystalline states are the equilibrium thermodynamic phases between the crystalline solid and the ordinary liquid. There are two classes of liquid crystals, thermotropic and lyotropic. In the thermotropic liquid crystals, with which we are exclusively concerned here, the liquid crystalline phase emerges as the solid of a certain organic compound is melted. In the lyotropic liquid crystals, on the other hand, the liquid crystalline phase is obtained in colloidal solution, and in this class, concentration is the primary controllable parameter, rather than temperature as in the thermotropic class.

Since Friedel [11], three basic types of liquid crystalline phases are distinguished according to their structural properties: "nematic," "cholesteric," and "smectic." In Fig.2.1, the arrangement of molecules in these phases are schematical-

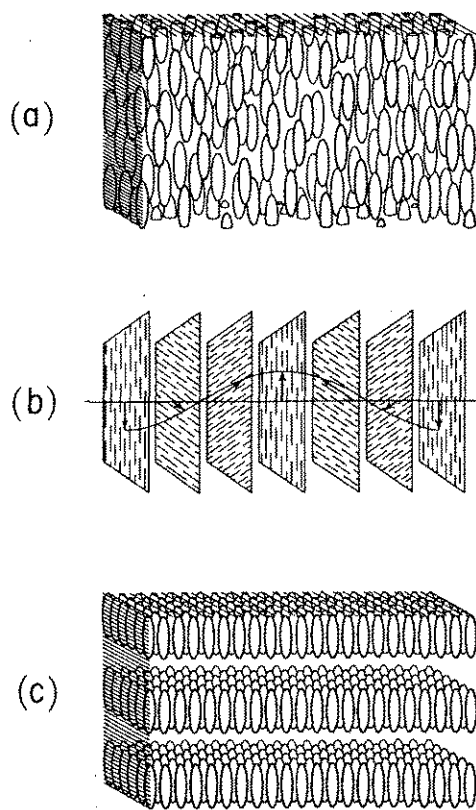
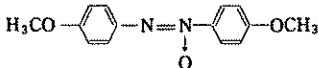
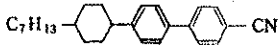
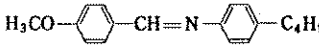
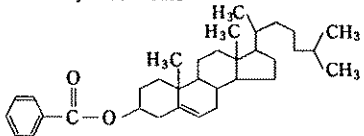
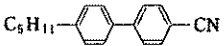
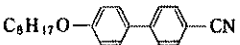


FIG.2.1. Arrangement of molecules in liquid crystal phases. (a) Nematic phase. (b) Cholesteric phase. (c) Smectic phase (smectic A).

ly illustrated.

Liquid crystals are found among organic compounds. The organic molecules which exhibit liquid crystalline phase have wide variety of chemical structures. However, certain common structural features can be found: (1) Highly non-spherical molecular shapes, i.e., rodlike, disclike, etc.; (2) Rigid backbone; (3) Strong dipoles or highly polarizable groups. In Table 2.1, typical thermotropic liquid crystalline compounds are listed together with their phase transformation sequence. The experiments to be described in this thesis have been exclusively performed on the chemically stable, room temperature nematic liquid crystal, *p*-*n*-pentyl-*p*'-cyanobiphenyl, which is usually referred to as 5CB.

TABLE 2.1. Typical liquid crystalline compounds and their phase transitions.

1. <i>p</i> -azoxyanisole (PAA)	5. <i>trans</i> -4-heptyl (4-cyanophenyl)cyclohexane (PCH-7.)
	
$\text{solid} \xrightleftharpoons{117.4^\circ\text{C}} \text{nematic} \xrightleftharpoons{134.4^\circ\text{C}} \text{isotropic}$	$\text{solid} \xrightleftharpoons{30^\circ\text{C}} \text{nematic} \xrightleftharpoons{57^\circ\text{C}} \text{isotropic}$
2. <i>p</i> -methoxybenzylidene- <i>p</i> '- <i>n</i> -butylaniline (MBBA)	6. Cholesteryl benzoate
	
$\text{solid} \xrightleftharpoons{22^\circ\text{C}} \text{nematic} \xrightleftharpoons{47^\circ\text{C}} \text{isotropic}$	$\text{solid} \xrightleftharpoons{147^\circ\text{C}} \text{cholesteric} \xrightleftharpoons{186^\circ\text{C}} \text{isotropic}$
3. <i>p</i> - <i>n</i> -pentyl- <i>p</i> '-cyanobiphenyl (5CB)	
	
$\text{solid} \xrightleftharpoons{24^\circ\text{C}} \text{nematic} \xrightleftharpoons{35^\circ\text{C}} \text{isotropic}$	
4. <i>p</i> - <i>n</i> -octyloxy- <i>p</i> '-cyanobiphenyl (8OCB)	
	
$\text{solid} \xrightleftharpoons{55^\circ\text{C}} \text{smectic A} \xrightleftharpoons{67^\circ\text{C}} \text{nematic} \xrightleftharpoons{80^\circ\text{C}} \text{isotropic}$	

2.1.1 The nematic phase

A. The director

The term "nematic" is derived from the Greek word, $\nu\eta\mu\alpha\tau\omicron\varsigma$ (nematos), meaning thread-like. This terminology is based on the naked-eye observation of nematic liquid crystals that there can be seen a large number of thin threads (see Fig.1.1), resulting from the arrangement of molecules in this state [Fig.2.1(a)].

The nematic phase is characterized by long-range orientational order, i.e., the long axes of molecules (symbolized by ellipses in Fig.2.1(a)) tend to align along a preferred direction. There is however no long-range order in the positions of the centers of mass of the molecules, though a certain degree of short-range order may remain as in ordinary liquids. The molecules can rotate quite frequently about their long axes, and there is no preferential orientation as regards the ends of molecules, i.e., opposite orientations are equally probable. The nematic phase has thus a uniaxial symmetry about this preferred direction, and its macroscopic physical properties, optical, electrical, magnetic, mechanical, hydrodynamic, etc., all exhibit corresponding anisotropy. The important concept in describing the nematic state is therefore the axis of symmetry. And, it is usually specified by a unit vector (along this axis) called the "director" \mathbf{n} . This picture of the nematic phase is supported by the results of X-ray and NMR studies.

Although the ground state configuration of the director corresponds to a spatially uniform one, the director may vary its direction from one point to the other through the nematic as a result of thermal fluctuations and/or of external agents such as electric and magnetic fields, or surfaces. The action of surfaces on the alignment of director is nothing but the surface-induced alignment. As will be described later, the spatial variation of

the director can be described with remarkable precision by means of the Frank theory of curvature elasticity. And, it is now well known that the opaque appearance of a nematic liquid is the consequence of the intense light scattering due to vigorous thermal fluctuations of the director [1].

B. The orientational order parameter

Another important concept in characterizing the nematic state is the orientational order parameter, which describes the degree to which each molecule is strictly oriented along the director. For simplicity, let us imagine that the molecules composing the nematic phase are rigid rod, whose orientation can be completely specified by a unit vector l ; it should be strictly distinguished from the director \mathbf{n} . Since the nematic phase has, as mentioned above, a center of symmetry, the average of l vanishes, and hence it is impossible to define an order parameter of vectorial character.

de Gennes [1] introduced the "tensor order parameter" which is defined as

$$Q_{ij} = \frac{1}{2} \langle 3l_i l_j - \delta_{ij} \rangle, \quad (2.1)$$

where $\langle \rangle$ denotes the thermal average, and δ_{ij} the Kronecker symbol. Q_{ij} is a symmetric traceless tensor. It is readily appreciated that Q_{ij} has a correct property as an orientational order parameter for the nematic phase. For example, if the molecules are perfectly aligned along the director in the x -axis, we find

$$Q_{xx}=1, \quad Q_{yy}=Q_{zz}=-1/2, \quad \text{and} \quad Q_{xy}=Q_{yz}=Q_{zx}=0. \quad (2.2)$$

And, if they are randomly oriented,

$$Q_{ij} = 0. \quad (2.3)$$

When the uniaxial symmetry prevails as in the nematic phase, the tensor order parameter can be rewritten in terms of the director as follows:

$$Q_{ij} = \frac{1}{2} Q(3n_i n_j - \delta_{ij}), \quad (2.4)$$

where

$$Q = \frac{1}{2} \langle 3\cos^2\theta - 1 \rangle, \quad (2.5)$$

with θ being the angle between the molecular axis and the director. Q is called the "scalar order parameter" or "order parameter" for short, which assumes 1 in the perfectly oriented nematic and 0 in the isotropic orientation. In Fig.2.2, the temperature dependence of the order parameter has been reproduced from Ref.12, for homologous series of n-alkyl-cyanobiphenyls.

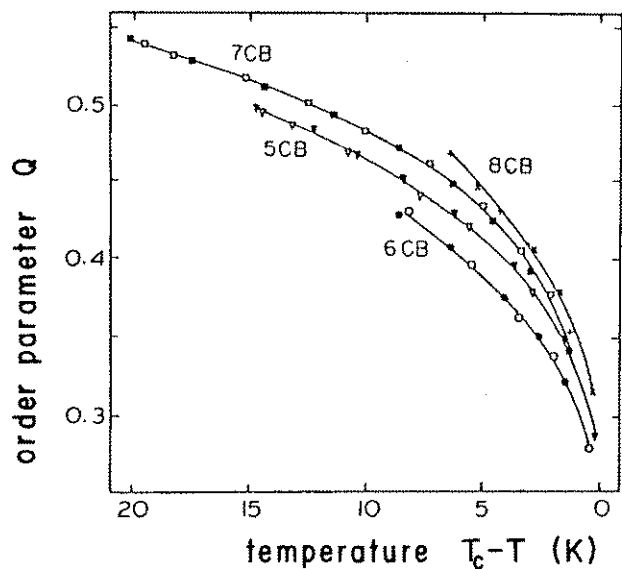


FIG.2.2. Order parameter as a function of temperature for alkyl-cyanobiphenyls (nCB). n stands for the number of carbons in the alkyl chain. From Ref.12.

C. Relationship between the order parameter and the macroscopic material constants of the nematic liquid crystal

The orientational order parameter can be related with the anisotropic part of various macroscopic properties of nematics. The most clear-cut example is the magnetic polarizability. Since nematics are diamagnetic with small magnetic polarizability, the local field correction can be to a good approximation ignored.

Thus, the polarizability of a macroscopic body is simply the sum of molecular polarizabilities. For a nematic consisting of simple rods, we have

$$\chi_{//} - \chi_{\perp} = c(A_{//} - A_{\perp})Q, \quad (2.6)$$

where $\chi_{//}$ and χ_{\perp} are the magnetic polarizability of the nematic in the directions parallel and perpendicular to the director, respectively, $A_{//}$ and A_{\perp} are the polarizabilities of one rod molecule parallel and perpendicular to its long axis, and c is the number of molecules per unit volume of the nematic. Due to the diamagnetic nature, $\chi_{//}$ and χ_{\perp} are negative, and further because of the aromatic rings, $\chi_{\perp} < \chi_{//}$.

The refractive index of a nematic is also anisotropic with respect to the director. The refractive index along the optic axis, i.e., the director, is written as n_e , and that perpendicular to it n_o . Although the local field correction is more significant this time than in the case of magnetic polarizability, we can roughly obtain

$$n_e - n_o \propto Q, \quad (2.7)$$

For obtaining a more precise relation, we have to resort to Vuks' formula or such [13]. In nematics, the extraordinary index n_e is larger than the ordinary index n_o (because of the aromatic rings again), and hence the optical properties of a uniform nematic are identical with those of an "optically positive" crystal. The refractive indices of 5CB have been accurately measured by Karat and Madhusudana [12, see also Chapter 7]. The birefringence $\Delta n = n_e - n_o$ decreases from 0.185 at 20 K below the nematic-isotropic transition point ($T_c = 308$ K) to 0.116 at 1.2 K below T_c for light of wavelength 632.8 nm. This reflects the degradation of the orientational order as the temperature is increased.

In the case of dielectric constants, however, it is no longer possible to draw a simple correlation with the order parameter as

above. As shown in Table 2.1, nematic molecules involve a group with substantial dipole moment. These dipoles contribute to the dielectric property in a very complicated manner, which is strongly dependent on the short range structure in nematics. In the case of 5CB, a cyano group exists, giving a dipole which is almost parallel to the geometrical long axis of the molecular core. So that, its dielectric constant is larger in the direction of the director; the difference between the dielectric constants parallel and perpendicular to the director,

$$\Delta \epsilon = \epsilon_{//} - \epsilon_{\perp} , \quad (2.8)$$

is called the dielectric anisotropy. In fact, the dielectric constants of 5CB are $\epsilon_{\perp} \sim 7$ and $\epsilon_{//} \sim 17$ [2], and the dielectric anisotropy is positive. In the case of MBBA, on the other hand, the dipole moment is almost perpendicular to the long axis of the molecule, thereby making the dielectric anisotropy negative.

2.2 Curvature elasticity

In any microscopic region of a nematic, the preferred axis can be precisely defined, giving rise to the local director. Even in equilibrium, however, the director can vary from one position to the other through the nematic by the action of external field and bounding surfaces. If such a variation occurs on a length scale much larger than the molecular dimension, the spatial configuration of the director for given external field and boundary condition can be analyzed with extreme rigor by means of the elastic continuum theory of nematics. The elasticity associated with the director configuration is conceptually very different from the usual elasticity of solids, and we shall refer to it as the "curvature elasticity." The theory of curvature elasticity was originated by Zocher [14] and Oseen [15], and completed in the present form by Frank [7].

The essential approach of the theory is completely the same as in the elastic theory of solids; first, we define the "curvature strain" and the "curvature stress," and assume a linear relation between them similar to Hook's law. This procedure can be systematically carried out by constructing a free energy density as a quadratic function of the curvature strain in such a way as to satisfy the symmetry requirement coming from the fundamental structure of the nematic.

In the ground state, the director is uniformly distributed in the nematic, so that the director field $\mathbf{n}(\mathbf{r})$ is a constant in space. It should be noted here that, in the infinite sample of a nematic, no preference exists for the director as long as they are invariant in space. Therefore, the free energy of the nematic is independent of \mathbf{n} in the ground state. This property of the nematic state is known as the Goldstone degeneracy [6,16], which is connected with the spontaneous symmetry breaking at the isotropic to nematic phase transition. Hence, the increase of

free energy is only associated with the relative variation of the director in space. The natural choice of the curvature strain is the spatial derivative of the director field $\mathbf{n}(\mathbf{r})$.

2.2.1 Deformation free energy and the normal modes

Up to second order in the curvature strain, the scalar function which is compatible with the uniaxial and inversion symmetry of the nematic can be readily constructed by way of direct calculations. We will not repeat the procedure here, and thus those who are interested in it are referred to the standard textbook of liquid crystals [1-6].

According to the Frank theory, the curvature strain can be decomposed into three independent modes, splay, twist, and bend. The director configurations corresponding to those modes are illustrated in Fig.2.3.

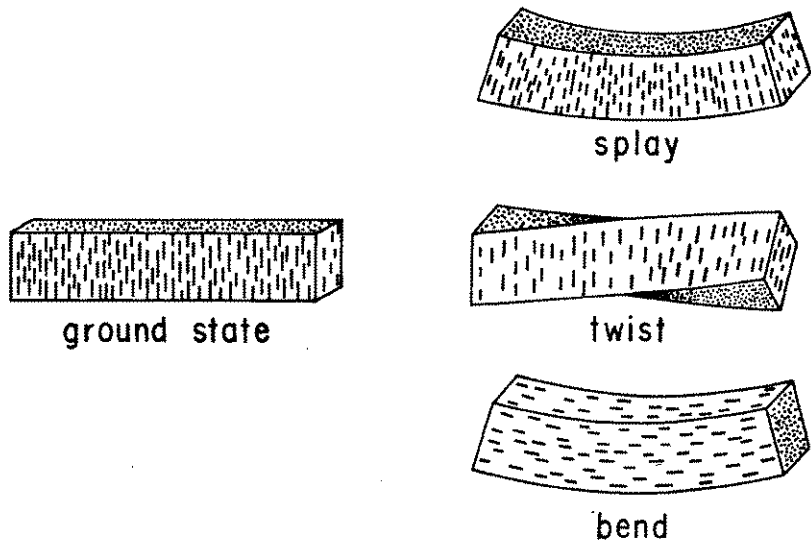


FIG.2.3. Principal modes of curvature strain in the nematic phase.

The free energy density f_d associated with the principal modes are written as follows:

$$f_d(\mathbf{r}) = \frac{1}{2} K_1 (\text{div} \mathbf{n})^2 + \frac{1}{2} K_2 (\mathbf{n} \cdot \text{rot} \mathbf{n})^2 + \frac{1}{2} K_3 (\mathbf{n} \times \text{rot} \mathbf{n})^2, \quad (2.9)$$

where K_1 , K_2 , and K_3 are the elastic moduli for the splay, twist, and bend modes, respectively. These elastic moduli are usually referred to as the Frank elastic constants. The actual values of the Frank constants of known nematics lie around 10^{-11} N. And, these constants are empirically known to satisfy the following inequality:

$$K_3 > K_1 > K_2. \quad (2.10)$$

Furthermore, according to the mean-field theory of the Frank constants due to Nehring and Saupe [17,18], the Frank constants are approximately shown to scale with the square of the order parameter:

$$K_1, K_2, K_3 \propto Q^2. \quad (2.11)$$

This relation can also be derived via a phenomenological approach based on the lowest-order expansion of the elastic deformation energy in terms of the tensor order parameter [8]. It should however be emphasized that this relation is highly approximately, and the higher order correction becomes in many cases important [19,20].

In the absence of external orientational field, the equilibrium director configuration is such that the total deformation energy,

$$F_d = \int f_d(\mathbf{r}) d\mathbf{r}, \quad (2.12)$$

should be minimized under the prescribed boundary condition.

2.2.2 Effect of electric field

Owing to the anisotropic dielectric property of nematics, electric fields are effective to rotate the director. In the presence of an electric field \mathbf{E} , the electrical displacement \mathbf{D} can be written as

$$\mathbf{D} = \epsilon_{\perp} \mathbf{E} + \Delta \epsilon (\mathbf{n} \cdot \mathbf{E}) \mathbf{n}. \quad (2.12)$$

So that, the dielectric energy density in the nematic medium F_e is given by

$$\begin{aligned} f_e &= \mathbf{D} \cdot \mathbf{E} / 2 = \epsilon_{\perp} E^2 / 2 + \Delta \epsilon (\mathbf{n} \cdot \mathbf{E})^2 / 2. \\ &= D^2 / (2 \epsilon_{\perp}) - (\Delta \epsilon / 2 \epsilon_{\perp} \epsilon_{\parallel}) (\mathbf{n} \cdot \mathbf{D})^2. \end{aligned} \quad (2.13)$$

In case the nematic is placed in an electric field produced by constant charges on a conductor, we should consider the process that occurs under constant electrical displacement. Therefore, from the last equation of the above, we see that, when the dielectric anisotropy $\Delta \epsilon$ is positive as in 5CB, the director tends to align in along the direction of \mathbf{D} . The actual configuration of the director in an electric field is determined in such a way as to minimize the sum of the deformation and the dielectric free energies under the boundary condition.

One of the most remarkable examples of the field-induced deformation of the director field may be the Fredericksz transition [1] which occurs when an electric or magnetic field is applied to a slab of nematic liquid crystal which is uniformly aligned by the action of the substrates. If the dielectric anisotropy is positive, and the initial orientation is planar, i.e., the director parallel to the substrate, no deformation of the director field does occur even in an electric field unless the field strength is below some threshold value given by

$$V_{th} = \pi (K_1 / \Delta \epsilon)^{1/2}, \quad (2.14)$$

where V_{th} is the threshold voltage across the slab. And, as the field strength is increased beyond the threshold, the director field begins to deform from the uniform configuration. The Freedericksz transition is in fact the basis of most liquid crystal displays including TN type, and also offers important means to probe the elastic property of the nematic [21].

2.2.3 Hydrostatic stress in deformed nematics

In ordinary liquids, the hydrostatic stress tensor is given by a symmetric tensor $-p\delta_{ij}$ with p the pressure. In a orientationally deformed nematic, the director deformation also contributes to the hydrostatic stress, and gives rise to an extra static pressure which should ultimately be balanced by an external force (not torque) applied at the boundary. This hydrostatic stress of orientational origin has a serious effect on the morphology of the interface of nematics [see Chapter 4].

The stress tensor in a deformed nematic can also be derived by means of the common approach based on the virtual displacement [1]. The resulting stress tensor can be written as

$$\sigma_{ij}^d = -\pi_{jk}(\partial n_k / \partial r_i), \quad (2.15)$$

where

$$\pi_{jk} = \partial f_d / \partial (\partial n_k / \partial r_j). \quad (2.16)$$

In Eq.(2.15), summation over the repeated subscript k should be performed. Then, adding the contribution from the pressure, we obtain

$$\sigma_{ij}^e = \sigma_{ij}^d - p\delta_{ij}, \quad (2.17)$$

where σ_{ij}^e is the total hydrostatic stress tensor in a deformed nematic, and is usually referred to as the "Ericksen stress tensor." For a surface element dS_j in the deformed nematic, the force exerted on the element in the i -direction is given by

$$f_i = \sigma_{ij}^e dS_j.$$

For the nematic to be in the mechanical equilibrium, the following condition must be satisfied:

$$\partial \sigma_{ij}^e / \partial r_j = 0. \quad (2.18)$$

By a direct calculation utilizing the equilibrium condition of the director profile, we can readily find that the pressure has to be given by

$$p(\mathbf{r}) = - f_d(\mathbf{r}) + \text{constant}. \quad (2.19)$$

Finally, it may be worth noting that, when the deformation is occurring only in one direction, say along the z-axis. It immediately follows from Eqs.(2.15) and (2.16) that

$$\sigma_{zz}^d = - 2f_d, \quad (2.20)$$

since f_d is the second order homogeneous function of $\partial n_k / \partial z$. Then, in combination with Eqs.(2.17) and (2.19), we find that the Ericksen stress is written as

$$\sigma_{zz}^e = - f_d + \text{constant}. \quad (2.21)$$

Because the above constant is the pressure at a point out side the deformed region, it is clear that the director deformation exerts a force on the confining boundary along the outward normal of the interface; in other words, so as to expand the deformed volume.

2.3 Landau-de Gennes theory of the isotropic to nematic phase transition

In this section, we shall briefly review the elements of the Landau-de Gennes theory, so as to facilitate the later application to interfacial problems.

Let us assume, following de Gennes [1,8], that the free energy density $g(p, T, Q_{ij})$ is an analytic function of the tensor order parameter Q_{ij} near the isotropic-nematic transition temperature T_c (the clearing temperature). And, we expand g in powers of Q_{ij} up to fourth order. Since the free energy must be invariant under uniform rotations of the system, all terms of the expansion must be scalar. The most general form satisfying this condition is shown to be

$$g = g_0 + \frac{1}{12} A Q_{ij} Q_{ij} - \frac{1}{18} B Q_{ij} Q_{jk} Q_{ki} + \frac{1}{144} C (Q_{ij} Q_{ij})^2, \quad (2.21)$$

where g_0 is the free energy of the isotropic phase, which is independent of Q_{ij} , and as before, summation over repeated indices is implied. The coefficients of expansion A , B , and C are in general functions of the temperature T and pressure p . However, we shall postulate that B and C are constants, and A has a temperature dependence of the form

$$A = a(T - T^*). \quad (2.22)$$

The equilibrium state is characterized by the order parameter which minimizes the free energy. The presence of the third order term demands that the phase transition should be of first order.

By using the uniaxial tensor order parameter Eq.(2.4), we can rewrite Eq.(2.21) in terms of the scalar order parameter:

$$g = g_0 + \frac{1}{2} A Q^2 - \frac{1}{3} B Q^3 + \frac{1}{4} C Q^4. \quad (2.23)$$

The equilibrium value of Q is given by that which makes the free energy minimum. The dependence of g on Q at several temperatures are shown in Fig.2.4. We see that there is a discontinuous phase transition at a temperature T_c slightly above T^* . The source of this first-order phase transition lies, as mentioned above, in the fact that there exists a third order term in Eq.(2.23). This is related to the fact that the state with Q and that with $-Q$ are not equivalent in the case of nematics. As immediately obvious from the definition of the order parameter, if the state with positive Q is optically positive, the state with negative Q is optically negative.

The actual value of Q corresponding to minimum free energy can be derived from Eq.(2.23) as

$$\begin{aligned}
 Q &= 0, & T > T_c, \\
 Q &= (B/2C)\{1 + [1 - 4aC(T-T^*)/B^2]^{1/2}\}, & T < T_c.
 \end{aligned}
 \tag{2.24}$$

The clearing temperature T_c is given by

$$T_c = T^* + 2B^2/(9aC), \tag{2.25}$$

and hence the order parameter at T_c by

$$Q_c = 2B/3C. \tag{2.26}$$

Furthermore, the latent heat of the transition is expressed as

$$q = aT_c Q_c^2/2. \tag{2.27}$$

The temperature T^* corresponds to the limit of metastability of the isotropic phase. It should be possible to supercool the

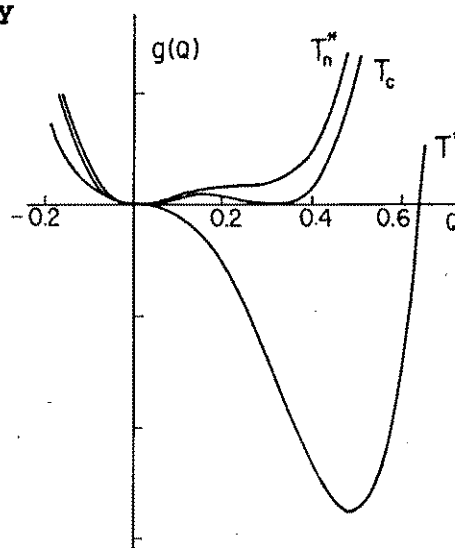


FIG.2.4. Landau-de Gennes free energy density as a function of the order parameter for various characteristic temperatures.

isotropic liquid to this temperature. Below T^* , the isotropic phase becomes absolutely unstable with respect to any degree of fluctuation of the order parameter. Similarly, it is also meaningful to consider the temperature at which the nematic phase becomes absolutely unstable. This temperature, T_n^* , is given by

$$\begin{aligned} T_n^* &= T^* + B^2/(4aC) \\ &= T_c + B^2/(36aC) = T_c + (T_c - T^*)/8. \end{aligned} \quad (2.28)$$

Coles [22] determined the parameters of the theory for n-alkyl-cyanobiphenyls by means of the pretransitional Kerr effects in the isotropic phase. His results for 5CB are listed in Table 2.2.

TABLE 2.2. Parameters in Landau-de Gennes free energy density for 5CB [Ref.22].

$T_c - T^*$	1.1 ± 0.3 K
a	$(0.13 \pm 0.01) \times 10^6$ J/m ³ K
B	1.6 ± 0.2 J/m ³ K
C	3.9 ± 0.3 J/m ³
Q_c	0.27 ± 0.01
q	$(1.47 \pm 0.15) \times 10^3$ J/kg

The value of Q_c has been calculated via Eqs.(2.25) and (2.26) and shows a good agreement with the result of the direct optical measurement [12, see Fig.2.2]. Further, since the latent heat of the crystal to nematic transition is about 17×10^3 J/kg, we see that the latent heat of the nematic-isotropic transition is about one order smaller than that. This is indeed one of the most dramatic feature of the transition, and indicates the weakly first order nature of the nematic-isotropic transition.

Chapter 3

CONCEPTS IN THE SURFACE-INDUCED ALIGNMENT OF NEMATICS

The surface-induced alignment of nematic liquid crystals is, as we have seen in Chapter 1, a kind of interfacial phenomenon known for over 70 years. Especially, in the last two decades, the surface-induced alignment has been a matter of great concern for both scientists and engineers, thereby stimulating quite a few studies in the field.

The spectrum of these researches are however enormously wide, ranging from empirical search for good aligning substrates to theoretical studies on the origin of alignment. And, still today, there seems to exist a large gap between the theoretical and the experimental sectors. As mentioned in Chapter 1, this article is an attempt to fill in the gap by setting forth an appropriate phenomenological framework on which various observations related to the surface-induced alignment can be settled and to which microscopic theory can be converged. To construct a good phenomenology, it is first of all necessary to figure out what is common to any interfacial orientation of nematics and what is not. The first step in so doing is to clarify what does the surface-induced alignment mean. Above all, we must have a language appropriate to express the point, before we start to discuss over the problem.

This section is devoted to the critical review of the conventional concepts concerning the surface-induced alignment, with a view to increasing our vocabulary and seeking more powerful words. We also present some facts and conjectures about the surface-induced alignment by focusing on the two most commonly employed techniques, "rubbing" and "oblique evaporation" methods,

with which we shall exclusively concern ourselves later.

3.1 Pretilt angle and the anchoring strength

The surface-induced alignment of practical significance can be classified into three basic types as shown in Fig.3.1.

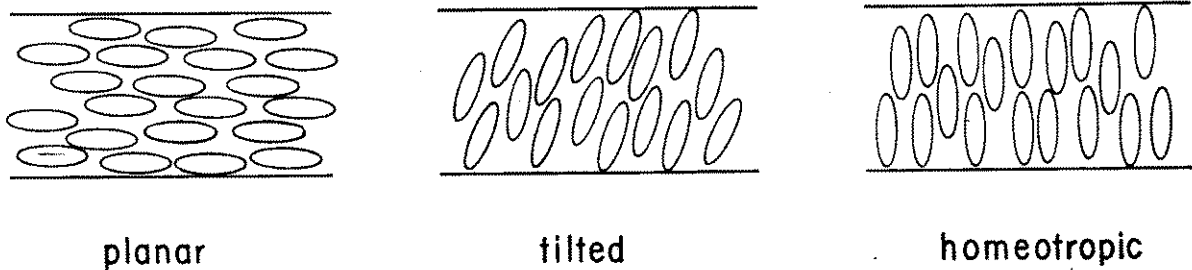


FIG.3.1. Basic types of the surface-induced alignment.

In the first type, the director is aligned parallel to the substrate, and this type of alignment is called "planar." In the second type, the director assumes an oblique angle with respect to the substrate surface, we call this type the "tilted" alignment. Finally, in the third type, the director is oriented normal to the substrate. This is referred to as the "homeotropic" alignment.

To be more quantitative, the alignment of the director on a solid substrate is schematically depicted in Fig.3.2. The fundamental quantity associated with the alignment is, as noted above, the angle that the director is making with the substrate, Θ_e and Φ_e . We refer to these angles as the "pretilt angles," and the former is especially the "polar" pretilt angle and the latter is the "azimuthal" pretilt angle. The concept of the pretilt angle is inevitably connected with the surface-induced alignment. And, it is sometimes used as a synonym of the surface-induced alignment.

In the operation of displays, the pretilt angle plays a

decisive role. So, various accurate methods have been devised for their measurements soon after the liquid crystal display become realistic. The commonest and most accurate method is the magnetic null method [1], with which one can easily determine the pretilt angle to an accuracy 0.1 degree.

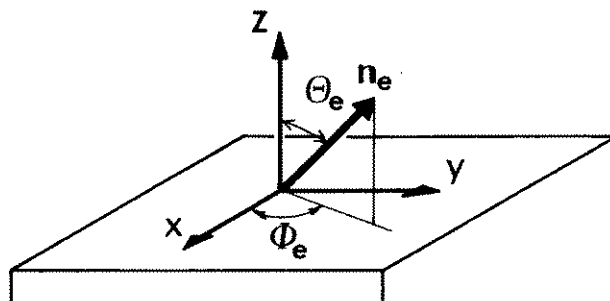


FIG.3.2. Pretilt angles at a nematic interface.

Another important concept associated with the surface-induced alignment is the anchoring strength. This was first introduced by Rapini and Papoular [2] to quantitatively account for the strength with which the director is restricted to the easy axis imposed by the substrate. They postulated that the interfacial free energy or tension of the nematic-substrate interface was written as a function of the actual angle of the director at the interface in the following form:

$$\gamma = \gamma_0 + \frac{1}{2} E_a^p \sin^2(\theta_0 - \theta_e) + \frac{1}{2} E_a^a \sin^2(\phi_0 - \phi_e), \quad (3.1)$$

where θ_0 and ϕ_0 are the actual polar and azimuthal angles of the director at the interface, respectively. Here, E_a^p and E_a^a are the positive constants respectively called the polar and azimuthal anchoring strength coefficients, or the polar and azimuthal anchoring energies. Obviously, the interfacial tension γ assumes a minimum value when the director coincides with the easy direction, i.e., $\theta_0 = \theta_e$ and $\phi_0 = \phi_e$. As the anchoring energies increase, the director becomes harder to rotate from the easy direction.

Equation (3.1) is usually used in conjunction with the Frank

elastic energy Eq.(2.12), and offers a basis to quantitatively take into account the effect of aligning substrate on the director configuration within the nematic in contact with it. As will be fully discussed in Chapters 4, 5, and 7, the anchoring strength is certainly an important concept characterizing the orientational property of a nematic interface. However, in comparison with the pretilt angle, it is rather abstract, and is also hard to measure experimentally. In fact, it is only recently that reliable measurement of the anchoring strength has become possible.

These two quantities do not exhaust all the concepts relevant for the characterization of nematic interface. Among other, we can conceive that the orientational order may be different in the interfacial region from that in the bulk, because of the aligning force exerted by the substrate. It is also expected to serve as a characterizing parameter. Indeed, we will emphasize the importance of the surface order parameter as an ingredient of the phenomenological description of a nematic interface.

Since the surface-induced alignment is unmistakably a macroscopic interfacial phenomena, it is not fair and insufficient to restrict the attention to those parameters which have direct connection with the orientation of molecules. Namely, we should also pay attention to such concepts as "adsorption," "surface entropy," and "surface energy" which are the central variables in the phenomenological description of the interfaces of ordinary liquids. We will theoretically pursue this direction in Chapter 4, and show that thermodynamically closed treatment of pretilt angle and anchoring strength is inevitably connected with those concepts.

3.2 Methods of surface-induced alignment and proposed mechanisms of alignment

3.2.1 Rubbing and oblique evaporation techniques

Today, we know quite a few methods to achieve uniform alignments of nematics shown in Fig.3.1. Those techniques were thoroughly reviewed by Cognard [3]. In assessing wide variety of alignment techniques with emphasis on reproducibility and reliability, he recommended the following methods for each type of alignment:

- (1) planar: rubbing a polymer film,
oblique evaporation of SiO [4].
- (2) tilted: oblique evaporation of SiO at a glancing angle,
crossed evaporation of SiO,
application of homeotropic aligning agents on
obliquely evaporated SiO.
- (3) homeotropic: application of surface active agents such
as lecithin, or silane coupling agents.

Those methods are useful both in industrial and in laboratory applications. Especially, since the planar alignment is a prerequisite for TN displays, the rubbing and the oblique evaporation methods are of great practical importance. Although rubbing is carried out by means of a sophisticated "rubbing machine" [5] in industries, rubbing by hand is still effective in laboratory for research purposes. The oblique evaporation of SiO is also an easy yet highly reproducible method. In this thesis, experimental works are largely concentrated on the substrate treated by these two methods. So, we shall here describe the actual procedure in some detail below.

In Fig.3.3, the process of rubbing is illustrated. A glass slide coated with polyvinylalcohol (PVA) is rubbed in one direction with lens paper. The weight is normally 45 g. For preparation of PVA coating, 1 wt% aqueous solution of PVA is deposited through 0.5 μm millipore filter on a spinning glass substrate. The deposited film is dried at 80 $^{\circ}\text{C}$ for 30 min. The thickness of the resulting PVA film is about 600 \AA .

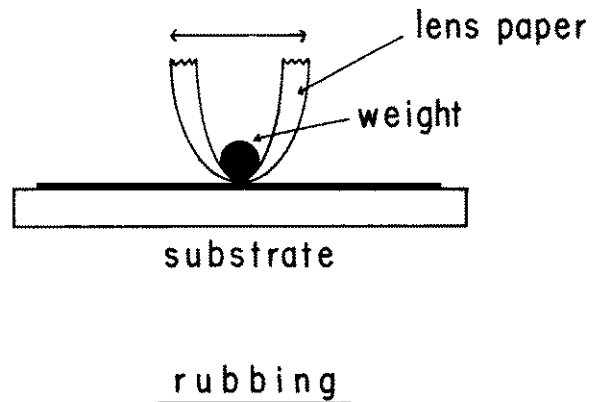


FIG.3.3. Rubbing arrangement.

The oblique evaporation of SiO_2 can be made in an ordinary vacuum evaporation (Fig.3.4). In our laboratory, powder of SiO_2 is heated in a Tantalum chimney in a vacuum of about 10^{-6} Torr. The glass substrate is inclined from the direction of deposition. According to the angle of inclination θ , the resulting film is here denoted as $\text{SiO}_2(\theta)$. The deposition rate is controlled to be 7 $\text{\AA}/\text{s}$ in terms of a substrate inclined to 60 degrees. The evaporation is continued for 90 s.

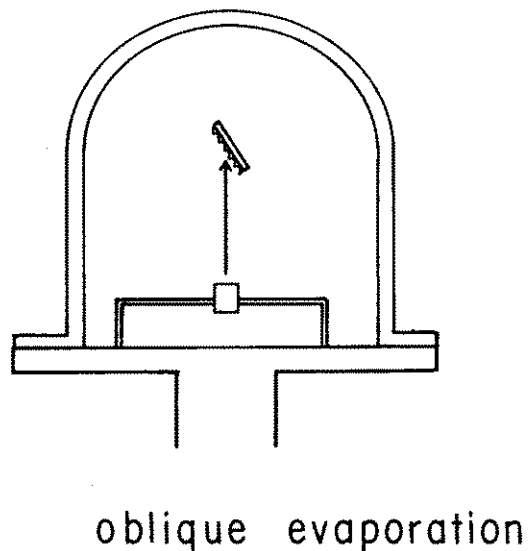


FIG.3.4. Oblique evaporation technique.

Although rubbing technique leads, in most cases, to the formation of near planar alignment with very small pretilt angle, the alignment on an obliquely evaporated SiO is known to yield planar as well as tilted alignments depending on the deposition angle θ [6,7]. When $\theta < 45^\circ$, random planar alignment results, but when $45^\circ < \theta < 72^\circ$, the director aligns in a direction perpendicular to the incident beam with a negligible polar pretilt angle. Furthermore, when $\theta > 75^\circ$, the nematic is oriented toward the direction of the deposition with the pretilt angle ranging from 15 to 25° [8,9]. In the last case, the pretilt angles are also known to be slightly dependent on the deposition condition and the liquid crystal used [10]. And it undergoes a marked temperature dependence near the nematic-isotropic transition point [11-13].

3.2.2 Conjectures on alignment mechanisms

Some conjectures have been presented as to the alignment mechanism on evaporated SiO films. The most popular idea is based on the structural anisotropy inherent in the obliquely deposited films, and explains the alignment as resulting from the minimization of the curvature elastic energy induced by the anisotropic structure of the film, i.e., Berreman's groove mechanism [14]. Although such anisotropic or columnar structures have been confirmed with electron microscopes [15-19], it is as yet hard to estimate the significance of the film structure relative to the physico-chemical interaction between the solid and the liquid crystal [20, 21].

On the other hand, the alignment mechanism on a rubbed substrate seems to be even more obscured. It was proposed long ago by Chatelain [22] that the orientation results from dipole interactions between an ordered layer of adsorbed fatty

contaminants and the nematic molecules. However, he did not rule out the role of structural modification of the substrate as conceived as regards the evaporated SiO films. What is even more confusing here is the presence of polymer film, in which polymer chains may to some extent reorient in the rubbing direction, producing aligning force in similar manner as a stretched polymer film aligns liquid crystals.

Thus, the mechanism of uniform alignments on these substrates is still a matter speculation. The correct answer may be something like that both structural and physico-chemical effects are important (of course in a varying degree) for the surface-induced alignment of nematics. However, this is not at all an answer to the original question. At present, it seems that no one knows what a truly well-posed question is like and what form the correct answer would take. Setting an either-or type question may not be fruitful.

Chapter 4.

THERMODYNAMICS OF THE NEMATIC LIQUID CRYSTAL INTERFACE

In this chapter, we will concern ourselves with the thermodynamic consequences of the orientational anisotropy of nematics on their interfacial properties [1]. Our primary objective here is to extend the Gibbs thermodynamics of fluid interfaces [2], originally developed for ordinary fluids, so as to encompass the interface between the nematic and another non-nematic media by taking explicit account of the orientational degrees of freedom inherent in the nematic phase.

The counter phase being in contact with the nematic may in principle be fluid or solid, but we shall always assume here that their bulk (thermodynamic) states are not influenced by the orientational degrees of freedom of the nematic as long as other thermodynamic variables are held constant. This assumption appears almost trivial in the case of "isotropic" fluids, and is also expected to remain realistic for highly refractory solids such as those which are in extensive use as a substrate for nematic liquid crystals. However, for those phases, including most of the liquid crystals, which have an elastic property comparable to that of nematics, this assumption might become far from being a good one. Accordingly, the intriguing problems concerning the interface between a nematic and a smectic phases, etc. must be excluded.

In this chapter, we will restrict our arguments to an interface between a nematic and a rigid solid or an isotropic fluid (not necessarily the "isotropic phase" of the nematic in question). Since both cases can be treated in an almost parallel fashion, we shall exclusively, unless otherwise noted, discuss the case of a nematic in contact with an isotropic fluid, which allows

for a thermodynamically more complete treatment than the other.

By describing the orientational state of the bulk nematic by means of the Frank theory of curvature elasticity and rigorously applying the Gibbs recipe, we are automatically led to the concept of the "surface of extrapolation." And, it is shown that the separation between the surface of extrapolation and the surface of tension should be identified with the extrapolation length, which as mentioned in Chapter 3 is a measure of the orientational anchoring strength at a nematic interface. Furthermore, we are able to give a thermodynamically and mechanically consistent definition of the anchoring strength as a natural generalization of the Rapini-Papoular formalism.

The present thermodynamic theory allows us to connect the orientation-related surface parameters of a nematic such as the pretilt angle and the extrapolation length with the common thermodynamic variables like temperature, pressure, and concentrations; thereby it helps us to appreciate and predict on a very general ground the behavior of those surface parameters in response to the changes of extraneous conditions. In particular, the changes of the adsorption and the surface entropy associated with the rotation of the nematic director are discussed in detail.

We also investigate the thermodynamic basis and implications of the alignment transition at nematic interfaces. Especially, when the pretilt angle or the anchoring strength undergoes a critical change in response to the variation of temperature and/or concentrations, the thermodynamics gives rise to criteria that the corresponding critical exponents have to obey.

We begin our argument with summarizing the elements of the Gibbs surface thermodynamics to an extent needed for later arguments, mainly following the treatment due to Hill [3]. Those who are familiar with the surface thermodynamics of ordinary fluids may skip to Section 4.2.

4.1 Gibbs' thermodynamics of fluid interfaces

As intuitively evident, an interface existing between a couple of real fluids is by no means a simple mathematical surface of discontinuity. Rather, when viewed closely, there must be a transition layer with finite thickness, over which the properties of the fluid change continuously from those of one phase to those of the other. Consequently, in order to apply the recipe of classical thermodynamics to a fluid interface, one needs to devise some tricks to cope with this inherent inhomogeneity.

The thermodynamics of a fluid interface has been thoroughly formulated by Gibbs[2] and his followers[3-6] in the case of ordinary "isotropic" fluids, by partitioning the extensive variables of the whole system into the bulk and the interface parts utilizing the concept of either the "dividing surface"[2-5] or the "surface phase" [6]. The former is an imaginary surface of demarcation with infinitesimal thickness, up to which the fluids in contact are assumed to be completely homogeneous, while the latter refers to a hypothetical "third phase" which are taken to embrace the inhomogeneous region associated with the interface. It is notable, at this point, that since both of these concepts are merely an instrumental construct to facilitate further thermodynamic treatments, none of their results, as long as they are physically relevant, depends on which pathway is to be actually adopted to reach them [7-9].

An interface between fluids may be planar or curved in equilibrium depending on the environmental conditions, as we often experience in daily life. The Laplace equation indeed tells us that the curvature of an interface should increase in proportion to the pressure difference across the interface (see 4.1.4). Though this is essentially a condition of "mechanical" equilibrium, the concomitant morphological variation has a rather far reaching consequence on the thermodynamic treatment of the

interface. For example, as we shall see later, the interfacial tension can be defined uniquely (independent of the position of the dividing surface or the surface phase) only when the interface is planar. But when the interface is curved, the numerical value of the interfacial tension varies with the choice of the dividing surface, reflecting the fact that the "area of the interface" is no longer a well-defined property. In the case of nematic liquid crystals, we have seen in Chapter 2 that the pressure and hence the stress tensor change according as the nematic is orientationally deformed. Therefore, it becomes in general necessary for our purpose to consider curved interfaces. In view of the application to a liquid crystal interface, we will here focus our attention to a "cylindrical interface", following the Gibbs approach based on the dividing surface.

4.1.1 The dividing surface and the definition of surface excess

Suppose a cylindrical interface between two distinct ordinary fluids (a and b), which are in complete thermodynamic and mechanical equilibrium (see Fig.4.1). We assume here that the fluid is uniform over cylindrical surfaces concentric with the interface; namely, the contours of equal density, etc., coincide with those cylindrical surfaces. We consider a fan-shaped region with unit thickness subtending an angle ω . We take the cylindrical bounda-

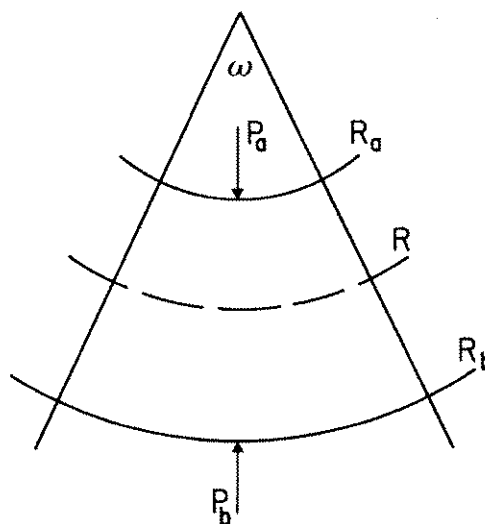


FIG.4.1. Geometry of cylindrical interface.

ries with the radii, R_a and R_b , as shown in Fig.4.1; at this stage, the choice of R_a and R_b is arbitrary, provided they are well inside the bulk phase. Then, the volume V of the fan-shaped region within those cylindrical boundaries is given by

$$V = \omega(R_b^2 - R_a^2)/2. \quad (4.1)$$

We place the dividing surface at the radius R as illustrated in Fig.4.1, dividing the volume V into V_a and V_b as

$$V = V_a + V_b \quad (4.2)$$

where

$$V_a = \omega(R^2 - R_a^2)/2, \quad \text{and} \quad V_b = \omega(R_b^2 - R^2)/2.$$

Now let X be an arbitrary extensive variable of the system pertaining to the volume V , and x_a and x_b be its densities in the bulk phases, a and b , respectively. We define the surface excess X^S of the property X via

$$X^S = X - V_a x_a - V_b x_b. \quad (4.3)$$

Namely, the surface excess stands for the residue when the fluids in contact are assumed to be completely bulk like right up to the dividing surface. In general, therefore, the surface excess is dependent on the position of the dividing surface.

4.1.2 Thermodynamics of a fluid interface

We consider the Helmholtz free energy F of the fluid within the volume V , and assume that F is a function of T (the absolute temperature), R_a , R_b , ω , and the number of molecules of i -th species N_i ($i=1\sim r$); the fluid in question is assumed to be of multicomponent, comprised of r different species. We denote the pressures in the bulk fluids by P_a and P_b (they are not in general identical for curved interfaces, as mentioned above). The entropy

and the chemical potential of the i -th species are written as S and μ_i , respectively.

For infinitesimal changes of T , N_i , R_a , R_b , and ω , the change of the Helmholtz free energy is written as

$$dF = - SdT + \sum \mu_i dN_i - P_b R_b \omega dR_b + P_a R_a \omega dR_a + \eta d\omega, \quad (4.4)$$

where

$$\eta = \left(\frac{\partial F}{\partial \omega} \right)_{T, N_i, R_a, R_b}.$$

In Eq.(4.4), the last three terms represent the external work associated with the geometrical changes of the fluid volume. In particular, $\eta d\omega$ represents the work when the angle of the cone is changed, while other variables are kept constant; this can obviously be defined without ambiguity regardless of the choice of the dividing surface. Integrating Eq.(4.4) with respect to ω under fixed T , μ_i , R_a , and R_b , we obtain

$$F = \sum \mu_i N_i + \eta \omega. \quad (4.5)$$

By using the area of the dividing surface $A = \omega R$ instead of ω and noting Eqs.(4.2) and (4.5), we can rewrite Eqs.(4.4) as

$$dF = - SdT + \sum \mu_i dN_i - P_a dV_a - P_b dV_b + \gamma dA + A \zeta dR, \quad (4.6)$$

where γ and ζ are given by

$$\gamma = [F - \sum \mu_i N_i + P_a V_a + P_b V_b] / A, \quad (4.7)$$

$$\zeta = (P_a - P_b) - \gamma / R = \partial \gamma / \partial R. \quad (4.8)$$

Note that Eq.(4.7) is just the expression to be obtained when Eq.(4.6) is integrated at constant T , μ_i , R , P_a , and P_b . Then by using Eq.(4.7) in Eq.(4.6), we arrive at the Gibbs-Duhem equation

which reads

$$A d\gamma = - S dT - \sum N_i d\mu_i + V_a dP_a + V_b dP_b + A \zeta dR. \quad (4.9)$$

It is clearly seen from Eq.(4.6) that γ has a meaning of the "interfacial tension", expressing the free energy increase resulting from a unit increase of the area of the interface. As readily found in the standard textbooks of thermodynamics [46],

$$\Omega = F - \sum \mu_i N_i \quad (4.10)$$

is the thermodynamic potential, which in a bulk fluid reduces to $-PV$. Hence Eq.(4.7) can be rewritten as

$$\gamma = [\Omega - \Omega_a - \Omega_b] / A. \quad (4.11)$$

This expression shows that the interfacial tension is just the surface-excess thermodynamic potential per unit area Ω^S/A .

It is worth emphasizing at this point that the interfacial tension of a curved interface depends on the position of the dividing surface R , as can be seen in Eqs.(4.7) and (4.8); in Eq.(4.6), however, the free energy itself is independent, as it should be, of the choice of the dividing surface, because of the presence of a term which depends on dR . This feature originates from the fact that the area of a curved interface can not be given unambiguously, independent of the dividing surface, as in the case of a planar interface. In fact, when the interface is planar, so that $P_a = P_b$ and $R \rightarrow \infty$, it is easily confirmed in the above that the interfacial tension does become independent of R .

In the bulk of a "homogeneous" multicomponent fluid, the pressure P satisfies the Gibbs-Duhem equation,

$$dP = s dT + \sum \rho_i d\mu_i, \quad (4.12)$$

where s and ρ_i are the entropy and the molecular number

densities, respectively. Applying this equation to the present bulk fluids a and b, we may rewrite Eq.(4.9) in a surface-thermodynamic form:

$$A d\gamma = - S^S dT - \sum N_i^S d\mu_i + A \zeta dR, \quad (4.13)$$

where

$$S^S = S - s_a V_a - s_b V_b,$$

$$N_i^S = N_i - \rho_{ai} V_a - \rho_{bi} V_b.$$

On the unit area basis, Eq.(4.13) is further rewritten as

$$d\gamma = - S^S dT - \sum \Gamma_i d\mu_i + \zeta dR, \quad (4.14)$$

where $\Gamma_i = N_i^S/A$ represents the adsorption per unit area of the i-th species with respect to the dividing surface, and the surface entropy (that is, the surface-excess entropy per unit area) is here denoted by the same symbol S^S as before for economy of notation. Equations (4.11) and (4.14) constitute the basis of the thermodynamics of a fluid interface.

4.1.3 Thermodynamic relations

A. Gibbs adsorption isotherm

We shall first concentrate our attention the processes which occur at constant temperature, in order to see how the variation of the fluid composition influences the interface property. According to the Gibbs-Duhem equation for a bulk phase, cf. Eq.(4.12), the chemical potentials are shown under this condition to satisfy

$$\rho_1 d\mu_1 + \rho_2 d\mu_2 + \rho_3 d\mu_3 + \dots = dP. \quad (4.15)$$

This equation applies to both phases being in contact. Then, subtracting the equation for the b phase from that for the a phase, we obtain (since chemical potentials are identical in both

phases)

$$\Delta \rho_1 d\mu_1 + \Delta \rho_2 d\mu_2 + \Delta \rho_3 d\mu_3 + \dots = d(P_a - P_b), \quad (4.16)$$

where

$$\Delta \rho_i = \rho_{ai} - \rho_{bi}. \quad (4.17)$$

By using this relation, Eq.(4.13) is reduced at fixed temperature to

$$Ad\gamma = - \frac{N_1^s}{\Delta \rho_1} d(P_a - P_b) - \sum [N_i^s - \frac{\Delta \rho_i}{\Delta \rho_1} N_1^s] d\mu_i + A\zeta dR, \quad (4.18)$$

where we have assumed $\Delta \rho_1 \neq 0$. It is noteworthy that the term in the square brackets is independent of the choice of the dividing surface. To see this property, we would recall the definition of surface excess, i.e.,

$$N_i = \rho_{ai}V_a + \rho_{bi}V_b + N_i^s.$$

Differentiating by R the both sides of this equation, we immediately have

$$0 = A \Delta \rho_i + \frac{d}{dR} N_i^s,$$

which is valid for any i , since N_i 's are by definition constants independent of R . Eliminating A with the use of the equation corresponding to $i=1$, we reach the desired result:

$$\frac{d}{dR} N_i^s - \frac{\Delta \rho_i}{\Delta \rho_1} \frac{d}{dR} N_1^s = 0, \quad (4.19)$$

which shows that the quantity in question is really an invariant. It can also be confirmed directly by way of Eq.(4.7) that the remaining part is independent of R , as required.

1. Two-component fluid

It is now convenient to take the dividing surface in such a way that the adsorption of the first component vanishes, i.e. $\Gamma_1=0$. So, we can simply write Eq.(4.18) as

$$d\gamma = - {}^1\Gamma_2 d\mu_2 + \zeta dR_0, \quad (4.20)$$

where the superscript "1" implies that $\Gamma_1=0$ (at $R=R_0$). Thus, we obtain

$$\left(\frac{\partial \gamma}{\partial \mu_2} \right)_{T,R} \Big|_{R=R_0} = - {}^1\Gamma_2 \quad (4.21)$$

This is the Gibbs adsorption equation for a curved interface. In the case of a plane interface, the left hand side becomes independent of R , resulting in the standard form of the Gibbs equation. It must be remarked here that the "Gibbs phase rule" [8] indicates that the region of a two-phase coexistence of a two-component fluid can be spanned by either two or three degrees of freedom depending on the interface is planar or curved; so that when the temperature is fixed, at least one of the pressures of the coexisting phases has to change as the composition is varied, although the pressure does not apparently appear in Eq.(4.21). Namely, in the two-component case, it is impossible to fix temperature and pressure all together, while changing the concentration.

To be a bit more specific, let us consider a liquid-vapor interface of a two-component fluid, regarding the vapor phase to be an ideal gas. Then, by denoting the partial pressures of the first and the second components by p_1 and p_2 , respectively, we can write the chemical potentials as [7]

$$\mu_i = kT \ln p_i + \chi_i(T), \quad i=1 \text{ or } 2, \quad (4.22)$$

where k is the Boltzmann constant. Using this expression in Eq.(4.21), we get

$$\frac{p_2}{kT} \left(\frac{\partial \gamma}{\partial p_2} \right)_{T,R} \Big|_{R=R_0} = - {}^1\Gamma_2. \quad (4.23)$$

This equation shows clearly that when the introduction of the second component is to reduce the tension of the interface, there must be a net positive adsorption of the second component at the interface.

2. Three-component fluid

Next we consider an interface between two immiscible liquids, each containing a small amount of solute (third component) as illustrated in Fig.4.2. In contrast to the two-component case, the phase rule now allows the temperature and pressure to be kept constant even when the concentration of the third component is changed. This case is of particular importance for our purpose, in that it essentially simulates the liquid crystal-substrate interface with which we are presently concerned. In this respect, we will refer to the fluids of first and second components as the "substrate" and the "solvent", respectively, here.

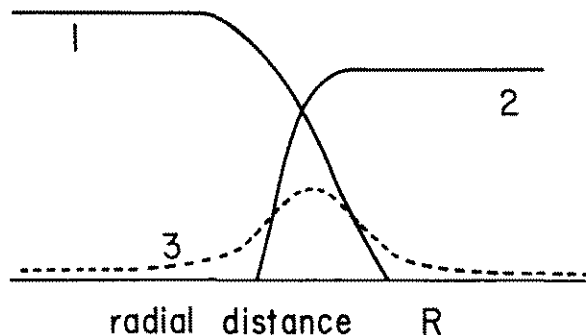


FIG.4.2. Concentrations near the interface.

We imagine that the solution is ideal with respect to the third component, so that we can write the chemical potentials of the solvent and the solute as

$$\mu_2 = \mu_0 - kT c, \quad (4.24)$$

$$\mu_3 = kT \ln c + \psi, \quad (4.25)$$

where $c = \rho_3/\rho_2$ is the concentration of the solute, and μ_0 denotes the chemical potential of the pure solvent. ψ is a

function only of the temperature and pressure. It is easily verified that Eqs.(4.24) and (4.25) indeed satisfy the Gibbs-Duhem equation [Eq.(4.12)] at fixed temperature and pressure.

Upon taking the dividing surface such that $\Gamma_1=0$, we substitute Eqs.(4.24) and (4.25) into Eq.(4.18), and obtain

$$\frac{c}{kT} \left(\left(\frac{\partial \gamma}{\partial c} \right)_{T,P,R} \Big|_{R=R_0} - kT \Gamma_2 \right) = - \Gamma_3. \quad (4.26)$$

This equation shows that the adsorption of the solute at an interface between immiscible liquids is dependent on the adsorption of the solvent as well as on the susceptibility of the interfacial tension to the solute.

It must be finally pointed out that if it can be assumed that the third component is not soluble in the substrate phase (made up of the first component), the solute does not affect the thermodynamic state of the substrate fixed at constant temperature and pressure. As a result, by taking the dividing surface at the zero adsorption of the solvent, we can write the adsorption equation for the three-component fluid in the same form as that for the solvent-solute two-component system, now at a constant pressure.

B. Surface entropy and surface energy

Let us consider an interface appearing in a single component fluid, e.g. liquid-vapor, nematic-isotropic, etc. With a dividing surface taken at the point of zero adsorption, we have from Eq.(4.14)

$$\left(\frac{\partial \gamma}{\partial T} \right)_R = - s^S. \quad (4.27)$$

In the case of a plane interface, the left-hand side of this equation is an absolutely measurable quantity, and when it is

negative, the surface entropy should be positive; this implies that the interfacial transition layer is less ordered than the bulk phase. It is indeed a common observation that the surface tension of a pure liquid, away from the liquid-vapor critical point, approximately follows a linear relationship with temperature [10]:

$$\gamma = \gamma_0 - S_0 T, \quad (4.28)$$

with S_0 being a positive constant [Fig.4.3]. Then, it follows from the thermodynamics that S_0 is just the surface entropy S^S .

The internal energy U of the system is related to the Helmholtz free energy F and the thermodynamic potential Ω via $U = F + TS = \Omega + \sum \mu_i N_i + TS$. Therefore, by taking the surface excess per unit area, we obtain

$$U^S = \gamma + \sum \mu_i \Gamma_i + TS^S. \quad (4.29)$$

For a single component fluid with the dividing surface taken at zero adsorption, this equation is rewritten, in view of Eq.(4.26), as

$$U^S = \gamma + TS^S = \gamma - T \left(\frac{\partial \gamma}{\partial T} \right)_R. \quad (4.30)$$

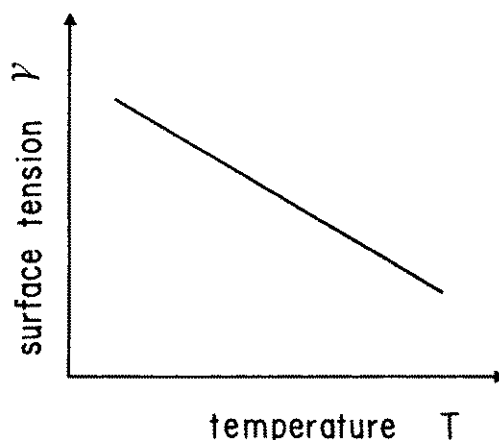


FIG.4.3. Typical temperature dependence of surface tension.

When the surface tension satisfies Eq.(4.28), this equation reveals that the surface energy U^S simply equals γ_0 , which is a constant independent of temperature. This implies that the linear temperature dependence of surface tensions is essentially an entropic effect which derives from the enhanced structural "disorder" of the surface region compared with the bulk phase.

4.1.4 The Laplace equation and the surface of tension

As already mentioned, the interfacial tension of a curved interface can not be defined uniquely without reference to the dividing surface only from a thermodynamic point of view. However, the surface or interfacial tension is originally a "mechanical" concept which was first introduced by Young [11] to expound the balance of force at an interface. It is, therefore, of interest to see how the thermodynamic and the mechanical concepts of interfacial tensions are connected to each other.

Consider now the mechanical equilibrium of the region shown

in Fig. 4.1. Let us also imagine that an interfacial tension γ is acting just at the interface located at R [see Fig. 4.4], and we conceive that the pressure is uniform within each region divided by the interface.

The condition of mechanical equilibrium can be most readily obtained by con-

sidering a shell of infinitesimal thickness around the interface. Then, the region in question is now comprised of three parts, two bulk phases and the shell. Obviously, the bulk phases separated by the shell should be in equilibrium in themselves. Therefore, it is only necessary to consider the equilibrium of the shell. Because the total force acting in the x direction should be zero, we obtain

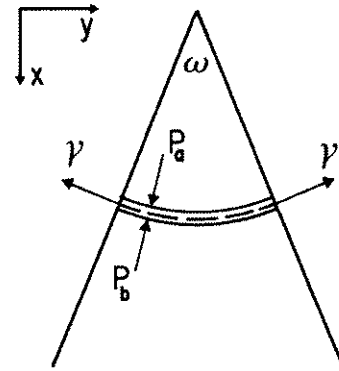


FIG.4.4. Definition of the surface of tension.

$$0 = R(P_a - P_b) \int_{-\omega/2}^{\omega/2} \cos\phi \, d\phi - 2\gamma \sin\omega/2,$$

$$= 2R(P_a - P_b)\sin\omega/2 - 2\gamma \sin\omega/2,$$

from which we obtain the "Laplace equation" for a cylindrical interface [5]:

$$P_a - P_b = \frac{\gamma}{R} \quad (4.31)$$

As it appears, the Laplace equation can be viewed, on the one hand, as relating the curvature of an interface to the pressure difference across the interface. On the other hand, however, it can also be regarded as giving a "mechanical definition" of the interfacial tension γ in terms of the pressure difference and the curvature. Unfortunately, the interfacial tension appearing in Eq.(4.31) is not necessarily identical with that defined thermodynamically [Eq.(4.7)]; indeed, at a fixed pressure difference, the former is linearly dependent on R , while the latter is nonlinearly. Only in the limit of plane interface, the Laplace equation becomes indeterminate and is thus trivially compatible with the thermodynamic definition.

We have derived the Laplace equation as if there were an infinitesimally thin boundary-layer which can sustain tensile force. So, the above mentioned fact indicates that not all the thermodynamical interfacial tensions do not allow a simple interpretation as a tensile force acting at the dividing surface. In order to reconcile the mechanistic and the thermodynamic views of an interfacial tension of a curved interface, we need therefore to take the dividing surface at a special point called the "surface of tension." By comparing the Laplace equation with the thermodynamic formula Eq.(4.8), we see that the surface of tension corresponds to the dividing surface for which

$$\left(\frac{\partial \gamma}{\partial R}\right)_{T,P,V,N_i} = 0, \quad (4.32)$$

where γ is the thermodynamic interfacial tension given by

Eq.(4.7). We will denote by R_s the R which satisfies the above equation and the corresponding interfacial tension by γ_s . From Eq.(4.32), it readily follows that on taking the dividing surface at R_s , we can treat a curved interface in a formally similar manner as a plane interface. As will be shown later, this property still holds for a nematic interface; however, Eq.(4.32) becomes no longer true, because of the orientational anisotropy of the nematic liquid crystal.

The interfacial tension depends in general on the curvature of the interface. In fact, we know from Eq.(4.14) for a single component fluid with the dividing surface taken at the point of zero adsorption that

$$d\gamma = [(P_a - P_b) - \gamma/R_0] dR_0. \quad (4.33)$$

On the right-hand side, dR_0 represents the change of the curvature of the interface induced by the variation of pressure, etc.; do not confuse it with the (non-physical) formal change of the dividing surface. When the surface of zero adsorption coincides with the surface of tension, the term in the square brackets vanishes due to the Laplace equation, and hence the interfacial tension becomes an invariant irrespective of whether the interface is planar or curved. Conversely, therefore, unless R_0 always equals R_s , the interfacial tension is to actually vary as the curvature is changed. In order to take a closer look at the curvature dependence, we rewrite the interfacial tension, Eq.(4.7), as

$$\gamma = \frac{1}{2} \gamma_s \left(\frac{R}{R_s} + \frac{R_s}{R} \right), \quad (4.34)$$

where we have used Eq.(4.31). Then, by taking the total differential of the above at $R=R_0$ and comparing it with Eq.(4.33), we have

$$\frac{R_s}{\gamma_s} \frac{\partial \gamma_s}{\partial R_s} = \frac{R_o^2 - R_s^2}{R_s^2 + R_o^2} \quad (4.35)$$

This equation describes how the tension of a cylindrical interface changes as the fluid cylinder thins.

For the more interesting cases of spherical drops, the above argument can be straightforwardly extended to give the Laplace equation for a spherical interface

$$P_a - P_b = 2 \frac{\gamma}{R_s} \quad (4.36)$$

and

$$\frac{R_s}{\gamma_s} \frac{\partial \gamma_s}{\partial R_s} = \frac{2(R_o^3 - R_s^3)}{R_s^3 + 2R_o^3} \quad (4.37)$$

which corresponds to Eq.(4.35); the thermodynamic interfacial tension of a spherical interface is given by the same formula Eq.(4.7) as that for the cylindrical interface. Formal integration of Eq.(4.37) leads to the Gibbs-Tolman-Koenig-Buff equation [5] for the curvature-dependence of the interfacial tension.

Up to first order in $1/R_s$, Eqs.(4.35) and (4.37) can be rewritten as

$$\frac{R_s}{\gamma_s} \frac{\partial \gamma_s}{\partial R_s} = \begin{cases} \delta_{\infty}/R_s, & \text{for cylinders,} \\ 2\delta_{\infty}/R_s, & \text{for spheres,} \end{cases} \quad (4.38)$$

where

$$\delta_{\infty} = \lim_{R_s \rightarrow \infty} (R_o - R_s).$$

Hence, integrating Eq.(4.36), we obtain

$$\gamma_s = \begin{cases} \gamma_o \exp(-\delta_{\infty}/R_s), & \text{for cylinders,} \\ \gamma_o \exp(-2\delta_{\infty}/R_s), & \text{for spheres,} \end{cases} \quad (4.39)$$

where γ_o denotes the tension of the plane interface. As both R_o and R_s lie within the interfacial transition layer, the above equation shows that the interfacial tension remains virtually

constant, until R_g becomes so small as to be comparable with the thickness of the transition layer.

Since the liquid-vapor interface is known to be a few-molecular layer thick at a point far from the critical point[13], the interfacial tension can be, to a good approximation, assumed constant for a system of macroscopic dimension. In the case of a nematic-isotropic interface, however, the interfacial tension is on the order of 10^{-5} J/m² [13-18], about 1/1000 of the surface tension of ordinary liquids, and also the thickness of the transition layer, which is mostly governed by the orientational correlation length, reaches a few hundred angstroms due to the nearly second-order nature of the nematic-isotropic transition [19,20]. Hence, the curvature effect is expected to manifest itself even in relatively large droplets and thereby play a significant role in the nucleation of new phase at the nematic-isotropic transition. However, very little is known on this matter at present.

4.2 The equilibrium shape of a nematic interface

In the above argument, we have seen that the shape of a fluid interface is determined such that the mechanical equilibrium of the phases in contact is established, and among others that the shape itself brings about a deep consequence on the thermodynamic treatment of the interface. So, it is obviously quite important to have a fair understanding of the geometry of the interface in question, prior to detailed thermodynamic discussions. We will now briefly investigate, from a mechanical view point, the relationship between the degree of deformation occurring in the nematic and the resulting distortion of the interface which is assumed to be planar in the absence of deformation [see Fig.4.5].

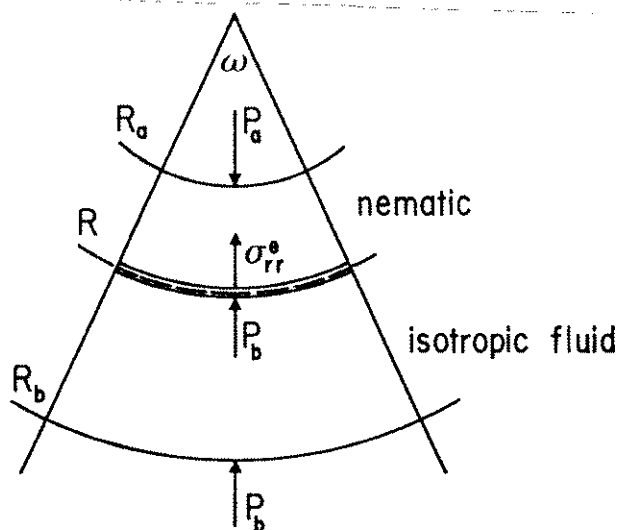


FIG.4.5. Mechanical equilibrium of an interface between an isotropic fluid and an orientationally deformed nematic. σ_{rr}^e denotes the rr -component of the Ericksen stress tensor. The interfacial tension γ is acting at the surface of tension located at R .

The overall shape of the interface depends not only on the pressure difference across the interface but also on what conditions are imposed at the circumference of the interface; in this respect, the cylindrical interface we have considered in the former section turns out to be a special case which may be attained when the interface is suspended over a long rectangular hole. In general, it can be shown that the interface adopts a shape which has a constant "mean curvature," as well known in the equilibrium-shape problem of a suspended soap film[12]. At

present, however, we imagine, without going into the detail, that a proper boundary condition is always imposed at the circumference so as to let the interface be cylindrical when the nematic is deformed. We also conceive that the volume of the nematic in question is always in contact with a large reservoir of the undeformed nematic held at temperature T and pressure P with prescribed concentrations. We shall further assume that the phase with which the nematic is in contact is an isotropic fluid whose thermodynamic state can be completely specified by its temperature, pressure, and concentrations, so that the state of this phase is indifferent to the orientational state of the nematic once the state of the reservoir is given.

We take the cylindrical polar coordinate with the z -axis parallel to the interface, and assume, as before, that the property of the system, including the orientation of the nematic molecules, is invariant with respect to the rotation and translation about the z -axis; so that we are to consider only the case of an interface which imposes a uniform orientational boundary condition on the nematic being in contact.

Now, let σ_{rr}^e be the rr -component of the Ericksen stress. Then by applying the same argument as used to derive the Laplace equation in the last section, we can write down the condition of the mechanical equilibrium of the interface as

$$-\sigma_{rr}^e - P_b = \gamma/R, \quad (4.40)$$

where γ is the interfacial tension of the deformed nematic interface, which has as yet been defined. From the hydrostatics of nematics described in Chapter 2, we can rewrite Eq.(4.40), under the condition of no external field, as

$$-\sigma_{rr}^d - f_d + P - P_b = \gamma/R. \quad (4.41)$$

where P stands for the pressure inside the nematic reservoir.

From our requirement that the interface be planar ($R \rightarrow \infty$) in the absence of deformations, we must have $P_b = P$; the first two terms disappear when the nematic is in the undeformed state and hence the interface is planar. Since P and P_b are constant regardless of the degree of deformation (because of the constancy of temperature and chemical potentials), we are left finally with

$$-\sigma_{rr}^d - f_d = \gamma/R. \quad (4.42)$$

This equation in principle gives the curvature of the (cylindrical) interface in terms of the orientational strain.

To proceed further, let us first note the fact that, for a system with cylindrical symmetry, the strain energy density f_d can be written in the following form:

$$f_d(r) = f_0(\mathbf{n}, \partial\mathbf{n}/\partial r) + f_1(\mathbf{n}, \partial\mathbf{n}/\partial r)/r + f_2(\mathbf{n})/r^2, \quad (4.43)$$

where the first term is the strain energy density corresponding to the case of zero curvature, i.e. $R \rightarrow \infty$, and the second and the third are the terms proportional to $1/r$ and $1/r^2$, respectively, and hence they vanish when $R \rightarrow \infty$. In terms of the components of the director in respect to the cylindrical coordinate, f_0 , f_1 , and f_2 are specifically given by

$$\begin{aligned} f_0(\mathbf{n}, \partial\mathbf{n}/\partial r) &= \frac{1}{2} K_1 \left(\frac{\partial n_r}{\partial r} \right)^2 + \frac{1}{2} K_2 \left[n_z \frac{\partial n_\phi}{\partial r} - n_\phi \frac{\partial n_z}{\partial r} \right]^2 \\ &+ \frac{1}{2} K_3 n_r^2 \left[\left(\frac{\partial n_r}{\partial r} \right)^2 + \left(\frac{\partial n_\phi}{\partial r} \right)^2 + \left(\frac{\partial n_z}{\partial r} \right)^2 \right], \end{aligned} \quad (4.44)$$

$$\begin{aligned} f_1(\mathbf{n}, \partial\mathbf{n}/\partial r) &= K_1 n_r \frac{\partial n_r}{\partial r} + K_2 n_z n_\phi \left[n_z \frac{\partial n_\phi}{\partial r} - n_\phi \frac{\partial n_z}{\partial r} \right] \\ &+ K_3 \left[n_r^2 n_\phi \frac{\partial n_\phi}{\partial r} - n_\phi^2 n_r \frac{\partial n_r}{\partial r} \right], \end{aligned} \quad (4.45)$$

and

$$f_2(\mathbf{n}) = \frac{1}{2} K_1 n_r^2 + \frac{1}{2} K_2 (n_z n_\phi)^2 + \frac{1}{2} K_3 n_\phi^2 (n_\phi^2 + n_r^2). \quad (4.46)$$

Note that f_0 corresponds to the deformation energy density calculated as if the interface were planar. Similarly, according to Eq.(2.00), σ_{rr}^d can be divided into two terms as

$$\sigma_{rr}^d = \sigma_{rr_0}^d + \sigma_{rr1}^d/r, \quad (4.47)$$

where in the present geometry, in particular, we have

$$\sigma_{rr_0}^d = -2 f_0(\mathbf{n}, \partial\mathbf{n}/\partial r), \quad (4.48)$$

$$\sigma_{rr1}^d = -f_1(\mathbf{n}, \partial\mathbf{n}/\partial r). \quad (4.49)$$

Then, by combining Eqs.(4.42), (4.43), and (4.47)-(4.49), we get

$$f_0 - f_2/R^2 = \gamma/R, \quad (4.50)$$

where f_0 and f_2 are to be evaluated at $r=R$ in the Gibbs' spirit; that is, by extrapolating the bulk orientation of the director to R . Equation (4.50) is the nematic version of the Laplace equation.

By solving Eq.(4.49), the curvature $1/R$ is given by

$$\frac{1}{R} = \frac{2f_0}{\gamma + (\gamma^2 + 4f_0f_2)^{1/2}}. \quad (4.51)$$

It is here illustrative to expand the above expression in terms of a (usually small) parameter $\varepsilon = (f_0f_2)^{1/2}/\gamma$ to give

$$\frac{1}{R} = \frac{f_0}{\gamma} [1 - \varepsilon^2 + O(\varepsilon^4)]. \quad (4.52)$$

Then it follows immediately that, up to first order in ε , the curvature of the interface is given by

$$1/R = f_0/\gamma. \quad (4.53)$$

The parameter of expansion ε has a rather clear physical meaning: Let λ be the characteristic length of orientational deformation, over which the director changes its direction appreciably, and K be a typical Frank constant; then, in view of Eqs.(4.44) and (4.46), we can have an order of estimate of ε as

$$\varepsilon \sim K/(2\gamma\lambda) \sim \lambda/R. \quad (4.54)$$

Therefore, we can conclude that the higher order corrections to Eq.(4.53) will be important only when λ gets so small that R becomes comparable with λ ; note that R itself is of the order of λ^2 and hence of ε^{-2} .

To make the point more specific, let us take $K=3 \times 10^{-11}$ N, $\gamma=30$ mN/m, which are typical values for the elastic constant and the surface tension of nematics, and assume that the deformation is occurring typically over $\lambda=1$ μ m. Putting these values in Eq.(4.54), we obtain $\varepsilon=5 \times 10^{-4}$ and $R=2$ mm. This shows that at a free surface of nematics, Eq.(4.53) holds to a good approximation for virtually all realistic cases. For an interface between nematic and isotropic phases, however, which has commonly an interfacial tension on the order of 10^{-2} mN/m, ε becomes as large as 0.5 ($R \sim 2$ μ m) under the same condition as above, indicating the need to retain the higher order terms. At a real nematic-isotropic interface, however, a number of other factors influence the shape of the interface [17,21-23], before the approximation in question actually breaks down.

Finally a word of caution is in order as to the meaning of the interfacial tension γ , which has been used without explicit definition in the above. We have started the present argument with the condition of mechanical equilibrium of the interface, conceiving that γ is a tensile force acting at the point R . As in the case of ordinary fluids, therefore, R is to specify the position of the "surface of tension" for the nematic interface,

when γ is chosen to be compatible with the thermodynamics. It is thus noteworthy that the mechanical formulas as Eqs.(4.50) and (4.53) offer an essentially distinct perspective as regards the interfacial tension, independent of the thermodynamics of the interface to be discussed below.

4.3 Orientational thermodynamic variables and thermodynamics of bulk nematics

A thermodynamic treatment of a macroscopic body begins invariably with counting out all the thermodynamic variables needed to completely specify the state of the system in question. One of the most fundamental assumptions of a traditional treatment of fluid interfaces is that the equilibrium state of the interface is attained automatically once the state of the bulk phases is specified; so that the thermodynamic variables for the bounded system are assumed to be completely identical with those for the bulk phase. Based on this assumption, therefore, it is only necessary to consider the thermodynamic variables relevant to bulk nematics.

As described in the previous chapters, the nematic liquid crystals have a long-range orientational order, yet still lacking a translational periodicity. Consequently, the equilibrium state of a nematic liquid is to depend not only on the temperature, the volume of the container, and the number of molecules in it, but also on the "orientational boundary condition" at the container wall and on its "shape" as well through the curvature elasticity of nematics. In its most general description, the orientational state of a nematic may depend on the director and its derivatives of all orders at the boundary. Here, we will base our argument on the Frank theory of curvature elasticity, by restricting the attention to the small deformation regime. Since the Frank theory is a kind of linear elastic theory, the number of orientational degrees of freedom will be greatly reduced, thereby making the problem mathematically tractable. The purpose of this section is to set out the most convenient set of thermodynamic variables to specify the orientational equilibria of nematic liquid crystals, and to discuss the thermodynamics of deformed bulk nematics.

4.3.1 The equilibrium configuration of the director in the bulk nematic with cylindrical symmetry

As described in Chapter 2, the equilibrium director profile should satisfy the Euler-Lagrange equation, which derives from the Frank elastic energy functional. Based on this equation, we will here work out some characteristic features of the director profile, which the nematic in question is expected to have when it is deformed with cylindrical symmetry. Since we are only concerned with the bulk property, it is completely immaterial whether or not the elastic energy density involves terms resulting from the so-called "second order elasticity." Here, we conceive deformation processes in which variables other than the director is kept constant.

Suppose a region of bulk nematic as shown in Fig.4.6. Taking the cylindrical coordinate system, the Frank elastic energy of the region F_d can be written as

$$F_d = \int_{R_1}^{R_2} [f_0(\mathbf{n}, d\mathbf{n}/dr) + f_1(\mathbf{n}, d\mathbf{n}/dr)/r + f_2(\mathbf{n})/r^2] r \omega dr. \quad (4.55)$$

where f_0 , f_1 , and f_2 are the functions of the components of the director and their derivatives, defined in Eqs.(4.44)-(4.46). Then the director profile in equilibrium can be in principle obtained under an appropriate boundary condition by directly applying the variational calculus to F_d . In order to see the qualitative features of those director profiles, however, it is far more convenient to work

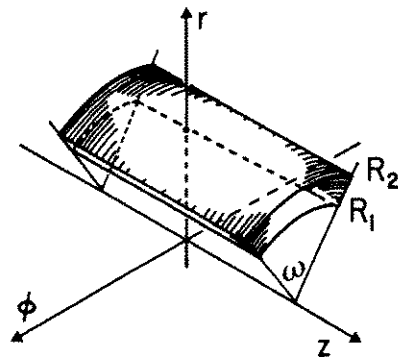


FIG.4.6. Cylindrical region of the bulk nematic.

with a new variable t defined by

$$t = \ln r. \quad (4.56)$$

Since f_0 , f_1 , and f_2 are, respectively, second, first, and zero-th order homogeneous functions of $d\mathbf{n}/dr$, it is readily shown that F_d can be rewritten in terms of t as

$$F_d = \int_{t_1}^{t_2} [f_0(\mathbf{n}, d\mathbf{n}/dt) + f_1(\mathbf{n}, d\mathbf{n}/dt) + f_2(\mathbf{n})] \omega dt, \quad (4.57)$$

where $f_0(\mathbf{n}, d\mathbf{n}/dt)$, etc. are the functions defined by Eqs.(4.44)-(4.46) in which $d\mathbf{n}/dr$ is merely replaced by $d\mathbf{n}/dt$, so that, for example, $f_0(\mathbf{n}, d\mathbf{n}/dt) = r^2 f_0(\mathbf{n}, d\mathbf{n}/dr)$. The Euler-Lagrange equation determining the equilibrium director profile now reads

$$\frac{d}{dt} \frac{\partial L_d}{\partial (dn_i/dt)} - \frac{\partial L_d}{\partial n_i} = h n_i, \quad (4.58)$$

where $L_d = f_0 + f_1 + f_2$, and the subscript i refers to either r , ϕ , or z , and h is the Lagrange multiplier to assure $\mathbf{n}^2 = 1$.

A. Director profile as a trajectory on a unit sphere

As noted by Thurston [24], a director profile, when it changes only in one dimension, can be regarded as a trajectory of a particle moving on a unit sphere. Though this analogy with a dynamical system adds nothing essentially new to the information contained in Eqs.(4.57), (4.58), etc., it is extremely powerful to visualize the characteristic features of the

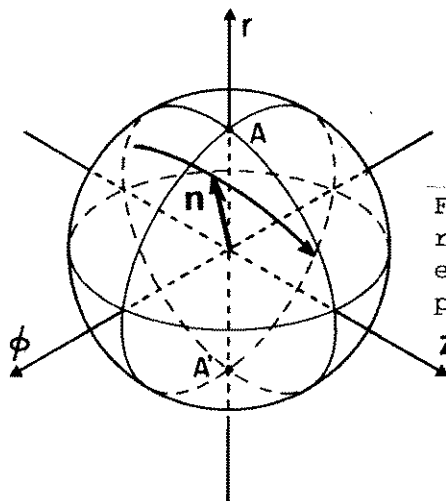


FIG.4.7. Unit sphere representation of an equilibrium director profile.

profile and thus to classify various profiles according to their global properties.

In this analogy, the director \mathbf{n} corresponds to the position of the particle, t to the time, and L_d to the Lagrangian. Accordingly, the Euler-Lagrange equation, Eq.(4.58), turns into the equation of motion for the particle. Let us now introduce a unit sphere, as illustrated in Fig.4.7, on which the director is to be plotted as a function of t . In the figure, z -, r -, and ϕ -axes should be understood as expressing the same directions as in Fig.4.6. Therefore, the point A, which is physically equivalent to the radially opposite point A' because of the equivalence of \mathbf{n} and $-\mathbf{n}$, corresponds to a director which is normal to the cylindrical surface. The points on the equator, on the other hand, express those directors which are tangential to the cylinder. For the sake of later calculations, we will occasionally utilize the spherical polar coordinate (Θ, Φ) as also defined in Fig.4.7.

At present, the Lagrangian L_d consists of three terms f_0 , f_1 , and f_2 . And, if we restrict ourselves to a region of the nematic not very far from the interface, i.e. $r/R = O(1)$, we can approximately write

$$\begin{aligned} \frac{dn_i}{dt} &= r \frac{dn_i}{dr} \\ &\sim \frac{R}{\lambda} = \varepsilon^{-1}. \end{aligned} \quad (4.59)$$

Then, considering the definition of f_0 , f_1 , and f_2 , we readily have

$$f_0(\mathbf{n}, d\mathbf{n}/dt)/K \sim O(\varepsilon^{-2}),$$

$$f_1(\mathbf{n}, d\mathbf{n}/dt)/K \sim O(\varepsilon^{-1}),$$

and

$$f_2(\mathbf{n})/K \sim O(1),$$

where K stands for a typical value of the Frank elastic constant.

From the above, we obtain

$$L_d(\mathbf{n}, d\mathbf{n}/dt) = f_0(\mathbf{n}, d\mathbf{n}/dt)[1 + O(\varepsilon)]. \quad (4.60)$$

Then, it follows that, for sufficiently small deformations and/or small interface curvature, we can neglect f_1 and f_2 terms in comparison with f_0 in the Lagrangian; in other words, the director profile can be treated, to lowest approximation, as though the interface remain planar even when the nematic is deformed. It must be emphasized that this result is nonetheless nontrivial, but intimately related to the fact that the radius of the interface R should diverge more rapidly than the characteristic length of deformation λ according as the deformation weakens.

In a dynamical system, there usually exist several conservation laws resulting from the inherent space-time symmetry of its Lagrangian. Now it is a straightforward task to see by way of Eq.(4.44) that L_d , as approximated above, remains unchanged under transformation of t and rotation of \mathbf{n} about the r -axis. So, the Hamiltonian H given by

$$\begin{aligned} H &= \sum_i \frac{\partial L_d}{\partial (dn_i/dt)} \frac{dn_i}{dt} - L_d = f_0(\mathbf{n}, d\mathbf{n}/dt) \\ &= r^2 f_0(\mathbf{n}, d\mathbf{n}/dr), \end{aligned} \quad (4.61)$$

and the r -component of the angular momentum,

$$\begin{aligned} M_r &= n_\phi \frac{\partial L_d}{\partial (dn_z/dt)} - n_z \frac{\partial L_d}{\partial (dn_\phi/dt)}, \\ &= [K_2(1-n_r^2) + K_3 n_r^2] \left(n_\phi \frac{dn_z}{dt} - n_z \frac{dn_\phi}{dt} \right), \end{aligned} \quad (4.62)$$

are both to be conserved along each allowed trajectory. This property can be easily confirmed by a direct calculation, if L_d is expressed in terms of Θ and Φ :

$$L_d = \frac{1}{2} K_3 \left[f(\theta) \left(\frac{d\theta}{dt} \right)^2 + g(\theta) \left(\frac{d\phi}{dt} \right)^2 \right], \quad (4.63)$$

where

$$\begin{aligned} f(\theta) &= (K_1 \sin^2 \theta + K_3 \cos^2 \theta) / K_3, \\ g(\theta) &= \sin^2 \theta (K_2 \sin^2 \theta + K_3 \cos^2 \theta) / K_3. \end{aligned} \quad (4.64)$$

Because M_r is written as

$$M_r = K_3 g(\theta) \frac{d\phi}{dt}, \quad (4.65)$$

in terms of those angles, it follows immediately from the Euler-Lagrange equation for ϕ coming from Eq.(4.63) that M_r is indeed constant in equilibrium. It is also notable at this stage that, while the Hamiltonian remains to be a constant of motion even when f_1 and f_2 are included, (though it is no longer equal to L_d as above), M_r can be strictly constant only when they are neglected.

The general solution of the equation of motion should contain at present four arbitrary constants, corresponding to the initial position and the velocity on the unit sphere. From the above argument, it is now clear that two out of the four constants are $H = L_d$ and M_r . Furthermore, since the Lagrangian is, as we have already seen, invariant with respect to arbitrary shift of time and rotation about the r-axis, we are generally allowed to write the equilibrium director configuration in the form,

$$\mathbf{n} = T(\phi_0) \mathbf{n}_s(t-t_0, H, M_r), \quad (4.66)$$

in terms of a special solution \mathbf{n}_s of the Euler-Lagrange equation with given H and M_r . Here, $T(\phi_0)$ denotes an operator to rotate the director about the r-axis by an angle ϕ_0 .

In order to further simplify the above expression, it is helpful to consider a scaling of t like

$$t \rightarrow \kappa t. \quad (4.67)$$

Upon application in Eqs.(4.61) and (4.62), we readily see that H and M_r transform as

$$H \rightarrow \kappa^{-2}H, \quad \text{and} \quad M_r \rightarrow \kappa^{-1}M_r. \quad (4.68)$$

Consequently, by taking $\kappa = H^{1/2}$, we can finally rewrite Eq.(4.66) to give

$$\mathbf{n} = T(\phi_0)\mathbf{n}_s[H^{1/2}(t-t_0), 1, M_r H^{-1/2}]. \quad (4.69)$$

This expression shows that trajectories having the same $M_r H^{-1/2}$ are isomorphic to each other by an appropriate rotation about the r -axis, apart from the scaling and the translation of t .

As far as the geometrical features are concerned, we can therefore characterize any allowed trajectory by a single parameter $M_r H^{-1/2}$. We will introduce here a dimensionless parameter β via

$$\beta = M_r^2 / (2K_3 H). \quad (4.70)$$

Then any equilibrium trajectory may be expressed in a simple form as

$$\mathbf{n} = T(\phi_0)\mathbf{n}_s[H^{1/2}(t-t_0), \beta], \quad (4.71a)$$

or in terms of r as

$$\mathbf{n} = T(\phi_0)\mathbf{n}_s[H^{1/2}\ln(r/r_0), \beta]. \quad (4.71b)$$

In summary, an equilibrium director trajectory (profile) is completely specified by four parameters β , H , r_0 , and ϕ_0 . The topology of the trajectory, however, is cast into β alone; H tells how fast the director traces the trajectory, and r_0 and ϕ_0 indicate where to start tracing on the unit sphere.

B. Geometrical properties of trajectories: the meaning of β

In order to appreciate the physical significance of the parameter β in some detail, we shall first quote some results

concerning the trajectories from Thurston[24] without proof:

(1) Any meridian is a possible trajectory.

[Meridian is a great circle passing the north and the south poles. Thus, along a meridian, $\Phi = \Phi_0 = \text{const.}$ and hence $\beta = 0$; no twist deformations exist.]

(2) The only trajectories through a pole ($\Theta = 0$ or π) are meridians.

[Only when $\beta = 0$, the director can be strictly normal to the surface of the cylinder, cf. Fig.4.6.]

(3) A trajectory cannot be tangent to a meridian.

[A twisting of the director about the r-axis, if any, never change its sense. ($d\Phi/dt$ has a fixed sign for a given M_r .)]

(4) The equator is a trajectory.

[The pure twist deformation with $\Theta = \pi/2$ is always possible, if boundary conditions allow.]

(5) There are no trajectories tangent to the equator.

[Along a trajectory on which $d\Theta/dt = 0$ does not always hold, $d\Theta/dt$ never be zero at $\Theta = 0$ for any choice of β .]

These properties are schematically illustrated in Fig.4.8.

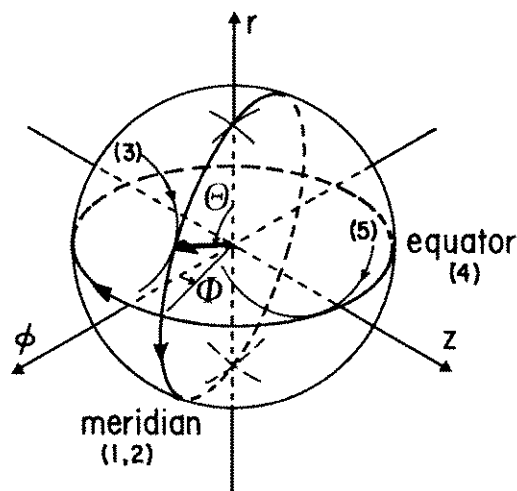


FIG.4.8. Basic geometrical properties of an equilibrium trajectory. Trajectories like (3) and (5) are not allowed.

In (1) and (3) of the above, we have learned that if and only if $\beta=0$, it is possible for $d\phi/dt$ to vanish, resulting in a director profile in which the rotation of the director is confined within a plane containing the r-axis. Therefore, in the presence of an aligning interface, which is of course assumed to have the cylindrical symmetry, it is naturally anticipated that such a planar configuration of the bulk director should exclusively excite the "out-of-plane" or "polar" mode of the orientational anchorage, regardless of the choices of H and r_0 . So, the director configurations with $\beta=0$, or equivalently the meridians are to play a special role (as a principal mode of bulk deformation) in connection with the interfacial properties of nematics.

From (4) and (5), on the other hand, we know that the equator, in which Θ is fixed at $\pi/2$, is a possible trajectory as far as the bulk equilibrium is concerned. This configuration may become a truly allowed one, if the boundary condition is such that the director is constrained to be perpendicular to the r-axis. In this special event, in particular, it is expected as regards the interfacial anchorage that the bulk deformation in question will excite only the "in-plane" or "azimuthal" mode of anchorage, in a similar manner as meridians do. As readily verified from Eqs.(4.63)-(4.65), β is in this case equal to $g(\pi/2)$. In contrast to meridians ($\beta=0$), however, the director configurations with $\beta=g(\pi/2)$ do not cover all the principal modes related to the in-plane anchorage; indeed, $\beta=g(\pi/2)$ only takes care of pure planar alignments.

Hence it is natural and also necessary to ask at this stage whether or not there is a possible trajectory with constant Θ for its arbitrary value other than $\pi/2$. Obviously, such a trajectory with, say, Θ_e , is to excite the in-plane mode of anchorage having the easy axis with Θ_e . Although the answer to this question is

in general negative as will be shown below, there always exists a trajectory [with $\beta = g(\Theta_e)$] which is tangent to the above hypothetical trajectory. So, it is indeed possible to excite the in-plane mode alone by means of those special trajectories with $\beta = g(\Theta_e)$.

In terms of β and $\zeta = t(2H/K_3)^{1/2}$, we can write Eq.(4.63) as

$$f(\Theta) \left(\frac{d\Theta}{d\zeta} \right)^2 + \frac{\beta}{g(\Theta)} = 1. \quad (4.72)$$

which leads to an inequality

$$g(\Theta) \geq \beta, \quad (4.73)$$

to be satisfied by Θ 's on a possible trajectory. At the point where the equality of Eq.(4.73) holds (at Θ_t), Eq.(4.72) yields $d\Theta/d\zeta = 0$. But this does not necessarily mean that $\Theta = \text{constant}$ along the trajectory. To see this point in detail, let us write down the Euler-Lagrange equation for Θ :

$$f(\Theta) \frac{d^2\Theta}{d\zeta^2} + f'(\Theta) \frac{d\Theta}{d\zeta} - \frac{1}{2} g'(\Theta) \left(\frac{d\Theta}{d\zeta} \right)^2 = 0. \quad (4.74)$$

This equation shows that only when $g(\Theta_t) = \beta$ and $g'(\Theta_t) = 0$ are simultaneously satisfied, second and all higher order derivatives vanish at this point and hence $\Theta = \Theta_t$ becomes an allowed trajectory.

In Fig.4.9, $g(\Theta)$ is plotted versus Θ for some values of

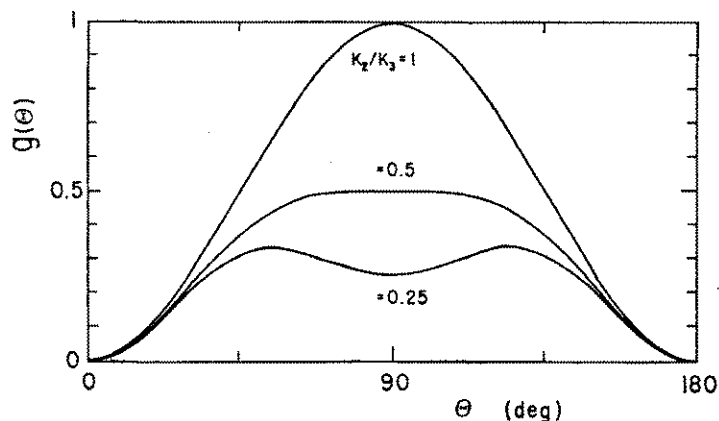


FIG.4.9. Function $g(\theta)$ for various values of K_2/K_3 .

K_2/K_3 . The allowed Θ 's are those beyond the horizontal line representing $g=\beta$. Then, unless Θ coincides with the extrema of $g(\Theta)$, Θ cannot be constant along a trajectory. In general, however, at the point where $g(\Theta_t)=\beta$, $d\Theta/d\zeta$ only changes its sign; we call this a "turning point" after Thurston[24]. At the turning point, the trajectory is tangent to a small circle on the unit sphere with a constant polar angle Θ_t , and as obvious from the above argument, the converse is also true, here.

4.3.2 Thermodynamics of bulk nematics

A. Director as an independent variable

As we are assuming that the nematic under discussion is always in contact with a large reservoir of undeformed nematic with given concentrations, it becomes convenient to work with the grand thermodynamic potential Ω . For the nematic region shown in Fig.4.6, held between the cylindrical surfaces at $r=R_1$ and R_2 subtending the azimuthal angle ω with unit length in z -direction, the cylindrical symmetry of the system allows us to write

$$\Omega = \Omega[\mathbf{n}(r); T, \omega, R_1, R_2, \mu_j], \quad (4.75)$$

where μ_j ($j=1\sim m$) are the chemical potentials of the constituents. At this stage, Ω is still regarded as a functional of the equilibrium director profile $\mathbf{n}(r)$, not as a function of β , H , t_0 , and Φ_0 . In view of the anisotropy of the nematic, the variation of Ω associated with an infinitesimal change of the thermodynamic state may in general be written as

$$d\Omega = - SdT - \sum_j N_j d\mu_j + \eta d\omega - P_2 \omega R_2 dR_2 + P_1 \omega R_1 dR_1 + \delta W_0, \quad (4.76)$$

where δW_0 represents the external work necessary to infinitesimally change the director profile within the volume from one equilibrium to another while keeping temperature, chemical

potentials, and geometry fixed. P_1 and P_2 denote the stress component normal to the boundary at $r=R_1$ and R_2 , respectively. η is defined ordinarily [cf. Eq.(4.4)] via

$$\eta = (\partial\Omega/\partial\omega)_{T, \mu_j, R_1, R_2, \mathbf{n}_{eq}}$$

We shall restrict the present argument to terms lowest-order in ε as before, and approximate the Frank energy density by f_0 . In order to formulate δW_0 , let us shortly consider those processes which occur by way of the change of the director profile alone. Under this circumstance, δW_0 has to be identical with the change of the Frank energy F_d . As a consequence, by applying the variational calculus to Eq.(4.57) (retaining only f_0), we obtain

$$\begin{aligned} \delta W_0 &= dF_d && (4.77) \\ &= \sum_i \omega R_2 \left. \frac{\partial f_0}{\partial (dn_i/dr)} \right|_{R_2} dn_i(R_2) - \sum_i \omega R_1 \left. \frac{\partial f_0}{\partial (dn_i/dr)} \right|_{R_1} dn_i(R_1). \end{aligned}$$

The first term in the above represents the orientational work performed across the (cylindrical) boundary at R_2 , and the second that across the boundary at R_1 . External work through other surfaces cancels out due to symmetry. Note that $\mathbf{n}(R_1)$ and $\mathbf{n}(R_2)$ can obviously be taken independently of each other (as far as the bulk configuration is concerned) and are at the same time sufficient to specify the equilibrium director configuration at given environmental conditions (as they contain essentially "four" independent parameters). So we can regard $\mathbf{n}(R_1)$ and $\mathbf{n}(R_2)$ as independent thermodynamic variables taking care of the director configuration inside the nematic.

We shall postulate here that the expression of the orientational work as given above can be extended as such to more

general processes involving the change of temperature, pressure, etc. So that, we may write

$$d\Omega = - SdT - N_j d\mu_j + \eta d\omega - P_2 \omega R_2 dR_2 + P_1 \omega R_1 dR_1 + \omega R_2 \left. \frac{\partial f_0}{\partial (dn_i/dr)} \right|_{R_2} dn_i(R_2) - \omega R_1 \left. \frac{\partial f_0}{\partial (dn_i/dr)} \right|_{R_1} dn_i(R_1), \quad (4.78)$$

where the subscript i runs over r , ϕ , and z , and for descriptive simplicity, we have employed Einstein's rule to imply summation over j and i . It must be strictly born in mind concerning Eq.(4.78) that $dn_i(R_1)$ and $dn_i(R_2)$ are the "net" differential of the director at the boundaries located at R_1 and R_2 , respectively; hence, they may change, even though $\mathbf{n}(r)$ is held constant, simply as a result of the motion of the boundary. According to the hydrostatics of nematics, therefore, we have to identify P_1 and P_2 with the negative of the rr -component of the Ericksen stress tensor. At R_1 for example, we see from Eqs.(2.00) and (4.47)-(4.49) that up to lowest order in ε

$$P_1 = -\sigma_{rr}^e(R_1) \sim R_1^{-2}H + P, \quad (4.79)$$

where P is the pressure of the nematic reservoir. In Eq.(4.79), f_0 has been replaced by H on account of Eq.(4.61). Similarly, η is given by

$$\eta = \int_{R_1}^{R_2} \sigma_{\phi\phi}^e r dr \sim H \ln(R_2/R_1) - (R_2^2 - R_1^2)P/2. \quad (4.80)$$

Combination of Eqs.(4.78)-(4.80) leads to

$$\begin{aligned}
d\Omega = & - SdT - N_j d\mu_j - PdV + H[\ln(R_2/R_1)]d\omega - H\omega d\ln(R_2/R_1) \\
& + \omega R_2 \left. \frac{\partial f_0}{\partial (dn_i/dr)} \right|_{R_2} dn_i(R_2) - \omega R_1 \left. \frac{\partial f_0}{\partial (dn_i/dr)} \right|_{R_1} dn_i(R_1),
\end{aligned} \tag{4.81}$$

where $V = \omega(R_2^2 - R_1^2)/2$ denotes the volume of the nematic region. The first three terms on the right hand side are formally the terms common in the thermodynamics of ordinary fluids, though it should be noted that the entropy S and the number of molecules N_j may change as the nematic is orientationally deformed. The last four terms are however concerned explicitly with the orientational deformations. Clearly they disappear when the nematic is free from deformations, i.e. $f_0=0$; in the undeformed state, therefore, the thermodynamics of a nematic liquid is no different from that of an isotropic fluid, being indifferent to the actual orientation of the nematic director in space.

B. H as an independent variable

In Eq.(4.81), the directors at the boundary have been utilized as thermodynamically independent variables to account for the orientational state of the nematic. As already noted, they are complete in the sense that they do have one-to-one correspondence with the equilibrium director profile, and thus should be complete thermodynamically as well. Here, we will attempt to replace these boundary directors with the trajectory parameters, H , β , r_0 , and Φ_0 , which are equally useful for the specification of the equilibrium director profile. We show that the thermodynamic potential involves H alone as an independent variable, while others as external parameters, leading to a quite simple formulation of the thermodynamics. Although the present approach toward bulk thermodynamics may seem unnecessarily complicated in the light of the rather trivial nature of the results it finally produces, it must be emphasized that its

conceptual clarity provides us with a systematic way to treat interface problems in later sections.

We begin our argument with the identity

$$[\ln(R_2/R_1)]H = \int_{R_1}^{R_2} f_0(T, \mu_j, \mathbf{n}, d\mathbf{n}/dr) r dr, \quad (4.82)$$

which directly follows from the spatial constancy of H in equilibrium. In the above, the dependence of f_0 on T and μ_j through the Frank elastic constants has been written explicitly. Upon taking the total differential of Eq.(4.82), we readily obtain

$$\begin{aligned} [\ln(R_2/R_1)]dH = & \int_{R_1}^{R_2} \left(\frac{\partial f_0}{\partial T} dT + \frac{\partial f_0}{\partial \mu_j} d\mu_j \right) r dr \\ & + R_2 \frac{\partial f_0}{\partial (dn_i/dr)} \Big|_{R_2} (dn_i)_{R_2} - R_1 \frac{\partial f_0}{\partial (dn_i/dr)} \Big|_{R_1} (dn_i)_{R_1}, \end{aligned} \quad (4.83)$$

where the symbol, $(dn_i)_R$, denotes the infinitesimal change of n_i at fixed R ; terms containing dR_1 or dR_2 cancel out on both sides. From the definition, $(dn_i)_R$ can be related to $dn_i(R)$ via

$$dn_i(R) = (dn_i)_R + \frac{dn_i}{dr} dR. \quad (4.84)$$

Substituting this equation into Eq.(4.83), we get

$$\begin{aligned} [\ln(R_2/R_1)]dH = & \int_{R_1}^{R_2} \left(\frac{\partial f_0}{\partial T} dT + \frac{\partial f_0}{\partial \mu_j} d\mu_j \right) r dr - 2Hd[\ln(R_2/R_1)] \\ & + R_2 \frac{\partial f_0}{\partial (dn_i/dr)} \Big|_{R_2} dn_i(R_2) - R_1 \frac{\partial f_0}{\partial (dn_i/dr)} \Big|_{R_1} dn_i(R_1), \end{aligned} \quad (4.85)$$

where use has been made of the fact that f_o is a second order homogeneous function of dn_i/dr , cf. Eq.(4.44). Finally, a combination of Eq.(4.85) with Eq.(4.81) yields

$$d\Omega = - [S + \omega \int_{R_1}^{R_2} \left(\frac{\partial f_o}{\partial T} \right)_n r dr] dT - [N_j + \omega \int_{R_1}^{R_2} \left(\frac{\partial f_o}{\partial \mu_j} \right)_n r dr] d\mu_j - PdV + Hd[\omega \ln(R_2/R_1)] + [\ln(R_2/R_1)]\omega dH. \quad (4.86)$$

This equation is identical with Eq.(4.81) in its essential content. But it is obviously far more transparent and useful.

To expound some fundamental consequences of this formula, let us integrate the above with respect to ω at fixed temperature, chemical potential, R_1 , and R_2 . During this process, P is apparently constant, so that we obtain

$$\Omega = - PV + H[\ln(R_2/R_1)]\omega. \quad (4.87)$$

The second term is just the Frank elastic energy of the volume F_d , and the first is the thermodynamic potential in the absence of deformation Ω_o . Consequently, Eq.(4.87) reduces to

$$\Omega = \Omega_o + F_d, \quad (4.88)$$

which is a trivial result coming from the definition of the Frank elastic energy. However, since $d\Omega_o = - S_o dT - N_{o_j} d\mu_j - PdV$, with S_o and N_{o_j} being the entropy and the number of molecules in the undeformed state, respectively, comparison of Eq.(4.88) with Eq.(4.86) leads to

$$S = S_o - \omega \int_{R_1}^{R_2} \left(\frac{\partial f_o}{\partial T} \right)_n r dr = S_o - \omega \frac{\partial K_q}{\partial T} \int_{R_1}^{R_2} \left(\frac{\partial f_o}{\partial K_q} \right)_n r dr, \quad (4.89)$$

$$N_j = N_{o_j} - \omega \int_{R_1}^{R_2} \left(\frac{\partial f_o}{\partial \mu_j} \right)_n r dr = N_{o_j} - \omega \frac{\partial K_q}{\partial \mu_j} \int_{R_1}^{R_2} \left(\frac{\partial f_o}{\partial K_q} \right)_n r dr, \quad (4.90)$$

which give the entropy and the number of molecules within the orientationally deformed bulk nematic in terms of the temperature and the chemical potential dependences of the Frank elastic constants; the subscript q should be summed over 1, 2, and 3, corresponding to the splay, twist, and bend elastic constants. Though it is in general difficult to express the integral in a closed form in terms of H , β , r_0 , and Φ_0 , we can draw some qualitative conclusions from the above as follows:

- (1) As the Frank elastic constants are usually decreasing functions of temperature, the entropy should increase when the nematic is isothermally deformed; note that the integral in the right hand side is always positive.
- (2) When deformed adiabatically, the temperature of the nematic must be lowered.
- (3) For a single component nematic, the density should be reduced as the nematic is deformed isothermally; because $\partial K_q / \partial \mu = (\partial K_q / \partial P) v^{-1}$, (>0 for most cases), with v the molecular volume.

Especially, when the Frank constants satisfy

$$\frac{1}{K_1} \frac{\partial K_1}{\partial X} = \frac{1}{K_2} \frac{\partial K_2}{\partial X} = \frac{1}{K_3} \frac{\partial K_3}{\partial X} = \frac{1}{K} \frac{\partial K}{\partial X}, \quad (4.91)$$

where X stands for T or μ_j , and K some appropriate function of T and μ_j , Eqs.(4.88) and (4.89) assume an extremely simple form as

$$S = S_0 - \frac{1}{K} \frac{\partial K}{\partial T} \omega H, \quad (4.92)$$

$$N_j = N_{0j} - \frac{1}{K} \frac{\partial K}{\partial \mu_j} \omega H. \quad (4.93)$$

Equation (4.91) is equivalent to require that the Frank elastic

constants be always proportional to each other, thus it in particular holds when the mean field prediction, i.e. $K_q \propto Q^2$, applies. Obviously, similar equations can also be derived, if the director configuration is comprised of a single mode of either splay, twist, or bend deformation.

From Eq.(4.93), we can see an interesting consequence for a binary mixture. When the concentration of the solute c is so small that the weak solution formulas such as Eqs.(4.24) and (4.25) apply, we can rewrite Eq.(4.93) to give

$$N_1 = N_{o1} + \frac{1}{kTK} \frac{\partial K}{\partial c} \omega H, \quad \text{and} \quad N_2 = N_{o2} - \frac{c}{kTK} \frac{\partial K}{\partial c} \omega H,$$

where the first and the second components refer to the solvent and the solute, respectively. So, if the solute is such that the Frank elastic constant is reduced as it is added more to the mixture, the solute is to accumulate in the deformed region, while the solvent is to be depleted. This is in accord with Le Chatelier's principle. More generally, in a multi-component nematic, the concentrations are no longer homogeneous when the director is distributed nonuniformly.

4.4 Thermodynamic formulation of a nematic interface

In Section 4.3, we have learned that the orientational thermodynamic state of a bulk nematic can be completely specified (within the limit of the Frank theory) either by the directors $\mathbf{n}(R_1)$ and $\mathbf{n}(R_2)$ or by H , β , r_0 , and Φ_0 . And, especially with the use of the latter set of variables, we could achieve a compact formulation of the thermodynamics of bulk nematics. Based on this formulation, we shall here extend the Gibbs thermodynamics of fluid surfaces to a nematic interface. In the first place, we identify the orientational thermodynamic variables relevant to a bounded nematic liquid, and in the second, we define the surface excess quantity with respect to an arbitrary dividing surface in the case of orientationally deformed nematics. Finally, we derive the nematic version of the Gibbs equation.

4.4.1 Orientational degrees of freedom of a bounded nematic

Let us consider again a region as shown in Fig.4.5 circumventing the interface of the nematic with another isotropic phase. Just as in the same manner as for bulk nematics, we can write the change of the thermodynamic potential Ω due to an infinitesimal change of the thermodynamic state as

$$d\Omega = - SdT - N_j d\mu_j + \eta d\omega + P_a \omega R_a dR_a - P_b \omega R_b dR_b + \delta W_0. \quad (4.94)$$

Contrary to Eq.(4.76), however, since only R_a is in the nematic medium, we have to discard now the first term in Eq.(4.77) to give

$$\delta W_0 = - \omega R_a \left. \frac{\partial f_0}{\partial (dn_i/dr)} \right|_{R_a} dn_i(R_a). \quad (4.95)$$

In the above equation, it is of course assumed that R_a is well inside the bulk nematic, so that the concept of the director and

the Frank theory hold to a good approximation at the boundary of the volume in question.

In the presence of an interface, it is no longer a trivial matter to affirm whether $\mathbf{n}(R_a)$ can be taken independent of other variables such as T , μ_j , etc., or not. In order to investigate this point in detail, let us generally write the director configurations in equilibrium above the interface Σ as follows:

$$\mathbf{n} = \mathbf{n}_{\Sigma}(r:T, \mu_j, \mathbf{X}), \quad (4.96)$$

where \mathbf{X} is a vectorial parameter characterizing the allowed profiles which are at present supposed to be generated by the action of a counter boundary placed outside the region under discussion. The number of the orientational degrees of freedom of such a bounded nematic is given by the dimension of \mathbf{X} . It must be noted at this stage that due to the Frank theory, the dimension of \mathbf{X} can never exceed four.

In order to determine the dimension of \mathbf{X} , it is convenient to consider a region of the nematic as shown in Fig.4.10 confined in between a couple of concentric interfaces (Σ_1 and Σ_2) which are separated by a large distance. The starting point of our present argument is the trivial conviction that, irrespective of the nature of those interfaces, there must be an equilibrium configuration of the director, $\mathbf{n}_{eq}(r:T, \mu_j)$, corresponding to the free energy minimum at the temperature T and the chemical potential μ_j , which is unique except for some

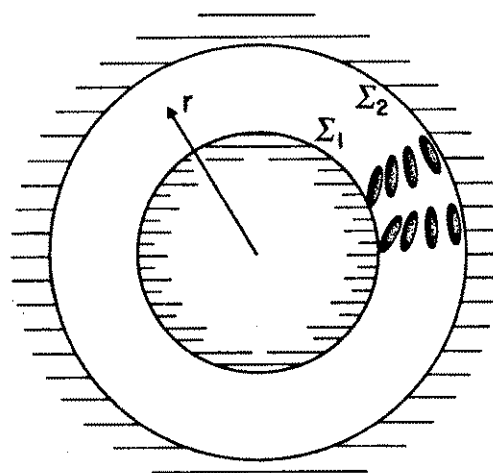


FIG.4.10. Nematic liquid crystal placed between two largely separated cylindrical boundaries.

special cases in which the multiple ground states exist.

As the equilibrium configuration must be compatible with both interfaces at R_1 and R_2 , there must be some appropriate vectors X_1 and X_2 satisfying

$$\begin{aligned} n_{\text{eq}}(r:T, \mu_j) &= n_{\Sigma_1}(r:T, \mu_j, X_1) \\ &= n_{\Sigma_2}(r:T, \mu_j, X_2). \end{aligned} \quad (4.97)$$

Since n_{Σ} 's themselves are the solutions of the Euler-Lagrange equation, Eq.(4.58), it is shown to be the necessary and sufficient condition for n_{Σ_1} and n_{Σ_2} to be identical for all r , as in Eq.(4.97), that they coincide at two arbitrary points. Therefore, Eq.(4.97) essentially reduces to four independent equations involving two unknowns X_1 and X_2 . In order that those equations can be uniquely solved for X_1 and X_2 at any T and μ_j , thereby giving rise to a unique director profile, the condition

$$\text{Dim}(X_1) + \text{Dim}(X_2) = 4 \quad (4.98)$$

should be met, where $\text{Dim}(X)$ denotes the dimension of the vector X . Furthermore, because the choice of Σ_1 and Σ_2 is arbitrary, we must have

$$\text{Dim}(X_1) = \text{Dim}(X_2) = 2, \quad (4.99)$$

which easily follows by applying reductio ad absurdum to Eq.(4.98). This indicates that the number of the orientational degrees of freedom is two in the case of a nematic liquid bounded on one of its side by an interface [see "Note" at the end of this section].

As appreciable from the course of derivation, this is a kind of phase rule (pertaining to the orientational state of a bounded nematic) analogous to the Gibbs phase rule. As a consequence of Eq.(4.99), in particular, we are allowed to regard $n(R_a)$ appearing in Eq.(4.95) as an independent thermodynamic variable.

So that we can write the equilibrium director profile in the presence of an interface Σ in the form,

$$\mathbf{n} = \mathbf{n}_{\Sigma}(r:T, \mu_j, \mathbf{n}(t_a)). \quad (4.100)$$

In terms of the trajectory parameters H , β , r_0 , and Φ_0 , on the other hand, it is readily shown by solving Eqs.(4.61) and (4.70) for X along with Eq.(4.96) that we can alternatively write

$$\mathbf{n} = \mathbf{n}_{\Sigma}(r:T, \mu_j, H, \beta), \quad (4.101a)$$

except for the following two cases: 1) H is always zero (so that the trajectory shrinks to a point on the unit sphere), and/or 2) Eq.(4.70) becomes an identity with a constant β .

In the former case, the nematic director is free to rotate as in an infinite sample, and hence the boundary condition imposed by the interface is fully degenerate, which is a situation of no interest to us here. As regards the latter case, it can immediately be shown that it occurs, even if possible, only at $\beta=0$: This is because, for $\beta \neq 0$, there is a turning point (of the trajectory on the unit sphere) with non-zero polar angle Θ_t satisfying $\beta = g(\Theta_t)$ [Section 4.3.1], so that, when $\mathbf{n}(R_a)$ which has $\Theta < \Theta_t$ is assumed in Eq.(4.100), β corresponding to $\mathbf{n}(R_a)$ should be smaller than the original one. Consequently, we see that for such a system which allows only meridians as its equilibrium trajectories, β can be a constant independent of X . Since meridians are differentiated from each other by the azimuthal angle Φ of the directors on it, it is possible to use Φ as an independent variable in place of β :

$$\mathbf{n} = \mathbf{n}_{\Sigma}(r:T, \mu_j, H, \Phi). \quad (4.101b)$$

The fact that the allowed trajectories are always meridians is equivalent to that the system in question does not stand a finite torque around the interface normal (r -axis). Such a

situation may arise if there is a cylindrical symmetry about the r-axis, and hence the orientational boundary condition due to the interface should be conical with respect to the rotation about the r-axis. Further, as we have seen in Section 4.3.2, the thermodynamic state of a bulk nematic is independent of Φ . Therefore, in those cases to which Eq.(4.101b) applies, the states differing only in Φ are thermodynamically equivalent. So, insofar as thermodynamics is concerned, we can treat Eq.(4.101b) as a special case of Eq.(4.101a) in which $\beta=0$.

Note:

In determining the number of the orientational degrees of freedom for a bounded system, the Frank theory has played a decisive role. Indeed, the resultant number of "two" is just the half of the number of the degrees of freedom of a bulk nematic. This in turn shows that two out of the four orientational degrees of freedom of a bulk nematic should give way to an interface, when the nematic is put into contact with another phase. This does not, however, mean that the property of a nematic interface can be fully characterized by a couple of parameters. Rather, it simply refers to the effect of an interface on the bulk orientation of the nematic director. Macroscopic description of an interface makes sense only when it is properly supplemented by that of the bulk phase, as illustrated in the following example: If we base our argument on an elasticity theory which incorporates the up to, say m-th ($m>1$), order derivatives of the director, we can show in the same way as in the text that the number of the orientational degrees of freedom of a bulk nematic becomes in general $4m (>4)$, and accordingly $2m (>2)$ degrees of freedom of the bulk are to be assigned to an interface!

4.4.2 Definition of the surface excess

Now it is a straightforward task to define the surface excess quantity for a nematic liquid crystal as an extension of the cases of ordinary fluids described in Section 4.1. However, special care must be exercised in the case of a nematic, in that neither the concentration nor the entropy density is in general uniform even in the bulk phase, when it is orientationally deformed (see Section 4.3.2). In stead of Eq.(4.3), therefore, we need here to define the surface excess of an extensive property X in a slightly different form:

$$X^S = X - X_a - X_b, \quad (4.3')$$

where X_a and X_b are, respectively, the hypothetical X 's which the a and b phases would have, when each of the bulk phases were "extrapolated" up to the dividing surface. This is evidently a generalization of the original definition, because, if the bulk phases are uniform, X_a and X_b may be given respectively by $V_a x_a$ and $V_b x_b$, thereby reducing Eq.(4.3') to Eq.(4.3). The extrapolation should be done in such a way as to conserve the state of the bulk phase, specified by the independent thermodynamic variables, say T , μ_j , H , and β . At present, this procedure simply corresponds to the analytical continuation of the bulk director profile, following the Euler-Lagrange equation.

By using Eq.(4.85) in combination with Eqs.(4.94) and (4.95), we obtain

$$\begin{aligned} d\Omega = & - SdT - N_j d\mu_j + \omega(P_a R_a dR_a - P_b R_b dR_b) + \eta d\omega \\ & + \omega[\ln(R_2/R_a)]dH + 2\omega H d[\ln(R_2/R_a)] \quad (4.102) \\ & - \omega \int_{R_a}^{R_2} \left(\frac{\partial f_o}{\partial T} dT + \frac{\partial f_o}{\partial \mu_j} d\mu_j \right) r dr - \omega R_2 \left. \frac{\partial f_o}{\partial (dn_i/dr)} \right|_{R_2} dn_i(R_2). \end{aligned}$$

In this expression of the thermodynamic potential, R_2 is still an arbitrary parameter. Hence, the right-hand side of Eq.(4.102) must be, as a whole, independent of R_2 . This property can be readily confirmed by expressing $dn_i(R_2)$ in terms of dH , $d\beta$, etc. In view of Eq.(4.101), we can generally write

$$dn_i(r) = \frac{dn_i}{dr}dr + \frac{\partial n_i}{\partial T}dT + \frac{\partial n_i}{\partial \mu_j}d\mu_j + \frac{\partial n_i}{\partial H}dH + \frac{\partial n_i}{\partial \beta}d\beta. \quad (4.103)$$

In conformity with the previous notation, we shall continue to use dn_i/dr in the sense of $(\partial n_i / \partial r)_{T, \mu_j, H, \beta}$, as long as there is no fear of confusion. Substituting the above into the last term of Eq.(4.102), there arise five terms, the first of which, involving dR_2 , is obviously $-\omega H d[\ln R_2^2]$. Next let us consider the term containing dH . Based on the Euler-Lagrange equation for n_i , we can readily show that

$$r \frac{d}{dr} \left[r \frac{\partial f_0}{\partial (dn_i/dr)} \frac{\partial n_i}{\partial H} \right] = r^2 \frac{\partial f_0}{\partial H} = 1.$$

Thus, by integrating with respect to r , we obtain

$$-\omega R_2 \frac{\partial f_0}{\partial (dn_i/dr)} \frac{\partial n_i}{\partial H} \Big|_{R_2} dH = -\omega [\ln(R_2/R_c)]dH, \quad (4.104)$$

where R_c is the constant of integration which is itself a function of T , μ_j , H , and β . As we shall see later, the orientational property of a nematic interface is wholly cast into the function R_c .

To proceed further, let us consider a special surface located, say, at R_{ex} , across which no orientational work is performed as the nematic is distorted at fixed T , μ_j , and β . Though it is not always the case, it may be illustrative to mention that the above condition is always fulfilled, if the

director is "rigidly" pinned on the surface at R_{ex} . So, in the same spirit as de Gennes [15] introduced the concept of the extrapolation length, it seems natural to entitle R_{ex} the "point of extrapolation" and the surface at R_{ex} the "surface of extrapolation." As shown in Eq.(4.95), the orientational work done through the surface at R_{ex} when H is changed by dH is given by

$$0 = \delta W_o = - \omega R_{ex} \left. \frac{\partial f_o}{\partial (dn_i/dr)} \right|_{R_{ex}} \frac{dn_i(R_{ex})}{dH} dH.$$

As R_{ex} is a function of H , the above equation can be rewritten as

$$0 = - \omega R_{ex} \left. \frac{\partial f_o}{\partial (dn_i/dr)} \right|_{R_{ex}} \left(\frac{\partial n_i}{\partial r} \frac{\partial R_{ex}}{\partial H} + \frac{\partial n_i}{\partial H} \right),$$

which is, on account of Eq.(4.104), further simplified to give

$$2 \frac{\partial \ln R_{ex}}{\partial \ln H} = - \ln(R_{ex}/R_c). \quad (4.105)$$

Therefore, once R_{ex} is given as a function of T , μ_j , H , and β , we can find R_c via Eq.(4.105), and vice versa. Using Eq.(4.105), we can rewrite Eq.(4.104) as

$$- \omega R_2 \left. \frac{\partial f_o}{\partial (dn_i/dr)} \frac{\partial n_i}{\partial H} \right|_{R_2} dH = \omega [\ln(R_{ex}/R_2) + 2 \frac{\partial \ln R_{ex}}{\partial \ln H}] dH. \quad (4.106)$$

Next, the term involving $d\beta$ is immediately obtained in a similar manner as we have done for Eq.(4.104):

$$- \omega R_2 \left. \frac{\partial f_o}{\partial (dn_i/dr)} \frac{\partial n_i}{\partial \beta} \right|_{R_2} d\beta = - \omega G(T, \mu_j, H, \beta) d\beta, \quad (4.107)$$

where $G(T, \mu_j, H, \beta)$ is a function independent of R_2 . Finally, the

terms with dT and $d\mu_j$ are evaluated directly from Eq.(4.83) to give

$$- \omega R_2 \frac{\partial f_0}{\partial (dn_i/dr)} \frac{\partial n_i}{\partial T} \Big|_{R_2} dT = \omega \int_{R_{ex}}^{R_2} \left(\frac{\partial f_0}{\partial T} dT \right) r dr - \omega R_2 \frac{\partial f_0}{\partial (dn_i/dr)} \frac{\partial n_i}{\partial T} \Big|_{R_{ex}} dT, \quad (4.108)$$

and the equation in which T is replaced by μ_j in the above. Then, the use of Eqs.(4.104)-(4.108) in Eq.(4.102) yields

$$\begin{aligned} d\Omega = & - [S + \omega \int_{R_a}^{R_{ex}} \left(\frac{\partial f_0}{\partial T} \right) r dr + \omega R_{ex} \frac{\partial f_0}{\partial (dn_i/dr)} \frac{\partial n_i}{\partial T} \Big|_{R_{ex}}] dT \\ & - [N_j + \omega \int_{R_a}^{R_{ex}} \left(\frac{\partial f_0}{\partial \mu_j} \right) r dr + \omega R_{ex} \frac{\partial f_0}{\partial (dn_i/dt)} \frac{\partial n_i}{\partial \mu_j} \Big|_{R_{ex}}] d\mu_j \\ & + \omega (P_a R_a dR_a - P_b R_b dR_b) + \eta d\omega - 2\omega Hd[\ln R_a] \\ & + \omega [\ln(R_{ex}/R_a) + 2 \frac{\partial \ln R_{ex}}{\partial \ln H}] dH - \omega G(T, \mu_j, H, \beta) d\beta. \end{aligned} \quad (4.109)$$

As required, Eq.(4.109) is independent of R_2 , and serves as the fundamental equation for the thermodynamic description of a bounded nematic, which plays the same role as that Eq.(4.4) does for ordinary fluids.

Now we can follow much the same procedure as that we taken from Eq.(4.4) through Eq.(4.14) to define various surface excess quantities for the nematic interface. As H and β are both intensive variables, an integration of Eq.(4.107) with respect to ω at constant T , μ_j , R_a , R_b , H , and β leads to

$$\Omega = \eta \omega, \quad (4.110)$$

which is the same as Eqs.(4.5) and (4.10). Let us now take the

dividing surface at R , and rewrite Eq.(4.109) in terms of $V_a = \omega(R^2 - R_a^2)/2$, $V_b = \omega(R_b^2 - R^2)/2$, and $A = \omega R$, to obtain an equation corresponding to Eq.(4.6) for ordinary fluid systems:

$$\begin{aligned}
d\Omega = & - [S + \omega \int_{R_a}^{R_{ex}} \left(\frac{\partial f_o}{\partial T} \right) r dr + \omega R_{ex} \left. \frac{\partial f_o}{\partial (dn_i/dr)} \frac{\partial n_i}{\partial T} \right|_{R_{ex}}] dT \\
& - [N_j + \omega \int_{R_a}^{R_{ex}} \left(\frac{\partial f_o}{\partial \mu_j} \right) r dr + \omega R_{ex} \left. \frac{\partial f_o}{\partial (dn_i/dr)} \frac{\partial n_i}{\partial \mu_j} \right|_{R_{ex}}] d\mu_j \\
& - PdV_a - P_b dV_b + d(H[\ln(R/R_a)]\omega) + \gamma dA + A \zeta dR \\
& + AR^{-1}[\ln(R_{ex}/R) + 2 \frac{\partial \ln R_{ex}}{\partial \ln H}] dH - AR^{-1}G(T, \mu_j, H, \beta) d\beta,
\end{aligned} \tag{4.111}$$

where use has been made of $P_a = P + HR_a^{-2}$, with P being the pressure in the nematic reservoir. The interfacial tension γ is defined ordinarily by

$$\begin{aligned}
\gamma & = [\Omega - \Omega_a - \Omega_b]/A \\
& = (\eta\omega + PV_a - H[\ln(R/R_a)]\omega + P_b V_b)/A,
\end{aligned} \tag{4.112}$$

and ζ by

$$\zeta = (P - P_b) - \gamma/R - H/R^2 = \partial\gamma/\partial R. \tag{4.113}$$

Then, by substituting Eq.(4.112) into Eq.(4.111) and making use of the Gibbs-Duhem equation for bulk phases, we obtain

$$\begin{aligned}
d\gamma = & - [S^s + R^{-1} \int_R^{R_{ex}} \frac{\partial f_o}{\partial T} r dr + \frac{R_{ex}}{R} \left. \frac{\partial f_o}{\partial (dn_i/dr)} \frac{\partial n_i}{\partial T} \right|_{R_{ex}}] dT \\
& - [\Gamma_j + R^{-1} \int_R^{R_{ex}} \frac{\partial f_o}{\partial \mu_j} r dr + \frac{R_{ex}}{R} \left. \frac{\partial f_o}{\partial (dn_i/dr)} \frac{\partial n_i}{\partial \mu_j} \right|_{R_{ex}}] d\mu_j \\
& + (P - P_b - \gamma R^{-1} - HR^{-2}) dR + R^{-1}[\ln(R_{ex}/R) + 2 \frac{\partial \ln R_{ex}}{\partial \ln H}] dH \\
& - R^{-1}G(T, \mu_j, H, \beta) d\beta,
\end{aligned} \tag{4.114}$$

where S^s and Γ_j are, respectively, the surface entropy and the adsorption of the j -th species per unit area of the dividing surface taken at R . As it stands, this is the extension of the Gibbs equation to interfaces of nematic liquid crystals, and gives the basis for their thermodynamic treatment. Besides the ordinary terms found in the original Gibbs equation [i.e., Eq.(4.14)], we see several additional contributions coming from the orientational anisotropy of the nematic. In what follows, we will study the effects of these factors in detail.

4.4.3 Hard wall-nematic interface

Before going into the detailed discussion of the various aspects of the generalized Gibbs equation, we would like to here derive the Gibbs equation when the nematic is interfaced against a planar hard wall (see Fig.4.11). Here, we mean by "hard wall" an athermal substrate which serves merely as a constant boundary field acting on the nematic [25]. Studying this idealized case is of much realistic importance, however, since it can be expected to well approximate the behavior of the nematic in a real solid substrate-nematic system, which is in extensive use for alignment control of nematic samples. Because the planar

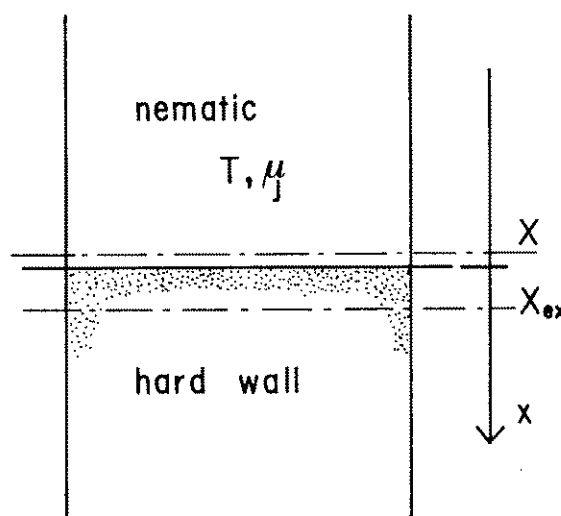


FIG.4.11. Planar interface between a hard wall and a deformed nematic. The origin of the x-axis is fixed with respect to the hard wall.

geometry of the interface is presently an auxiliary condition which must be satisfied regardless of the state of the nematic phase, we are to find some characteristic differences in its thermodynamics, as shown in later sections, in comparison with the case of a fluid-nematic interface which is assuming a near-planar geometry under an infinitesimally small orientational deformation.

The Gibbs equation for the hard wall-nematic interface can be at present most easily obtained by formally taking the planar limit of Eq.(4.114), while neglecting the contribution from the substrate phase. In order to actually perform this procedure, we have to recall the fact that, as $R \rightarrow \infty$, the variable H is to in general diverge, because, from its definition, we have

$$H = R^2 f_o(\mathbf{n}, d\mathbf{n}/dR).$$

Then, upon taking the interface normal pointing toward the wall as the x -axis as shown in Fig.4.11, we get

$$\lim_{R \rightarrow \infty} H/R^2 = \lim_{R \rightarrow \infty} f_o(\mathbf{n}, d\mathbf{n}/dR) = f_d(\mathbf{n}, d\mathbf{n}/dx), \quad (4.115)$$

where f_d denotes the unapproximated Frank strain energy density [see Eq.(4.43)]. Furthermore, since

$$df_d/dx = \lim_{R \rightarrow \infty} d(H/R^2)/dR = \lim_{R \rightarrow \infty} [-2f_o/R] = 0,$$

f_d converges to a constant independent of x as the interface gets planar; hence, f_d can be used as a thermodynamic variable in place of H . The variable β , on the other hand, is obviously unaffected by this limiting procedure. Consequently, in view of Eq.(4.107), we can define a new function G_p in such a way that

$$G_p(T, \mu_j, f_d, \beta) = \lim_{R \rightarrow \infty} R^{-1} G(T, \mu_j, H, \beta). \quad (4.116)$$

We shall here denote the positions of the dividing surface and that of the surface of extrapolation as X and X_{ex} ,

respectively. Using Eq.(4.116) and replacing dR and dR_{ex} by dX and dX_{ex} in Eq.(4.114) while making R and R_{ex} go to infinity and neglecting the contribution from the substrate phase, we obtain

$$\begin{aligned}
 d\gamma^* = & - [S^{S+} \int_X^{X_{ex}} \left(\frac{\partial f_d}{\partial T} \right) dx + \frac{\partial f_d}{\partial (dn_i/dx)} \frac{\partial n_i}{\partial T} \Big|_{X_{ex}}] dT \\
 & - [\Gamma_j + \int_X^{X_{ex}} \left(\frac{\partial f_d}{\partial \mu_j} \right) dx + \frac{\partial f_d}{\partial (dn_i/dx)} \frac{\partial n_i}{\partial \mu_j} \Big|_{X_{ex}}] d\mu_j \\
 & - (-P+f_d)dX + (X_{ex} - X + 2f_d \frac{\partial X_{ex}}{\partial f_d}) df_d - G_p(T, \mu_j, f_d, \beta) d\beta,
 \end{aligned} \tag{4.117}$$

where the tension of the hard wall-nematic interface has been denoted as γ^* . It is not difficult to confirm that this equation is identical with that we obtain by starting directly from Eq.(4.94).

Finally, a word of comment is in order as to the relationship between the hard wall-nematic interface with which we have concerned ourselves here and a real solid-nematic interface. It is crucial at present to notice that most of the solid substances (like glass) which are in use as a substrate of nematic samples are in effect perfectly rigid when compared with the curvature elasticity of the nematic liquid; so that, we can, to a good approximation, neglect a change of the thermodynamic state of the solid itself which would occur in response to the variation of the orientational state of the nematic. It must furthermore be pointed out here that the aligning surface layers such as polymeric films etc. may be treated simply as an adsorbed layer from a thermodynamic point of view.

Based on the assumption of infinitely rigid solid, we can generally divide the thermodynamic potential Ω_t of the whole system including both solid and nematic phases as [25],

$$\Omega_t = \Omega_{sol} + \Omega^*, \quad (4.118)$$

where Ω_{sol} is the thermodynamic potential of the solid when it exists alone in vacuum; we assume here the solid has a vanishing vapor pressure and is also immiscible to the nematic phase. And, as clear from the above, Ω^* takes care of the remainder of Ω_t after the individual contribution of the solid is subtracted. According to the statistical mechanics of the rigid solid-fluid interface (see Chapter 5), it is shown that Ω^* can be identified with the thermodynamic potential of the nematic phase which is in equilibrium under the external field produced by the solid phase. Consequently, we have to relate the interface tension γ in Eq.(4.117) with Ω^* as follows:

$$\Omega^* = \Omega_a + A\gamma, \quad (4.119)$$

where Ω_a is, same as that in Eq.(4.112), the thermodynamic potential of the hypothetical bulk nematic when the dividing surface is taken at X. The interfacial tension defined this way is usually referred to as the "boundary tension" [26-28]; hence, in order to discriminate it from the interfacial tension in the usual sense, we denote the boundary tension as γ^* . Comparing Eqs.(4.119) and (4.118) with Eq.(4.112), we can write

$$\gamma^* = \gamma - (\Omega_{sol} - \Omega_b)/A. \quad (4.120)$$

Then, γ^* and γ coincide with each other, only when the dividing surface is taken in such a way that $\Omega_b = \Omega_{sol}$.

4.5 The surface of tension and the surface of extrapolation

As we have seen in Section 4.1.4, the surface of tension can be regarded as a specially chosen dividing surface for which the thermodynamic and the mechanical concepts of interfacial tension become compatible. In this section, we shall investigate how the physical meaning of the surface of tension may be modified in the case of a nematic interface and how it is related to the orientational property of the interface.

4.5.1 Some elementary properties of the surface of tension

When the (mechanical) interfacial tension is given by γ_s , while the elastic strain energy density stored in the nematic is (to lowest order) f_0 at the point of the interface, it has been shown in Section 4.2 that the radius of curvature of the (cylindrical) interface R_s can be written as

$$R_s = \gamma_s / f_0, \quad (4.53')$$

provided the (undeformed) nematic reservoir and the fluid in contact with the deformable nematic are held at a common hydrostatic pressure P .

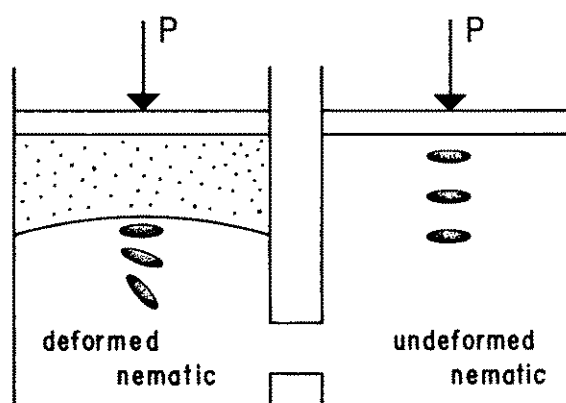


FIG.4.12. Equilibrium shape of a deformed nematic-fluid interface. The interface is planar in the absence of deformation, but as it is orientationally deformed under a fixed external pressure, the interface tends to curve to seek a mechanical equilibrium.

Noting the relation $H = R_s^2 f_0$, we can now rewrite Eq.(4.53') to give

$$R_s = H/\gamma_s. \quad (4.121)$$

Equations (4.53) and (4.53') have been derived via a mechanical argument, hence they are meaningful only when the surface of tension is taken at the dividing surface. It must be noticed in particular that Eq.(4.121) indicates that H should diverge to infinity as the interface tends to be planar ($R_s \rightarrow \infty$), in contrast to the fact that f_0 goes to zero. This might at a glance appear unphysical, in that H is proportional to the deformation energy density and that the interface be planar when the nematic is undeformed. Here, however, we must recall that, only when observed at a fixed point relative to the cylindrical coordinate, H can be proportional to the deformation energy; and in Eq.(4.121), indeed, H should be measured just at the position of the interface which moves outward as the elastic deformation near the interface weakens. So, the fact that $H \rightarrow \infty$ as $f_0 \rightarrow 0$ is nothing but an indication that the radius of the interface R_s increases overwhelmingly in comparison with the decrease in f_0 .

The thermodynamic interfacial tension γ with respect to an arbitrary dividing surface at R is generally defined by Eq.(4.112). Then, by combining Eqs.(4.112) and (4.121), while setting $P_b = P$ as required here, we can now express γ in terms of γ_s , R_s , and R :

$$\gamma = \gamma_s \frac{R_s}{R} [1 + \ln(R_s/R)],$$

which is an equation corresponding to Eq.(4.34) derived for ordinary fluids. In particular, if $|(R_s - R)/R_s| \ll 1$, i.e., the dividing surface is sufficiently near the surface of tension, then we can expand the logarithm to obtain

$$\gamma = \gamma_s \frac{R_s^2}{R^2} \quad (4.122)$$

This result shows that at constant T , μ_j , H , and β , the tension of a nematic interface does not exhibit an extremum as a function of R , as the interfacial tension of ordinary fluids does. This is a manifestation of the fact that at constant H and β , orientational as well as translational work must be performed across the dividing surface so as to shift its location. As obvious from the physical meaning of the surface of tension, it only takes care of the equilibrium with respect to normal stress at the interface.

Indeed, by regarding the "director at the dividing surface" as an independent thermodynamic variable in place of H and β [see Section 4.4.1], it is easy to show, on account of the definition of the interfacial tension, that Eq.(4.114) should be written as

$$d\gamma = -S^s dT - \Gamma_j d\mu_j - (\gamma R^{-1} - HR^{-2})dR - \left. \frac{\partial f_0}{\partial (dn_i/dr)} \right|_R dn_i(R). \quad (4.123)$$

This expression shows clearly that, for fixed T , μ_j , and $n(R)$, the interfacial tension takes a minimum value at $R=R_s$, in much the same manner as in ordinary fluids.

In the generalized Gibbs equation, there have appeared a couple of surface orientational functions, R_{ex} and $G(T, \mu_j, H, \beta)$, the former of which gives the position of the surface of extrapolation. Thermodynamically, the latter can be shown to be connected with the surface of tension as:

$$G(T, \mu_j, H, \beta) = -H \frac{\partial \ln R_s}{\partial \beta}, \quad (4.124)$$

which immediately follows from the generalized Gibbs equation by substituting Eq.(4.121) at fixed T , μ_j , and H with the surface of

tension adopted as the dividing surface. This may be enough to reveal the important role played by the surface of tension as to the orientational properties of nematic interfaces.

4.5.2 Curvature dependence of the interfacial tension

In order to determine γ_s as a function of H , let us consider Eq.(4.114) at constant T , μ_j , and β (with $P_b=P$):

$$d\gamma = - (\gamma + R^{-1}H)R^{-1}dR + R^{-1}[\ln(R_{ex}/R) + 2 \frac{\partial \ln R_{ex}}{\partial \ln H}]dH. \quad (4.125)$$

Substituting $\gamma_s (=H/R_s)$ and R_s for γ and R in the above, we find

$$\frac{\partial \ln \gamma_s}{\partial \ln H} = \ln(R_{ex}/R_s) + 2 \frac{\partial \ln(R_{ex}/R_s)}{\partial \ln H}. \quad (4.126)$$

Thus, it is seen that when the surface of tension and the surface of extrapolation coincide with each other (i.e. $R_s=R_{ex}$), γ_s should always be a constant independent of H and β :

$$\gamma_s(T, \mu_j, H, \beta) = \gamma_o(T, \mu_j),$$

where γ_o denotes, as before, the interfacial tension when the interface is planar (in the absence of orientational deformations).

When $R_s \neq R_{ex}$, however, γ_s is no longer in general a constant and is to change as the curvature of the interface increases in response to the orientational deformations in the nematic. To look more into this point, we rewrite Eq.(4.126) as

$$\frac{\partial \ln \gamma_s}{\partial H} = \frac{2}{H^{1/2}} \frac{\partial}{\partial H} [H^{1/2} \ln(R_{ex}/R_s)]. \quad (4.126')$$

Because γ_s converges to γ_o as $H \rightarrow \infty$, the right-hand side of the above equation has to be integrable over $0 < H \leq \infty$. Hence, we see that, at large H , the right-hand side must decrease at least

faster than H^{-1} . This fact then assures that

$$\ln(R_{\text{ex}}/R_s) \rightarrow 0, \quad \text{as } H \rightarrow \infty. \quad (4.127)$$

So that,

$$\lim_{H \rightarrow \infty} R_{\text{ex}}/R_s = 1, \quad (4.128)$$

Based on Eq.(4.121), we have

$$R_{\text{ex}} \sim H/\gamma_0, \quad \text{at large } H. \quad (4.129)$$

Then, by-part integration of Eq.(4.126') yields

$$\gamma_s = \gamma_0 \frac{R_{\text{ex}}^2}{R_s^2} \exp\left[\int_{\infty} \ln(R_{\text{ex}}/R_s) d(\ln H)\right]. \quad (4.130)$$

When the deformation is weak, in particular, Eq.(4.130) can be approximated as

$$\gamma_s = \gamma_0 \frac{R_{\text{ex}}^2}{R_s^2} \exp\left[-\int_0 (R_{\text{ex}} - R_s)/\gamma_0 df_0\right], \quad (4.131)$$

where we have used $H \sim \gamma_0^2/f_0$ as obtained from Eqs.(4.53') and (4.121), and expanded $\ln(R_{\text{ex}}/R_s)$ as $(R_{\text{ex}} - R_s)/R_s$ on account of Eq.(4.128). Finally, in combination with Eq.(4.123), we obtain

$$\gamma = \gamma_0 \frac{R_{\text{ex}}^2}{R^2} \exp\left[-\int_0 (R_{\text{ex}} - R_s)/\gamma_0 df_0\right]. \quad (4.132)$$

A. Normal behavior: $\lim_{f_0 \rightarrow 0} (R_{\text{ex}} - R_s) < \infty$

Equations (4.128) and (4.129) do not necessarily imply that the separation between R_s and R_{ex} should always remain finite as the orientational deformation disappear; but, they only demand that $(R_{\text{ex}} - R_s)^{-1} = o(f_0)$. However, as we will see in the next section, it is possible to show that $R_{\text{ex}} - R_s$ is just the orientational extrapolation length, hence if $(R_{\text{ex}} - R_s) \rightarrow \infty$ according as $f_0 \rightarrow 0$, it must be concluded in the Rapini-Papoular's

sense that the anchoring strength at the interface is infinitely weak. Based on this observation, we shall call it a "normal behavior," if $R_{ex} - R_s$ converges to a finite value, and if not, a "singular behavior."

Although Eqs.(4.131) and (4.132) are valid for both normal and singular behaviors alike, they can be reduced to a particularly simple form in the case of a normal behavior, which is readily comparable with the results for ordinary fluid interfaces. As in the case of ordinary fluids, let us now write

$$\delta_{\infty} = \lim_{R \rightarrow \infty} (R_{ex} - R_s). \quad (4.133)$$

Then, in view of $R_s \sim \gamma_o/f_o$ which is valid for small f_o 's, we can transform Eq.(4.131), up to first order in f_o , as

or
$$\gamma_s \sim \gamma_o(1 + \delta_{\infty}/R_s), \quad (4.134a)$$

$$\gamma_s \sim \gamma_o(1 + f_o \delta_{\infty}/\gamma_o). \quad (4.134b)$$

Note that, apart from the sign of the exponent, Eq.(4.134b) has an identical form with that derived for an ordinary fluid interface [see Eqs.(4.35) and (4.39)]. This equation indicates that γ_s remains virtually constant as long as R_s is large in comparison with δ_{∞} . As will be shown later, δ_{∞} gives a measure of the orientational anchoring strength at the interface: the larger δ_{∞} becomes, the weaker the anchoring. Thus, Eq.(4.134b) additionally shows that the interfacial tension at a nematic interface is more likely to be affected by the orientational deformation when the anchoring gets weaker and/or the interfacial tension smaller.

The value of the interfacial tension when the dividing surface is taken at R_{ex} can be approximately evaluated from Eq.(4.132):

$$\gamma_{ex} \sim \gamma_0 \exp(-\delta_{\infty}/R_g). \quad (4.135)$$

The surface of extrapolation has been defined as a hypothetical surface through which the orientational work done by the environment would vanish when the nematic were extrapolated to it. Since a finite orientational work through a dividing surface implies a change of the interfacial tension, we can redefine the surface of extrapolation as a dividing surface with which the orientational work does not contribute to the change of the interfacial tension. On the other hand, the surface of tension designates, as clear from its definition, a special dividing surface where the work associated with the Ericksen stress does not alter the value of the interfacial tension. As a result, if both of these surfaces are identical, neither director rotation nor Ericksen stress are to change the interfacial tension, so that it remains constant even when the nematic is orientationally deformed to a varying degree. We have already noticed this point in connection with Eq.(4.125).

It is generally impossible, however, to simultaneously eliminate both of the contributions from director rotation and from the Ericksen stress only by appropriately choosing the dividing surface. Indeed, with the dividing surface taken at R_g , the director rotation will change the interfacial tension, and at R_{ex} , the Ericksen stress will do the same thing. Equa-

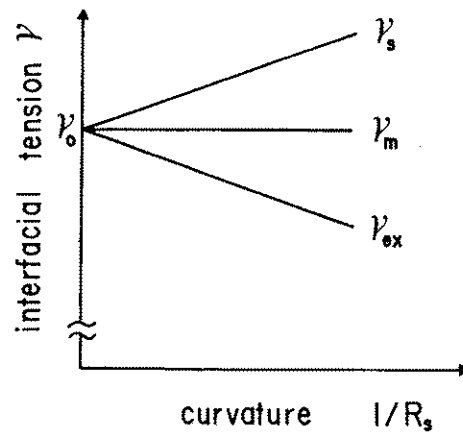


FIG.4.13. Variations of interfacial tension with the increase in the interface curvature.

tions (4.134a) and (4.135) show that they are, roughly speaking, same in magnitude while opposite in sign as shown in Fig.4.13. At the present level of approximation, the interfacial tension is linearly dependent on the position of the dividing surface, hence we can conclude that by taking the dividing surface at

$$R_m = (R_s + R_{ex})/2, \quad (4.136)$$

the interfacial tension is given by the geometrical mean of those at R_s and at R_{ex} , which is fixed at γ_0 up to first order in f_0 as a result of cancellation between the rotational and the translational works across this dividing surface.

4.5.3 Thermodynamic potential

In order to further appreciate the physical significance of the surface of tension and the surface of extrapolation, it is also instructive to see how the thermodynamic potential itself changes under weak orientational deformations. As the thermodynamic potential is independent of the choice of the dividing surface, we may locate it at R_s . By using Eqs.(4.112) and (4.134b) along with the assumption of normal behavior, we get

$$\Omega = -PV + A_s[(R_{ex} - R_a)f_0] + A_s\gamma_0, \quad (4.137)$$

in which $A_s = \omega R_s$ designates the area of the dividing surface. Since the total deformation energy F_d stored in the hypothetical bulk region between R_{ex} and R_a with the area A can be written as

$$F_d \sim A(R_{ex} - R_a)f_0,$$

as long as the deformation is weak, Eq.(4.137) shows that the contribution from the orientational deformation can be treated as if the nematic were extended up to R_{ex} with its bulk properties completely retained. In this respect, the term, "surface of extrapolation," appears to be a reasonable nomenclature.

Concerning Eq.(4.137), however, it must be remembered that the area of the interface A refers to the surface of tension. If the area is measured at a different point, thereby resulting in a numerically different value, it becomes no longer possible to make such a simple interpretation of the orientational part of the thermodynamic potential as denoting the deformation energy for a hypothetical volume of the nematic.

As mentioned above, the change of an interfacial tension is in general comprised of translational and orientational parts, and for example, the former disappears when the dividing surface is taken at R_g . Thus, $\delta\Omega = \Omega + PV - A\gamma_0$ turns out to be solely orienta-

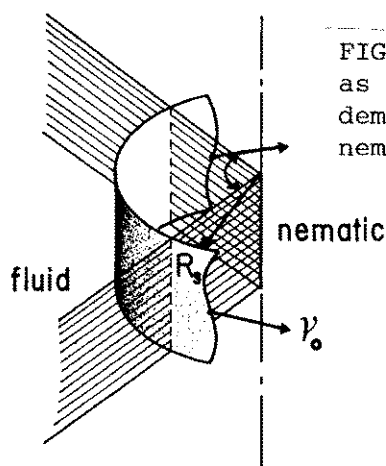


FIG.4.14. Surface of tension as an effective interface demarcating deformed "bulk" nematic from bulk fluid.

tional, if A is taken at the surface of tension. By virtue of this property, the particular expression of the thermodynamic potential as given by Eq.(4.137) is consistent with a naive picture of the system as shown in Fig.4.14, which can be regarded as an extension of the Rapini-Papoular model [29] to a curved interface; namely, the nematic and the isotropic fluid are separated by an infinitely thin membrane which is sustaining a tension γ_0 , and both phases in contact are completely bulklike right up to the membrane, except that the nematic director is subjected to some local boundary condition at the membrane. Insofar as we are concerned with the orientational property of the interface, this suggests that it is most natural to regard the surface of tension as a virtual position of the nematic-fluid interface.

4.5.4 The surface of extrapolation at a hard wall-nematic interface

Before closing this section, we shall list some properties of the surface of extrapolation at a hard wall-nematic interface so as to facilitate comparison with and further elaboration of the relevant formulas for the nematic-fluid interface.

Integrating Eq.(4.117) with respect to f_d at fixed T , μ_j , β , and X , we readily find

$$\gamma^* = \gamma_o^* + \int_0^{f_d} (X_{ex} - X + 2f_d \frac{\partial X_{ex}}{\partial f_d}) df_d. \quad (4.138)$$

In the case of a rigid solid-nematic interface, we can replace γ^* by the interfacial tension γ to give

$$\gamma = \gamma_o + \int_0^{f_d} (X_{ex} - X + 2f_d \frac{\partial X_{ex}}{\partial f_d}) df_d. \quad (4.139)$$

Especially, in case X_{ex} remains finite at $f_d=0$ (normal behavior), we can obtain to first order in f_d the following equations:

$$\gamma = \gamma_o + (X_{ex} - X)f_d \quad (4.140)$$

and hence

$$\Omega = -PV + A[(X_{ex} - X_a)f_d] + A\gamma_o. \quad (4.141)$$

Note that Eqs.(4.140) and (4.141) have, respectively, an identical form with Eqs.(4.134b) and (4.137), provided the position of the dividing surface X is understood to be referring to the surface of tension; the arbitrariness in the choice of X appearing in the above equations is a consequence of the fact that, when the interface is planar, the concept of the surface of tension loses its meaning whatever the nature of the interface. Conversely, it may also be argued that they show that the thermodynamics of a curved nematic interface can be treated as if

it were planar, in a very limited sense though, when the dividing surface is taken at the surface of tension.

4.6 Geometrical properties of the point of extrapolation and the Connection with the Rapini-Papoular formalism

In this section, we shall focus our attention on investigating the relation between the surface-thermodynamic orientational parameters, R_{ex} and $G(T, \mu_j, H, \beta)$, introduced in the former section, and the conventional phenomenological parameters appearing in the Rapini-Papoular formalism [29] of the surface-induced alignment. This enables us to apply the present thermodynamic theory to existing experimental results, which have mostly been formulated and analyzed on the basis of the Rapini-Papoular type formalism. Although the present consideration is mainly concerned with the case of a nematic-fluid curved interface, the argument applies to the solid-nematic case without change, when the planar limit is formally carried out.

4.6.1 Equilibrium director profile as a function of R_{ex} and G

A. General formulas

According to Eq.(4.71b), the equilibrium director profile is generally written in the form

$$\mathbf{n} = T(\phi_0)\mathbf{n}_s[\zeta, \beta]. \quad (4.71b)$$

where $\zeta = (2H/K_3)^{1/2} \ln(r/r_0)$, and $T(\phi_0)$ represents a rotation matrix acting on the (r, ϕ, z) components of the director:

$$T(\phi_0) = \begin{pmatrix} 1 & 0 & 0 \\ 0 & \cos\phi_0 & -\sin\phi_0 \\ 0 & \sin\phi_0 & \cos\phi_0 \end{pmatrix}. \quad (4.142)$$

Because Eq.(4.71b) involves only two arbitrary constants ϕ_0 and r_0 besides H and β , it should be in principle possible to express them as functions of R_{ex} and G .

Let us denote the director in the absence of deformation as \mathbf{n}_e (the unit vector along the easy axis). So that, as the

deformation weakens near the interface, i.e. $H^{1/2} \ln(r/r_0) \sim f_0^{1/2} (r-r_0) \rightarrow 0$, the director profile has to shrink to the single point \mathbf{n}_e . Here, we will consider only such profiles that converge continuously to \mathbf{n}_e as $f_0 \rightarrow 0$ with a fixed β ; then, we find from Eq.(4.71b)

$$\lim_{\zeta \rightarrow \infty} T(\Phi_0) \mathbf{n}_s[\zeta, \beta] = T[\Phi(0)] \mathbf{n}_s[0, \beta] = \mathbf{n}_e. \quad (4.143)$$

Since the origin of Φ_0 is arbitrary, we can assume without loss of generality that

$$\mathbf{n}_s[0, \beta] = \mathbf{n}_e. \quad (4.144)$$

In order that there exists such \mathbf{n}_s that passes through \mathbf{n}_e , it is necessary and sufficient that β be chosen to satisfy the following inequality [cf. Eq.(4.73)]:

$$\beta \leq g(\Theta_e), \quad (4.145)$$

where Θ_e denotes the polar angle of \mathbf{n}_e . This condition is not to deny the existence of equilibrium profiles with $\beta > g(\Theta_e)$; but, as Eq.(4.143) shows, such trajectories must cease to be an equilibrium director profile at a sufficiently small, yet nonzero deformation.

Consequently, the region on the (f_0, β) plane, corresponding to equilibrium director configurations, may be expressed as something like the shaded area depicted in Fig.4.15. Within the region in between $\beta = g(\pi/2)$ and the shaded region, [where Eq.(4.144) does not of

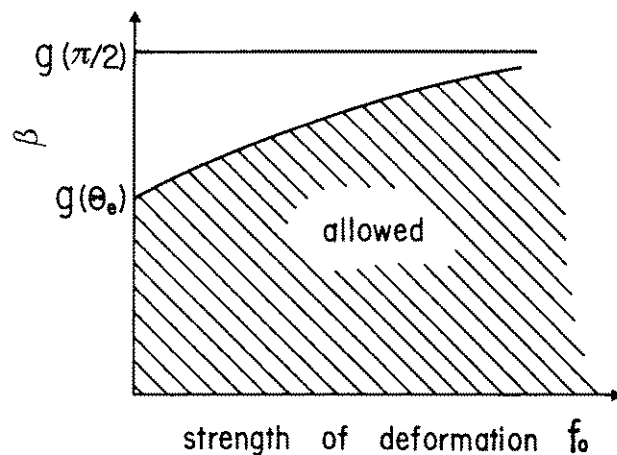


FIG.4.15. Region of f_0 and β corresponding to an allowed state of a bounded nematic.

course hold], we cannot find a set of r_0 and Φ_0 which is compatible with the boundary condition imposed by the nematic interface.

For $\beta \leq g(\Theta_e)$, on which Eq.(4.144) holds, r_0 and Φ_0 can be easily expressed in a closed form as a function of R_{ex} and G . Before substituting Eq.(4.71b) into the definitions of R_{ex} and G , it is helpful to note the following identity. For an arbitrary variable w which is a function of H and β , the value of the partial derivative of \mathbf{n} with respect to w at $r=r_0$ can be written as

$$\left. \frac{\partial \mathbf{n}}{\partial w} \right|_{r_0} = \frac{\partial \Phi_0}{\partial w} \mathbf{A} \mathbf{n} - r_0 \left. \frac{\partial \mathbf{n}}{\partial r} \right|_{r_0} \left[\frac{\partial}{\partial w} \ln r_0 \right], \quad (4.146)$$

where

$$\mathbf{A} = \begin{pmatrix} 0 & 0 & 0 \\ 0 & 0 & -1 \\ 0 & 1 & 0 \end{pmatrix}, \quad \text{and} \quad \mathbf{n} = \begin{pmatrix} n_r \\ n_\phi \\ n_z \end{pmatrix}.$$

Here, use has been made of the fact that $\partial \mathbf{n}_s / \partial \beta = 0$ at $r=r_0$ as coming from the assumption of Eq.(4.144). Using this result in Eqs.(4.106) and (4.107), while in turn substituting H and β for w , we find

$$\pm (2HK_3\beta)^{1/2} \frac{\partial \Phi_0}{\partial H} = -2H^{1/2} \frac{\partial}{\partial H} [H^{1/2} \ln(R_{ex}/r_0)], \quad (4.147)$$

and

$$\pm (2HK_3\beta)^{1/2} \frac{\partial \Phi_0}{\partial \beta} = 2H \frac{\partial}{\partial \beta} (\ln r_0) + G(T, \mu_j, H, \beta). \quad (4.148)$$

where the positive and negative signs on the left-hand side corresponds, respectively, to whether the azimuthal angle Φ increases or decreases with r :

$$\pm (2HK_3\beta)^{1/2} = r \left[n_\phi \frac{\partial f_0}{\partial (dn_z/dr)} - n_z \frac{\partial f_0}{\partial (dn_\phi/dz)} \right]. \quad (4.149)$$

An integration of Eq.(4.147) with the initial condition, $\Phi_0=0$ at $H=\infty$ ($f_0=0$), yields

$$\Phi_0 = \frac{1}{4} (2H/K_3\beta)^{1/2} \ln(R_{ex}/r_0). \quad (4.150)$$

Then, differentiating this expression by β and substituting into Eq.(4.148), we obtain

$$\ln r_0 = \ln R_{ex} - 2\beta \frac{\partial}{\partial \beta} \ln R_{ex} - \beta G/H. \quad (4.151a)$$

Use of the thermodynamic relation for G , Eq.(4.124), in the above leads to

$$\begin{aligned} \ln r_0 &= \ln R_{ex} - \beta \frac{\partial}{\partial \beta} \ln(R_{ex}^2/R_s), \\ &= \ln R_{ex} - 2\beta \frac{\partial}{\partial \beta} \ln(R_{ex}/R_s) + \beta \frac{\partial}{\partial \beta} \ln r_s, \end{aligned}$$

which, upon application of Eq.(4.130), yields

$$\ln r_0 = \ln R_{ex} + \beta \frac{\partial}{\partial \beta} \int_{\infty} \ln(R_{ex}/R_s) d(\ln H). \quad (4.151b)$$

Although Eq.(4.151a) is a purely geometrical expression, Eq.(4.151b) is a geo-thermodynamic formula, which depends not only on the present state of the system but, as it stands, on the process through which the system is brought from the planar geometry. Now, by combining Eqs.(4.150) and (4.151b), we get

$$\Phi_0 = \frac{1}{4} (2H\beta/K_3)^{1/2} \frac{\partial}{\partial \beta} \int_{\infty} \ln(R_{ex}/R_s) d(\ln H). \quad (4.152)$$

B. Geometrical significance of R_{ex} : the point of closest approach

Equation (4.152) show that, under a finite deformation, Φ_0 does not in general vanish; so, it cannot necessarily be possible to find a point on an arbitrary trajectory where the director

coincide with \mathbf{n}_e . There are however some special cases wherein such event does occur: (1) when $\beta=0$, and hence when the deformation is purely polar, (2) when $R_{ex}=R_s$, and (3) when the integral is not dependent on β . The first is obviously a geometrical requirement of any polar deformation satisfying the condition that $\mathbf{n} \rightarrow \mathbf{n}_e$ as $f_o \rightarrow 0$. The second and the third will be later shown to correspond to the cases of an infinitely strong and a direction-independent orientational anchorages, respectively. Anyway, in all of the above listed situations, we have $r_o=R_{ex}$ from Eq.(4.151b) and vice versa, showing that R_{ex} represents the point of "closest approach" to \mathbf{n}_e .

In case there exists a point where $\mathbf{n}=\mathbf{n}_e$ holds, it is intuitively quite obvious that it should occur at R_{ex} , because R_{ex} refers to a hypothetical surface of demarcation across which no orientational work is done as the nematic is deformed.

1. General cases

Let \mathbf{n}_p and \mathbf{n}_a be, respectively, the unit vectors along the meridian and the azimuth circle at \mathbf{n}_e as shown in Fig.4.16.

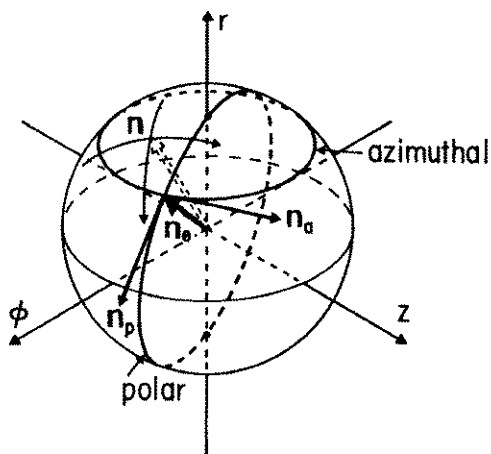


FIG.4.16. Definition of the polar and the azimuthal unit vectors. Under a finite deformation, the equilibrium trajectory does not necessarily pass through the easy axis.

Then, for sufficiently small Φ_0 and $\zeta = (2H/K_3)^{1/2} \ln r/r_0$, $\mathbf{n}(\zeta, \beta)$ may be expanded to give

$$\begin{aligned} \mathbf{n}(\zeta, \beta) &\sim [I + \delta T(\Phi_0)] [\mathbf{n}_e + \zeta \partial \mathbf{n}_s(0, \beta) / \partial \zeta] \\ &= \mathbf{n}_e + \Phi_0 \sin \theta_e \mathbf{n}_a + \zeta \left[\frac{\partial \theta(0)}{\partial \zeta} \mathbf{n}_p + \sin \theta_e \frac{\partial \Phi(0)}{\partial \zeta} \mathbf{n}_a \right], \end{aligned} \quad (4.153)$$

where I denotes the unit tensor. According to Eq.(4.74), this expression is shown to be valid as long as $|r-r_0| \ll \lambda$, with λ being the characteristic length of director deformation.

Further, from Eq.(4.63), we have

$$\begin{aligned} \partial \theta(0) / \partial \zeta &= \pm [1 - \beta / g(\theta_e)]^{1/2} / f(\theta_e)^{1/2}, \\ \partial \Phi(0) / \partial \zeta &= \pm \beta^{1/2} / g(\theta_e). \end{aligned} \quad (4.154)$$

Reflecting the cases in which θ and Φ increase or decrease with ζ , there arise four possible trajectories for each β as shown in Fig.4.16. Putting Eqs.(4.150) and (4.154) into Eq.(4.153), we obtain

$$\begin{aligned} \mathbf{n}(\zeta, \beta) &\sim \\ &\mathbf{n}_e \pm [2H/K_3 f(\theta_e)]^{1/2} \left[1 - \frac{\beta}{g(\theta_e)} \right]^{1/2} \ln(r/r_0) \mathbf{n}_p \\ &\mp (2H/K_3 \beta)^{1/2} \left[\ln(R_{ex}/r_0) - \frac{\beta}{g(\theta_e)} \ln(r/r_0) \right] \sin \theta_e \mathbf{n}_a. \end{aligned} \quad (4.155)$$

The separation between the director on an equilibrium trajectory and \mathbf{n}_e is therefore in general seen to be a quantity of the order of $f_0^{1/2}$, except that

$$r_0 = R_{ex}, \quad \text{or} \quad \beta = g(\theta_e),$$

under which the director satisfies $\mathbf{n}(R_{ex}) = \mathbf{n}_e + o(f_0^{1/2})$. The former is just the condition discussed above in relation to the case wherein $\mathbf{n}(R_{ex}) = \mathbf{n}_e$ is rigorously satisfied. On the other hand, the latter is a condition for specifying a trajectory which

is tangent to the azimuth passing through \mathbf{n}_e , namely the azimuthal deformation. In this case, although the director at R_{ex} does not strictly coincide with \mathbf{n}_e under a finite deformation, Eq.(4.155) shows that it asymptotically approaches the easy axis at a relatively faster rate [$o(f_o^{1/2})$] than at any other point on the trajectory.

To be more quantitative, let us define the element of distance on the unit sphere by

$$ds^2 = f(\Theta)d\Theta^2 + g(\Theta)d\Phi^2, \quad (4.156)$$

which reduces the determination of the equilibrium trajectory between two arbitrary points to the exploration of the trajectory with the shortest path length on the unit sphere [24]. Based on this measure of length, it immediately follows from Eq.(4.155) that the separation between $\mathbf{n}(r)$ on an equilibrium trajectory and \mathbf{n}_e is given by

$$\begin{aligned} \Delta s^2 / (2H/K_3) = & \left[1 - \frac{\beta}{g(\Theta_e)} \right] [\ln(r/r_o)]^2 \\ & + \frac{g(\Theta_e)}{\beta} \left[\ln(R_{ex}/r_o) - \frac{\beta}{g(\Theta_e)} \ln(r/r_o) \right]^2. \end{aligned}$$

Hence, it is now clear that for any β , the trajectory comes closest to \mathbf{n}_e at the point of extrapolation, i.e. $r=R_{ex}$. This is of course valid up to the order of $f_o^{1/2}$.

2. Summary of result

If the special measure of length as defined in Eq.(4.156) is employed, the point of extrapolation acquires a very transparent geometrical significance as the point where the separation between the director and the easy axis becomes minimum. However, only in either of the following three cases,

$$(1) \quad \beta = 0, \quad (2) \quad \beta = g(\Theta_e),$$

$$\text{and (3) } \frac{\partial}{\partial \beta} \int_{\infty} \ln(R_{\text{ex}}/R_s) d(\ln H) = 0, \quad (4.157)$$

the point of closest approach bears a qualitatively different status, asymptotically at least, which allows its interpretation as a position where the director behaves as if it were always pinned along the easy axis regardless of the strength of orientational deformations. [see Fig.4.17].

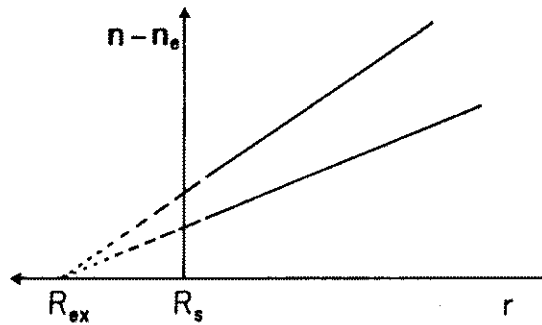


FIG.4.17. Geometrical concept of the point of extrapolation.

4.6.2 Connection with the Rapini-Papoular formalism

A. The model

As a natural and a most general extension of the original Rapini-Papoular model of a planar nematic interface [29], we would postulate that the thermodynamic potential Ω of a volume including a curved nematic interface may be expressed as a functional of the director field $\mathbf{n}(r)$ in the following form:

$$\Omega[\mathbf{n}; \omega, R_a, R_b, R] = -PV + F_d[\mathbf{n}; \omega, R_a, R] + \omega R \gamma_{\text{RP}}(\mathbf{n}_o), \quad (4.158)$$

where F_d represents the Frank elastic energy for a bulklike nematic volume subtending the angle ω in between the boundary at R_a and the nematic interface at R [cf. Eq.(4.55)], and γ_{RP} , which is here regarded as a function of the director at the interface \mathbf{n}_o alone, is the tension of an infinitely thin membrane demarcating the nematic from the substrate fluid. This expression

now involves two unknowns, the position of the interface R and the director field $\mathbf{n}(r)$; they are determined in such a way as to minimize the thermodynamic potential under given boundary conditions. In this type of model, it is of course required that the equilibrium director profile, derived this way, and the resulting thermodynamic potential should correctly reproduce the actual ones in equilibrium. This constraint imposes some restrictions on the model and facilitates a bridge with the equilibrium thermodynamics.

B. The allowed choice of the interface in the Rapini-Papoular model

Subjecting Eq.(4.158) to a virtual change in R , we find

$$0 = \frac{\delta \Omega}{\delta R} = \omega R(\sigma_{rr}^e + P) + \omega \gamma_{RP}, \quad (4.159)$$

where σ_{rr}^e is the rr -component of the Ericksen stress. As mentioned above γ_{RP} must be in equilibrium equal to the thermodynamic interfacial tension relative to the dividing surface at R . So, Eq.(4.159) is just the Laplace equation for a curved nematic interface [see Eqs.(4.40) and (4.42)]. Therefore, (as the Laplace equation is satisfied only at the surface of tension,) in the present form of the Rapini-Papoular model, only the surface of tension can be regarded as the "effective" interface of the nematic:

$$R = R_s. \quad (4.160a)$$

As a consequence, we must also have in equilibrium

$$\gamma_{RP} \Big|_{eq} = \gamma_s. \quad (4.160b)$$

By adopting the director at the surface of tension \mathbf{n}_s as an independent thermodynamic variable in stead of H and β , it follows from Eq.(4.160b) that

$$\gamma_{RP} \Big|_{eq} = \gamma_{RP}(\mathbf{n}_s) = \gamma_s(\mathbf{n}_s). \quad (4.160c)$$

Therefore, γ_{RP} should be uniquely determined when the director at the "interface" is given. As clear from the argument in Section 4.4.1, this is a direct consequence of the use of a linear formalism, the Frank theory, for describing the curvature elasticity of bulk nematics. Hence, in the Rapini-Papoular context, there is no room for γ_{RP} to involve the spatial derivatives of the director as additional independent variables besides \mathbf{n}_o as suggested by Dubois-Violette and Parodi[30], and Mada[31]. This fact also precludes the possibility of treating the "second order elasticity" term, introduced by Nehring and Saupe [32], as a purely surface term to supplement the Frank elastic energy for bulk nematics [23,33,34]. These restrictions have also been pointed out recently by Barbero, et al.[35], and Oldano and Barbero [36,37] based on the consideration of the uniqueness of the equilibrium director profile. Nevertheless, it should be emphasized that the above result is not to deny the role played by such terms, but is only to imply that these contributions, even if exist, should be expressed in one way or another as a function of \mathbf{n}_o for the sake of thermodynamically consistent treatments. This point will also be discussed in Chapter 5 from a statistical mechanical view point.

That Eqs.(4.160a-c) are also compatible with the condition of equilibrium with respect to the director can be readily confirmed as follows. By applying the variational calculus to Eq.(4.158) with regard to $\mathbf{n}(r)$, we obtain the Euler-Lagrange equation for bulk profile, which is formally independent of interfacial properties, and the torque balance equation at the interface which reads

$$-\frac{\partial f_o}{\partial (dn_i/dr)} \Big|_{R_s} = \frac{\partial \gamma_{RP}}{\partial n_{oi}} \Big|_{\mathbf{n}_s} + h n_{si}, \quad (4.161)$$

where h is the Lagrange multiplier to take care of $|\mathbf{n}|=1$. Substituting Eq.(4.160c) into the right-hand side of the above, we find

$$-\left. \frac{\partial f_0}{\partial (dn_i/dr)} \right|_{R_s} = \frac{\partial \gamma_s}{\partial n_{si}} + h n_{si}, \quad (4.162)$$

which is just the equation which follows from the generalized Gibbs equation, when the dividing surface located at R_s [cf. Eq.(4.123)]. Since the bulk profile is clearly invariant as long as the director at the boundary is fixed, this result shows that the Rapini-Papoular model, as envisaged in Eq.(4.158), can be consistent with thermodynamics, if and only if the "interface" appearing in the model is identified with the surface of tension.

C. The anchoring energy and its relationship with the thermodynamic parameters

Let us now focus on the weak deformation regime in order to elucidate the connection of R_{ex} with the anchoring strength as defined in the Rapini-Papoular formalism. As \mathbf{n} now resides more or less near \mathbf{n}_e , we can approximately write

$$\mathbf{n} \sim \mathbf{n}_e + C_p \mathbf{n}_p + C_a \mathbf{n}_a, \quad (4.163)$$

where \mathbf{n}_p and \mathbf{n}_a are the unit vectors defined in Fig.4.16; and, C_p and C_a denote the respective components of \mathbf{n} . According to Rapini and Papoular, we assume that, when the director is sufficiently near the easy axis, the interfacial tension $\gamma_{RP}(\mathbf{n}_0)$ may be written as

$$\gamma_{RP}(\mathbf{n}_0) = \gamma_0 + \frac{1}{2} E_a(p)(C_{0p})^2 + \frac{1}{2} E_a(a)(C_{0a})^2, \quad (4.164)$$

where $E_a(p)$ and $E_a(a)$ are the polar and the azimuthal anchoring energies, respectively.

In equilibrium, the director at the surface of tension can be

approximately obtained with the use of Eqs.(4.151b) and (4.155) to give

$$C_{sp} = \pm [2H/K_3 f(\theta_e)]^{1/2} \left[1 - \frac{\beta}{g(\theta_e)} \right]^{1/2} \times \left[\ln(R_{ex}/R_s) + \beta \frac{\partial}{\partial \beta} \int_{\infty}^{\infty} \ln(R_{ex}/R_s) d(\ln H) \right], \quad (4.165a)$$

$$C_{sa} = \pm (2H\beta/K_3)^{1/2} \sin \theta_e \times \left\{ \left[1 - \frac{\beta}{g(\theta_e)} \right] \frac{\partial}{\partial \beta} \int_{\infty}^{\infty} \ln(R_{ex}/R_s) d(\ln H) - \frac{\ln(R_{ex}/R_s)}{g(\theta_e)} \right\}. \quad (4.165b)$$

For purely polar [$\beta=0$] and azimuthal [$\beta=g(\theta_e)$] deformations, therefore, Eq.(4.164) yields

(i) Polar:

$$\begin{aligned} \gamma_{RP} \Big|_{eq} &= \gamma_o + E_a(p) H [\ln(R_{ex}/R_s)]^2 / K_3 f(\theta_e), \\ &\sim \gamma_o + E_a(p) f_o (R_{ex}-R_s)^2 / K_3 f(\theta_e), \end{aligned} \quad (4.166a)$$

(ii) Azimuthal:

$$\begin{aligned} \gamma_{RP} \Big|_{eq} &= \gamma_o + E_a(a) \sin^2 \theta_e H [\ln(R_s/R_{ex})]^2 / K_3 g(\theta_e), \\ &\sim \gamma_o + E_a(a) \sin^2 \theta_e f_o (R_{ex}-R_s)^2 / K_3 g(\theta_e). \end{aligned} \quad (4.166b)$$

As noted in Eq.(4.160c), γ_{RP} has to be, in equilibrium, equal to γ_s . At small f_o , it is readily shown from Eq.(4.131) that γ_s can be written as

$$\gamma_s = \gamma_o + 2f_o (R_{ex}-R_s) - \int_0^{f_o} (R_{ex}-R_s) df_o. \quad (4.167)$$

Thus, by combining Eqs.(4.166a,b) and Eq.(4.167) while taking the limit of $f_o \rightarrow 0$, we arrive at an expression for the anchoring energies:

(i) Polar:

$$E_a(p)/K_3 f(\theta_e) = \lim_{f_o \rightarrow 0} 1/(R_{ex}-R_s), \quad (4.167a)$$

(ii) Azimuthal:

$$E_a(a) \sin^2 \theta_e / K_3 g(\theta_e) = \lim_{f_0 \rightarrow 0} 1 / (R_{ex} - R_s). \quad (4.167b)$$

As shown in Section 4.6.1, in the case of a single mode anchorage, R_{ex} gives (at least approximately) a point where the director would lie along the easy direction, if the bulk profile were extrapolated. So that, $R_{ex} - R_s$ must be regarded as the extrapolation length in de Gennes' sense. Consequently, the above results are seen to be completely consistent with the ordinary formula relating the extrapolation length to the anchoring energy.

Finally, the physical meaning of the previously made distinction between the "normal" and "singular" behaviors as regards $\lim(R_{ex} - R_s)$ is now clear. In the former case, which is characterized by the fact that $(R_{ex} - R_s)$ converges to a finite value, Eqs.(4.167a,b) show that the orientational anchorage is of finite or infinite strength. In the latter, however, since $(R_{ex} - R_s) \rightarrow \infty$, we see that the anchoring energy should vanish, allowing an almost free rotation of the director at the interface. Except that the symmetry of the system demands, it is obviously a rather uncommon situation.

4.7 Generalized Gibbs equation in the near planar regime and the thermodynamic definition of the anchoring strength

Though it is possible to derive various thermodynamic relations by directly starting from the original form of the generalized Gibbs equation, (which is valid as long as the orientational torque per unit area is much smaller than the interfacial tension), the results are not necessarily convenient to figure out the nature of the nematic interface in an intuitively comprehensible manner. Here, we transform the Gibbs equation into more specialized forms which hold at small interface curvatures, so as to facilitate an easy bridge from the results in the former sections to physically transparent thermodynamic relations. This also enables us to define the anchoring strength in a thermodynamically meaningful manner.

4.7.1 Expansion in terms of the curvature

As the interfacial tension becomes large and/or the elastic deformation weak, the interface tends to assume an almost planar configuration [Fig.4.18].

We shall first derive an equation which is valid for any degree of deformation as long as the curvature of the interface is sufficiently small.

This is technically a recurrence of the case of a hard wall-nematic interface, in which we started the argument with the relation

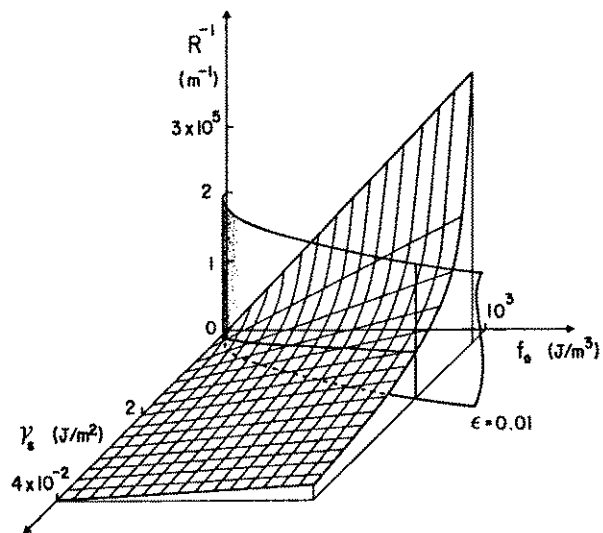


FIG.4.18. Relationship among the interface curvature R^{-1} , the interfacial tension γ_s , and the Frank elastic energy density f_o .

$$H = r^2 f_0.$$

As H is spatially constant, we see from the above that

$$0 = df_0/dr + 2f_0/r,$$

so that we find that f_0 should also be spatially invariant up to first order in the curvature of the interface R^{-1} .

Putting $H=R^2 f_0$ into Eq.(4.114) and retaining only the terms of lowest order in R^{-1} , we obtain

$$\begin{aligned} d\gamma = & - [S^s + \int_R^{R_{ex}} \frac{\partial f_0}{\partial T} dr + \left. \frac{\partial f_0}{\partial (dn_i/dr)} \right|_{R_{ex}} \frac{\partial n_i(R_{ex})}{\partial T}] dT \\ & - [\Gamma_j + \int_R^{R_{ex}} \frac{\partial f_0}{\partial \mu_j} dr + \left. \frac{\partial f_0}{\partial (dn_i/dr)} \right|_{R_{ex}} \frac{\partial n_i(R_{ex})}{\partial \mu_j}] d\mu_j \\ & + 2d[f_0(R_{ex} - R)] + (R_s - R_{ex})df_0 - [G_p(T, \mu_j, f_0, \beta) + 2f_0 \frac{\partial R_{ex}}{\partial \beta}] d\beta. \end{aligned} \quad (4.168)$$

where $n(R_{ex})$ implies that the director at the point of extrapolation should always be taken during differentiation. Furthermore, it follows from Eq.(4.124) that G_p thermodynamically satisfies

$$G_p(T, \mu_j, f_0, \beta) = - f_0 \frac{\partial R_s}{\partial \beta}. \quad (4.169)$$

It must finally be remembered that the higher order correction to the above is of the order of $O[(R_{ex}-R)/R]df_0^{1/2}$.

If we wish to focus on a particular mode of anchorage, we need to regard the variable β as a function of T and μ_j ; for example, in order to exclusively deal with the azimuthal anchorage, we have to set $\beta=g(\Theta_e)$. In this case, Eq.(4.174) can be rewritten in a bit simpler form, which reads

$$\begin{aligned}
d\gamma = & - [S^S + \int_R^{R_{ex}} \frac{\partial f_o}{\partial T} dr + \left. \frac{\partial f_o}{\partial (dn_i/dr)} \right|_{R_{ex}} \frac{\partial n_i(R_{ex}, \beta)}{\partial T}] dT \\
& - [\Gamma_j + \int_R^{R_{ex}} \frac{\partial f_o}{\partial \mu_j} dr + \left. \frac{\partial f_o}{\partial (dn_i/dr)} \right|_{R_{ex}} \frac{\partial n_i(R_{ex}, \beta)}{\partial \mu_j}] d\mu_j \\
& + 2d[f_o(R_{ex} - R)] + (R_s - R_{ex})df_o.
\end{aligned} \tag{4.170}$$

Finally, it is of interest to note that, when $R=R_s$, Eqs.(4.168) and (4.170) are reduced to essentially the same form as those for a hard wall-nematic interface [cf. Eq.(4.117)]. Although, in the latter remains an additional term, $-f_o dX$, which comes from the athermal nature of the hard wall, this contribution vanishes when the dividing surface is located at a point fixed relative to the hard wall.

4.7.2 Expansion in terms of the elastic energy: Formulation based on the stress-strain relationship

For weak deformations, Eq.(4.151b) can be approximated to give

$$r_o - R_{ex} = \beta \frac{\partial}{\partial \beta} (R_{ex} - R_s).$$

Then, substituting the above into Eq.(4.155), we can write the polar and the azimuthal angles of the director at R_{ex} as

$$\begin{aligned}
\theta_{ex} &= \theta_e \mp [2f_o/K_3 f(\theta_e)]^{1/2} \left[1 - \frac{\beta}{g(\theta_e)}\right]^{1/2} \beta \frac{\partial}{\partial \beta} (R_{ex} - R_s), \\
\phi_{ex} &= \phi_e \pm [2\beta f_o/K_3]^{1/2} \left[1 - \frac{\beta}{g(\theta_e)}\right] \frac{\partial}{\partial \beta} (R_{ex} - R_s).
\end{aligned} \tag{4.171}$$

These are correct up to the order of $f_o^{1/2}$, and clearly, when $\beta=0$, $\beta=g(\theta_e)$, or $\partial(R_{ex}-R_s)/\partial\beta=0$, we have $\mathbf{n}(R_{ex})=\mathbf{n}_e$.

Next, utilizing the expression of the Frank elastic energy

density in terms of polar and azimuthal angles, i.e.,

$$f_0 = \frac{1}{2} K_3 \left[f(\theta) \left(\frac{d\theta}{dr} \right)^2 + g(\theta) \left(\frac{d\phi}{dr} \right)^2 \right],$$

we generally find

$$\left(\frac{\partial f_0}{\partial T} \right)_n = f_0 \left\{ \left[1 - \frac{\beta}{g(\theta)} \right] \frac{\partial}{\partial T} \ln[K_3 f(\theta)] + \frac{\beta}{g(\theta)} \frac{\partial}{\partial T} \ln[K_3 g(\theta)] \right\}. \quad (4.172)$$

Similar equations are obtainable for chemical potentials also. In relation to the above, it should be pointed out that, when the Frank elastic constants are assumed to be proportional to each other,

$$K_1 \propto K_2 \propto K_3, \quad (4.173)$$

Eq.(4.172) can be very simplified to

$$\left(\frac{\partial f_0}{\partial T} \right)_n = f_0 \frac{\partial}{\partial T} \ln K_3, \quad (4.172')$$

as we have already noted as regards the thermodynamics of bulk nematics [cf. Eq.(4.91)]. Equation (4.173) is a much weaker constraint than the so-called "one-constant approximation," and we shall hereafter refer to it as the "scaling constant approximation."

As a final preparation, we derive an expression for the curvature stress L . According to the elasticity theory, the curvature stress components, L_p and L_a , along the polar and azimuthal directions are respectively defined by

$$L_p = - n_{pi} \frac{\partial f_0}{\partial (dn_i/dr)}, \quad \text{and} \quad L_a = - n_{ai} \frac{\partial f_0}{\partial (dn_i/dr)},$$

which are, in terms of spherical polar coordinate, rewritten as

$$L_p = - K_3 f(\theta) \frac{d\theta}{dr}, \quad \text{and} \quad L_a = - K_3 g(\theta) / \sin\theta \frac{d\phi}{dr}. \quad (4.174a)$$

These represent the orientational torque per unit area transmitted along the interface normal (r-axis). Because of the presence of the torque which is laterally transmitted through the boundary surface parallel to the r-axis, the over all balance of the torque does not necessarily require L to be spatially constant throughout the nematic. However, since this lateral contribution is of the order of f_0 , L_p and L_a can be regarded to be a constant of deformation as far as terms on the order of $f_0^{1/2}$ are concerned. In terms of f_0 and β , L_p and L_a can be readily written, up to an appropriate order, as

$$\begin{aligned} L_p &= \mp [2f_0 K_3 f(\theta_e)]^{1/2} [1 - \beta/g(\theta_e)]^{1/2}, \\ L_a &= \mp [2f_0 K_3 \beta]^{1/2} / \sin \theta_e. \end{aligned} \quad (4.174b)$$

Likewise, the curvature strain, which is defined by $\mathbf{n} - \mathbf{n}_e = C_p \mathbf{n}_p + C_a \mathbf{n}_a$, can be expressed on account of Eqs.(4.155) and (4.174b) as

$$\begin{aligned} C_p &= [L_p / K_3 f(\theta_e)] [R_{ex} - R + \beta \frac{\partial}{\partial \beta} (R_{ex} - R_s)], \\ C_a &= [L_a / K_3 g(\theta_e)] \sin^2 \theta_e \{R_{ex} - R + [\beta - g(\theta_e)] \frac{\partial}{\partial \beta} (R_{ex} - R_s)\}. \end{aligned} \quad (4.175)$$

Combining Eqs.(4.171)-(4.174) with Eq.(4.170), we get

$$\begin{aligned} d\gamma &= - S^s dT - \Gamma_j d\mu_j + L_p d\theta_{ex} + L_a d\phi_{ex} \\ &- f_0 (R_{ex} - R) \left[1 - \frac{\beta}{g(\theta_e)} \left\{ d[\ln K_3 f(\theta_e)] - \frac{\partial}{\partial \theta_e} \ln f(\theta_e) d\theta_e \right\} \right. \\ &- f_0 (R_{ex} - R) \frac{\beta}{g(\theta_e)} \left\{ d[\ln K_3 g(\theta_e)] - \frac{\partial}{\partial \theta_e} \ln g(\theta_e) d\theta_e \right\} \\ &\left. + 2d[f_0 (R_{ex} - R)] + (R_s - R_{ex}) df_0. \right. \end{aligned} \quad (4.176a)$$

Furthermore, this equation adopts an extremely simple form in the

case of a single mode anchorage as follows:

(1) Polar [$\beta=0$],

$$\begin{aligned}
 d\gamma = & - S^S dT - \Gamma_j d\mu_j + L_p d\theta_e \\
 & - f_o(R_{ex} - R) \{ d[\ln K_3 f(\theta_e)] - \left[\frac{\partial}{\partial \theta_e} \ln f(\theta_e) \right] d\theta_e \} \\
 & + 2d[f_o(R_{ex} - R)] + (R_s - R_{ex}) df_o, \quad (4.176b)
 \end{aligned}$$

(2) Azimuthal [$\beta=g(\theta_e)$],

$$\begin{aligned}
 d\gamma = & - S^S dT - \Gamma_j d\mu_j + L_a d\phi_e \\
 & - f_o(R_{ex} - R) \{ d[\ln K_3 g(\theta_e)] - \left[\frac{\partial}{\partial \theta_e} \ln g(\theta_e) \right] d\theta_e \} \\
 & + 2d[f_o(R_{ex} - R)] + (R_s - R_{ex}) df_o. \quad (4.176c)
 \end{aligned}$$

Finally, when the dividing surface is located at R_s , these equations can be expressed in a compact form in terms of the curvature stress and strain as follows:

$$\begin{aligned}
 d\gamma_s = & - S^S dT - \Gamma_j d\mu_j + L_p d\theta_e + L_a d\phi_e + L_p dC_{sp} + L_a dC_{sa} \\
 & - f_o(R_{ex} - R_s) \left\{ \left[1 - \frac{\beta}{g(\theta_e)} \right] \frac{\partial}{\partial \theta_e} \ln f(\theta_e) + \frac{\beta}{g(\theta_e)} \frac{\partial}{\partial \theta_e} \ln g(\theta_e) \right\} d\theta_e, \\
 & - L_a C_{sa} \cot \theta_e d\theta_e \quad (4.177)
 \end{aligned}$$

which is, as it should be, identical with what follows directly from Eq.(4.123).

4.7.3 Thermodynamic definition of the anchoring strength: The extrapolation length and the anchoring energy

The Rapini-Papoular's definition of the anchoring strength is thermodynamically quite unsatisfactory. First, their definition is

based on a semi-microscopic concept of the "director at the interface," which, as already noted, needs further specification from a thermodynamic point of view. Next, another serious shortcoming is the fact that the functional form for the interfacial tension was chosen on a rather ad hoc basis without regard to its thermodynamic foundation; accordingly, the phenomenological meaning of the anchoring energies were left ambiguous, thereby having made them useful only for limited descriptive purposes. We shall here offer a thermodynamic definition of the anchoring strength.

In Section 4.6, we have seen that, for both $\beta=0$ and $\beta=g(\Theta_e)$, the limiting distance between the surface of extrapolation and the surface of tension $d_{e\circ}=\lim_{f_{\circ}\rightarrow 0}(R_{ex}-R_s)$ can be identified, insofar as it exists, with the extrapolation length in Rapini-Papoular's sense. In addition, we have seen in Section 4.6 that, when $R_{ex}-R_s=0$, the equilibrium director profile passes through \mathbf{n}_e at $R_{ex}=R_s$, and in this case furthermore, the interfacial tension remains at the value of the undeformed state even when the nematic is deformed. These are all the correct properties that an infinitely strong anchoring must have, which are familiar in the Rapini-Papoular context. Based on these properties, it appears natural to generally define the "thermodynamic extrapolation length" via

$$d_e = R_{ex} - R_s. \quad (4.178a)$$

Note that this definition is not restricted to an infinitesimal deformation, but remains meaningful however strongly the nematic is deformed. In the case of a hard wall-nematic interface, this may be replaced by

$$d_e = X_{ex} - X. \quad (4.178b)$$

It is also illuminating to recall the fact that at the point of

extrapolation, the director approaches closest to the easy axis, when the director configuration in the bulk nematic is extrapolated. This also shows that the definition of the extrapolation as given above can be regarded as a generalization of de Gennes' concept of the extrapolation length.

From Eq.(4.168) or (4.170), we readily obtain

$$\left(\frac{\partial \gamma_s}{\partial f_0}\right)_{T, \mu_j, \beta} = R_{ex} - R_s + 2f_0 \frac{\partial}{\partial f_0} (R_{ex} - R_s). \quad (4.179a)$$

In particular, we find from this equation that the limiting value of the extrapolation length d_e is given by

$$\lim_{f_0 \rightarrow 0} \left(\frac{\partial \gamma_s}{\partial f_0}\right)_{T, \mu_j, \beta} = d_{e0}. \quad (4.179b)$$

In contrast to Rapini-Papoular's definition, these formulas express the anchoring strength in the form of a susceptibility of the interfacial tension to the Frank elastic energy density in the bulk nematic, both of which are well-defined regardless of whatever inhomogeneity exists within the interfacial transition region. As a result, if the interfacial tension is measured as a function of the orientational deformation, the extrapolation length can be calculated via the above equations. This point has an important consequence for statistical mechanical treatments of the orientational anchoring strength [see Chapter 5]. Since it does not matter much in most cases which of d_e or d_{e0} is actually employed, we shall hereafter express both of them simply by d_e ; when there is a need of distinction, we write the former as $d_e(f_0)$ by explicitly showing its function dependence on f_0 .

Next, let us define the anchoring energy, in a slightly generalized form than Rapini-Papoular's, and investigate how it is related to the extrapolation length. Recall the fact that, as an independent orientational variable, we can take the equilibrium

director at an arbitrary point instead of (H, β) or (f_0, β) . Therefore, it follows in particular that γ_s can be written as a function of the director \mathbf{n}_s at the surface of tension. By focusing on the weak deformation regime, we can write

$$\gamma_s = \gamma_s(C_{sp}, C_{sa}), \quad (4.180)$$

where C_{sp} and C_{sa} are, respectively, the polar and the azimuthal components of \mathbf{n}_s with respect to the local rectangular coordinate taken at \mathbf{n}_e [cf. Eq.(4.163)]; see also Eqs.(4.165a,b) and Fig.4.16. It should be emphasized that although Eq.(4.180) is formally similar to the Rapini-Papoular interfacial free-energy functional, they are radically different from each other in that the former is strictly an equilibrium quantity expressed as a function of the thermodynamic variables C_{sp} and C_{sa} .

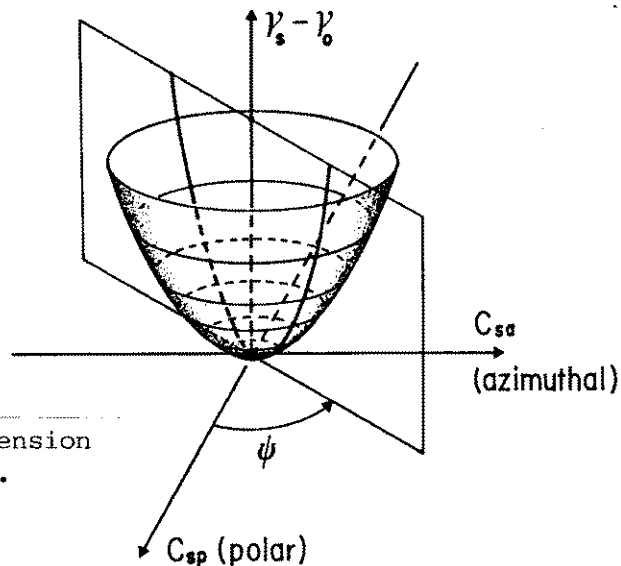


FIG.4.19. Interfacial tension as a function of strain.

At $C_{sp}=C_{sa}=0$, which corresponds to a planar interface, γ_s is equal to γ_0 , and, as C_{sp} and C_{sa} move away from the origin, γ_s will increase or decrease depending on the sign of the extrapolation length, $R_{ex}-R_s$. In Fig.4.19, γ_s is schematically illustrated over the $C_{sp}-C_{sa}$ plane.

In the Rapini-Papoular formalism, the anchoring energy is introduced as a coefficient denoting the rate of increase of the interfacial tension when the director at the interface undergoes a deviation from the easy axis. Let us consider the change of γ_s for each mode of anchorage specified by β . At constant β , C_{sp} and C_{sa} move on a straight line in sufficient vicinity of the origin, and now we would like to introduce a measure of the separation between the interface director \mathbf{n}_s and the easy axis via

$$C_r = \frac{[f(\theta_e)C_{sp}^2 + g(\theta_e)C_{sa}^2/\sin^2\theta_e]^{1/2}}{\{f(\theta_e)[1-\beta/g(\theta_e)] + \beta/\sin^2\theta_e\}^{1/2}}, \quad (4.181a)$$

which is rewritten, by using Eqs.(4.174b) and (4.175), as

$$C_r = \frac{(2f_0/K_3)^{1/2} \{d_e^2 + \beta[g(\theta_e) - \beta](\partial d_e / \partial \beta)^2\}^{1/2}}{\{f(\theta_e)[1-\beta/g(\theta_e)] + \beta/\sin^2\theta_e\}^{1/2}}. \quad (4.181b)$$

Obviously from the former equation, $C_r = C_{sp}$ and $C_r = C_{sa}$ for purely polar and azimuthal deformations, respectively. Furthermore, it should be noted that C_r is, except for the denominator, identical with the measure of length on the unit sphere used in the last section, which has allowed the interpretation of R_{ex} as the point of closest approach to \mathbf{n}_e .

For each β , we define the anchoring energy E_a by the curvature (with respect to C_r) at the origin of the curve of intersection between $\gamma_s(C_{sp}, C_{sa})$ and the perpendicular plane containing the straight line as noted above:

$$E_a = \left(\frac{\partial^2 \gamma_s}{\partial C_r^2} \right)_{T, \mu_j, \beta}, \quad \text{at } C_r = 0, \quad (4.182)$$

This definition yields the Rapini-Papoular anchoring energies $E_a(p)$ and $E_a(a)$ for pure polar and azimuthal anchorages [see Eq.(4.167)]. For an arbitrary mode of anchorage, straightforward calculations show that

$$E_a = \frac{K_3}{d_e} \frac{f(\Theta_e)[1-\beta/g(\Theta_e)] + \beta/\sin^2\Theta_e}{1 + \beta[g(\Theta_e)-\beta][\partial \ln(d_e)/\partial \beta]^2} . \quad (4.183)$$

Because the second factor is always positive, E_a has the same sign as that of the extrapolation length. However, it is in general only in the cases of purely polar or azimuthal deformations that the formula, $E_a \propto 1/d_e$, is obtained, as is familiar in the Rapini-Papoular formalism. This is not an artifact resulting from the present choice of C_r . To illustrate this point, let us consider the case in which d_e is finite, but $\partial d_e / \partial \beta = \infty$. Equation (4.183) now indicates that $E_a = 0$, i.e., a vanishing anchoring strength. And, in accordance with this result, Eqs.(4.175) and (4.179) show that, for finite C_{sp} and C_{sa} , we must have $f_o = 0$ and hence $\gamma_s = \gamma_o$. This is just the property reminiscent of the zero anchoring strength. Therefore, the thermodynamic definition of the anchoring energy as given above is dependent not only on the extrapolation length d_e for the particular mode of anchorage in question, but also on how d_e behaves for neighboring modes. However, when d_e is independent of β , E_a can be written in a very simple form,

$$E_a = 1 / \left[\frac{\beta}{g(\Theta_e)} \frac{1}{E_a(a)} + \left(1 - \frac{\beta}{g(\Theta_e)} \right) \frac{1}{E_a(p)} \right], \quad (4.184)$$

which shows that the anchoring energy for a mode of β is given by a weighted harmonic mean of the anchoring energies for the polar and the azimuthal anchoring energies.

As appreciable from the above discussions, the extrapolation length is a more fundamental concept in thermodynamics than the anchoring energy; the anchoring energy comes afterward via some additional definition (Rapini-Papoular formula is a kind of this). And, even more significantly, the extrapolation length, though it might be understood to be meaningful for only infinitesimal

deformations, can be naturally generalized to finite deformation regime in a thermodynamically consistent manner by defining it as $R_{ex} - R_s$.

One of the remarkable features of Eq.(4.183) is that the β -dependence of E_a can in principle be quite complicated, showing a sharp contrast with the simple dependence assumed in the Rapini-Papoular formalism. Put differently, this is an indication that thermodynamics tells nothing on how the anchoring strength should be influenced by the mode of deformation to couple. This is indeed a task of microscopic theories. From the stress-strain formulation of the thermodynamics, i.e., Eqs.(4.123) and (4.177), we have at fixed temperature and chemical potentials

$$d\gamma_s = L_p dC_{sp} + L_a dC_{sa}.$$

Consequently, the Rapini-Papoular form of the interfacial tension as in Eq.(4.164) amounts to assume (arbitrarily) a linear relationship as

$$L_p = E_a(p)C_{sp}, \quad \text{and} \quad L_a = E_a(a)C_{sa}.$$

4.7.4 Thermodynamic inequalities for the stability of macroscopic alignment: Finiteness of the anchoring strength

Let us finally give a formal proof for an intuitively obvious fact that the anchoring strength is thermodynamically related to the stability of the macroscopic alignment. Here, we suppose that the system in question (including the interface) is immersed in a huge environment comprised of the deformed nematic within the boundary located at R_a [see Fig.4.5]; $R_b - R_a \ll R_a$.

As well known, the condition of thermodynamic equilibrium can be stated in the form that the minimum work needed to bring the system from the equilibrium to any neighboring state should be positive [38]. Let Ω_{env} be the grand thermodynamic potential of

the environment. For a process taking place at fixed temperature, volume, and chemical potentials, the minimum work δW_{\min} is required when the process is reversible; so that, it follows that

$$\delta W_{\min} = \delta \Omega + \delta \Omega_{\text{env}}. \quad (4.185)$$

Furthermore, on the assumption that the environment itself is always in thermodynamic and mechanical equilibrium, the condition of the equilibrium of the system reduces to

$$\delta W_{\min} = \delta \Omega + \omega R_a \frac{\partial f_0}{\partial (dn_i/dr)} \Big|_{R_a} \delta n_i(R_a) > 0. \quad (4.186)$$

Expanding $\delta \Omega$ in powers of $\delta n_i(R_a)$ by regarding Ω as a function of $n_i(R_a)$, we find up to second order

$$\delta \Omega = \frac{\partial \Omega}{\partial n_i} \delta n_i + \frac{\partial^2 \Omega}{\partial n_i \partial n_j} \delta n_i \delta n_j. \quad (4.187)$$

Upon substitution of the above into Eq.(4.184), the first term cancels out when combined with the second in Eq.(4.184), and we are left with

$$- \left[\frac{\partial}{\partial n_i} \frac{\partial f_0}{\partial (dn_j/dr)} \right] \delta n_i \delta n_j > 0, \quad (4.188)$$

where use has been made of Eqs.(4.94) and (4.95). Note that the quantity in the square brackets is symmetrical concerning the exchange of n_i and n_j . The above inequality should be satisfied for any infinitesimal rotations of the director, obeying $|\mathbf{n}|=1$.

For small deformations, Eq.(4.186) can be transformed to

$$\frac{\partial L_p}{\partial C_p} (\delta C_p)^2 + \left[\frac{\partial L_p}{\partial C_a} + \frac{\partial L_a}{\partial C_p} \right] \delta C_p \delta C_a + \frac{\partial L_a}{\partial C_a} (\delta C_a)^2 > 0, \quad (4.189)$$

where C_p and C_a are the polar and the azimuthal components of $\mathbf{n}-\mathbf{n}_e$ at R_a . In order that this inequality holds for any δC_p and δC_a , the following two conditions should be satisfied:

$$\frac{\partial L_p}{\partial C_p C_a} > 0, \quad (4.190)$$

and

$$\frac{\partial L_p}{\partial C_p} \frac{\partial L_a}{\partial C_a} > \frac{\partial L_p}{\partial C_a} \frac{\partial L_a}{\partial C_p}. \quad (4.191)$$

In terms of the Jacobian, the latter can be further written as

$$\frac{\partial(L_p, L_a)}{\partial(C_p, C_a)} > 0.$$

So that, we find

$$\frac{\partial(L_p, L_a) / \partial(L_p, C_a)}{\partial(C_p, C_a) / \partial(L_p, C_a)} = \frac{\partial L_p}{\partial C_p C_a} \frac{\partial L_a}{\partial C_a L_p} > 0,$$

which, in combination with Eq.(4.188), yields

$$\frac{\partial L_a}{\partial C_a L_p} > 0. \quad (4.192)$$

Equations (4.188) and (4.190) are the thermodynamic inequalities characterizing the stable and metastable orientational states of a surface-aligned nematic under curvature stress. Qualitatively, they indicate that, as the director is rotated from the easy axis, the restoring force should monotonically increase.

The inequalities derived above can be translated to a condition for the extrapolation length by changing the independent variables from C_p and C_a to f_0 and β . As clear in Eqs.(4.174b) and (4.175), the curvature strain and stress are proportional to $f_0^{1/2}$ under weak deformations; so that, by temporally defining the functions of β , $x(\beta)$, $y(\beta)$, $X(\beta)$ and $Y(\beta)$ via $L_p = \mp f_0^{1/2} x(\beta)$, $L_a = \mp f_0^{1/2} y(\beta)$, $C_p = -f_0^{1/2} X(\beta)$, and $C_a = -f_0^{1/2} Y(\beta)$, we can rewrite Eqs.(4.188) and (4.190) as follows:

$$\frac{\partial(L_p, C_a)}{\partial(C_p, C_a)} = \frac{\partial(L_p, C_a) / \partial(f_0, \beta)}{\partial(C_p, C_a) / \partial(f_0, \beta)} = \frac{xY' - x'Y}{XY' - X'Y} > 0,$$

and

$$(4.193)$$

$$\frac{\partial(L_a, L_p)}{\partial(C_a, L_p)} = \frac{\partial(L_a, L_p) / \partial(f_o, \beta)}{\partial(C_a, L_p) / \partial(f_o, \beta)} = \frac{yx' - y'x}{Yx' - Y'x} > 0.$$

The, substituting x , y , X , and Y as obtained from Eqs.(4.174b) and (4.175), we find after some straightforward calculations that if

$$|d_e| < \infty, \quad \left| \frac{\partial}{\partial \beta} d_e \right| < \infty, \quad \text{and} \quad \left| \frac{\partial^2}{\partial \beta^2} d_e \right| < \infty \quad (4.194)$$

are simultaneously satisfied, there exists a critical thickness $d=d_c$ for each β , beyond which the thermodynamic inequalities hold. The appearance of the critical thickness is obviously related to the inhomogeneous nature of the system under consideration; so, it is natural to expect that d_c is the quantity of the same order of magnitude with the physical thickness of the interfacial layer. The first two inequalities of Eq.(4.194) is, as observed from Eq.(4.183), equivalent to require that $|E_a| < \infty$. So that, they are seen to be connected with the stability of the director configuration with respect to the director rotation which conserves β . The final one is thus related to the stability for the change of mode at fixed elastic energy.

When, in particular, the deformation is restricted to be of single mode, the condition of local stability reduces to

$$|d_e| < \infty, \quad (4.195)$$

which also implies a non-zero anchoring strength. When the equality holds in the above, the alignment becomes unstable. This case may correspond to an "orientational critical point" where the alignment undergoes some kind of phase transition. We will discuss this point in more detail in Section 4.9.

4.8 Thermodynamic relations

By applying Maxwell's relation to the generalized Gibbs equation, Eqs.(4.170), (4.186a), or (4.177), it is now a straightforward matter, for any mode of anchorage, to derive formal thermodynamic relations which hold among interfacial quantities. However, unless the anchorage is polar, azimuthal, or isotropic, this procedure yields in general a very complicated expression involving the β -derivative of the extrapolation length d_e . Though this may well be of theoretical interest, there is at present available no experimental information on how a nematic interface does behave, when subjected to such a mixed-mode curvature deformation. So, we shall here limit the argument to the cases of simple anchorages, whenever it becomes otherwise too lengthy.

4.8.1 Adsorption at a deformed nematic-fluid interface

A. Adsorption as a function of orientational deformation

As already noted in relation to the case of ordinary fluids in two-phase equilibria, the temperature and the chemical potentials can not be in general changed independently of each other. From the Gibbs-Duhem equations for the bulk (isotropic) fluid and the nematic reservoir mutually in equilibrium under a common pressure P [cf. Eq.(4.12)], we get

$$0 = \Delta s dT + \Delta \rho_1 d\mu_1 + \Delta \rho_2 d\mu_2 + \dots, \quad (4.196)$$

where Δs and $\Delta \rho_j$ are, respectively, the phase-to-phase differences of the entropy density and of the molecular number density of the j -th species. For a process taking place at constant temperature, substituting $d\mu_1$ from Eq.(4.196) into Eq.(4.170) yields

$$\begin{aligned}
d\gamma = & - [\Gamma_j + \int_R^{R_{ex}} \frac{\partial f_0}{\partial \mu_j} dr - \frac{\Delta \rho_j}{\Delta \rho_1} (\Gamma_1 + \int_R^{R_{ex}} \frac{\partial f_0}{\partial \mu_1} dr)] d\mu_j \\
& - \frac{\partial f_0}{\partial (dn_i/dr)} \Big|_{R_{ex}} \left[\frac{\partial n_i(R_{ex}, \beta)}{\partial \mu_j} - \frac{\Delta \rho_j}{\Delta \rho_1} \frac{\partial n_i(R_{ex}, \beta)}{\partial \mu_1} \right] d\mu_j \\
& + 2d[f_0(R_{ex} - R)] + (R_s - R_{ex})df_0,
\end{aligned}
\tag{4.197}$$

where the summation over j runs over all components but the first. As we have done for ordinary fluids [Section 4.1.3], it is easy to show, on account of the expression for bulk densities [Eq.(4.90)], that the quantity in the first square brackets is independent of the position of the dividing surface R .

Next by applying Maxwell's relation to μ_j and f_0 in the above and integrating by f_0 at fixed T and μ_m ($m \neq 1$), we obtain

$$\begin{aligned}
{}^1\Gamma_j = & {}^1\Gamma_{0j} - \int_R^{R_{ex}} \frac{\partial f_0}{\partial \mu_j} dr - \frac{\partial f_0}{\partial (dn_i/dr)} \Big|_{R_{ex}} \frac{\partial n_i(R_{ex}, \beta)}{\partial \mu_j} \\
& + \int_0^{f_0} \frac{\partial}{\partial \mu_j} (R_{ex} - R_s) df_0, \quad (j \geq 2).
\end{aligned}
\tag{4.198}$$

In this expression, μ_1 is regarded as a function of T and μ_m ($m \geq 2$), and ${}^1\Gamma_j$ stands for the adsorption of the j -th component relative to the first, i.e., ${}^1\Gamma_j = \Gamma_j - (\Delta \rho_j / \Delta \rho_1) \Gamma_1$; the subscript 0 denotes the quantity at $f_0=0$. It should be noted that, in an orientationally deformed nematic, ${}^1\Gamma_j$ is no longer a constant independent of the location of the dividing surface as in ordinary liquids. The above equation also applies to the case of a hard wall-nematic interface, provided the variables are reread appropriately.

For weak single-mode deformations with the dividing surface taken at R_s , we obtain from Eq.(4.176b):

(i) Polar anchorage ($\beta=0$),

$${}^1\Gamma_{sj} = {}^1\Gamma_{\circ j} + [L_p + L_p^2 \frac{d_e}{2K_3 f(\theta_e)} \frac{\partial}{\partial \theta} \ln f(\theta_e)] \frac{\partial \theta_e}{\partial \mu_j} + L_p^2 \frac{\partial}{\partial \mu_j} \frac{d_e}{2K_3 f(\theta_e)} + o(f_0), \quad (4.199a)$$

where L_p is, as before, the torque transmitted per unit area across the interface as given by $L_p = \mp [2f_0 K_3 f(\theta_e)]^{1/2}$. For the azimuthal anchorage, on the other hand, we obtain from Eq.(4.176c) a slightly different expression:

(ii) Azimuthal anchorage [$\beta=g(\theta_e)$],

$${}^1\Gamma_{sj} = {}^1\Gamma_{\circ j} + L_a \frac{\partial \Phi_e}{\partial \mu_j} + L_a^2 \frac{d_e}{2K_3 g(\theta_e)} \frac{\partial}{\partial \theta} \ln g(\theta_e) \frac{\partial \theta_e}{\partial \mu_j} + L_a^2 \frac{\partial}{\partial \mu_j} \frac{d_e}{2K_3 g(\theta_e)} + o(f_0), \quad (4.199b)$$

where $L_a = \mp [2f_0 K_3 g(\theta_e)]^{1/2}$. In particular, when the scaling constant approximation ($K_1 \ll K_2 \ll K_3$) holds, Eqs.(4.199a,b) reduce to

(i)

$${}^1\Gamma_{sj} = {}^1\Gamma_{\circ j} + L_p \frac{\partial \theta_e}{\partial \mu_j} + L_p^2 \frac{1}{2f(\theta_e)} \frac{\partial}{\partial \mu_j} \frac{d_e}{K_3}, \quad (4.200a)$$

and (ii)

$${}^1\Gamma_{sj} = {}^1\Gamma_{\circ j} + L_a \frac{\partial \Phi_e}{\partial \mu_j} + L_a^2 \frac{1}{2g(\theta_e)} \frac{\partial}{\partial \mu_j} \frac{d_e}{K_3}, \quad (4.200b)$$

respectively. Here, it must be noticed that Eq.(4.200a) is completely identical with Eq.(4.198) restricted to polar anchorage owing to the fact that $\mathbf{n}(R_{ex}, \beta=0) = \mathbf{n}_e$ and $\partial f_0 / \partial \mu_j = f_0 \partial \ln K_3 / \partial \mu_j$. Obviously, this is not necessarily the case for an azimuthal anchorage. In terms of the strain components at the surface of tension C_{sp} and C_{sa} given by Eq.(4.175), the above

equations can be transformed, under sufficiently weak deformations, to give

$$(i) \quad {}^1\Gamma_{sj} = {}^1\Gamma_{\circ j} + C_{sp} \frac{K_3 f(\theta_e)}{d_e} \frac{\partial \theta_e}{\partial \mu_j} - C_{sp}^2 \frac{f(\theta_e)}{2} \frac{\partial}{\partial \mu_j} \frac{K_3}{d_e}, \quad (4.200c)$$

and (ii)

$${}^1\Gamma_{sj} = {}^1\Gamma_{\circ j} + C_{sa} \frac{K_3 g(\theta_e)}{d_e} \frac{\partial \theta_e}{\partial \mu_j} - C_{sa}^2 \frac{g(\theta_e)}{2} \frac{\partial}{\partial \mu_j} \frac{K_3}{d_e}. \quad (4.200d)$$

The above results indicate that the adsorption at a deformed nematic-fluid interface is affected by the orientational deformation of the nematic in two ways: (1) the change of the pretilt angle induced by composition (or pressure) variation, and (2) that of the anchoring strength. In particular, it is worth pointing out that the effect of the anchoring strength is quadratic in the curvature stress (and strain), so that it is uniquely determined only by the absolute strength of the deformation, in whatever direction the director is distorted. As to the contribution from the pretilt angle, however, the adsorption may increase or decrease depending on the sign of the curvature stress. Specifically, when the nematic is deformed in such a way as to enhance (oppose) the effect of the addition of the j -th component, the adsorption will be increased (decreased) as the nematic is more and more deformed. This is in accord with Le Chatelier's law.

To make an order-of-magnitude estimate, let us assume that the j -th component is a trace impurity with the mole fraction c_j ; so that we can use the ideal solution formula. For simplicity, furthermore, we adopt the scaling constant approximation. Then, in the case of a polar anchorage, Eq.(4.200a) is rewritten as

$${}^1\Gamma_{sj} = {}^1\Gamma_{\circ j} + \frac{L_p c_j}{kT} \frac{\partial \theta_e}{\partial c_j} + \frac{L_p^2 c_j}{2kTf(\theta_e)} \frac{\partial}{\partial c_j} \frac{d_e}{K_3}, \quad (4.201)$$

where k is the Boltzmann constant. In Fig.4.20 shown is an example of the change of the adsorption with L_p ; wherein, we have assumed

$$c_j \frac{\partial \Theta_e}{\partial c_j} = -10, \quad \text{and} \quad \frac{c_j}{2f(\Theta_e)} \frac{\partial}{\partial c_j} \frac{d_e}{K_3} = 10^5 \text{ m}^2/\text{J}.$$

Since no systematic measurement has ever been made on the changes of the pretilt angle and, especially, of the anchoring strength associated with the addition of an impurity, these values were adopted rather arbitrarily here, with the situation as shown in Fig.4.21 in mind. Although this choice of parameters corresponds to the case wherein the pretilt angle and the anchoring strength should change drastically over a rather narrow range of impurity concentration, those values may not be so unrealistic in view of the fact that the alignment of nematics is often forced to change from planar to homeotropic by a fractional variation in the amount of adsorbed surface-active agent on

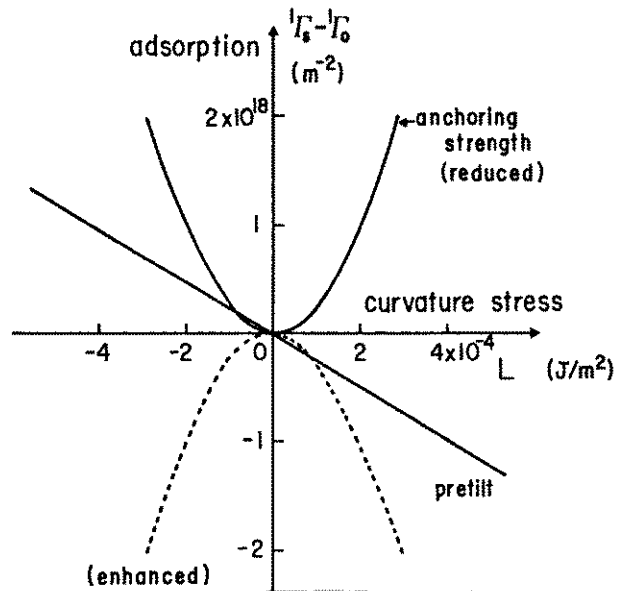


FIG.4.20. Variation of the adsorption with the application of a curvature stress.

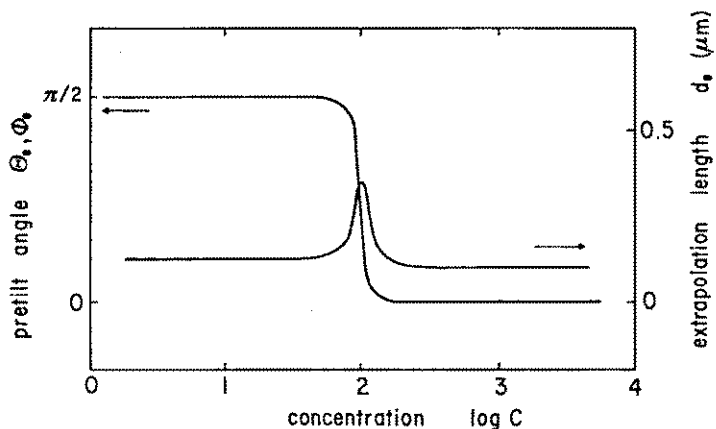


FIG.4.21. Conceived variation of the pretilt angle and the extrapolation length associated with the change of the impurity concentration.

a solid substrate [39].

Figure 4.20 reveals that at an L_p as large as 10^{-4} J/m², almost sub-monolayer adsorption (or desorption) of the impurity is induced. If we denote the characteristic length of the elastic deformation as λ , L_p is approximately given by $K_3 f(\Theta_e)/\lambda$. Then, assuming $K_3 f(\Theta_e) = 10^{-11}$ N, we obtain $\lambda = 0.1$ μ m for $L_p = 10^{-4}$ J/m². This is a level of deformation which is often achieved under an electric field in practical liquid crystal cells. It should, however, be pointed out that at this rather strong deformation, the strain C_{sp} assumes a value as large as 1 at the nematic interface in question having $d_e \sim 0.1$ μ m.

B. Gibbs adsorption isotherm

Suppose a process associated with the change of chemical potentials occurring at constant T and f_0 . By substituting Eq.(4.198) into Eq.(4.197), we obtain the Gibbs adsorption isotherm for a nematic interface:

$$d\gamma_s = - [{}^1\Gamma_{0j} - 2 \frac{\partial}{\partial \mu_j} (R_{ex} - R_s) + \int_0^{f_0} \frac{\partial}{\partial \mu_j} (R_{ex} - R_s) df_0] d\mu_j, \quad (4.202a)$$

where, as before, j is restricted to 2 and over, and μ_1 and β are considered to be functions of the rest of the chemical potentials. This equation is valid for any mode of anchorage, and agrees with what we obtain by directly differentiating Eq.(4.167). In the case of a normal behavior, Eq.(4.202a) reduces, up to first order in f_0 , to

$$d\gamma_s = - [{}^1\Gamma_{0j} - f_0 \frac{\partial}{\partial \mu_j} d_e] d\mu_j. \quad (4.202b)$$

In contrast to the adsorption itself, the above equations lack the (direct) contribution from the pretilt angle, but contains only

the part of the anchoring strength.

When the orientational strain $\Delta \mathbf{n}_s = \mathbf{n}_s - \mathbf{n}_e$ is fixed, instead of f_o , while the chemical potentials are changed, we find from Eq.(4.123)

$$d\gamma_s = - [{}^1\Gamma_{sj} + \frac{\partial f_o}{\partial (dn_i/dr)} \Big|_{R_s} \frac{\partial n_{ei}}{\partial \mu_j}] d\mu_j, \quad (4.203a)$$

which can be, upon application of Eqs.(4.199a,b), transformed to

$$d\gamma_s = - [{}^1\Gamma_{oj} + f_o \frac{\partial}{\partial \mu_j} d_e] d\mu_j, \quad (4.203b)$$

provided the anchorage is purely polar or azimuthal. Equations (4.202b) and (4.203b) show that, depending on which of f_o and $\Delta \mathbf{n}_s$ is fixed, the orientational deformation contributes to the interfacial tension in an opposite direction. Intuitively speaking, f_o may be almost constant when the boundary opposite to the interface, which is inducing the orientational deformation, is located sufficiently far from the interface in comparison with the extrapolation length; and on the other hand, $\Delta \mathbf{n}_s$ is expected to stay almost fixed when the counter boundary is very close to the interface. As a result, they may well be viewed as representing the two extreme boundary conditions. The actual experimental situations lie somewhere in between, depending on the details of how the deformation is brought about.

To illustrate the numerical consequences of those formulas, let us investigate the case of a three-component fluid which is comprised of a couple of mutually immiscible fluids, the components "1" and "2," dissolved with a small amount of surface active agent, the component "3." We regard here that the phase consisting of the first component is in the nematic state, and the phase with the second component is serving as a substrate for it. And, to make the point clear, we further assume that the added

surface active agent is not miscible to the substrate, either.

Because of the immiscibility, the chemical potential of the substrate phase, μ_2 , is not influenced, at constant temperature and pressure, by an application of the third component. For the nematic phase, we have, from the ideal solution formula

$$d\mu_1 = -kT dc, \quad \text{and} \quad d\mu_3 = (kT/c) dc,$$

where c is the concentration of the third component with respect to the second. From Eq.(4.202b), we get

$$\left(\frac{\partial \gamma_s}{\partial c}\right)_{f_0} = -(kT/c)^1 \Gamma_{o_3} + f_0 \frac{\partial}{\partial c} d_e, \quad (4.204a)$$

and especially for polar or azimuthal anchorage, we further obtain

$$\left(\frac{\partial \gamma_s}{\partial c}\right)_{\Delta n_s} = -(kT/c)^1 \Gamma_{o_3} - f_0 \frac{\partial}{\partial c} d_e. \quad (4.204b)$$

So, if the surface active agent is to reduce the anchoring strength, we should observe a decrease or an increase in the interfacial tension as the nematic is orientationally deformed, according to which of f_0 and Δn_s is fixed during the deformation. If we take $K \sim 10^{-11}$ N and $\lambda \sim 10^{-7}$ m as before, we have $f_0 \sim 5 \times 10^2$ J/m³. Therefore, if the extrapolation length varies by 10^{-7} m during the addition of 10^{-4} mole fraction of the agent, we find from the above that the orientational contribution to $\partial \gamma_s / \partial c$ is about ± 1 J/m²·(mol fraction), and hence the absolute change of γ_s is $\pm 10^{-4}$ J/m². Although the rate of change is remarkably large, the absolute magnitude of the change is negligibly small in comparison with the interfacial tension of ordinary fluids, which is normally $10^{-3} \sim 10^{-1}$ J/m².

Nevertheless, the change of the anchoring strength associated with the addition of a surface active agent may not be necessarily linearly dependent on its concentration as depicted in Fig.4.21.

This presents a good contrast with the Langmuir type adsorption, which is, at small concentrations, linearly dependent on the concentration. Therefore, even though the absolute effect is not large, the orientational effect is expected to presents a qualitatively different feature characterized by the nonlinearity and the dependence on the degree of orientational deformation.

4.8.2 Surface entropy and the temperature-dependence of the interfacial tension

A. Surface entropy as a function of orientational deformation

In completely the same manner as for adsorption, we can write down an expression for the surface entropy:

$$\begin{aligned}
 {}^1S^S = {}^1S_0^S - \int_R^{R_{ex}} \frac{\partial f_0}{\partial T} dr - \left. \frac{\partial f_0}{\partial (dn_i/dr)} \right|_{R_{ex}} \frac{\partial n_i(R_{ex}, \beta)}{\partial T} \\
 + \int_0^{f_0} \frac{\partial}{\partial T} (R_{ex} - R_s) df_0, \quad (j \geq 2),
 \end{aligned}
 \tag{4.205}$$

where ${}^1S^S$ represents the relative surface entropy with respect to the first component as defined by

$${}^1S^S = S^S - (\Delta s / \Delta \rho_1) \Gamma_1.$$

Here, too, μ_1 and β are regarded as a function of other variables. For a polar anchorage under a weak deformation, we obtain, up to first order in f_0 ,

$$\begin{aligned}
 {}^1S_s^S = {}^1S_0 + [L_p + L_p^2 \frac{d_e}{2K_3 f(\theta_e)} \frac{\partial}{\partial \theta} \ln f(\theta_e)] \frac{\partial \theta_e}{\partial T} \\
 + L_p^2 \frac{\partial}{\partial T} \frac{d_e}{2K_3 f(\theta_e)},
 \end{aligned}
 \tag{4.206a}$$

where the dividing surface is located at the surface of tension. For an azimuthal anchorage, we get

$$\begin{aligned}
1_{S_s}^{SS} = 1_{S_o} + L_a \frac{\partial \phi_e}{\partial T} + L_a^2 \frac{d_e}{2K_3 g(\theta_e)} \frac{\partial}{\partial \theta} \ln g(\theta_e) \frac{\partial \theta_e}{\partial T} \\
+ L_a^2 \frac{\partial}{\partial T} \frac{d_e}{2K_3 g(\theta_e)}.
\end{aligned} \tag{4.206b}$$

If the scaling constant approximation holds, the above equations are respectively rewritten as

$$1_{S_s}^{SS} = 1_{S_o} + L_p \frac{\partial \theta_e}{\partial T} + L_p^2 \frac{1}{2f(\theta_e)} \frac{\partial}{\partial T} \frac{d_e}{K_3}, \tag{4.207a}$$

$$1_{S_s}^{SS} = 1_{S_o} + L_a \frac{\partial \phi_e}{\partial T} + L_a^2 \frac{1}{2g(\theta_e)} \frac{\partial}{\partial T} \frac{d_e}{K_3}. \tag{4.207b}$$

Furthermore, for sufficiently weak deformations, they can be written in terms of the strain components as follows:

$$1_{S_s}^{SS} = 1_{S_o} + C_{sp} \frac{K_3 f(\theta_e)}{d_e} \frac{\partial \theta_e}{\partial T} - C_{sp}^2 \frac{f(\theta_e)}{2} \frac{\partial}{\partial T} \frac{k_3}{d_e}, \tag{4.207c}$$

$$1_{S_s}^{SS} = 1_{S_o} + C_{sa} \frac{K_3 g(\theta_e)}{d_e} \frac{\partial \theta_e}{\partial T} - C_{sa}^2 \frac{g(\theta_e)}{2} \frac{\partial}{\partial T} \frac{k_3}{d_e}. \tag{4.207d}$$

As evident in these results, the surface entropy is affected by orientational deformations, if and only if there is a temperature-induced change of the easy axis and/or of the anchoring strength. The effect of the anchoring strength, in particular, is always such that when the anchorage weakens with temperature, the surface entropy increases as the nematic is orientationally deformed; therefore, the ordering near the interface should be deteriorated more rapidly in the interfacial region than in the bulk nematic under a curvature stress. On the other hand, the contribution from the pretilt-angle variation is dependent on the direction of the director deformation. When the nematic is deformed in such a way as to enhance (oppose) the variation of \mathbf{n}_e with temperature, the surface entropy increases (decreases) for suffi-

ciently small deformations. In other words, upon application of an orientational torque so as to pull back the director at the interface toward the direction that the director assumes at lower temperatures, the interfacial layer should be brought into a more ordered state!

Figure 4.22 shows the surface entropy as a function of the applied torque L_p , calculated based upon the scaling constant approximation. Here, we have used the following values,

$$\frac{\partial \theta_e}{\partial T} = -0.1 \text{ rad/K}, \quad \text{and} \quad \frac{\partial}{\partial T} \frac{d_e}{K_3} = 3.4 \times 10^{-4} \text{ m}^2/\text{J K},$$

in view of the experimental results for the free surface of MBBA (4-methoxybenzylidene-4'-butylaniline) reported by Chiarelli, et al.[40,41]. From the

figure, we see that the orientational contribution to surface entropy reaches a value as large as $2 \times 10^{-4} \text{ J/m}^2 \cdot \text{K}$ at $L_p = 10^{-4} \text{ J/m}^2$. But, as evident from its almost symmetrical shape about the ordinate axis, the contribution of the pretilt-angle part is at present negligibly small.

For a free surface of undeformed nematic, the surface entropy can be estimated from the temperature dependence of the surface tension

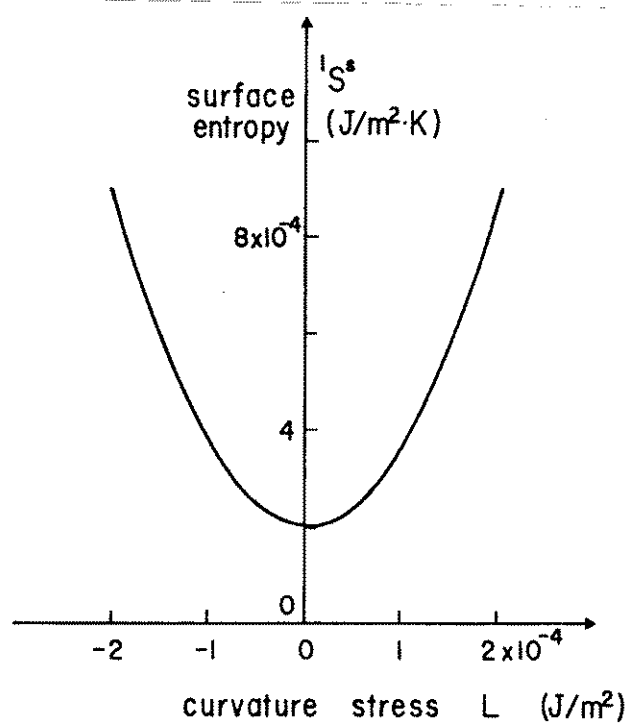


FIG.4.22. Example of the change of surface entropy with the applied curvature stress.

as in ordinary fluids. According to the measurement due to Krishnaswamy and Shashidhar[42], the surface tension of MBBA decreases with temperature by about $1\sim 2 \times 10^{-4}$ J/m² per 1 K in the nematic phase; so that, the surface entropy is estimated to be about $1\sim 2 \times 10^{-4}$ J/K·m². This shows that the orientational deformation can exert significant influence on the interfacial structure of nematic liquid crystals, if either the easy axis or the anchoring strength undergoes a spontaneous variation associated with temperature.

B. Temperature-dependence of the interfacial tension

As already noted, the temperature-induced change of an interfacial tension is intimately related to the surface entropy. By using Eq.(4.204) in Eq.(4.197), while keeping f_0 and μ_m ($m \geq 2$) fixed, we obtain

$$d\gamma_s = - [^1S_0^s - 2 \frac{\partial}{\partial T} (R_{ex} - R_s) + \int_0^{f_0} \frac{\partial}{\partial T} (R_{ex} - R_s) df_0] dT,$$

Consequently, when normal behavior is assumed, the above equation is reduced to

$$\left(\frac{\partial \gamma_s}{\partial T} \right)_{f_0} = -^1S_0^s - f_0 \frac{\partial}{\partial T} d_e. \quad (4.208a)$$

Similar to Eq.(4.204b), when Δn_s is fixed instead of f_0 , we obtain

$$\left(\frac{\partial \gamma_s}{\partial T} \right)_{\Delta n_s} = -^1S_0^s + f_0 \frac{\partial}{\partial T} d_e, \quad (4.208b)$$

for purely polar or azimuthal anchorage. Therefore, we observe here again that the contribution of the pretilt angle disappears in relation to the variation of the interfacial tension. This result indicates that, concerning the interface of a deformed nematic, the variation of the interfacial tension with temperature does not faithfully reflect the surface entropy in the same sense

that it does in the case of ordinary fluids; it is only related to the part coming from the variation of the anchoring strength.

Equations (4.208a,b) show that, the contribution of orientational deformation can be in opposite direction, depending on the choice of the independent orientational variable. Indeed, when f_0 (or Δn_g) is fixed during the temperature variation, the interfacial tension should behave as if the surface entropy were increased (or decreased) relative to that in the undeformed state. For an order-of-magnitude estimate, let us assume that d_e increases at a rate of about 100 nm/K, which roughly corresponds to the parameter taken above. Then, Eqs.(4.208a,b) predict that at $f_0=10^3 \text{ J/m}^3$ ($L_p \sim 10^{-4} \text{ J/m}^2$), the interfacial tension has to vary at a rate of about $10^{-4} \text{ J/m}^2 \cdot \text{K}$, which is on the same order as that for ordinary fluid surfaces. Obviously, at higher orientational stress, the deformational contribution can be overwhelmingly large when compared to the temperature-dependence of the surface tension in the undeformed state. This suggests that precise measurements of surface tension of nematics, for instance by means of Wilhelmy plate method, require extra care to take account of the states of deformation and of anchoring strength near the point where the tension is actually in action.

4.9 Alignment transition at nematic interfaces: Thermodynamic inequalities for critical exponents

The pretilt angle and the anchoring strength are in general functions of temperature, pressure, and composition. And, in some instances, they undergo a variation which can be regarded as a kind of "phase transition." Especially, when the transition is accompanied by a singularity at a point in the phase space, it is possible to set forth some thermodynamic criteria for critical exponents governing the behavior of the pretilt angle and the anchoring strength around this point. This section is devoted to formulate such conditions, and to discuss a few recent experiments on the continuous alignment-transition observed at a nematic free surface in the light of these results.

4.9.1 Critical behavior of the anchoring strength

We shall first consider the case in which only the anchoring strength undergoes a critical behavior. Though the criticality may in principle emerge in connection with any of temperature, pressure, and/or composition, we restrict the present argument to the case of temperature, since other cases can be treated in completely the same manner, resulting in identical conditions.

Imagine that the temperature derivative of the extrapolation length diverges at a temperature T_0 :

$$\lim_{T \rightarrow T_0} \frac{\partial d_e}{\partial T} = \infty, \quad (4.209)$$

At temperatures near T_0 , therefore, the extrapolation length may be expressed as

$$d_e \sim d_{e0} + A |(T_0 - T)/T_0|^\eta, \quad (4.210)$$

with A being a temperature-independent constant, and η is the critical exponent satisfying

$$\eta < 1. \quad (4.211)$$

Consequently, according as $\eta < 0$ or $0 < \eta < 1$, d_e exhibits two qualitatively different behaviors as illustrated in Fig.4.23; in the former case, the anchoring strength becomes infinitely weak at T_0 , i.e., $d_e \rightarrow \infty$ or $E_a \rightarrow 0$, but in the latter it remains finite.

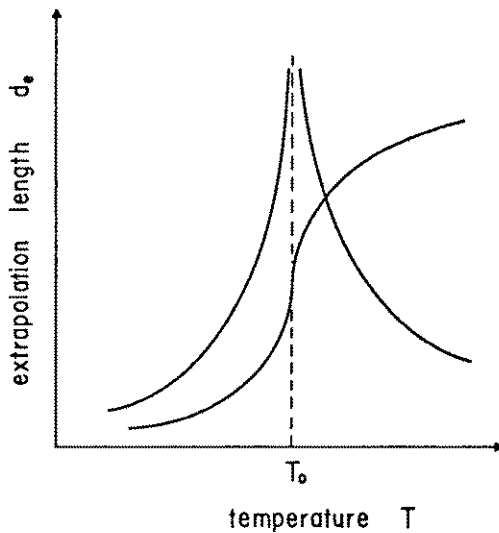


FIG.4.23. Two possible cases of the critical variation of the extrapolation length. The extrapolation length cannot assume an infinite gradient as long as it is finite.

The basis of our present argument is the formulas for surface entropy as derived in Section 4.8.2. Introducing Eq.(4.210) into Eq.(4.206) and collecting only (potentially) singular terms, we obtain

$${}^1 S_s^s = S_n(T) \mp \frac{L_p^2}{2K_3 f(\Theta_e)} \frac{\eta A}{T_0} |(T_0 - T)/T_0|^{(\eta - 1)}, \quad (4.212)$$

where $S_n(T)$ represents the noncritical part, and the upper and the lower signs before the second term correspond to $T < T_0$ and $T > T_0$, respectively. A similar equation can also be derived for the case of azimuthal anchorage.

Since thermodynamic state functions such as entropy and internal energy cannot diverge at any finite temperature, one might conclude from Eq.(4.212) that it is in any case impossible for the extrapolation length to show a critical behavior as conceived above. This is indeed true when the extrapolation length

remains finite even at the critical point, i.e., $\eta > 0$. Hence, we can conclude that d_e cannot have a diverging slope as long as it is finite.

However, it is clear that, when the anchoring strength tends to vanish as the critical point is approached, i.e., $\eta < 0$, the interface cannot indefinitely support a finite orientational torque L_p . So, in this case, it is no longer allowed to consider L_p as a constant independent of temperature. In order to take account of this point, we have to rewrite the above equation in terms of the strain, $\Delta n_s = n_s - n_e$, as in Eqs.(207c,d). Using Eq.(4.175), Eq.(4.206) can be generally rewritten as

$$1_{S_S}^S = 1_{S_0}^S + \frac{K_3 f(\theta_e)}{d_e} \left[C_{sp} + \frac{C_{sp}^2}{2} \frac{\partial}{\partial \theta} \ln f(\theta_e) \right] \frac{\partial \theta_e}{\partial T} - \frac{C_{sp}^2}{2} \frac{\partial}{\partial T} \frac{K_3 f(\theta_e)}{d_e}. \quad (4.213)$$

Hence, upon substitution of Eq.(4.210), we find

$$1_{S_S}^S \sim S_n(T) \mp \frac{C_{sp}^2}{2} \frac{K_3 f(\theta_e)}{AT_0} \eta \left| (T_0 - T)/T_0 \right|^{-(\eta+1)}, \quad (\eta < 0). \quad (4.214)$$

This equation shows that for any "finite" strain, the entropy should diverge if $0 > \eta > -1$. Since it is intuitively evident that the strain at the surface of tension C_{sp} can be arbitrarily chosen regardless of the anchoring strength, the requirement of nondivergence of the left-hand side of Eq.(4.214) results in the following condition to be satisfied by the critical exponent:

$$\eta \leq -1. \quad (4.215)$$

This inequality means that the anchoring strength, when it exhibits a critical decrease, should behave with a sufficiently strong singularity. The behavior of the anchoring energy at this type of critical point is schematically shown in Fig.4.24.

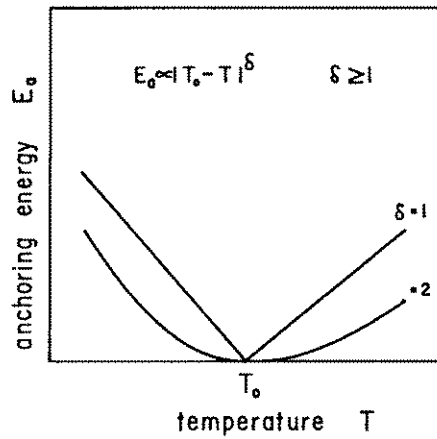


FIG.4.24. Possible singular behaviors of the anchoring energy at the critical temperature T_0 .

4.9.2 Critical behavior of the pretilt angle

A. Continuous transition

Next, we consider the case in which the pretilt angle also experiences a critical variation when the temperature, pressure, or composition is changed. Here, let us suppose that the polar angle of \mathbf{n}_e varies with temperature, exhibiting a diverging slope at the critical point T_0 . [see Fig.4.25].

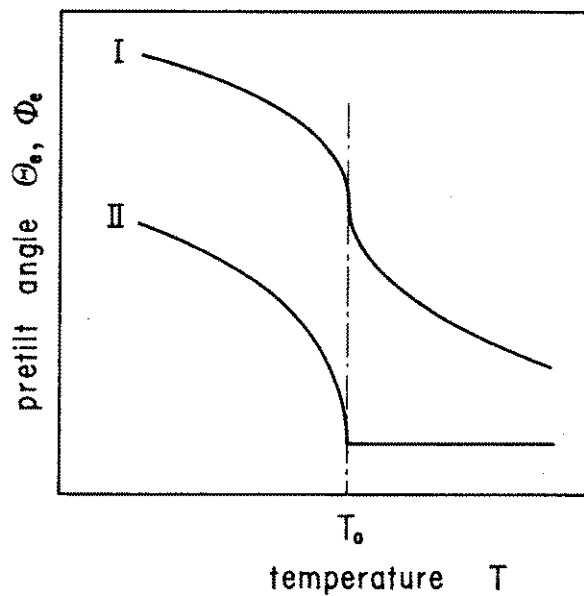


FIG.4.25. Two possible cases of the critical behavior of the pretilt angle.

Since the pretilt angle is a bounded function, we may now write

$$\Theta_e \sim \Theta_{e0} + B |(T_0 - T)/T_0|^\nu, \quad (4.216)$$

with

$$0 < \nu < 1.$$

Then, substituting Eq.(4.216) into Eq.(4.213), it follows immediately that, as long as the anchoring strength remains finite, the surface entropy is doomed to go to infinity as T_0 is approached. Because the second and the third terms in Eq.(4.213) have distinct dependences on C_{sp} , they have to separately remain finite at the critical temperature in order to prevent the surface entropy from diverging. So, the critical behavior of the pretilt angle must always be accompanied by the critical weakening of the anchoring strength. Not to mention, the critical exponent of the extrapolation length has to satisfy the inequality as envisaged in Eq.(4.214). As in Section 4.9.1, this result applies not only to the temperature-induced rotation of the easy axis but also to pressure- and composition-induced rotations, and to the azimuthal angle as well.

As illustrated in Fig.4.25, we may distinguish two cases as to how the pretilt angle behaves around the critical point: In the first case (I), the slope, $\partial\Theta_e/\partial T$, diverges on both sides of the critical point; but, in the second case (II), $\partial\Theta_e/\partial T$ shows a critical divergence on only one of the sides of T_0 , while it remains finite on the other. Although it is clear from the above argument that, the anchoring strength has to exhibit a critical weakening on such a side of T_0 where $\partial\Theta_e/\partial T$ diverges, it is not immediately apparent whether this remains true even when T_0 is approached along the non-critical side in case II. However, since it is trivial that two orientational states with a same pretilt angle but with different anchoring strengths cannot coexist in equilibrium, we can conclude that the anchoring strength must

continuously vanish even under such a circumstance. So, once it is established that the slope of the pretilt angle diverges in one way or another at some temperature, pressure, and composition, the anchoring strength should be absolutely critical at this point as shown in Fig.4.25.

B. Discontinuous transition

So far, we have considered only the case wherein the pretilt angle undergoes a continuous transition. However, there may also be an occasion, as observed experimentally [43,44], that the pretilt angle changes discontinuously as schematically shown in Fig.4.26. As clear from the above arguments, the thermodynamics presents no criterion as to the "discontinuous" transition itself, but it appears to be of some interest here to discuss how such a transition can be related to continuous ones.

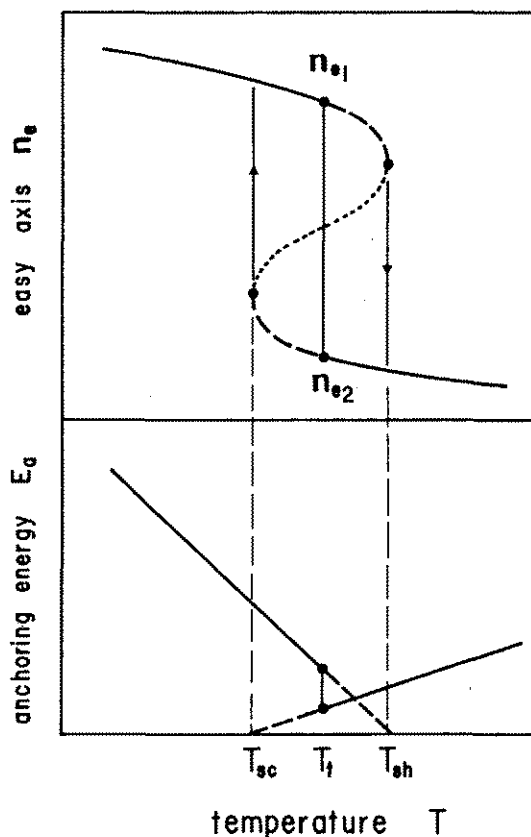


FIG.4.26. Discontinuous transition of the alignment and the relation with the anchoring energy. The broken lines correspond to a metastable region of the surface alignment, and the dotted line denotes the unstable region. At the end point of the metastable region, the anchoring strength vanishes.

Let us imagine that, as the temperature is increased in complete thermodynamic equilibrium, the easy direction n_e jumps abruptly from the lower branch with n_{e1} to the upper with n_{e2} at a transition temperature T_t . The thermodynamic potentials of upper and lower branches become identical at this temperature in the absence of orientational deformation. So that, the corresponding interfacial tensions, γ_{s1} and γ_{s2} , when expressed as functions of the strain, may be schematically drawn as in Fig.4.27 around T_t .

Analogous to liquid-vapor transitions, each branch is expected to be accompanied by a region of metastable orientation (broken line in the figure) which terminates at the temperature where the orientation becomes completely unstable. Further pursuing this analogy, we would expect that the metastable regions are connected with each other via the

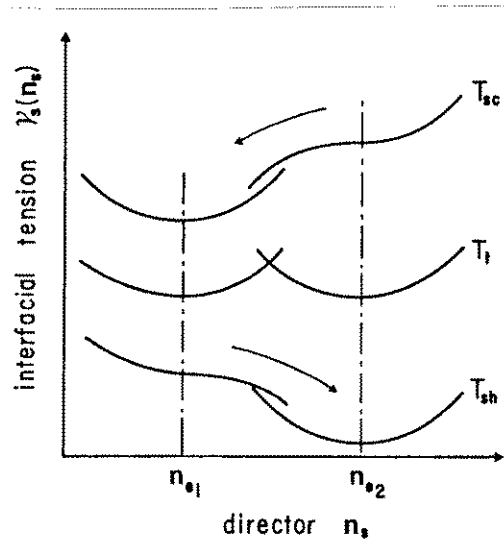


FIG.4.27. Behavior of the interfacial tension around the discontinuous transition point of the pretilt angle.

region of instability (dotted line), resulting in a sigmoidal curve as shown in Fig.4.26. Hence, there must be some degree of super heating and super cooling, which gives rise to a hysteretic behavior of the easy axis along heating and cooling cycles.

As clear from the figure, the boundary between the metastable and unstable regions is characterized by the divergence of $\partial n_e / \partial T$; in the case of liquid-vapor transition, this point corresponds to the "spinodal point." Therefore, according to the

present thermodynamics, which may be valid even in the metastable region, the anchoring strength has to vanish at this orientational spinodal point with a critical exponent satisfying Eq.(4.215). Now that the pretilt angle changes by a finite amount through the transition from one branch to the other, there is no reason to require the anchoring strength to be continuous, in contrast to the case of continuous transition of the pretilt angle. Accordingly, the anchoring strength is also expected to show a hysteretic behavior as illustrated in Fig.4.26.

4.9.3 Phase diagram for surface-induced alignment

As clear from the above arguments, the regions (in the phase diagram) which are separated by an alignment transition, be it continuous or discontinuous, are also demarcated by the line of zero anchoring strength, i.e., $d_e = \infty$ or $E_a = 0$. In the case of an n-component fluid in two-phase equilibria, the Gibbs phase rule indicates that the number of the degrees of freedom is n, apart from the orientational degrees of freedom. Therefore, the equation

$$E_a(T, P, \mu_j) = 0 \quad (4.217)$$

is to determine a hypersurface in this n-dimensional phase space.

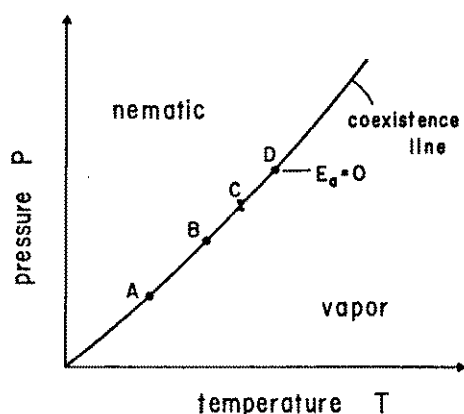


FIG.4.28. Alignment phase diagram for a single component nematic. Transition of the alignment or the anchoring strength occurs at isolated points on the coexistence curve.

In the case of a pure nematic substance, for example, the nematic-vapor coexistence line may be drawn as in Fig.4.28. Hence, due to Eq.(4.217), the zero anchoring strength, even if it might happen, should be in general realized only at isolated points on the coexistence line. Especially, when there are a couple of orientational spinodal points (B & D), the easy direction n_e becomes a multi-valued function in between these points, and undergoes a discontinuous change at C.

Let us next consider a two-component fluid. Then, Eq.(4.204) now specifies a line of zero anchoring strength in the phase space spanned by T, P, and c (the concentration of the second component) as shown in Fig.4.29. In the figure depicted is a situation in which the line in question is separated into several parts each of which corresponds to a different alignment transition. This is obviously a feature which is impossible to emerge in the case of a single component fluid. Within the region surrounded by a pair of orientational spinodal lines, terminating at the intercepts C and D with the lines of continuous alignment transition, n_e is again a multi-valued function.

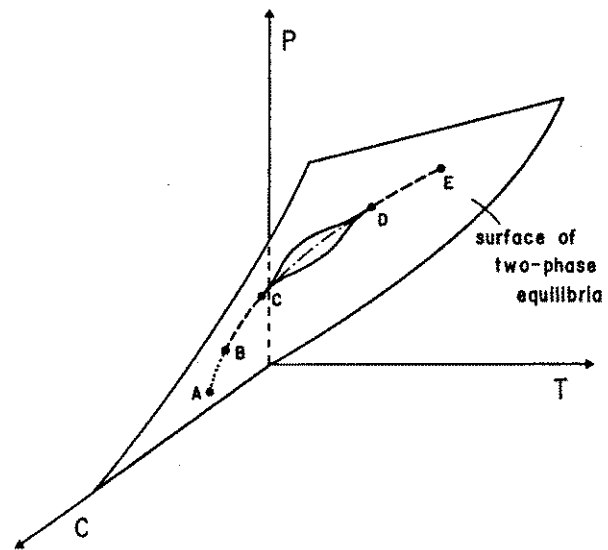


Fig.4.29. Alignment phase diagram for a two component system. the alignment transition occurs along a line on the equilibrium surface.

4.9.3 Experimental situation

For such substrates which induce an invariant alignment in nematics, the temperature-dependence of the anchoring strength has been so far measured only by a few authors. The substrates examined include a surfactant-treated glass [45], a vacuum-evaporated SiO film [1,46,47], and a rubbed polyvinylalcohol film. And, especially, in the first two cases, in which the alignments were homeotropic and planar respectively, the anchoring strengths were found to exhibit an apparently critical weakening toward the clearing temperature. The critical exponents are however between 0 and -1, and hence are inconsistent with the thermodynamic inequality, Eq.(4.215), characterizing the true critical behavior. This indicates that the weakening has to terminate at a finite value or to turn into a more singular one. For more details, see Chapter 7, where the measurements of the anchoring strength and their results are fully described.

The control of pretilt angles at a solid-nematic interface is one of the issues of greatest concern in LCD technology. As a result, its measurement have been quite extensively carried out in the last two decades[48]. Although the effects of temperature and of surface active agents on the pretilt angle on a solid surface have been examined sporadically, they were mostly qualitative, and moreover, no correlational study has been done to elucidate their connection with the anchoring strength. However, it should be pointed out that some cases are now known in which the pretilt angle undergoes a nearly critical change or a discontinuous transition. The results of those studies are compiled also in Chapter 7 with some thermodynamic discussions.

As far as the present author knows, the only one investigation which is truly comparable with the thermodynamic theory formulated in this section is the series of studies

conducted by Chiarelli, et al. [40,41], who measured the temperature-induced continuous transition of the pretilt angle and the concomitant change of the anchoring strength at a free surface of MBBA. They observed, as reproduced in Fig.4.30, that there is a critical temperature T_0 (about 1 K below the clearing point) toward which the polar angle of the director Θ_e tends to

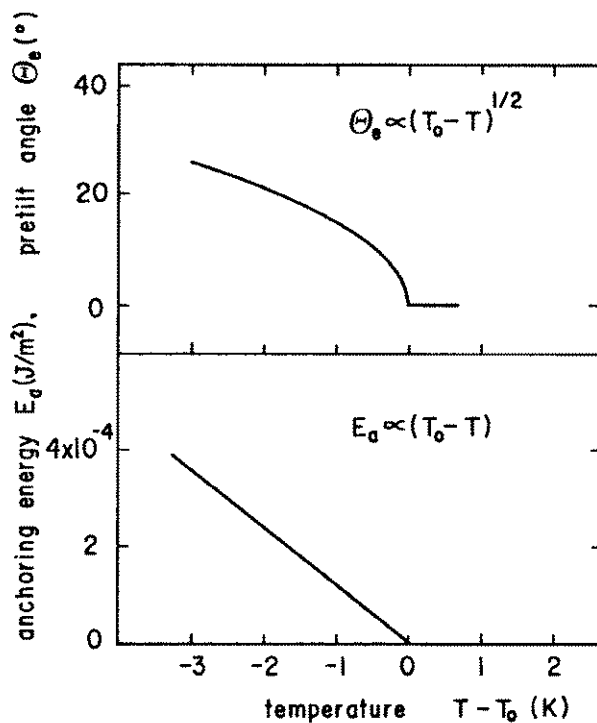


FIG.4.30. Critical behavior of the pretilt and the anchoring energy at the free surface of MBBA observed by Chiarelli et al. (Ref.40 and 41)

zero obeying $\Theta_e \sim B[(T_0 - T)/T_0]^{1/2}$, ($T < T_0$). And, above T_0 , the director remains perpendicular to the surface, i.e., the homeotropic alignment. Furthermore, they measured the temperature-dependence of the anchoring strength, showing that the anchoring energy decreases with temperature toward T_0 with a linear relationship $E_a \sim A(T_0 - T)/T_0$.

Because $\partial \Theta_e / \partial T$ diverges at T_0 , the present thermodynamic theory requires that the anchoring strength should vanish at T_0 . This is just what was observed in their experiments. Furthermore, it should be noted that the linear relationship they found is

consistent with the thermodynamic inequality for the critical exponent, Eq.(4.215).

Finally, it should be pointed out that for both pretilt angle and anchoring strength, no quantitative investigation has ever been made as to the influence of composition. However, as we have seen in the last three sub-sections, at an interface of a multicomponent nematic, even richer variety of orientational phenomena can be expected to occur than at an interface of a single component nematic. This appears to be a promising field open to future investigations.

Chapter 5

STATISTICAL MECHANICAL THEORIES

In the former chapter, we have made an extensive thermodynamic argument as to the orientational properties of a nematic interface subjected to a curvature stress, and have revised the concepts of the anchoring energy and of the extrapolation length, which have so far been naively understood based on the Rapini-Papoular formalism. The purpose of this chapter is to provide some microscopic bases for the surface-induced alignment phenomena so as to supplement the argument in the former chapter from a microscopic view point. Since our primary interest in this thesis is focused on the phenomenological description of the nematic interfaces, we will not make any attempt here to perform detailed statistical mechanical calculations to quantitatively predict the molecular alignment at nematic interfaces. Here, we shall be contented with setting a conceptual bridge between the macroscopic and the microscopic worlds, leaving such molecular approaches to the literature and future investigations.

The first two sections of this chapter are devoted to the development of rigorous statistical mechanical theories for the interfacial tension and the anchoring strength, respectively. Though the derivation of an exact formula for fundamental quantities characterizing the nematic interface is of interest in its own right, our present aim is, as emphasized above, to figure out the qualifications that an appropriate phenomenological description of the nematic interface should have. In the last four sections, we indeed show that the Landau-de Gennes type phenomenological theory of the nematic interface as developed by Sluckin and Poniewierski [1] is just of this kind; it is general

enough to take care of all the basic properties of a nematic interface, yet still simple enough to allow for easy treatment. Within this theoretical framework, we investigate several orientational phenomena of experimental interest such as (1) Orientational wetting transition, (2) Contact angle phenomena at nematic-isotropic transition, and (3) Interfacial anchoring. As we shall show in Chapters 6 and 7, the observations of those interfacial phenomena provide us with crucial and substantial information as to the orientational nature of the nematic interface. The theoretical development in the present chapter helps us appreciate the basic physics underlying the actual observations.

5.1 Statistical mechanical theory of the interfacial tension of nematics

5.1.1 Theoretical background

The interfacial tension of nematics, both in undeformed and in deformed states, plays a fundamental role for characterizing the orientational properties of a nematic interface. Since Kirkwood and Buff formulated an exact statistical mechanical expression of the surface tension of simple liquids, there have appeared quite a few attempts of rigorous formulation of various interfaces involving not only monatomic but also polyatomic (molecular) liquids [2]. Today, there are essentially two distinct approaches for deriving exact expressions for the interfacial tension [2]: one is the thermo-mechanical approach taken by Kirkwood and Buff [3], and the other is an approach based on the direct correlation function, due originally to Triezenberg and Zwanzig [4]. Though these approaches result in apparently distinct expressions based respectively on the intermolecular potential and the pair distribution function and on the density profile and the Ornstein-Zernike direct correlation function, they have recently been shown (almost rigorously) to be equivalent to each other [5,6].

Though both of these approaches were originally concerned with simple liquids (whose constituents have only translational degrees of freedom), these can be rather straightforwardly extended to the free surface of a polyatomic liquid, which has orientational degrees of freedom as well. Gray and Gubbins [7,8], and Davis[9] have derived a formally exact expression for the surface tension of molecular liquid in the Kirkwood-Buff form. The Triezenberg-Zwanzig approach has been extended to the free surface of molecular liquids by Sluckin [10]. Furthermore, Navascues and Berry [11] have applied the Kirkwood-Buff theory to

a wall-simple liquid interface, proving an exact formula for the boundary tension of a simple liquid to be useful in the study of adsorption at solid surfaces.

As we have seen in the former chapter, the surface of a nematic liquid crystal can be treated, when the bulk phase is free from orientational deformation, as if it were no different from the surface of ordinary molecular liquids. Hence, the exact formulas as mentioned above are directly applicable to the calculation of surface and interfacial tensions of nematics. Parsons [12], Murakami [13], Croxton [14], and Parsons [15] took this approach based on the Kirkwood-Buff formula, and obtained (with extensive approximations as to the density profile and the pair distribution function in the surface region, however) the surface tension [12-15], the pretilt angle [12,15], and the degree of orientational order near the interface [14,15].

There are several characteristic interfacial phenomena of (presumably) orientational origin which those molecular statistical theories have been aimed to explain: Firstly, it is of course the occurrence of an easy axis at an interface; secondly, the small but finite jump of the surface tension of nematics often observed at the temperature of the nematic to isotropic transition [16-20]; and, thirdly, the reversal of the temperature dependence of the surface tension in the vicinity of the nematic-isotropic transition point [16,17]. The theoretical treatments cited above are indeed partially successful for explaining these observations. It should be commented, however, that despite these endeavors, it is as yet hardly possible to satisfactorily trace back all the aspects of the actual nematic interfaces to the intermolecular interactions operating at the interface. Generally speaking, the degree of success of such a microscopic theory is very difficult to assess, because of the good deal of approximations often involved in such theories. Indeed, even when a certain theory

fails to explain one observation or the other, it is not usually clear which of the intermolecular interaction employed or the approximation is inadequate. Even more seriously, the orientational contribution to the interfacial tension is believed to occupy only a very small part ($10^{-1} \sim 10^{-5}$) of the entire tension of the interface. This is in part making the theoretical estimate of the orientational contribution extremely difficult. This situation clearly signifies the importance of a statistical mechanical route which allows for the construction of a at least "qualitatively" correct picture of the nematic interface.

In this section, we would like to show up some qualitative aspects of the interface between a rigid wall and an undeformed nematic from a statistical mechanical view point. Extending the theory due to Navascues and Berry [11], we derive a formally exact expression for the tension of a rigid wall-nematic interface taking explicit account of the steric repulsion between the wall and the nematic molecule. On the basis of this exact expression, we point out that the measurement of the contact angle at the nematic-isotropic-solid three-phase line of contact (to be observable at the clearing point) is a promising experiment for extracting information on the anisotropic interaction working at the interface.

The present formula for the interfacial tension consists of the contributions from the "direct interaction between the wall and the nematic" and from the "structural perturbation near the interface." The latter contribution, in particular, is the factor which most of the existing molecular theories of the nematic interface neglect, in spite of the fact that because of the long range nature of the orientational order in nematics, the structural variation induced by the solid has considerable influence on the orientational property of the nematic interface. As pointed out by Navascues and Berry, this point also indicates

the inadequacy of the Girifalco-Good-Fowkes "semi-empirical" equation, which has sometimes been applied to nematics for estimating the interfacial tension between a solid and a nematic from the knowledge of the individual surface tensions of the solid and the nematic phases. We will emphasize this point through the consideration of an exact criterion that the interfacial tension of nematics should obey.

The present exact formula provides a microscopic basis for the heuristic argument due to Okano [21] who showed that the anisotropic steric interaction between the wall and the nematic always favors a planar alignment. And it can also be expected to serve as a good conceptual background for the mean-field theories developed by Kimura [22-24], Telo da Gama [25,26], and Sullivan [27], which were shown to provide qualitatively good explanation for the alignment and tension at various nematic interfaces.

5.1.2 Formal expression of the wall-nematic interfacial tension

Let us consider a single component nematic in contact with a rigid and structureless wall in the absence of an external field. We imagine that the surface of the wall, i.e., the surface of zero-adsorption of the solid phase, is located at $z=0$, and that the nematic occupies the semi-infinite region $z>0$ [Fig.5.1]. We assume that the nematic is comprised of lath-like molecules as shown in Fig.5.2 whose orientation is

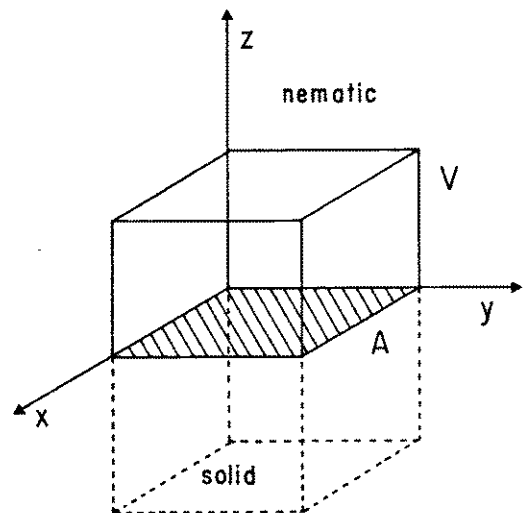


FIG.5.1. Geometry of the model.

fully specified by a unit vector ω . Here, we work with the Helmholtz free energy F of a volume V having the area A parallel to the interface. We assume that the nematic molecules are interacting via pairwise potential

$$\phi(\mathbf{r}_i, \omega_i, \mathbf{r}_j, \omega_j) = \phi_{ij},$$

and that the wall exerts a

potential $V_w(z, \omega)$ on nematic molecules, which we assume to be uniform in the plane parallel to the interface. We separate $V_w(z, \omega)$ into the long-range attractive part $V_a(z, \omega)$ and the steric repulsive part which goes to infinity when the molecule and the wall overlap with each other; namely, for each orientation ω , the center of mass of a molecule can approach up to the distance $Z(\omega)$ from the wall surface as shown in Fig.5.2.

Here, we follow the method of Navascues and Berry [11]. Let N and N_s be the number of molecules of the nematic and of the solid phases, respectively. Then, according to Eq.(4.6), the interfacial tension may be written as

$$\gamma = \left(\frac{\partial F}{\partial A} \right)_{T, V, N, N_s} \quad (5.1)$$

Because of the assumption of the rigid solid, it is immediately clear the Eq.(5.1) can also be written as

$$\gamma = \left(\frac{\partial F}{\partial A} \right)_{T, V_0, N} \quad (5.2)$$

where V_0 is the volume above the zero-adsorption plane of the solid phase ($z=0$).

Let Z_c be the configurational partition function defined by

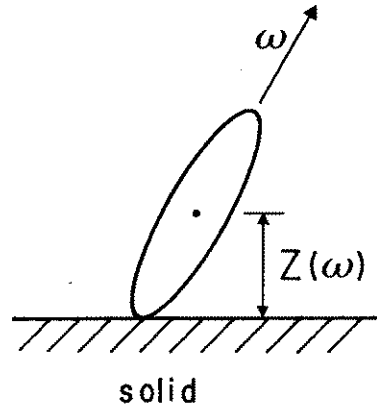


FIG.5.2. Nematic molecule in contact with a hard wall. Due to the hard core repulsion, a molecule with ω cannot come closer to the wall than $Z(\omega)$.

$$Z_C(T, V, A, N_s, N) = \frac{1}{N!} \int \{d\mathbf{r}d\omega\} \exp[-U_T/kT], \quad (5.3)$$

where $U_T(\mathbf{r}_1, \omega_1, \dots, \mathbf{r}_N, \omega_N)$ is the total potential energy of the system. Here, it should be noted that because of the rigidity of the solid, it is only necessary to integrate the Gibbs factor over the coordinate of the molecules in the nematic phase. By writing the kinetic part of the partition function as Z_{kin} , the Helmholtz free energy can now be given by

$$F = -kT \ln(Z_{kin}Z_C). \quad (5.4)$$

Therefore, using Eq.(5.4) in Eq.(5.1), we obtain

$$\gamma = -kT \frac{1}{Z_C} \left(\frac{\partial Z_C}{\partial A} \right)_{T, V, N, N_s}. \quad (5.5)$$

The total internal energy can be dividing into the following three contributions,

$$U_T = U_{ss} + U_{sn} + U_{nn}, \quad (5.6)$$

corresponding to the solid-solid, solid-nematic, and nematic-nematic interactions. Due to the assumption of the rigid solid, the first term is completely determined for given A and N_s . In terms of the intermolecular and the wall-nematic potentials, we may further write

$$U_{sn} = \sum_i V_w(\mathbf{r}_i, \omega_i), \quad \text{and} \quad U_{nn} = \sum_{i>j} \phi(\mathbf{r}_i, \omega_i, \mathbf{r}_j, \omega_j). \quad (5.7)$$

Denoting $U_{sn}+U_{nn}$ by U_T^* , the configurational partition function can be decoupled into the part coming from the solid-solid interaction and that from the rest of the internal energy U_T^* :

$$Z_C = \exp[-U_{ss}/kT] \cdot \frac{1}{N!} \int \{d\mathbf{r}d\omega\} \exp[-U_T^*/kT] \equiv Z_{ss} \cdot Z^*. \quad (5.8)$$

Consequently, using Eq.(5.8) in Eq.(5.5), we see that the interfacial tension can also be split into individual contributions to give

$$\gamma = \gamma_S + \gamma^*, \quad (5.9)$$

where

$$\gamma_S = -kT \frac{1}{Z_{SS}} \left(\frac{\partial Z_{SS}}{\partial A} \right)_{T, V, N_S} = \left(\frac{\partial U_{SS}}{\partial A} \right)_{T, N_S}, \quad (5.10)$$

$$\gamma^* = -kT \frac{1}{Z^*} \left(\frac{\partial Z^*}{\partial A} \right)_{T, V_0, N_S}. \quad (5.11)$$

γ_S and γ^* are, respectively, the surface tension of the solid phase and the boundary tension of the nematic phase with respect to the dividing surface located at the point of zero-adsorption of the solid phase [see Section 4.4.3].

The calculation of γ^* can be readily facilitated by means of a modified Green's method [28]. Let L_x , L_y , and L_z be the lengths of the nematic volume in question along x-, y-, and z-axes, respectively [see Fig.5.3]; i.e.,

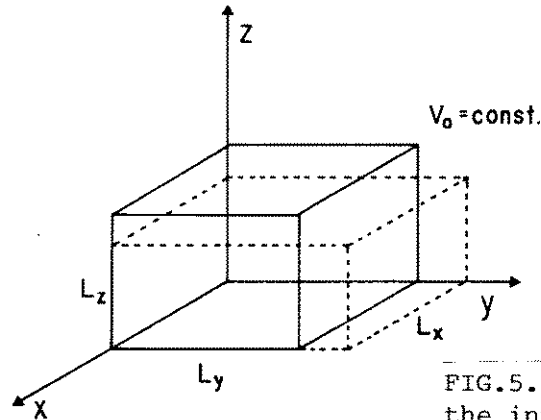


FIG.5.3. Variation of the interface area at constant volume.

$V_0 = L_x L_y L_z$. Green's method consists in the change of integration variables in such a way that the volume change can be entirely cast into the change in interaction potentials:

$$x' = x/L_x, \quad y' = y/L_y, \quad (5.12)$$

and, here, in order to take explicit account of the hard-core interaction between the wall and the nematic, we especially define

$$z' = [z - Z(\omega)] / [L_z - Z(\omega)], \quad (5.13)$$

for each molecular orientation ω . The Jacobian associated with this scaling transformation of linear dimension is not simply the volume V_0 as in the original Green's method, but is given by

$$\begin{aligned} J(\{\omega\}) &= \frac{\partial(\mathbf{r}'_1, \mathbf{r}'_2, \dots, \mathbf{r}'_N)}{\partial(\mathbf{r}'_1, \mathbf{r}'_2, \dots, \mathbf{r}'_N)} \\ &= (L_x L_y)^N \prod_{i=1}^N [L_z - Z(\omega_i)]. \end{aligned} \quad (5.14)$$

Thus, in terms of the new variables, the partition function Z^* can be written as

$$\begin{aligned} Z^* &= \frac{1}{N!} \int d\omega_1 \dots d\omega_N \int_0^1 dx'_1 \int_0^1 dy'_1 \int_0^1 dz'_1 \dots \int_0^1 dz'_N J(\{\omega\}) \\ &\quad \times \exp\{-[\sum_i V_a(\mathbf{r}_i, \omega_i) + \sum_{i>j} \phi(\mathbf{r}_i, \omega_i, \mathbf{r}_j, \omega_j)] / kT\}. \end{aligned} \quad (5.15)$$

in which the range of integration on z' has been restricted beyond $z'=0$ in view of the hard-core repulsion between the wall and the nematic, and hence the full singlet potential V_w due to the wall has been replaced by its attractive part V_a .

In order to calculate γ^* , we chose to differentiate Z^* by L_y at fixed V_0 and N ; note here that, since the interfacial tension is now defined as a surface-excess thermodynamic potential per unit area [Eq.(4.11)], it should not in equilibrium depend on the manner in which the interface is expanded; further, it must be strictly discerned from the surface stress [29].

The L_y -derivative of Z^* consists of two terms resulting from the derivative of the Jacobian and that of the Gibbs factor. For example, since the Jacobian is differentiated at constant volume to give

$$\frac{\partial}{\partial L_y} J(\{\omega\}) = -(1/L_y) J(\{\omega\}) \left\{ \sum_i \frac{Z(\omega_i)}{L_z - Z(\omega_i)} \right\}, \quad (5.16)$$

it is readily confirmed on account of Eqs.(5.11) and (5.15) that this term gives rise to a contribution to the interfacial tension as

$$\gamma^{*(J)} = \frac{kT}{A} \int_{V_0} d\mathbf{r} d\omega \frac{Z(\omega)}{L_z - Z(\omega)} \rho(\mathbf{r}, \omega), \quad (5.17)$$

after transforming back to the original variables, where $\rho(\mathbf{r}, \omega)$ is the density of a molecule with the orientation ω at the point \mathbf{r} . In much the same manner, we get the part which comes from the derivatives of the Gibbs factor:

$$\begin{aligned} \gamma^{*(G)} = & \frac{1}{2A} \int d\mathbf{r}_1 d\omega_1 d\mathbf{r}_2 d\omega_2 \left[y_{12} \frac{\partial \phi_{12}}{\partial y_{12}} - z_{12} \frac{\partial \phi_{12}}{\partial z_{12}} \right] \\ & \times \rho_2(\mathbf{r}_1, \omega_1, \mathbf{r}_2, \omega_2) \\ & - \frac{1}{A} \int d\mathbf{r} d\omega z \frac{\partial v_a(z, \omega)}{\partial z} \rho(\mathbf{r}, \omega) \\ & - \frac{1}{A} \int d\mathbf{r}_1 d\omega_1 d\mathbf{r}_2 d\omega_2 \left[\frac{z_1 - L_z}{L_z - Z(\omega_1)} Z(\omega_1) \frac{\partial \phi_{12}}{\partial z_{12}} \right] \\ & \times \rho_2(\mathbf{r}_1, \omega_1, \mathbf{r}_2, \omega_2) \\ & - \frac{1}{A} \int d\mathbf{r} d\omega \frac{z - L_z}{L_z - Z(\omega)} Z(\omega) \frac{\partial v_a(z, \omega)}{\partial z} \rho(\mathbf{r}, \omega), \end{aligned} \quad (5.18)$$

where $\rho_2(\mathbf{r}_1, \omega_1, \mathbf{r}_2, \omega_2)$ is the pair distribution function, and y_{12} and z_{12} denote $y_1 - y_2$ and $z_1 - z_2$, respectively. Furthermore, upon using the first member of the Yvon-Born-Green hierarchy [2],

$$\begin{aligned} kT \frac{\partial}{\partial z_1} \rho(\mathbf{r}_1, \omega_1) - \rho(\mathbf{r}_1, \omega_1) \frac{\partial}{\partial z_1} v_a(z_1, \omega_1) \\ = \int d\mathbf{r}_2 d\omega_2 \frac{\partial}{\partial z} \phi_{12} \rho_2(\mathbf{r}_1, \omega_1, \mathbf{r}_2, \omega_2), \end{aligned}$$

which rigorously holds for $z_1 > Z(\omega_1)$ at present. The last two terms of Eq.(5.18) can be transformed, in combination with

Eq.(5.17), to a surface term, and we finally obtain

$$\begin{aligned}
 \gamma^* = & \frac{1}{2} \int dz_1 \int d\omega_1 d\mathbf{r}_2 d\omega_2 \left[y_{12} \frac{\partial \phi_{12}}{\partial y_{12}} - z_{12} \frac{\partial \phi_{12}}{\partial z_{12}} \right] \\
 & \times \rho_2(z_1, \omega_1, \mathbf{r}_2, \omega_2) \\
 & - \int dz d\omega z \frac{\partial V_a(z, \omega)}{\partial z} \rho(z, \omega) \\
 & + kT \int d\omega Z(\omega) \rho[Z(\omega)+0, \omega].
 \end{aligned} \tag{5.19}$$

Here, we have used the fact that $\rho(\mathbf{r}, \omega) = \rho(z, \omega)$.

This offers an exact statistical mechanical expression for the boundary tension at a rigid solid-nematic liquid crystal interface. This is a generalization of the result of Navascues and Berry [11] to a polyatomic liquid interface. We see that γ^* is comprised of two qualitatively distinct contributions $\gamma^*(1)$ and $\gamma^*(2)$ which represent, respectively, the part of the interaction among nematic molecules and that of the direct interaction between the solid and the nematic:

$$\gamma^* = \gamma^*(1) + \gamma^*(2), \tag{5.20}$$

where $\gamma^*(1)$ stands for the first term in Eq.(5.19), and $\gamma^*(2)$ the remaining two terms. Note that in the absence of the solid wall, Eq.(5.19) reduces to the exact formulas derived by Gray and Gubbins [7,8], and Davis [9] for molecular liquid surfaces, which also applies to a free surface of a nematic liquid and to a nematic-isotropic interface. Finally, it is of interest to point out that the last term of the above represents the contribution of the hard-core interaction between the rigid wall and the nematic, and as such, it provides a formal proof for the result due to Okano [21]. Namely, the last term in Eq.(5.19) tends to orient nematic molecules parallel to the interface so as to increase the packing entropy. Evidently, this is one of many factors which

may influence the alignment at the interface, and the true orientation should be determined via the competition among the various contributions existing in Eq.(5.19).

**A. Separation into isotropic and anisotropic contributions:
Contact angle at the nematic-isotropic-solid three-phase line of
contact [18-20]**

Concerning the orientational property of a nematic interface, the point of primary interest is the anisotropic part of the interfacial tension. And, it is indeed the aim of experiments to extract that part from various observations of a nematic interface.

In order to gain some insight from the present exact formula into this point, it is convenient to separate the density into the isotropic and the anisotropic part:

$$\begin{aligned} \rho(z, \omega) &= \langle \rho(z, \omega) \rangle_{\omega} + \rho_a(z, \omega) \\ &\equiv \rho_o(z) + \rho_a(z, \omega), \end{aligned} \quad (5.21)$$

$$\begin{aligned} \rho_2(\mathbf{r}_1, \omega_1, \mathbf{r}_2, \omega_2) &= \langle \rho_2(\mathbf{r}_1, \omega_1, \mathbf{r}_2, \omega_2) \rangle_{\omega_1, \omega_2} \\ &\quad + \rho_{2a}(\mathbf{r}_1, \omega_1, \mathbf{r}_2, \omega_2), \end{aligned} \quad (5.22)$$

where $\langle \rangle_{\omega}$ denotes an unweighted average over ω , and $\rho_a(z, \omega)$ represents the anisotropic part of the density which vanishes when averaged over the molecular orientation. In terms of the radial distribution function $g(\mathbf{r}_1, \omega_1, \mathbf{r}_2, \omega_2)$, the pair distribution function can be written as

$$\rho_2(\mathbf{r}_1, \omega_1, \mathbf{r}_2, \omega_2) = \rho(\mathbf{r}_1, \omega_1) \rho(\mathbf{r}_2, \omega_2) g(\mathbf{r}_1, \omega_1, \mathbf{r}_2, \omega_2).$$

Then, we can also make a division of the pair distribution function as follows:

$$\begin{aligned} \rho_2(\mathbf{r}_1, \omega_1, \mathbf{r}_2, \omega_2) = & \rho_o(z_1) \rho_o(z_2) \langle g(\mathbf{r}_1, \omega_1, \mathbf{r}_2, \omega_2) \rangle_{\omega_1, \omega_2} \\ & + \rho_{2a}(\mathbf{r}_1, \omega_1, \mathbf{r}_2, \omega_2), \end{aligned} \quad (5.23)$$

where the last term is the collection of all the anisotropic terms.

Corresponding to these distinctions between the isotropic and the anisotropic parts, the interfacial tension is also seen to be divided into the respective parts:

$$\gamma^* = \gamma_{iso}^* + \gamma_a^*, \quad (5.24)$$

and hence, by adding γ_s to both sides, we have

$$\gamma = \gamma_{iso} + \gamma_a^*, \quad (5.25)$$

where γ_a^* is the anisotropic part which comes from ρ_a and ρ_{2a} . As clear from the course of derivation, γ_{iso} is the interfacial tension between the solid and a reference "simple" liquid in which the orientation dependence of the nematic phase is smeared out. Obviously, the anisotropic part of the nematic-nematic and the wall-nematic interactions contributes only to γ_a^* .

According to the generalized van der Waals theory of nematic interfaces due to Telo da Gama [25,26], the interfacial tension between a nematic and a vapor, and even that between a nematic and its isotropic liquid are primarily dominated by the change of (orientation-averaged) density across the interface; it should be pointed out, however, that Sluckin [1] argued that the dominance of the density change at the nematic-isotropic interface is an artifact of the model of Telo da Gama. Anyway, unless the interfacial tension is extremely small as in the case of nematic-isotropic interface, we can conceive that γ_{iso} is the main contribution to the total interfacial tension.

Let us now consider the contact angle of a drop of a nematic liquid crystal placed on a solid surface [Fig.5.4]. On negligence of a small effect due to gas adsorption on the solid surface, we see from Young's equation that the contact angle of the nematic θ should satisfy

$$\gamma_S = \gamma_{sn} + \gamma_{nv} \cos \theta, \quad (5.26)$$

where γ_{sn} is the solid-nematic interfacial tension, i.e., γ in the present notation. So that, according to Eqs.(5.23) and (5.24), we find

$$-\gamma^*/\gamma_{vn} = -(\gamma_{iso}^* + \gamma_a^*)/\gamma_{vn} = \cos \theta. \quad (5.27)$$

Therefore, except for an accidental case in which γ_{iso}^* becomes as small as γ_a^* , the anisotropic contribution to the contact angle is obscured by the isotropic contribution.

Next we consider a contact angle of a nematic droplet in a bit different setting as shown in Fig.5.5. Here, the nematic drop is placed at the interface between its own isotropic liquid, which is coexisting with the nematic phase at the transition temperature, and a solid wall. We can show that the contact angle α gives a direct measure of γ_a^* .

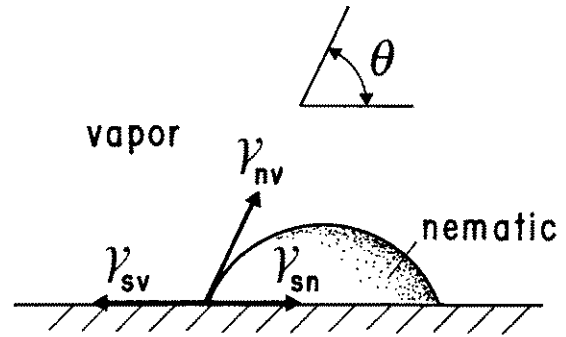


FIG.5.4. Contact angle of a nematic drop at a solid-vapor interface.

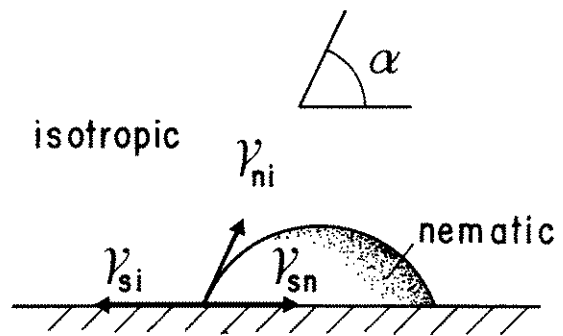


FIG.5.5 Contact angle of a nematic drop at a solid-isotropic interface

Since the density of a nematic liquid crystal changes only less than one percent across the nematic-isotropic transition, it is expected to be a good approximation, at least near the clearing temperature, to assume that $\langle \rho(z, \omega) \rangle_\omega$ and $\langle g(r_1, \omega_1, r_2, \omega_2) \rangle_{\omega_1, \omega_2}$ is invariant across the nematic-isotropic transition. Under this condition, the relevant interfacial tensions can be written as

$$\gamma_{sn} = \gamma_{iso} + \gamma_{an}^* \quad (5.28)$$

$$\gamma_{si} = \gamma_{iso} + \gamma_{ai}^* \quad (5.29)$$

where γ_{an}^* and γ_{ai}^* are the anisotropic parts of the solid-liquid interfacial tension when the liquid is in the nematic and the isotropic states at T_c , respectively. Using Eqs.(5.28) and (5.29) in the relevant Young's equation, we obtain

$$\frac{\gamma_{ai}^* - \gamma_{an}^*}{\gamma_{ni}} = \cos \alpha. \quad (5.30)$$

This equation clearly shows that the contact angle of the nematic liquid at the nematic-isotropic-solid three-phase line of contact at the temperature of nematic-isotropic coexistence is determined only by the anisotropic part of the interfacial tension and the tension of the nematic-isotropic interface. So, in contrast to the ordinary contact angles at a solid-vapor interface, the contact angle α is expected to provide direct information on the anisotropic nature of the solid-nematic interface.

Extensive measurements [18-20] of this type of contact angle at various solid-nematic systems will be described in Chapter 7.

5.1.3 Fundamental properties of the tension of a solid wall-undeformed nematic interface

A. Work of adhesion and related problems

The work of adhesion between a solid and a nematic liquid can be defined in the same manner as for an ordinary liquid-solid system. Let us imagine that, initially the solid and the nematic liquid are separated by a large distance, being in equilibrium with their vapor phase, and then are reversibly put into contact with each other to form a planar interface [Fig.5.6]. Now the work of adhesion is defined as the amount of work which the system can perform to the environment during this process. Obviously, it can be equivalently defined as the work needed to reversibly separate the solid and the nematic liquid to infinite distance.

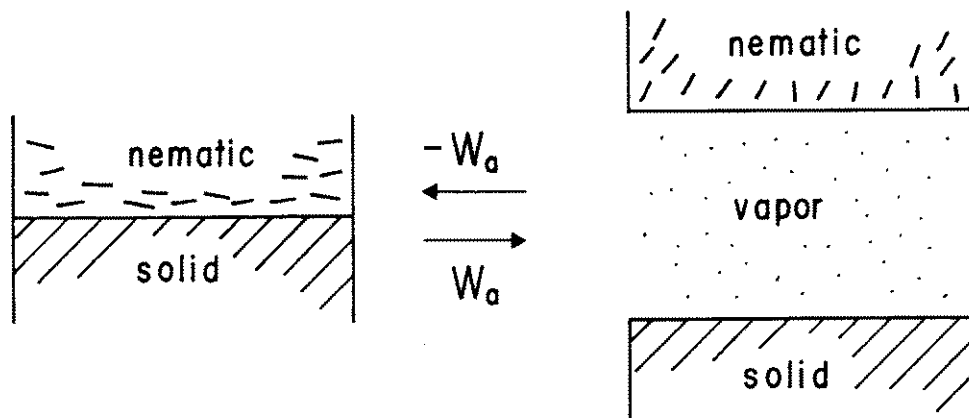


FIG.5.6. Defining process of the work of adhesion between a solid and a nematic liquid crystal.

Let us denote the tensions of the solid-nematic, solid-vapor, and nematic-vapor interfaces by γ_{sn} , γ_{sv} and γ_{nv} respectively. Then, by definition, the work of adhesion W_a can be written as

$$W_a = \gamma_{vn} + \gamma_{sv} - \gamma_{sn}. \quad (5.31)$$

By subtracting the surface tension of the solid γ_S from γ_{sv} and from γ_{sn} , Eq.(5.31) can be rewritten in the form,

$$W_a = \gamma_{vn} + \gamma_{sv}^* - \gamma_{sn}^*, \quad (5.32)$$

where the asterisk on the last two terms denotes the boundary tension defined in the former section.

Navascues and Berry [11] devised a convenient way to clearly show up the underlying physics of Eq.(5.32). The procedure of separation of the nematic and the solid as depicted in Fig.5.6 can be regarded as a sequence of two stages [see Fig.5.7] as follows: In the first stage, the nematic liquid is removed from the solid without changing the density profile, i.e. a mere translation of $\rho(z, \omega)$; and in the second, the nematic is relaxed to its equilibrium nematic-vapor density profile. Let us denote the

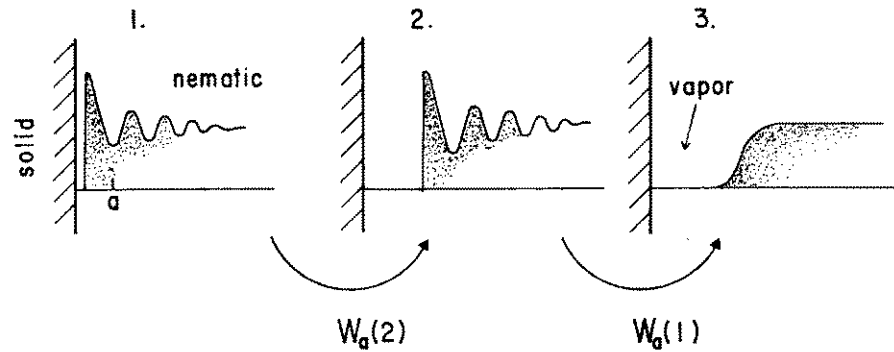


FIG.5.7. Two stages of separation between a nematic and a solid wall. From 1 to 2, the interfacial structure of the liquid is fixed, and from 2 to 3, it is allowed to relax.

amount of work associated with these two processes by $W_a(2)$ and $W_a(1)$, then we readily find from Eqs.(5.19) and (5.20) that

$$W_a = W_a(2) + W_a(1), \quad (5.33)$$

where

$$W_a(2) = - \gamma^*(2), \quad (5.34)$$

$$W_a(1) = \gamma_{nv} - \gamma^*(1). \quad (5.35)$$

Here, we have neglected γ_{sv}^* in comparison with γ_{sn}^* , because

the density in the vapor phase is much smaller than that in the nematic phase near its triple point; as shown in Eq.(5.19), γ^* is at least linear in the density in the medium in contact with the solid.

Equation (5.33) shows that the work of adhesion between a solid and a nematic consists of the (solid-nematic) interaction term $W_a(2)$ and the relaxation term $W_a(1)$. In contrast to the simple liquid treated by Navascues and Berry [11], the relaxation term of a polyatomic liquid involves the contribution from the relaxation of the orientational structure in the interfacial region. In particular, since the nematic liquid crystal has a long range orientational order, such an orientational relaxation will not be localized within a few molecules distance from the interface, as is often the case for oscillating density profile found at a wall-simple liquid interface, but will extend over a range on the order of the coherence length of the nematic order. This situation is shown in Fig.5.8 in relation to the two stages of separation as already conceived.

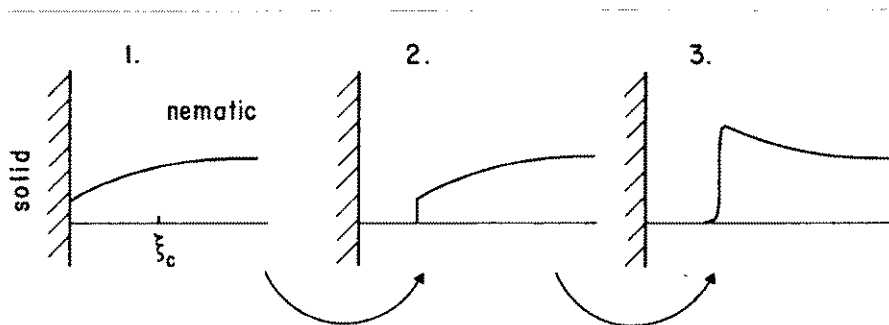


FIG.5.8. Changes of the order parameter profile near the interface associated with the two stages of separation. Here, the order parameter changes over the length of the order of coherence length ξ_c , which is much larger than the atomic dimension a .

The importance of this long-ranged orientational structure near the interface is indeed one of the most striking factors of the nematic interface, which is deeply reflected in its various macroscopic properties such as those listed at the beginning of this section. We will present some more examples of relevant experimental observations in Chapters 6 and 7.

1. Girifalco-Good-Fowkes theory of the work of adhesion

In the light of the present theory, we would like to briefly review the conventional theories of the work of adhesion, which have been applied to the problem of the surface-induced alignment.

The theory due to Girifalco and Good [30,31] and its second version extended by Fowkes [32] are the best-known and the most frequently used theory of the solid-liquid interfacial tension. Their theory rests on the direct calculation of the force acting between a solid and a liquid media on an assumption that the arrangement of molecules in these phases are invariant regardless of the separation between them. In analogy with the Berthelot relation between unlike molecules, they have write down the work of adhesion between two media, a and b, in terms of the surface tensions of a and b:

$$W_{ab} = 2\Phi(\gamma_a\gamma_b)^{1/2}, \quad (5.36)$$

and hence the interfacial tension γ_{ab} as

$$\gamma_{ab} = \gamma_a + \gamma_b - 2\Phi(\gamma_a\gamma_b)^{1/2}. \quad (5.37)$$

And, by direct calculation of the force between them, Φ is expressed in terms of the molar volume of consituents, V_a and V_b , as follows:

$$\Phi = 4V_a^{1/3}V_b^{1/3}/(V_a^{1/3}+V_b^{1/3})^2. \quad (5.38)$$

And they showed that for most organic liquids, Φ is something around unity. Furthermore, Fowkes considered the contributions of

the various intermolecular interactions, i.e. polar (p), dispersion (d), hydrogen-bonding (h), etc., to be independent, and expressed the interfacial tension as a sum of each contribution:

$$\gamma = \gamma(p) + \gamma(d) + \gamma(h) + \dots \quad (5.39)$$

And, he applied Eq.(5.37) with $\phi=1$ to each component of the interfacial tension.

In spite of this clearly very crude nature of the theory, it is now widely accepted that the formula reproduces the interfacial tension fairly well in a wide range of materials. However, it should be strictly emphasized that, the theory is not at all rigorous, but is intended to provide an empirical formula for the interfacial tension which is not readily measurable. As they themselves admitted [30], the formula may involve an error as large as a few 10^{-3} J/m², and thus it can be regarded as a good one if and only if an error of this level is permissible.

The orientational part of the interfacial tension γ_a^* is, if it can be identified with the anchoring energies, in reality less than 10^{-3} J/m². It seems to shed considerable doubt on the applicability of this theory to the surface-alignment of liquid crystals unless it is subjected to close scrutiny.

As pointed out by Navascues and Berry, the source of error in the Girifalco-Good-Fowkes theory is hard to assess from a rigorous statistical mechanical point of view. However, the apparent drawback of their theory is the neglect of the possible structural relaxations near the interface. In an attempt to calculate the alignment and anchoring energy at a solid-nematic interface, Mada [33], Okano and Murakami [34], Bernasconi, et al.[35], and Okano, et al. [36] have employed a similar approach to calculate the interfacial tension between a nematic and a solid based on the Lifshitz theory of van der Waals force. They assumed the

structure of those media are everywhere bulklike, and compared the interaction free energies when the nematic director is parallel or perpendicular to the interface. In this respect, their theories are essentially identical with the Girifalco-Good-Fowkes theory, thereby suffering from the same pitfall as the latter. Below we present one example which clearly demonstrates the importance of a structural consideration so as to reach a correct picture of the nematic interface.

B. Rigorous criteria for the interfacial tension of nematics

Let us consider a nematic interface at the temperature of nematic-isotropic transition. And, we address a question how large a discontinuity the interfacial tension can experience as the bulk phase transforms from one phase to the other.

Since the interfacial tension for a planar interface is an excess thermodynamic potential per unit area, it must assume the minimum value in equilibrium at constant temperature and chemical potential. It can therefore be shown that the absolute difference between γ_n and γ_i , which are respectively the interfacial tensions when the bulk phase is in the nematic and the isotropic phases, is bounded by the nematic-isotropic interfacial tension:

$$|\gamma_n - \gamma_i| \leq \gamma_{ni}. \quad (5.40)$$

This inequality follows immediately from the consideration of the situation as shown in Fig.5.9.

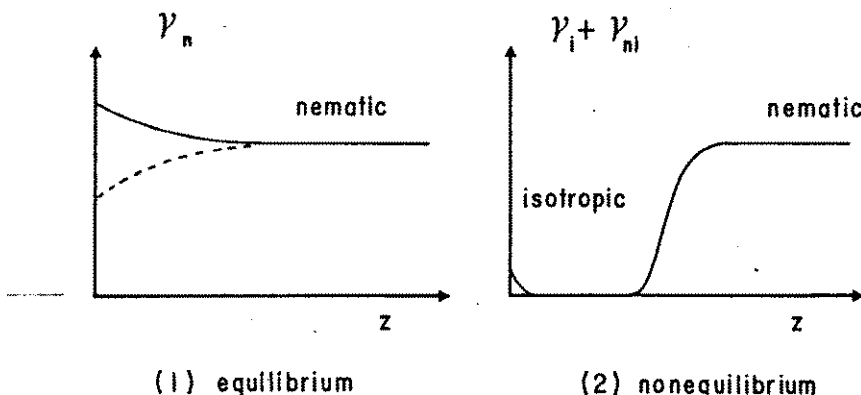


FIG.5.9. Schematic proof of the inequality. By placing a macroscopic layer of the isotropic liquid between the substrate and the nematic phase, the resulting interfacial tension must be larger than the equilibrium value.

For example, when it happens that

$$\gamma_i > \gamma_n + \gamma_{ni} \quad (5.41)$$

we can reduce the interfacial tension γ_i , at worst, to $\gamma_n + \gamma_{ni}$ by placing a macroscopic layer of the nematic liquid in between the wall or vapor and the isotropic bulk phase. However, since the real system can do even better, we must always have

$$\gamma_i \leq \gamma_n + \gamma_{ni} \quad (5.42)$$

By exchanging the role of the nematic and the isotropic phases, we can similarly obtain

$$\gamma_n \leq \gamma_i + \gamma_{ni} \quad (5.43)$$

It completes the proof of the desired inequality. This is a rigorous criterion, first explicitly pointed out by Telo da Gama [25], which a nematic interface should obey at the nematic-isotropic transition temperature. As clear from this heuristic argument, when the equality holds, we expect that the nematic or the isotropic liquid completely wets the interface intruding in between the two phases in contact. This condition is often violated in mean-field calculations in which the structure relaxation near the nematic interface is neglected.

5.2 Density functional theory of the anchoring strength

So far in this chapter, we have considered only a nematic interface in the absence of bulk orientational deformations. This section is devoted to a theoretical study of how a bounded nematic behaves under an externally applied curvature stress, with a view to formulating a statistical mechanical expression for the anchoring strength. For the sake of brevity, we shall restrict our attention to a nematic in contact with a rigid and structureless wall, which can be expected to serve as a good model of a real solid-nematic interface.

5.2.1 Introduction

As we have already shown in Chapter 4, the anchoring strength at a nematic interface is a kind of surface-specific elastic constant which describes the response of the interface to a curvature stress existing in the bulk nematic [see section 4.7.3]. Recently, several rigorous statistical mechanical theories have been developed for the bulk elastic constants of condensed media including liquid crystals [37-42]. In comparison with the classical molecular theories of curvature elasticity [43-48], those theories share distinctive characteristics in common. Namely, the microscopic structure of the matter plays the primary role, while the molecular interaction between constituent particles are implicitly taken into account through the structure. By virtue of this property, the elastic constants, which are always defined in relation to structural perturbations, can be rigorously expressed in terms of structural correlation functions. In view of the "fluctuation-dissipation theorem," it appears quite natural that such structural approaches have been far more successful than conventional interaction-based approaches.

The density functional theory [2], on which those structure-

oriented theories are invariably based, was originally developed as a tool to treat interacting electron gas. Later, however, it has proved to be remarkably useful in the study of inhomogeneous liquids. It offers a general and systematic way to treat the statistical mechanical aspects of structural problems. In this section, we apply the density functional theory to the interface involving an orientationally deformed nematic, and on the basis of the thermodynamic definition of the anchoring strength as given in the former chapter, we develop a formally exact structure-based expression for the extrapolation length. Furthermore, by discriminating the "energetic" and the "geometrical" extrapolation lengths, which coincide with each other in equilibrium, we prove a simple variational property that these extrapolation lengths to obey. And, by using a simple trial function, we show that the extrapolation length consists of two distinct contributions which respectively allow interpretations as coming from the interaction between the wall and the nematic and from the interfacial anomaly of the Frank elastic constants. Finally, we will shortly discuss the problem concerning the second order elasticity.

5.2.2 Density functional theory

Here, we summarize some fundamental concepts and formulas of the density functional theory [2,10] so as to aid the understanding of later arguments.

We consider a single component liquid comprised of rod like molecules in the volume V under an external potential V_{ext} . We assume that the molecule is rigid so that its position can be specified by \mathbf{r} and the orientation by a unit vector ω along the long axis of the molecule. We consider a grand canonical ensemble at temperature T and chemical potential μ ; then the equilibrium probability density f for N molecules can be written as

$$\bar{f}_0 = \Xi^{-1} \exp[-(H_N - \mu N)/kT], \quad (5.44)$$

where k is the Boltzmann constant, and H_N the Hamiltonian for N molecules given by

$$H_N = \sum_{i=1}^N T_i + U(\mathbf{r}_1, \omega_1, \dots, \mathbf{r}_N, \omega_N) + \sum_{i=1}^N V_{\text{ext}}(\mathbf{r}_i, \omega_i),$$

with T_i being the kinetic energy of the i -th molecule and U being the potential energy due to intermolecular interactions. And, Ξ represents the grand partition function, which is connected with the grand thermodynamic potential Ω via

$$\Omega = -(1/kT) \ln \Xi \quad (5.45)$$

The equilibrium density $\rho_0(\mathbf{r}, \omega)$ is given as an ensemble average of the density operator $\hat{\rho}(\mathbf{r}, \omega) = \sum \delta(\mathbf{r} - \mathbf{r}_i) \delta(\omega - \omega_i)$:

$$\rho_0(\mathbf{r}, \omega) = \langle \hat{\rho}(\mathbf{r}, \omega) \rangle, \quad (5.46)$$

where $\langle \rangle$ denotes the ensemble average.

It is clear from the above equations that, once the external potential V_{ext} is given, the probability density f_0 and hence $\rho(\mathbf{r}, \omega)$ are determined at every temperature and chemical potential. Furthermore, it is possible to prove that the converse is also true, namely that for an arbitrary $\rho(\mathbf{r}, \omega)$, there exists a unique external potential which gives rise, in equilibrium, to the density in question [2]. Thus, it becomes possible to conceive \bar{f}_0 as a functional of $\rho(\mathbf{r}, \omega)$. Consequently, we can define the key quantity in the density functional theory, the "intrinsic" Helmholtz free energy $F_{\text{in}}[\rho]$, as a functional of the density by

$$\begin{aligned} F_{\text{in}}[\rho] &= T_r \bar{f}_0(\sum T_i + U + kT \ln \bar{f}_0), \\ &= \langle \sum T_i + U + kT \ln \bar{f}_0 \rangle \end{aligned} \quad (5.47)$$

where T_r is the trace operator performing the configurational

average in the phase space. The other important quantity is the grand thermodynamic potential (also a functional of ρ) which is defined by

$$\Omega[\rho] = \int d\mathbf{r}d\omega \rho(\mathbf{r}, \omega) V_{\text{ext}} + F_{\text{in}}[\rho] - \mu \int d\mathbf{r}d\omega \rho(\mathbf{r}, \omega). \quad (5.48)$$

It is readily confirmed that at the equilibrium density ρ_0 , the above functional correctly gives the equilibrium thermodynamic potential. It is also shown that the equilibrium thermodynamic potential is the minimum value of the $\Omega[\rho]$:

$$\Omega[\rho_0] < \Omega[\rho], \quad (5.49)$$

for any $\rho \neq \rho_0$. This condition is essentially equivalent to the thermodynamic inequality Eq.(4.186) specifying the criterion of equilibrium. Hence by taking the functional derivative of Eq.(5.48), we get

$$0 = V_{\text{ext}}(\mathbf{r}, \omega) + \mu_{\text{in}}[\rho_0; \mathbf{r}, \omega] - \mu, \quad (5.50)$$

where μ_{in} is the intrinsic chemical potential defined by

$$\mu_{\text{in}}[\rho; \mathbf{r}, \omega] = \frac{\delta F_{\text{in}}[\rho]}{\delta \rho}. \quad (5.51)$$

Let $\Phi[\rho] = F_{\text{id}}[\rho] - F_{\text{in}}[\rho]$, where $F_{\text{id}}[\rho]$ is the Helmholtz free energy of the ideal gas as given by

$$F_{\text{id}}[\rho] = kT \int d\mathbf{r}d\omega \rho(\mathbf{r}, \omega) \{ \ln[\lambda^3 \rho(\mathbf{r}, \omega) - 1] \}, \quad (5.52)$$

where $\lambda^3 = z_{\text{kin}}$ is the kinetic part of the partition function due to rotational as well as translational motions of the molecule. As obvious, $\Phi[\rho]$ represents the contribution from the intermolecular interaction.

The hierarchy of correlation functions can be generated by

successive functional differentiation of $\Phi[\rho]$ as follows:

$$C[\rho; \mathbf{r}, \omega] = (1/kT) \frac{\delta \Phi[\rho]}{\delta \rho(\mathbf{r}, \omega)}, \quad (5.53)$$

$$\begin{aligned} C[\rho; \mathbf{r}_1, \omega_1, \mathbf{r}_2, \omega_2] &= (1/kT) \frac{\delta^2 \Phi[\rho]}{\delta \rho(\mathbf{r}_1, \omega_1) \delta \rho(\mathbf{r}_2, \omega_2)} \\ &= (1/kT) \frac{\delta^2 \Phi[\rho]}{\delta \rho(\mathbf{r}_2, \omega_2) \delta \rho(\mathbf{r}_1, \omega_1)} = C[\rho; \mathbf{r}_2, \omega_2, \mathbf{r}_1, \omega_1], \end{aligned} \quad (5.54)$$

and so on.

On using Eq.(5.53) in Eq.(5.50), the equilibrium density is expressed as

$$\rho_o(\mathbf{r}, \omega) = \lambda^{-3} \exp(\mu/kT) \exp\{-V_{\text{ext}}(\mathbf{r}, \omega)/kT + c[\rho_o; \mathbf{r}, \omega]\}. \quad (5.55)$$

so that, $-kTc[\rho_o; \mathbf{r}, \omega]$ gives the additional, effective one-body potential which self-consistently determines the equilibrium density. The second member of the correlation functions, $c[\rho_o; \mathbf{r}_1, \omega_1, \mathbf{r}_2, \omega_2]$, is referred to as the Ornstein-Zernike direct correlation function, which satisfies the well-known Ornstein-Zernike equation in combination with the two-body density-density correlation function.

Finally, we would like to note the following identity, which derives readily from the definitions of the direct correlations functions. Imagine that the density is continuously changed from that of some reference fluid, $\rho_r(\mathbf{r}, \omega)$, according to

$$\rho_\alpha = \rho_r + \alpha(\rho - \rho_r), \quad (5.56)$$

in which α changes from 0 to 1. Then, starting from the obvious identity,

$$\Phi[\rho] = \Phi[\rho_r] + \int_0^1 \partial \Phi[\rho_\alpha] / \partial \alpha \, d\alpha, \quad (5.57)$$

we readily obtain

$$\begin{aligned}
\Phi[\rho] = & \Phi[\rho_r] + kT \int d\mathbf{r} d\omega [\rho(\mathbf{r}, \omega) - \rho_r(\mathbf{r}, \omega)] c[\rho_r; \mathbf{r}, \omega] \\
& + kT \int_0^1 d\alpha \int_0^1 d\alpha' \int d\mathbf{r}_1 d\omega_1 \int d\mathbf{r}_2 d\omega_2 \alpha [\rho(\mathbf{r}_1, \omega_1) - \rho_r(\mathbf{r}_1, \omega_1)] \\
& \quad \times [\rho(\mathbf{r}_2, \omega_2) - \rho_r(\mathbf{r}_2, \omega_2)] c[\rho_{\alpha\alpha'}; \mathbf{r}_1, \omega_1, \mathbf{r}_2, \omega_2].
\end{aligned}
\tag{5.58}$$

5.2.3 Statistical expression for the extrapolation length

A. Grand thermodynamic potential in an orientationally deformed state

Let us consider the equilibria of a semi-infinite nematic liquid crystal bounded by a rigid and structureless wall, and take the rectangular coordinate with its origin at the point of zero-adsorption of the wall as shown in Fig.5.10. As in Section 5.1, the rigidity of the wall allows us to disregard the wall variables, and to assume that its effect is only to produce an external potential $V_w(z, \omega)$ acting on the nematic. We imagine that the nematic and the wall are both uniform in the plane parallel to the wall surface (x-y plane). In order to apply the thermodynamic definition of the anchoring strength, Eq.(4.179b), we need first to calculate the grand thermodynamic potential in the presence of a curvature stress. Here, we conceive that the director deformation is brought about by an orientational force applied a point well inside the bulk nematic, and in conformity with the thermodynamics, we only con-

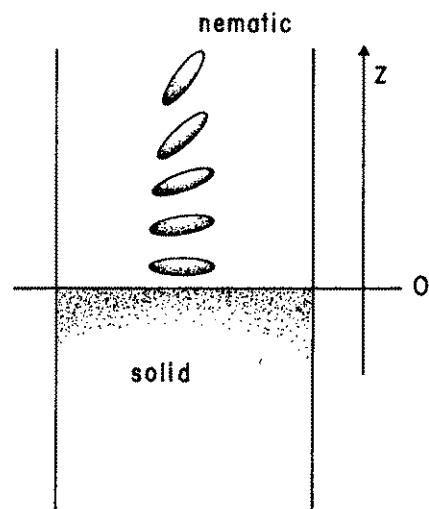


FIG.5.10. Rigid solid-nematic interface under a curvature stress.

sider the region where such an artificial field is absent, so that the nematic can be regarded as being deformed only elastically.

In the bulk nematic, the macroscopic alignment of the nematic should obey the Frank theory of elasticity as long as the deviation from the uniform orientation is of sufficiently long wave-length. Thus, as discussed in Section 4.4.1, the state of the system must be completely specified by the elastic energy density f_d , which is uniform in the bulk nematic, and the variable β indicating the mode of deformation. Once f_d and β are given, therefore, the density is uniquely given at any point in the nematic in question as $\rho(f_d, \beta; \mathbf{r}, \omega)$. By denoting the density in the absence of bulk orientational deformation as $\rho_o(\mathbf{r}, \omega)$, we define

$$\delta\rho(f_d, \beta; \mathbf{r}, \omega) = \rho(f_d, \beta; \mathbf{r}, \omega) - \rho_o(\mathbf{r}, \omega). \quad (5.59)$$

Expansion of Ω in powers of $\delta\rho$ can be readily carried out by way of Eq.(5.58). If we regard ρ_o as the reference density, then, up to second order in $\delta\rho$, we can set

$$c[\rho_{\alpha\alpha'}; \mathbf{r}_1, \omega_1, \mathbf{r}_2, \omega_2] = c[\rho_o; \mathbf{r}_1, \omega_1, \mathbf{r}_2, \omega_2],$$

in Eq.(5.58). Furthermore, because Ω should be minimum at ρ_o , there appears no term linear in $\delta\rho$. Hence, by making use of Eqs.(5.48), (5.52), and (5.58), we get

$$\begin{aligned} \Omega[\rho] = \Omega[\rho_o] + (kT/2) \int d\mathbf{r}_1 d\omega_1 d\mathbf{r}_2 d\omega_2 \delta\rho(f_d, \beta; \mathbf{r}_1, \omega_1) \\ \times \delta\rho(f_d, \beta; \mathbf{r}_2, \omega_2) C_2[\rho_o; \mathbf{r}_1, \omega_1, \mathbf{r}_2, \omega_2], \end{aligned} \quad (5.60)$$

where

$$\begin{aligned} C_2[\rho_o; \mathbf{r}_1, \omega_1, \mathbf{r}_2, \omega_2] = \frac{\delta(\mathbf{r}_1 - \mathbf{r}_2) \delta(\omega_1 - \omega_2)}{\rho_o(\mathbf{r}_1, \omega_1)} \\ - c[\rho_o; \mathbf{r}_1, \omega_1, \mathbf{r}_2, \omega_2]. \end{aligned} \quad (5.61)$$

B. Frank elastic energy and the statistical mechanical formulation of elastic constants

In order to obtain the expression of the interfacial tension, it is necessary to identify the part which approaches the Frank elastic energy density f_d as z goes to infinity. For this purpose, we utilize the following identity:

$$\begin{aligned} \delta\rho(\mathbf{r}_1, \omega_1)\delta\rho(\mathbf{r}_2, \omega_2) = & \\ & \frac{1}{2}[\delta\rho(\mathbf{r}_1, \omega_1)\delta\rho(\mathbf{r}_1, \omega_2) + \delta\rho(\mathbf{r}_2, \omega_1)\delta\rho(\mathbf{r}_2, \omega_2)] \\ & + \frac{1}{2}[\delta\rho(\mathbf{r}_1, \omega_1)\delta\rho(\mathbf{r}_2, \omega_2) - \delta\rho(\mathbf{r}_1, \omega_2)\delta\rho(\mathbf{r}_2, \omega_1)] \\ + \frac{1}{2}[\delta\rho(\mathbf{r}_1, \omega_1) - \delta\rho(\mathbf{r}_2, \omega_1)][\delta\rho(\mathbf{r}_2, \omega_2) - \delta\rho(\mathbf{r}_1, \omega_2)], \end{aligned} \quad (5.62)$$

where the dependence on f_d and β is not written explicitly for the sake of simplicity. Substituting Eq.(5.62) into Eq.(5.60), we obtain

$$\begin{aligned} \Omega[\rho] = \Omega[\rho_0] & \\ + (kT/2) \int d\mathbf{r}_1 d\omega_1 d\mathbf{r}_2 d\omega_2 \delta\rho(\mathbf{r}_1, \omega_1)\delta\rho(\mathbf{r}_1, \omega_2) & \\ \quad \times c_2[\rho_0; \mathbf{r}_1, \omega_1, \mathbf{r}_2, \omega_2] & \\ - (kT/4) \int d\mathbf{r}_1 d\omega_1 d\mathbf{r}_2 d\omega_2 \delta\rho(\mathbf{r}_1, \omega_1)\delta\rho(\mathbf{r}_2, \omega_2) & \\ \quad \times (c[\rho_0; \mathbf{r}_1, \omega_1, \mathbf{r}_2, \omega_2] - c[\rho_0; \mathbf{r}_2, \omega_1, \mathbf{r}_1, \omega_2]) & \\ + (kT/4) \int d\mathbf{r}_1 d\omega_1 d\mathbf{r}_2 d\omega_2 [\delta\rho(\mathbf{r}_1, \omega_1) - \delta\rho(\mathbf{r}_2, \omega_1)] & \\ \quad \times [\delta\rho(\mathbf{r}_1, \omega_2) - \delta\rho(\mathbf{r}_2, \omega_2)] c[\rho_0; \mathbf{r}_1, \omega_1, \mathbf{r}_2, \omega_2], & \end{aligned} \quad (5.63)$$

where use has been made of the symmetry property of the Ornstein-Zernike direct correlation function, Eq.(5.54).

It follows from Eq.(5.63) that the thermodynamic potential can be rewritten in the form,

$$\Omega[\rho] = \Omega[\rho_0] + \int f(\mathbf{r}) d\mathbf{r}, \quad (5.64)$$

$$f(\mathbf{r}) = f_1(\mathbf{r}) + f_2(\mathbf{r}) + f_3(\mathbf{r}), \quad (5.65)$$

where

$$f_1(\mathbf{r}) = (kT/2) \int d\mathbf{u} d\omega_1 d\omega_2 \delta\rho(\mathbf{r}, \omega_1) \delta\rho(\mathbf{r}, \omega_2) \\ \times c_2[\rho_0; \mathbf{r}, \omega_1, \mathbf{r}+\mathbf{u}, \omega_2],$$

$$f_2(\mathbf{r}) = - (kT/4) \int d\mathbf{u} d\omega_1 d\omega_2 \delta\rho(\mathbf{r}, \omega_1) \delta\rho(\mathbf{r}+\mathbf{u}, \omega_2) \\ \times \{c[\rho_0; \mathbf{r}, \omega_1, \mathbf{r}+\mathbf{u}, \omega_2] - c[\rho_0; \mathbf{r}+\mathbf{u}, \omega_1, \mathbf{r}, \omega_2]\},$$

$$f_3(\mathbf{r}) = (kT/4) \int d\mathbf{u} d\omega_1 d\omega_2 [\delta\rho(\mathbf{r}, \omega_1) - \delta\rho(\mathbf{r}+\mathbf{u}, \omega_1)] \\ \times [\delta\rho(\mathbf{r}, \omega_2) - \delta\rho(\mathbf{r}+\mathbf{u}, \omega_2)] c[\rho_0; \mathbf{r}, \omega_1, \mathbf{r}+\mathbf{u}, \omega_2].$$

In the uniformly oriented bulk nematic, it follows from the translational and rotational symmetry of the nematic phase [49] that

$$c[\rho_0; \mathbf{r}, \omega_1, \mathbf{r}+\mathbf{u}, \omega_2] = c[\rho_0; 0, \omega_1, \mathbf{u}, \omega_2] \\ = c[\rho_0; -\mathbf{u}, \omega_1, 0, \omega_2] \\ = c[\rho_0; \mathbf{u}, \omega_1, 0, \omega_2] \\ = c[\rho_0; \mathbf{r}+\mathbf{u}, \omega_1, \mathbf{r}, \omega_2], \quad (5.66)$$

so that, $f_2(\mathbf{r})$ should disappear as $z \rightarrow \infty$. Furthermore, in case the nematic is subjected only to an infinitesimal curvature stress under constant temperature and chemical potential, the density can be written, upon negligence of terms on the order of f_d , in the following form [cf. Eq.(4.93)]:

$$\rho(\mathbf{r}, \omega) = \rho_0(\mathbf{n} \cdot \omega), \quad (5.67)$$

where \mathbf{n} represents the local "director" at \mathbf{r} . Consequently,

$\delta \rho$ reduces to

$$\delta \rho(\mathbf{r}, \omega) = \rho'_0(\mathbf{n} \cdot \omega)(\delta \mathbf{n} \cdot \omega), \quad (5.68)$$

where the prime over ρ_0 denotes the differentiation with respect to $\mathbf{n} \cdot \omega$. Hence, in the bulk nematic, $f_1(z)$ can be regarded, to first order in f_d , as an extra energy needed to homogeneously rotate the orientation of a nematic by $\delta \mathbf{n}$. As well known, a uniform rotation of the director is a Goldstone mode [50] in the nematic phase, namely a mode which does not require any external work for its excitation; hence, $f_1(\mathbf{r})$ is also seen to vanish in the bulk phase. Therefore, $f_1(\mathbf{r})$ and $f_2(\mathbf{r})$ are non-zero only in the vicinity of the nematic-wall interface, due respectively to the break down of the Goldstone degeneracy and of the inversion symmetry.

As a result of the above property, we are left only with $f_3(\mathbf{r})$ in an infinitesimally deformed bulk nematic; thus it should be identified with the Frank elastic energy density. Here, we show that a rigorous expression for the Frank elastic constants immediately follows from the present formalism in complete agreement with the result due to Poniewierski and Stecki based on the rather complicated star-integral approach. For a director configuration which is spatially slowly varying about the easy direction \mathbf{n}_e , we obtain from Eq.(5.68),

$$\delta \rho(\mathbf{r}, \omega) - \delta \rho(\mathbf{r} + \mathbf{u}, \omega) \sim -u_z \rho'_0(\mathbf{n}_e \cdot \omega) \frac{d\mathbf{n} \cdot \omega}{dz}. \quad (5.69)$$

where we have used the fact that the density is one-dimensionally varying only along the z-axis, i.e., $\rho(\mathbf{r}, \omega) = \rho(z, \omega)$.

Using Eqs.(5.68) and (5.69), $f_3(\mathbf{r})$ can be expressed in the form,

$$f_3(\mathbf{r}) = \frac{1}{2} K_{ij} \frac{dn_i}{dz} \frac{dn_j}{dz}, \quad (5.70)$$

where

$$K_{ij} = (kT/2) \int d\mathbf{u} d\omega_1 d\omega_2 u_z^2 \rho_0(\mathbf{n}_e \cdot \omega_1) \rho_0(\mathbf{n}_e \cdot \omega_2) \times \omega_{1i} \omega_{2j} c[\rho_0; \mathbf{u}, \omega_1, \theta, \omega_2]$$

$$= K_{ji}. \quad (5.71)$$

When $\mathbf{n} \sim \mathbf{n}_e$ holds, $d\mathbf{n}/dz$ can be approximately written as

$$\frac{d\mathbf{n}}{dz} \sim \frac{d\theta}{dz} \mathbf{n}_p + \sin\theta_e \frac{d\phi}{dz} \mathbf{n}_a, \quad (5.72)$$

where θ and ϕ are the spherical polar angles of \mathbf{n} , and \mathbf{n}_p and \mathbf{n}_a are the unit vectors perpendicular to \mathbf{n}_e as shown in Fig.5.11; in Section 4.6, they have been referred to as the polar and the azimuthal vectors, respectively. Introducing Eq.(5.72) into Eq.(5.70), we find

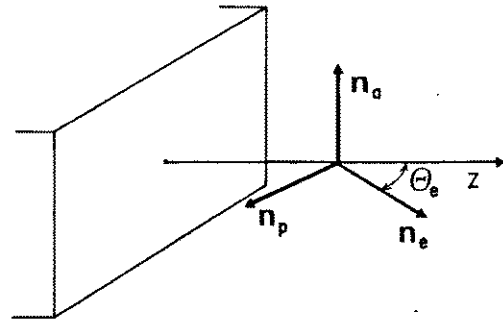


FIG.5.11. Definition of the unit vectors.

$$f_3(\mathbf{r}) = \frac{1}{2} (K_{ij} n_{pi} n_{pj}) \left(\frac{d\theta}{dz} \right)^2 + \frac{1}{2} (K_{ij} n_{ai} n_{aj}) \sin^2 \theta_e \left(\frac{d\phi}{dz} \right)^2, \quad (5.73)$$

where the cross term has been eliminated due to the reflection symmetry in the uniform nematic about the plane including \mathbf{n}_e . In order that this equation becomes identical with the Frank elastic energy density in an infinitesimal deformation, cf. Eq.(4.63), it is necessary and sufficient that

$$K_{ij} n_{pi} n_{pj} = K_1 \sin^2 \theta_e + K_3 \cos^2 \theta_e$$

and

$$K_{ij} n_{ai} n_{aj} = K_2 \sin^2 \theta_e + K_3 \cos^2 \theta_e, \quad (5.74)$$

where summations over the subscripts i and j are of course

implied.

As shown in Fig.5.11, \mathbf{U} can be decomposed as

$$\mathbf{U} = u_e \mathbf{n}_e + u_p \mathbf{n}_p + u_a \mathbf{n}_a,$$

and hence we get

$$u_z^2 = u_e^2 \cos^2 \theta_e + 2u_e u_p \sin \theta_e \cos \theta_e + u_p^2 \sin^2 \theta_e. \quad (5.75)$$

Substituting Eq.(5.75) into Eq.(5.74) by way of Eq.(5.71) and comparing the coefficients of $\cos^2 \theta_e$ and $\sin^2 \theta_e$, we finally obtain

$$K_1 = (kT/2) \int d\mathbf{U} d\omega_1 d\omega_2 u_p^2 \rho'(\mathbf{n}_e \cdot \omega_1) \rho'(\mathbf{n}_e \cdot \omega_2) \\ \times \omega_{1p} \omega_{2p} c[\rho_0; \mathbf{U}, \omega_1, 0, \omega_2],$$

$$K_2 = (kT/2) \int d\mathbf{U} d\omega_1 d\omega_2 u_p^2 \rho'(\mathbf{n}_e \cdot \omega_1) \rho'(\mathbf{n}_e \cdot \omega_2) \\ \times \omega_{1a} \omega_{2a} c[\rho_0; \mathbf{U}, \omega_1, 0, \omega_2],$$

$$K_3 = (kT/2) \int d\mathbf{U} d\omega_1 d\omega_2 u_e^2 \rho'(\mathbf{n}_e \cdot \omega_1) \rho'(\mathbf{n}_e \cdot \omega_2) \\ \times \omega_{1p} \omega_{2p} c[\rho_0; \mathbf{U}, \omega_1, 0, \omega_2],$$

$$= (kT/2) \int d\mathbf{U} d\omega_1 d\omega_2 u_e^2 \rho'(\mathbf{n}_e \cdot \omega_1) \rho'(\mathbf{n}_e \cdot \omega_2) \\ \times \omega_{1a} \omega_{2a} c[\rho_0; \mathbf{U}, \omega_1, 0, \omega_2],$$

(5.76)

where ω_p and ω_a denote $\omega \cdot \mathbf{n}_p$ and $\omega \cdot \mathbf{n}_a$, respectively; the term involving $u_e u_p$ disappears on symmetry ground. These equations offer the exact statistical mechanical expressions for the Frank elastic constants, in complete agreement with the results given by Poniewierski and Stecki [37].

5.2.4 The extrapolation length

We can now derive the statistical mechanical expression for the anchoring strength at the rigid-wall nematic interface on the basis of the thermodynamic definition of the anchoring strength Eq.(4.179b). As regards a planar interface between a rigid wall and a single component nematic, the definition can be readily translated to give

$$\lim_{f_d \rightarrow 0} \left(\frac{\partial \gamma^*}{\partial f_d} \right)_{T, \mu, \beta} = d_e, \quad (5.77)$$

where d_e is the extrapolation length, which in the present geometry is given by

$$d_e = z_d - z_{ex}. \quad (5.78)$$

Here, γ^* is the "boundary tension" with respect to the dividing surface located at z_d , and z_{ex} represents the point of extrapolation.

As noted in Section 4.4.3, the boundary tension for the interface of an orientationally deformed nematic must be written as

$$\gamma^* = (\Omega - \Omega_a)/A \quad (5.79)$$

where Ω_a is the thermodynamic potential for the hypothetical volume of the nematic which is assumed to be completely bulklike right up to the dividing surface, i.e.,

$$\Omega = \Omega_0 + V f_d. \quad (5.80)$$

Here, Ω_0 is the thermodynamic potential of the hypothetical volume in the absence of an orientational deformation.

In order to apply the above equations to the density functional formulas derived in the previous section, it is sufficient to recall the fact that as $z \rightarrow \infty$, $f(\mathbf{r})$, as defined in

Eq.(5.65), approaches the Frank elastic energy density f_d . Thus, it is immediately clear that the boundary tension can be written as

$$\gamma^* = \gamma_0^* + \frac{1}{A} \int d\mathbf{r} (z-z_d) \frac{\partial}{\partial z} f(\mathbf{r}), \quad (5.81)$$

where γ_0^* denotes the boundary tension in the absence of deformation. On using the fact that $f_1(\mathbf{r})$ and $f_2(vR)$ are localized near the interface, Eq.(5.81) can be further transformed to

$$\gamma^* = \gamma_0^* + \frac{1}{A} \int d\mathbf{r} [f_1(\mathbf{r}) + f_2(\mathbf{r}) + (z-z_d) \frac{\partial}{\partial z} f_3(\mathbf{r})]. \quad (5.82)$$

Now it is a straightforward task to derive the desired expression, by substituting Eq.(5.82) into Eq.(5.77). In order to make the resulting equation compact, let us introduce a position-dependent density response function $\eta(z, \omega)$ to a curvature stress applied in the bulk nematic:

$$\eta(z, \omega) = \lim_{f_d \rightarrow 0} \left(\frac{\partial \rho [f_d, \beta; z, \omega]}{\partial f_d^{1/2}} \right)_{T, \mu, \beta}. \quad (5.83)$$

Then, combining Eqs.(5.64), (5.82), and (5.83) with Eq.(5.77), we obtain

$$\begin{aligned} d_e = & \frac{kT}{2A} \int d\mathbf{r} \int d\mathbf{u} d\omega_1 d\omega_2 \eta(z, \omega_1) \eta(z, \omega_2) \\ & \times C_2[\rho_0; \mathbf{r}, \omega_1, \mathbf{r}+\mathbf{u}, \omega_2] \\ & - \frac{kT}{4A} \int d\mathbf{r} \int d\mathbf{u} d\omega_1 d\omega_2 \eta(z, \omega_1) \eta(z+u_z, \omega_2) \\ & \times (c[\rho_0; \mathbf{r}, \omega_1, \mathbf{r}+\mathbf{u}, \omega_2] - c[\rho_0; \mathbf{r}+\mathbf{u}, \omega_1, \mathbf{r}, \omega_2]) \\ & + \frac{kT}{4A} \int d\mathbf{r} (z-z_d) \frac{\partial}{\partial z} \int d\mathbf{u} d\omega_1 d\omega_2 [\eta(z, \omega_1) - \eta(z+u_z, \omega_1)] \\ & \times [\eta(z, \omega_2) - \eta(z+u_z, \omega_2)] c[\rho_0; \mathbf{r}, \omega_1, \mathbf{r}+\mathbf{u}, \omega_2]. \end{aligned} \quad (5.84)$$

This equation rigorously expresses the extrapolation length in terms of the density response function and the Ornstein-Zernike direct correlation function in the uniform nematic liquid crystal. Clearly, the first and the second terms are, roughly speaking, concerned with the broken symmetry in the vicinity of the interface, and the third with the anomaly of the curvature elasticity.

As apparent from its definition, the density response function is the one which vanishes steeply as one moves across the interface from the nematic liquid toward the wall. Because of this quasi-singularity near the interface, it is not necessarily a straightforward task to construct a reliable approximation scheme for $\eta(z, \omega)$ near the interface. So, it becomes sometimes desirable to transform the above equation into an equivalent form which involves only a less singular response function except for the density itself. This can be facilitated by normalizing $\eta(z, \omega)$ by the equilibrium density in the undeformed state; we define

$$\bar{\eta}(z, \omega) = \eta(z, \omega) / \rho_0(z, \omega). \quad (5.85)$$

It can be shown that $\bar{\eta}(z, \omega)$ is continuous even across an interface between a hard repulsive wall and a fluid consisting of hard molecules [51]. Similarly, we define

$$\begin{aligned} \bar{c}[\rho_0; \mathbf{r}_1, \omega_1, \mathbf{r}_2, \omega_2] &= \rho_0(\mathbf{r}_1, \omega_1) \rho_0(\mathbf{r}_2, \omega_2) \\ &\quad \times c[\rho_0; \mathbf{r}_1, \omega_1, \mathbf{r}_2, \omega_2], \end{aligned} \quad (5.86)$$

and also

$$\begin{aligned} \bar{C}_2[\rho_0; \mathbf{r}_1, \omega_1, \mathbf{r}_2, \omega_2] &= \rho_0(\mathbf{r}_1, \omega_1) \rho_0(\mathbf{r}_2, \omega_2) \\ &\quad \times C_2[\rho_0; \mathbf{r}_1, \omega_1, \mathbf{r}_2, \omega_2]. \end{aligned}$$

Then, repeating the same procedure by which we have derived Eq.(5.84), we arrive at the same expression as Eq.(5.84) but with the following exchanges, $\eta \rightarrow \bar{\eta}$, $c \rightarrow \bar{c}$, and $C_2 \rightarrow \bar{C}_2$, incorporated.

It is finally worth noting that, in the bulk nematic where the state of its orientation is specified by the director, the density response function $\eta(z, \omega)$ reduces to

$$\begin{aligned} \eta(z, \omega) &= \rho_0 (\mathbf{n}_e \cdot \omega) \frac{\partial \mathbf{n} \cdot \omega}{\partial f_d}^{1/2} \\ &= \rho_0 (\mathbf{n}_e \cdot \omega) \left\{ \pm [2/K_3 f(\theta_e)]^{1/2} \left[1 - \frac{\beta}{g(\theta_e)} \right]^{1/2} (z_0 - z) (\mathbf{n}_p \cdot \omega) \right. \\ &\quad \left. \mp (2/K_3 \beta)^{1/2} [z_0 - z]_{\text{ex}} - \frac{\beta}{g(\theta_e)} (z_0 - z) \right\} \sin \theta_e (\mathbf{n}_a \cdot \omega), \end{aligned} \quad (5.87)$$

which follows directly from Eq.(4.155); z_0 is a constant corresponding to r_0 . Consequently, $\eta(z, \omega)$ and $\bar{\eta}(z, \omega)$ turn out to be a linear function of z in the bulk nematic for each mode of deformation specified by β .

5.2.5 Variational principle

It is possible to prove, based on the minimum property of the thermodynamic potential, that the extrapolation length satisfies a simple variational principle when regarded as a functional of the density response function $\eta(z, \omega)$. For this purpose, we need to distinguish two types of extrapolation lengths which derive respectively from the energetic and the geometrical significances of the extrapolation length.

We consider such distribution of nematic molecules at fixed temperature and chemical potential that correspond, in the region sufficiently far from the interface, to some equilibrium state specified by an appropriate set of f_d and β ; that is, we are to take up only those density profiles in which a deviation from the equilibrium one, if any, should be localized near the wall-nematic interface. As pointed out in Section 4.6, the point of extrapolation has, on the one hand, a meaning as the point where

the director, when the bulk profile is extrapolated to the interface region, approaches closest to the easy axis \mathbf{n}_e [based on the measure of length as defined in Eq.(4.156)]. We shall refer to the extrapolation length in this sense as the "geometrical" extrapolation length, and denote it as $d_e(G)$.

On the other hand, as embodied by the thermodynamic definition of the extrapolation length itself, we can interpret it as giving a distance over which the bulk nematic should be extrapolated so as to regard the increase in the interfacial tension due to the curvature stress as entirely a bulk contribution [see Sections 4.5.3 and 4.5.4]. Also writing the boundary tension in nonequilibrium case as γ^* , this "energetic" extrapolation length $d_e(E)$ is thus given by

$$d_e(E) = \Delta\gamma^*/f_d, \quad (5.88)$$

where $\Delta\gamma^*$ denotes the orientational part of the boundary tension. In equilibrium, we have of course

$$d_e(E) = d_e(G). \quad (5.89)$$

Let $\eta(z, \omega)$ be an arbitrary (not necessarily equilibrium) density response function which is constrained to approach the equilibrium form, Eq.(5.87), as $z \rightarrow \infty$. And, we shall regard the extrapolation length d_e as given by Eq.(5.84) as a functional of $\eta(z, \omega)$. As clear from the course of derivation, $d_e[\eta]$ is just the energetic extrapolation length $d_e(E)$ associated with the change in density,

$$\delta\rho(z, \omega) = f_d^{1/2} \eta(z, \omega). \quad (5.90)$$

We begin with the consideration of the minimum condition of the thermodynamic potential for a total system including both the system in question and its environment [see Fig.12]:

$$\Omega_t = \Omega + \Omega_{env}. \quad (5.91)$$

We assume that the director is fixed at the boundary of the environment, which is itself far away from the boundary between the environment and the system located at z_a . Then, under this condition, Ω_t should assume a minimum value for an equilibrium density as shown in Eq.(5.49). Suppose a deviation from the equilibrium density at fixed T , μ , f_d , and β , yet associated with the variations in $d_e(G)$ and $d_e(E)$. In the bulk nematic (especially in the nematic environment), the change from d_e to $d_e(G)$ amounts to translate the equilibrium director profile from $n(z)$ to $n[z+d_e(G)-d_e]$; so that, just as in Eq.(4.186), we obtain

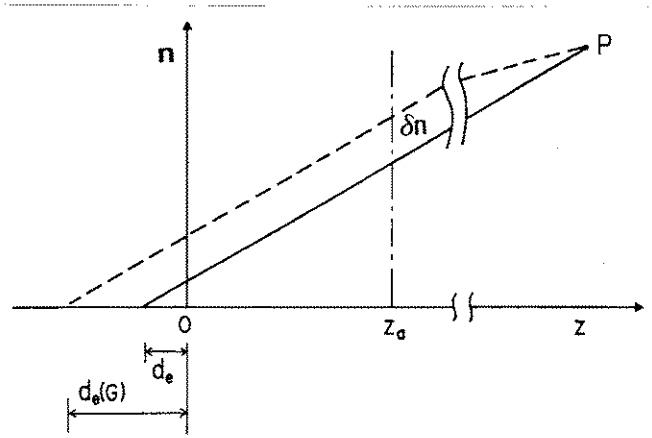


FIG.5.12. Virtual translation of the equilibrium director profile. The director is fixed at a far off point P. The extrapolation length changes from the equilibrium value d_e to $d_e(G)$.

$$\begin{aligned} \delta \Omega_{env} &= -A \left. \frac{\partial f_d}{\partial (dn_i/dz)} \right|_{z_a} \delta n_i(z_a) \\ &\sim 2Af_d[d_e - d_e(G)], \end{aligned} \quad (5.92)$$

where d_e represents the equilibrium extrapolation length. From Eqs.(5.80) and (5.81), we get

$$\delta \Omega = Af_d[d_e(E) - d_e]. \quad (5.93)$$

Thus, in terms of Eqs.(5.92) and (5.93), Eq.(5.49) can be translated to

$$0 < \delta \Omega_t = Af_d[d_e + d_e(E) - 2d_e(G)],$$

which yields

$$d_e > 2d_e(G) - d_e(E). \quad (5.94)$$

The equality holds in equilibrium, in which $d_e(G)=d_e(E)=d_e$. This result shows that by using a trial function for $\eta(z, \omega)$, we can at least set a lower bound for the extrapolation length; in other words, the upper bound for the anchoring strength.

Let us briefly illustrate how this variational principle works, by means of a Rapini-Papoular type model of the nematic interface. Though it is not a statistical mechanical model, it would serve as a good caricature of the interface for the purpose of illustration. We imagine that the nematic is completely bulklike right up to the interface at $z=0$, and that, by taking the dividing surface at $z=0$, the boundary (interfacial) tension γ^* is written as a function of the director at the interface; for simplicity, we consider the one-dimensional case in which only the polar angle of the director θ varies over space. In terms of the anchoring energy E_a , therefore, γ^* can be written as

$$\Delta \gamma^* = \frac{1}{2} E_a (\theta - \theta_e)^2. \quad (5.95)$$

Furthermore, we have

$$\theta - \theta_e = \pm [2f_d/K_3 f(\theta_e)]^{1/2} d_e(G). \quad (5.96)$$

The energetic extrapolation is thus given by

$$d_e(E) = d_e(G)^2 [E_a/K_3 f(\theta_e)]. \quad (5.97)$$

Using the above in Eq.(5.94), we find

$$d_e > 2d_e(G) - d_e(G)^2 [E_a/K_3 f(\theta_e)]. \quad (5.98)$$

The right-hand side assumes the maximum value $K_3 f(\theta_e)/E_a$, when

$$d_e(G) = d_e(E) = K_3 f(\theta_e)/E_a. \quad (5.99)$$

This is just the value of the extrapolation length that we expect for the Rapini-Papoular model [see Eq.(4.167a)].

5.2.6 Variational calculation of the extrapolation length

Equation (5.84) has revealed that a first principle calculation of the anchoring strength requires the knowledge on the Ornstein-Zernike direct correlation function and the density response function both in the bulk and in the inhomogeneous region near the nematic-wall interface. However, the calculation of such functions in an inhomogeneous liquid is still far from a settled problem, and in general needs an extensive computer simulations and/or some approximate formulas. As emphasized previously, the present purpose of microscopically treating the nematic interface is not to perform such microscopic calculations, but to found a conceptual basis for the phenomenology of the nematic interface. Indeed, on the basis of the variational principle derived above, we can qualitatively figure out the principal factors affecting the anchoring strength in some detail. The microscopic approaches will be pursued elsewhere.

For simplicity, let us consider the case of a purely polar anchorage [$\beta=0$]. In view of Eq.(5.87), we adopt a simplest possible trial function for the normalized density response function as

$$\bar{\eta}(z, \omega) = \chi_e(\omega) [2/K_3 f(\Theta_e)] 1/2 [z - z_d + d_e(G)], \quad (5.100)$$

where

$$\chi_e(\omega) = (\mathbf{n}_p \cdot \omega) \rho \delta(\mathbf{n}_e \cdot \omega) / \rho_0(\mathbf{n}_e \cdot \omega).$$

Substituting Eq.(5.100) into Eq.(5.84) with the dividing surface located at $z_d=0$ (the point of zero-adsorption of the solid phase), we find that the energetistic extrapolation length $d_e(E)$ can now be written in the following form:

$$d_e(E) = [B_2 + 2B_1 d_e(G) + B_0 d_e(G)^2 + J_2 + 2J_1 d_e(G) + J_0 d_e(G)^2 + M_0] / K_3 f(\Theta_e), \quad (5.101)$$

where B's, J's, and M_0 are the constants independent of $d_e(G)$, which are specifically given by

$$\begin{pmatrix} B_0 \\ B_1 \\ B_2 \end{pmatrix} = \frac{kT}{A} \int d\mathbf{r} \int d\mathbf{u} d\omega_1 d\omega_2 \begin{pmatrix} 1 \\ z \\ z^2 \end{pmatrix} \chi_e(\omega_1) \chi_e(\omega_2) \times \bar{c}_2[\rho_0; \mathbf{r}, \omega_1, \mathbf{r}+\mathbf{u}, \omega_2],$$

$$\begin{pmatrix} J_0 \\ J_1 \\ J_2 \end{pmatrix} = -\frac{kT}{2A} \int d\mathbf{r} \int d\mathbf{u} d\omega_1 d\omega_2 \begin{pmatrix} 1 \\ z+u_z/2 \\ z^2+zu_z \end{pmatrix} \chi_e(\omega_1) \chi_e(\omega_2) \times (\bar{c}[\rho_0; \mathbf{r}, \omega_1, \mathbf{r}+\mathbf{u}, \omega_2] - \bar{c}[\rho_0; \mathbf{r}+\mathbf{u}, \omega_1, \mathbf{r}, \omega_2]),$$

$$M_0 = \frac{kT}{2A} \int d\mathbf{r} z \frac{\partial}{\partial z} \int d\mathbf{u} d\omega_1 d\omega_2 \chi_e(\omega_1) \chi_e(\omega_1) \times \bar{c}[\rho_0; \mathbf{r}, \omega_1, \mathbf{r}+\mathbf{u}, \omega_2].$$

(5.102)

In comparison with Eq.(5.84), it is clear that B's and J's are respectively connected with the break-down of the Goldstone degeneracy and of the inversion symmetry in the interfacial inhomogeneous region. Under the present approximation, however, it should be noted that J's vanish identically; as clear from Eq.(5.84), the contribution of this term disappear, whenever $\eta(z, \omega)$ can be factorized as $\eta_1(z)\eta_2(\omega)$ or given by a sum of this type of functions.

In order next to appreciate the physical meaning of M_0 in some detail, we rewrite the above equation as follows:

$$\begin{aligned} M_0 &= \frac{kT}{2A} \int dz z \frac{\partial}{\partial z} \int dx dy d\mathbf{u} d\omega_1 d\omega_2 \chi_e(\omega_1) \chi_e(\omega_1) \\ &\quad \times \bar{c}[\rho_0; \mathbf{r}, \omega_1, \mathbf{r}+\mathbf{u}, \omega_2]. \\ &\equiv \int dz z \frac{\partial}{\partial z} K_{\text{eff}}(z). \end{aligned} \quad (5.103)$$

In view of Eqs.(5.74) and (5.76), it is clear that

$$\lim_{z \rightarrow \infty} K_{\text{eff}}(z) = K_3 f(\Theta_e), \quad (5.104)$$

so that, it appears reasonable to call $K_{\text{eff}}(z)$ the effective Frank elastic constant at the point z , as a generalization of the bulk constant into the inhomogeneous region. According to Eq.(5.103), M_0 is further transformed to

$$M_0 = \int_{-\infty}^{z_a} K_{\text{eff}}(z) dz - z_a K_3 f(\Theta_e). \quad (5.105)$$

So, M_0 can be interpreted as the surface excess of the Frank elastic constant relative to the dividing surface at $z_d=0$. The fact that K_{eff} has a correct property as an elastic constant can be confirmed, qualitatively at least, by applying the gradient expansion approximation with respect to the density or the (normalized) density response function in Eq.(5.53) or in Eq.(5.84).

When it can be assumed that the inhomogeneous region is localized virtually within a region having a thickness negligibly small compared with $d_e(G)$, it follows from Eq.(5.103) that B_1 and B_2 can be neglected compared with B_0 in Eq.(5.101) to give

$$d_e(E) = [B_0 d_e(G)^2 + M_0] / K_3 f(\Theta_e). \quad (5.106)$$

Then, using Eq.(5.106) in Eq.(5.98) and maximizing with respect to $d_e(G)$, we obtain

$$d_e > \frac{K_3 f(\Theta_e)}{B_0} - \frac{M_0}{K_3 f(\Theta_e)}, \quad (5.107)$$

which, upon the use of Eq.(5.105), reduces to

$$d_e > \frac{K_3 f(\Theta_e)}{B_0} + \int_{-\infty}^{\infty} \left[1 - \frac{K_{\text{eff}}(z)}{K_3 f(\Theta_e)} \right] dz. \quad (5.108)$$

Besides negligence of B_1 and B_2 , this is a rigorous inequality for the equilibrium extrapolation length. Although it is beyond the scope of the present argument to give a quantitative estimate for each terms appearing in the above, we can draw a few important (qualitative) consequences from this result on the nature of the anchoring of nematics at their interfaces:

(1) The extrapolation length is comprised of two independent contributions resulting from the broken symmetry and the direct interaction across the nematic-wall interface (B and J terms) and the anomaly of the elasticity in the interfacial transition region (structural effect);

(2) When the orientational restoring force, represented by B and J in the above, becomes small, the anchoring strength should weaken irrespective of the elastic property of the interfacial region of the nematic;

(3) Conversely, as the interfacial region grows, where the curvature elasticity is relatively weaker than in the bulk nematic, the extrapolation length can be arbitrarily large, independent of the strength of the orientational restoring force.

Note that the first of the above shows close correspondence with the results in Section 5.1 as regards the factors determining the interfacial tension of a wall-undeformed nematic. Finally, it must be pointed out that by using a more sophisticated trial functions, the estimate for the extrapolation can be readily improved. So, the present formula for the extrapolation length, armed with the variational property, seems to be especially suited for simulation studies of the anchoring processes.

5.3 The Landau-de Gennes theory of the nematic interface

5.3.1 Background

The Landau-de Gennes theory of the nematic-isotropic transition has been described in Chapter 2. This is a phenomenological theory which consists in expanding the free energy in powers of the orientational order parameter. It is therefore clear that, when properly supplemented with a surface term, it can be readily applied to interfacial phenomena as well. As a theory to describe the structure of an interface, it is essentially similar to the van der Waals theory, or gradient expansion theory, of the interface of simple liquids, which are known to provide qualitatively (and often quantitatively) good account of the interfacial properties of ordinary liquid systems [52]. The only difference between the Landau-de Gennes and the van der Waals theories is the order parameter with which the free energy is expanded. Both of These theories stand out as a good example of few existing theories that can yield meaningful information on the structure of the interface without detailed knowledge on the intermolecular interaction supporting the interface.

The Landau-de Gennes and other related theories of the nematic-wall, nematic-vapor, and nematic-isotropic interfaces have been explored by a number of workers [1,53-67]. The advantage of the Landau-de Gennes type theory is that it automatically allows us to take account of, in a phenomenological manner though, the spatial inhomogeneity of the orientational structure near the interface and the direct interaction between a nematic liquid and a solid or fluid. As emphasized in Section 5.1, both of them are expected to play an important role in determining the macroscopic orientational property of the nematic interface; and, at present, there is no molecular theory which can properly take care of the

former factor, in particular. In view of the success of van der Waals type theories in the case of ordinary fluid interface, it appears reasonable to expect that the Landau-de Gennes theory based on the expansion in terms of the order parameter and its spatial derivatives will produce a correct description, qualitatively at least, of the nematic liquid crystal interface.

In this section, we will formulate the model of a nematic interface in the Landau-de Gennes type theory, following the treatment due to Sluckin and Poniewierski [1,65,66]. And in the following three sections, we shall apply the theory to some specific orientational phenomena, with which we will concern ourselves in the experimental chapters. Since the details of the theoretical analyses are well documented in the literature, the description is limited to such an extent as to facilitate an intuitive appreciation of the physical content of the phenomena. Those who are interested in details are encouraged to consult original articles.

5.3.2 Description of the model

Let us consider a semi-infinite nematic liquid crystal in contact with a solid wall, whose surface is located at $z=0$ as in the previous section. The fundamental postulate of the Landau-de Gennes type model is that the thermodynamic potential Ω of the nematic be expressed as a functional of the orientational tensor order parameter (Q_{ij}). In case the system is uniform in the plane parallel to the interface, in particular, the thermodynamic potential is written as

$$\Omega[Q_{ij}(z)]/A_s = \int_0^{\infty} \sigma[Q_{ij}(z)] + \sigma_g[dQ_{ij}/dz] dz + \sigma_s(Q_{oij}), \quad (5.109)$$

where the area of the denoted by A_s . $\sigma[Q_{ij}]$ is the free energy

density of a uniform nematic with the order parameter $Q_{ij}(z)$, σ_g the additional contribution from the spatial variation of the order parameter, and $\sigma_s(Q_{oij})$ is the solid-nematic interaction term which is also regarded as a function of the order parameter at the interface $Q_{oij}=Q_{ij}(0)$. The equilibrium structure of the nematic interface is given by $Q_{ij}(z)$ which minimizes the thermodynamic potential Ω . In comparison with the exact formula derived in Section 5.1, we can see that the first and the second terms in the above are directly connected with $\gamma^*(1)$ and $\gamma^*(2)$ in Eq.(5.20), respectively.

As mentioned in Chapter 2, the tensor order parameter can be given, for a uniaxial nematic, by

$$Q_{ij} = \frac{1}{2} Q(3n_i n_j - \delta_{ij}), \quad (5.110)$$

where n_i is the i -th component of the director, and Q the scalar order parameter. In the ordinary form of the Landau-de Gennes theory [53-55], σ and σ_g are written respectively as

$$\sigma = \sigma_o(T) + \frac{1}{2} A Q^2 - \frac{1}{3} B Q^3 + \frac{1}{4} C Q^4, \quad (5.111)$$

and

$$\sigma_g = \frac{1}{2} L_1 (\partial_z Q_{ij})(\partial_z Q_{ij}) + \frac{1}{2} L_2 (\partial_z Q_{iz})(\partial_z Q_{iz}), \quad (5.112)$$

where σ_o is the isotropic contribution dependent only on the temperature, and ∂_z denotes the differentiation with respect to z . Usually, A is assumed to depend linearly on temperature, i.e.,

$$A = a(T - T^*), \quad (5.113)$$

with T^* being the supercooling limit of the isotropic phase. Here, a , B , and C are regarded as temperature-independent constants, and as mentioned in Chapter 2, σ is a function having double minima at $Q=0$ and Q_b (at least, sufficiently near the

clearing point T_c). L_1 and L_2 are the elastic constants for the spatial variation of the order parameter. In terms of Q and \mathbf{n} , Eq.(5.111) amounts to a rather complicated expression in which derivatives of Q and \mathbf{n} are coupled with each other, unless $L_2 \neq 0$. When $L_2=0$, however, Eq.(5.112) reduces to a simple decoupled form,

$$\sigma_g = \frac{3}{4} L_1 \left(\frac{dQ}{dz} \right)^2 + \frac{9}{4} L_1 Q^2 H_d(\mathbf{n}, d\mathbf{n}/dz),$$

where

$$H_d(\mathbf{n}, d\mathbf{n}/dz) = (\text{div}\mathbf{n})^2 + (\mathbf{n} \cdot \text{rot}\mathbf{n})^2 + (\mathbf{n} \times \text{rot}\mathbf{n})^2. \quad (5.114)$$

Sheng [56,57], Tarczon and Miyano [60], and Allender [61] used this simplified form (at $\mathbf{n}=\text{const.}$) in combination with Eq.(5.112) for studying the orientational phase transition at a wall-nematic interface. Poniewierski and Sluckin [65,66], however, adopted a Maier-Saupe Free energy density in stead of Eq.(5.111), supplemented also with Eq.(5.114) with the constant director. Below we shall use the fourth-order polynomial expression for σ with B and C being temperature-independent constant as in Eq.(5.111), but do not necessarily stick to the temperature dependence of A as assumed in Eq.(5.113) in accordance with de Gennes' original treatment [53].

To fully specify the model, it is finally necessary to give an expression for the solid-nematic interaction term σ_s . Following Poniewierski and Sluckin [1,65,66], we expand σ_s with respect to $Q_{\circ ij}$ up to quadratic order. But, here, we use the unit vector \mathbf{n}_e along the easy axis [58], instead of the interface normal they have used:

$$\begin{aligned} \sigma_s = \sigma_{s^0} - G Q_{\circ ij} n_{ei} n_{ej} + 4a_s Q_{\circ ij} Q_{\circ ij} \\ + 4b_s Q_{\circ ij} n_{ej} Q_{\circ ik} n_{ek} + 4c_s (Q_{\circ ij} n_{ei} n_{ej})^2, \end{aligned} \quad (5.115)$$

where G , a_s , b_s , and c_s are the coefficients of expansion. Upon

introduction of (5.110), Eq.(5.115) reduces to

$$\sigma_s = \sigma_{s0} + W_0(Q_0) + W_2(Q_0)[1 - (\mathbf{n} \cdot \mathbf{n}_e)^2]/2 + W_4(Q_0)[1 - (\mathbf{n} \cdot \mathbf{n}_e)^2]^2/4 \quad (5.116)$$

where

$$W_0(Q_0) = -GQ_0 + (a_s + 4b_s + 4c_s)Q_0^2 \equiv -GQ_0 + UQ_0^2/2,$$

$$W_2(Q_0) = 3GQ_0 - 6(b_s + 4c_s)Q_0^2 \equiv G_2Q_0 + U_2Q_0^2/2,$$

$$W_4(Q_0) = 36c_sQ_0^2 \equiv U_4Q_0^2/2.$$

In the absence of W_4 , Eq.(5.116) just gives the Rapini-Papoular form of the interfacial tension, which has also be given by Parsons [57] for the free surface of nematics.

$W_0(Q_0)$ is a term which is dependent only on the surface order parameter Q_0 . Since, when the director is along the easy axis, the second and the third terms disappear in Eq.(5.116), the surface property of an undeformed nematic is solely expressed by the form W_0 . According to Sluckin and Poniewierski [67], the second term of W_0 , which involves U_0 , is related to the reduction of the orientational mean field near the interface due to the smaller number of neighboring molecules near the interface than in the bulk phase; it can therefore be regarded as corresponding to the relaxation term $\gamma^*(1)$ in Eq.(5.19). Accordingly, we may conceive that this term is expressing the "disordering effect" of the interface, so that U_0 may approximately be regarded as a positive constant. The first term of W_0 , on the other hand, is a contribution of an external interfacial torque field, including the solid-nematic interaction, which tends to orient the nematics along the easy axis [58,63,67]. So, it is essentially expressing an "ordering effect" of the interface, implying a positive g .

Furthermore, in order for the easy axis to be a stable direction for the director, we should have $W_2 > 0$. In the sense that the easy axis is incorporated in the expression of σ_s from

the very beginning, the present model is more phenomenology-oriented than the original Poniewierski-Sluckin model.

Here, a word of caution is in order concerning the validity of Eqs.(5.115) and (5.116). As pointed out by Sluckin and Poniewierski [1], when \mathbf{n}_e does not coincide with the interface normal, there is always a symmetry breaking over the interface between the direction along the projection of \mathbf{n}_e and that normal to it. As a result, very close to the interface, one should find a "biaxial" ordering of nematic molecules (as in smectic C phase). However, in view of the fact that such a biaxial order is essentially short-ranged, and also that the representation of the thermodynamic potential in terms of the tensor order parameter cease to be valid very close to the surface (even when Q_{ij} is uniaxial or biaxial), it seems reasonable to expect that at least to the present level of approximation, the expression Eq.(5.116) remains to be valid.

Before going into the specific analysis of this model, it is convenient to transform the above equations into dimensionless forms. Note that the bulk nematic-isotropic transition occurs when

$$\sigma(Q_c) = d\sigma(Q_c)/dQ = 0, \quad (5.117)$$

where Q_c is the order parameter of the nematic phase at the point of transition. Then, from Eqs.(5.111) and (5.114), we obtain

$$Q_c = 2B/3C, \quad (5.118)$$

and various other quantities at the transition point T_c :

$$A(T_c) = 2B^2/9C, \quad \xi_c = [3L_1/2A(T_c)]^{1/2}, \quad \text{and} \quad \gamma_{ni} = (3CL_1)^{1/2} Q_c^3/12, \quad (5.119)$$

where ξ_c is the coherence length of the order parameter at T_c , and γ_{ni} is the nematic-isotropic interfacial tension within the context of the present model [53,54]. In terms of those

parameters, we now define the normalized variables as follows:

$$q = Q/Q_c, \quad (5.120)$$

$$\zeta = z/\xi_c, \quad (5.121)$$

$$\eta(T) = 9A(T)C/(2B^2). \quad (5.122a)$$

In particular, if a linear temperature dependence as in Eq.(5.113) is assumed for $A(T)$, $\eta(T)$ can be rewritten as

$$\eta(T) = \frac{T - T^*}{T_c - T^*}. \quad (5.122b)$$

In order to simplify the solid-nematic interaction term, we introduce a dimensionless solid-nematic potential via

$$\bar{\sigma}_s = \sigma_s/(6\gamma_{ni}), \quad (5.123)$$

and accordingly normalize the coefficients appearing in Eq.(5.116) as

$$g = GQ_c/(6\gamma_{ni}), \quad u_o = U_oQ_c^2/(6\gamma_{ni}), \quad \text{etc.} \quad (5.124)$$

For example, when $\mathbf{n}=\mathbf{n}_e$, we obtain

$$\bar{\sigma}_s(q_o) = -gq_o + u_oq_o^2/2.$$

Using these new variables, we can finally express the thermodynamic potential as

$$\begin{aligned} \Omega_a/(3\gamma_{ni}A_s) = & \int_0^\infty [\eta(T)q^2 - 2q^3 + q^4 + \left(\frac{dq}{d\zeta}\right)^2 \\ & + 3q^2H_d(\mathbf{n}, d\mathbf{n}/d\zeta)] d\zeta + 2\bar{\sigma}_s(q_o), \end{aligned} \quad (5.125)$$

where Ω_a is the anisotropic part of the thermodynamic potential, remaining after subtraction of the isotropic contribution due to σ_o .

5.4 Wall-induced pretransitional birefringence: Orientational wetting transition

5.4.1 Variation of the order parameter near the interface

Let us first consider how the orientational order of a nematic should be (locally) modified, when put into contact with a solid wall. It is naturally expected that if the solid wall is such that a nematic molecule feels a stronger orienting field in the vicinity of the solid than in the bulk phase, the orientational order may be enhanced near the wall [Fig.5.13(a)]. Conversely, if the solid acts in such a way as to reduce the mean field for the nematic molecule, we expect that the orientational order should be deteriorated near the wall [Fig.5.13(b)]. We shall refer to the former case as the "surface-induced ordering" and the latter as the "surface-induced disordering." The term "Wall-induced pretransitional birefringence" derives from the fact that this phenomenon was first observed by Miyano [68,69] through a measurement of locally induced birefringence near the wall at temperatures above the clearing point.

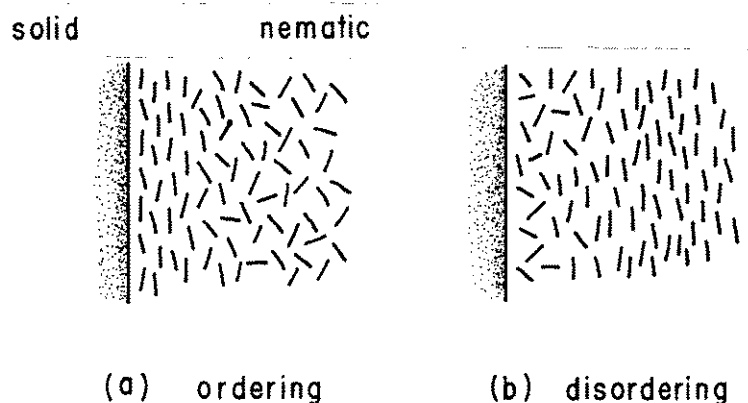


FIG.5.13. Surface-induced ordering (a) and disordering(b) transitions in nematic liquid crystals.

Once the order parameter at the interface ($z=0$) is given, the calculation of the order parameter profile can be readily carried

out by applying the variational calculus to Eq.(5.125). We assume that the director is spatially invariant; then, from Eq.(5.125), the Euler-Lagrange equation for the order parameter becomes

$$\frac{d^2q}{d\zeta^2} = \frac{d}{dq} \bar{\sigma}(q)/2, \quad (5.126)$$

where $\bar{\sigma}(q) \equiv (\sigma(Q) - \sigma_0)/(3\gamma_{ni}) = \eta(T)q^2 - 2q^3 + q^4$,

together with the boundary condition at the solid surface

$$\frac{dq}{d\zeta} = \frac{d}{dq} \bar{\sigma}_s, \quad \text{at } \zeta=0. \quad (5.127)$$

By integrating Eq.(5.126) once with the condition at infinity, i.e., $dq/d\zeta \rightarrow 0$, we obtain

$$\left(\frac{dq}{d\zeta}\right)^2 = \bar{\sigma}(q) - \bar{\sigma}(q_b), \quad (5.128)$$

where q_b is the normalized equilibrium order parameter in the bulk phase; at $T > T_c$, $q_b = 0$, and at $T < T_c$, $q_b \neq 0$. More specifically, q_b is given by

$$q_b = \{3 + [9 - 8\eta(T)]^{1/2}\} / 4, \quad \text{for } T < T_c. \quad (5.129)$$

Then, we find

$$\begin{aligned} \bar{\sigma}(q) - \bar{\sigma}(q_b) &= (q - q_b)^2 [q^2 + (q_b - 1)(2q + q_b)], & \text{for } T < T_c, \\ &= \eta(T)q^2 - 2q^3 + q^4, & \text{for } T > T_c. \end{aligned} \quad (5.130)$$

Inverting Eq.(5.128), we can write the profile of the order parameter as an implicit function of ζ as

$$\zeta = \int_{\min(q_0, q)}^{\max(q_0, q)} [\bar{\sigma}(q) - \bar{\sigma}(q_b)]^{-1/2} dq, \quad (5.131)$$

where q_0 is the order parameter at the solid surface ($\zeta=0$), which must be determined via the boundary condition Eq.(5.127). An important quantity, which is experimentally measurable, is the surface excess of the order parameter defined by

$$\Gamma_{\text{ord}} = \int_0^{\infty} [Q(z) - Q_b] dz. \quad (5.132)$$

This is directly connected with the surface excess birefringence at the solid surface.

Using Eq.(5.130) in Eqs.(5.131) and (5.132), we can readily write down the profile of the order parameter as follows:

(i) $T < T_c$ (nematic bulk-phase),

$$q = q_b - \frac{(4q_b^2 - 3q_b)}{2q_b - 1 + (q_b - 1)^{1/2} \sinh[\pm \zeta (4q_b^2 - 3q_b)^{1/2} + \phi_n]}, \quad (5.133)$$

where the positive sign should be adopted before ζ when $q_0 < q_b$, and the negative sign when $q_0 > q_b$, and

$$\phi_n = \sinh^{-1} \frac{2(q_b + q_0)(q_b - 1) + q_0}{(q_b - q_0)(q_b - 1)^{1/2}},$$

(ii) $T > T_c$ (isotropic bulk-phase),

$$q = \frac{\eta}{1 + (\eta - 1)^{1/2} \sinh[\eta^{1/2} \zeta + \phi_i]}, \quad (5.134)$$

where

$$\phi_i = \sinh^{-1} \frac{\eta - q_0}{q_0(\eta - 1)^{1/2}}.$$

At the nematic-isotropic transition point T_c , in particular, these equations can be reduced to

(i') nematic bulk-phase,

$$q = 1 - \frac{1 - q_0}{1 - q_0 + q_0 \exp \zeta}, \quad (5.135)$$

(ii') isotropic bulk-phase,

$$q = \frac{q_0}{q_0 - (1 - q_0) \exp \zeta}. \quad (5.136)$$

5.4.2 Orientational wetting transition in the isotropic phase

In Fig.5.14 shown are the profiles of the order parameter calculated at various temperatures above T_C . Focusing on the features that emerge as T_C is approached, we can distinguish two distinct behaviors which occur depending on whether the surface order parameter is larger or smaller than Q_C , i.e. $q_0 > 1$ or < 1 . Namely, when q_0 remains smaller than unity, the order parameter invariably decays over the length on the order of the coherence length, i.e., $\zeta \sim 1$. However, when $q_0 > 1$, we observe that the orientationally ordered interfacial region grows indefinitely, resulting in a nematic like layer with a macroscopic thickness; the solid surface is wetted by the nematic liquid.

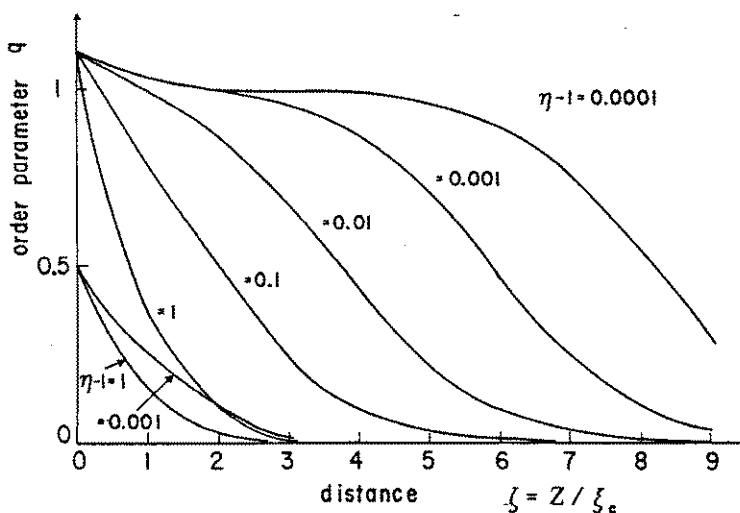


FIG.5.14. Profiles of the order parameter at various temperatures above T_C . η is a variable specifying the temperature. The surface order parameters are $q_0 = 1.1$ and 0.5 .

In analogy with the wetting transition at the interfaces of ordinary liquids [70,71], it may be called the "orientational wetting transition" [1]. This is one of few examples of the surface-induced critical phenomena associated with a first-order bulk transition. Lipowsky [72] also called this type of critical phenomenon the "interface depinning transition" in the sense that the interface between the ordered and the disordered region is liberated from the boundary as the transition temperature is approached.

As shown above, in a semi-infinite sample, the thickness of the ordered layer diverges (as long as $q_0 > 1$) as the temperature is decreased toward T_c . In real samples of finite dimension, it is obviously impossible to occur, and more over, because of the shift of the bulk coexistence temperature, there appears an upper bound for the thickness of the surface ordered layer. Lipowsky [72] argued that the upper bound is given, for a sample with a thickness d , by $\ln(d)$, and hence the actually observable thickness of the ordered layer is expected not to be very large even for a macroscopically thick samples.

The surface excess of the order parameter can also be obtained by substituting Eq.(5.134) into Eq.(5.132):

$$\Gamma_{\text{ord}} = Q_c \xi_c \ln \frac{1 - q_0 - [(q_0 - 1)^2 + \eta - 1]^{1/2}}{1 - \eta^{1/2}}. \quad (5.137)$$

Since the birefringence Δn of a nematic liquid is approximately proportional to the order parameter, the surface excess Γ_{ord} can be identified, except for a constant factor, with the surface excess birefringence. Especially, when the bulk phase is in the isotropic state, the absence of birefringence in the bulk phase allows us to directly measure the surface excess birefringence. This is indeed the principle of the Wall-induced pretransitional birefringence measurement originated by Miyano [60,68,69].

The quantity which is measurable in real experiments is the optical phase retardation R defined by

$$R = \frac{2\pi}{\lambda} \int_0^{\infty} \Delta n(z) dz, \quad (5.138)$$

where λ is the wavelength of the probe monochromatic light, and $\Delta n(z)$ denotes the local birefringence in the nematic. Therefore, writing $R_c = \Delta n_c \xi_c$, with Δn_c being the birefringence at T_c , we obtain the following relation

$$\frac{\Gamma_{ord}}{Q_c \xi_c} = \frac{R}{R_c}. \quad (5.139)$$

Thus, if the retardation R is measured for a known η , the surface order parameter can in principle be directly evaluated from Eq.(5.137):

$$q_0 = 1 - \cosh(R/R_c) + \eta^{1/2} \sinh(R/R_c). \quad (5.140)$$

When R/R_c is large, however, this equation becomes quite sensitive to an error in R/R_c , because q_0 is given by a difference between two large quantities. Consequently, in case the orientational wetting transition does occur, the value of the surface order parameter determined from the data of the wall-induced pretransitional birefringence should be subjected to an even more significant error as the temperature approaches T_c .

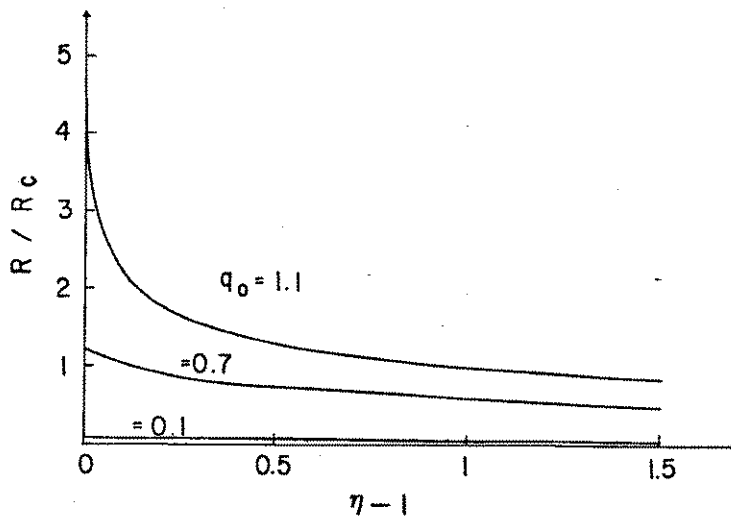


FIG.5.15. Temperature dependence of the reduced wall-induced birefringence for various surface order parameters. For $q_0 > 1$, the birefringence logarithmically diverges toward T_c ($\eta=1$).

In Fig.5.15, R/R_c is shown as a function of η^{-1} (which goes to 0 as $T \rightarrow T_c$) with the assumption of constant q_0 . As apparent from Eq.(5.132), when $q_0 > 1$, Γ_{ord} and hence R should diverge logarithmically with η^{-1} . In particular, if η^{-1} is linearly dependent on temperature as in a common Landau-de Gennes model, we find (in the vicinity of T_c)

$$R/R_c \sim \ln(T - T_c) + c, \quad \text{when } q_0 > 1, \quad (5.141)$$

where c is a function only of q_0 . This equation indicates that for a sufficiently large surface order parameter, the retardation diverges logarithmically as the temperature approaches the clearing point. This is an immediate consequence of the logarithmic divergence of the thickness of the ordered layer for $q_0 > 1$.

On the other hand, if $q_0 \ll 1$ holds, Eq.(5.137) can be approximated to give

$$\Gamma_{ord} \sim Q_c \xi_c \frac{q_0}{\eta^{1/2}}.$$

Under the same condition as above, we see that

$$R/R_c \sim q_0 (T_c - T^*)^{1/2} / (T - T^*)^{1/2}, \quad \text{when } q_0 \ll 1. \quad (5.142)$$

5.4.3 Orientational wetting transition in the nematic phase

The case in which the bulk phase is in the nematic state can be treated in much the same manner as above. The order parameter profile for this case is shown in Fig.5.16. In this case, however, an orientational wetting transition occurs when $q_0 \leq 0$, for which a "disordered" surface layer is observed to completely wet the solid wall as T_c is approached from below. This is the surface-induced disordering transition in Lipowsky's terminology.

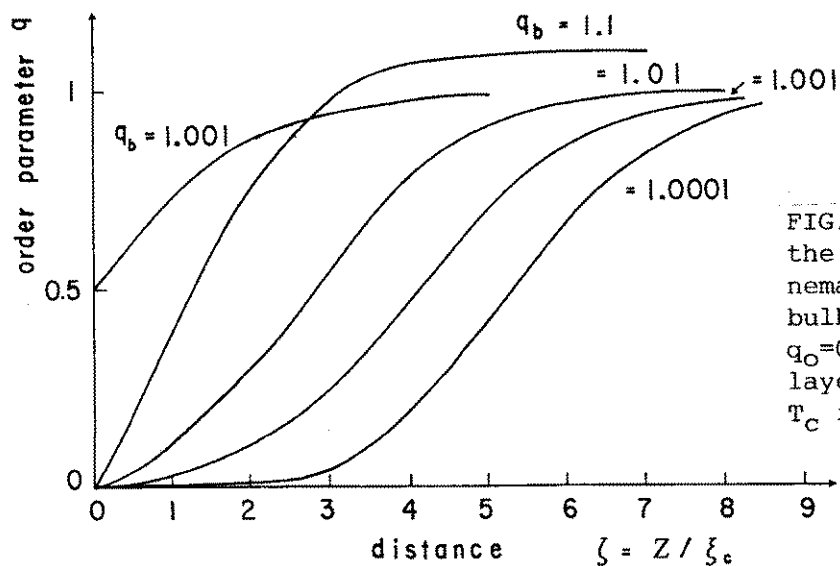


FIG.5.16. Spatial variation of the order parameter in the nematic phase for various bulk order parameters. When $q_0=0$, the disordered interface layer grows indefinitely as T_c is approached from below.

When the surface order parameter is larger than 0, the inhomogeneity of the order parameter is more or less restricted within the region away from the solid surface by ξ_c or so. This situation is essentially identical with what we have seen above T_c when q_0 is below q_b . In contrast to the case of wall-induced pretransitional birefringence, however, the surface-induced order or disorder in the nematic phase has as yet been unambiguously observed in experiment due primarily to the hazard resulting from the large optical anisotropy in the bulk nematic phase. So, we will not present the formula for the surface excess order parameter.

Nevertheless, it should be pointed out that the anomaly of surface order in the nematic phase does manifest itself, in an indirect manner though, in those orientational phenomena which we will treat later sections.

5.4.4 Surface order parameter

So far, we have tacitly assumed that the order parameter at the solid-nematic interface is given in advance. In reality, however, we must determine it so as to satisfy the boundary condition Eq.(5.127). By using Eqs.(5.124), (5.128), and (5.130), we can rewrite the boundary condition in the form

$$\begin{aligned}
 & (q_b - q_o)[q_o^2 + (q_b - 1)(2q_o + q_b)]^{1/2}, & (T \leq T_c), \\
 -g + u_o q_o = & \\
 & -q_o[\eta(T) - 2q_o + q_o^2]^{1/2}, & (T \geq T_c). \\
 & & (5.143)
 \end{aligned}$$

where we have used the fact that when $q_o > q_b$, $dq/d\zeta$ must be negative, and when $q_o < q_b$, it should be positive. To illustrate the physical content of the above equation, it is convenient to utilize a graphical representation as shown in Fig.5.17.

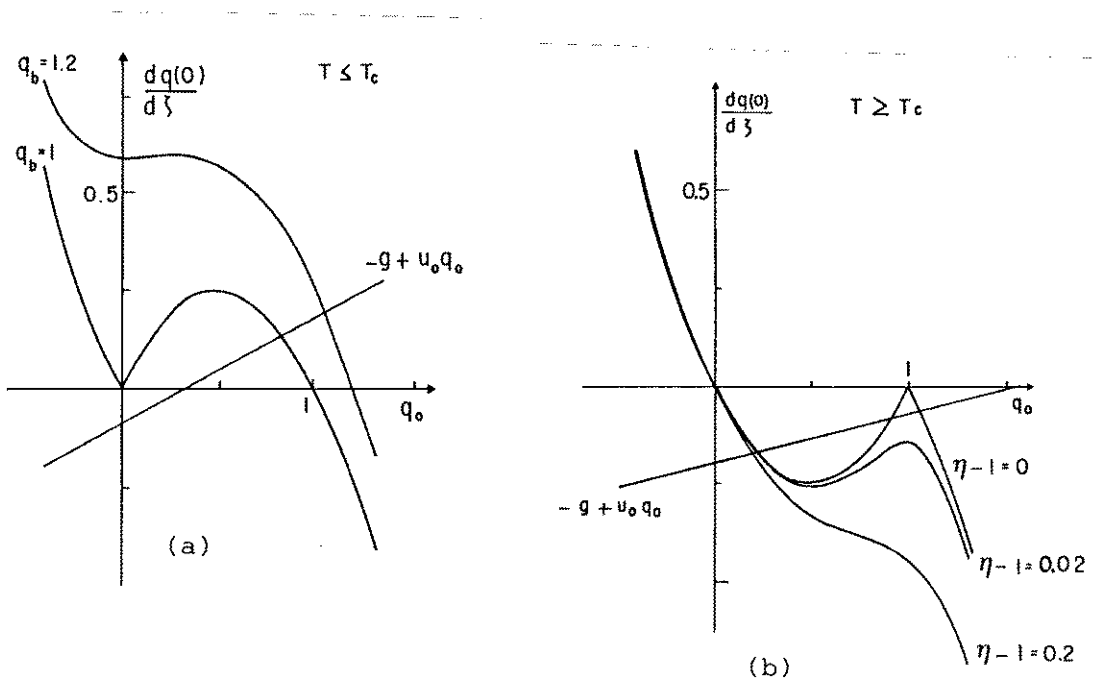


FIG.5.17. Graphical representation of the boundary condition Eq.(5.143): (a) $T \leq T_c$; (b) $T \geq T_c$.

In view of the aforementioned interpretations of g and u_0 terms in W_0 as expressing, respectively, the ordering and the disordering effects of the interface, we always assume here that

$$g > 0, \quad \text{and} \quad u_0 > 0. \quad (5.144)$$

Under this condition, it follows from Fig.5.17(a) that, when the bulk phase is in the nematic state, there exists a unique solution for the surface order parameter. And we see that q_0 increases as g increases and/or u_0 decreases, just as intuitively clear from their physical meaning. For constant g and u_0 , the surface order parameter continuously decreases with the increase in temperature.

When the bulk phase is in the isotropic state, however, the behavior of the surface order parameter is more complicated, and shows a rich variety of phenomena as discussed by Sheng [63], and Sluckin and Poniewierski [1]. At a temperature $1 \leq \eta \leq 9/4$, there may be one or three solutions depending on the magnitudes of g and u_0 . In particular, for a narrow range of g and u_0 , the surface order parameter jumps discontinuously on cooling from a small to a large value at a temperature slightly above T_c . This is an interfacial orientational transition called the "prewetting transition." So far, however, no experimental observation of this transition has been reported, due probably to the difficulty to control in actual systems for g and u_0 to lie in that narrow range as required by the theoretical prediction.

When g is sufficiently large or small and/or u_0 is large enough, Eq.(5.143) allows only one solution. The surface order parameter, this time, continuously decreases with temperature at constant g and u_0 . Obviously, if the ordering component g is absent, the surface order parameter always remains to be zero.

Anyway, the measurement of wall-induced pretransitional birefringence gives rise to the surface order parameter $q_0(\text{obs})$ and hence specifies a single relationship between g and u_0 , i.e.,

$q_0(\text{obs})=q_0(g,u_0)$. If we have independent information on these phenomenological parameters, we can in general determine g and u_0 . In the next section, we shall more specifically consider how the surface order parameter is affected by g and u_0 in relation to the contact angle at the nematic-isotropic-solid line of contact, by focusing the attention on the behavior at the clearing temperature.

5.5 Contact-angle phenomena at the clearing point [73]

As mentioned in Section 5.1, the contact angle at the line where the nematic, isotropic, and solid phases meet is far more sensitive to the orientational contributions in the relevant interfacial tensions in comparison with the familiar contact angle that one obtains in nematic-vapor-solid systems. In this section, we shall investigate more specifically within the framework of the Landau-de Gennes theory how the contact angle is related to the anisotropic part of the wall-nematic interaction, and is also connected with the orientational ordering at the interface.

In order to obtain an explicit expression for the contact angle of a nematic drop [see Fig.5.18], we need to find the interfacial tensions of the nematic and isotropic phases relative to the solid wall at the clearing temperature. Since the free energy density $\bar{\sigma}(q)$

vanishes in the bulk phase, where $q_b=0$ or 1 at T_c , the interfacial tension becomes identical with Ω_a/A_s as given in Eq.(5.125). Then, using Eq.(5.128), we obtain

$$\gamma/(3\gamma_{ni}) = \int_{\min(q_o, q_b)}^{\max(q_o, q_b)} 2[\bar{\sigma}(q) - \bar{\sigma}(q_b)]^{1/2} dq + 2\bar{\sigma}_s(q_o), \quad (5.145)$$

which applies to both nematic and isotropic phases. Substituting Eq.(5.130) at T_c , we can readily express γ as a function of the surface and bulk order parameters:

(i) nematic bulk-phase ($q_o \geq 0$),

$$\gamma_{sn}(q_o) = \gamma_{ni}[1 - 3q_o^2 + 2q_o^3 - 6gq_o + 3u_oq_o^2], \quad (5.146)$$

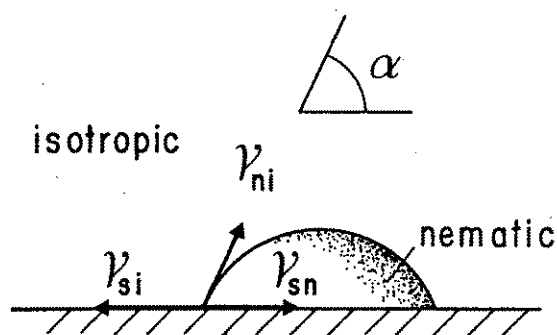


FIG.5.18. Contact angle of a nematic drop at a solid-isotropic interface.

(ii) isotropic bulk-phase,

(a) $q_o \leq 1$,

$$\gamma_{si}(q_o) = \gamma_{ni}[3q_o^2 - 2q_o^3 - 6gq_o + 3u_oq_o^2], \quad (5.147a)$$

(b) $q_o \geq 1$,

$$\gamma_{si}(q_o) = \gamma_{ni}[2 - 3q_o^2 + 2q_o^3 - 6gq_o + 3u_oq_o^2], \quad (5.147b)$$

where we have ignored the isotropic contribution from σ_g , since it does not influence the final result on the contact angle.

For each phase, the equilibrium value of the interfacial tension can be obtained by minimizing the above expression with respect to the surface order parameter. This condition of equilibrium reduces, as it must be, to Eq.(5.143). As noted in the former section, when the bulk phase is the nematic liquid, there is only one surface order parameter q_{on} for each set of $g > 0$ and $u_o > 0$:

$$q_{on} = \{1 - u_o + [(1-u_o)^2 + 4g]^{1/2}\}/2. \quad (5.148)$$

When the bulk is in the isotropic state, however, the following three cases are possible: (1) when $2g < u_o$, there is one stable solution $q_{oi}(L) \leq 1$; (2) when $2g^{1/2} < 1+u_o < 2g+1$, there are a low order-parameter and a high order-parameter (metastable) solutions, $q_{oi}(L) \leq 1$ and $q_{oi}(H) \geq 1$, along with one unstable solution; (3) when $1+u_o < 2g^{1/2}$, there is again only one stable solution $q_{oi}(H) \geq 1$:

$$q_{oi}(L) = \{1 + u_o - [(1+u_o)^2 - 4g]^{1/2}\}/2,$$

and

$$q_{oi}(H) = q_{on}. \quad (5.149)$$

The first case denotes the regime in which the disordering effect due to u_o term is overwhelming the ordering effect of g . In the second case, both effects are comparable. And, in the third case, the interface is strongly ordering. Therefore, the surface order parameter tends to increase as the condition of the interface

changes from the first toward the third. For example, if the ordering field is absent, i.e., $g=0$, we have $q_{o_i}=0$ and $q_{o_n}<1$; and, if the disordering field is absent, i.e., $u_o=0$, we have $q_{o_i}>0$ and $q_{o_n}>1$.

In the first case, we see from Fig.5.17 and Eqs.(5.148) and (5.149) that

$$q_{o_i}(L) \leq q_{o_n} \leq 1. \quad (5.150)$$

And, it is also clear that for fixed q_{o_n} (or q_o), we can choose appropriate g and u_o so that $q_{o_i}(L)$ (or q_{o_n}) can take an arbitrary value as long as it satisfies the above inequality. Furthermore, it should be noted that, regardless of the values of g and u_o , $q_{o_i}(L)$ is always smaller than unity. Now, combining Eqs.(5.146) and (5.147a) with Young's equation, i.e., $\gamma_{si} = \gamma_{sn} + \gamma_{ni} \cos \alpha$, we can express the contact angle as a function of the surface order parameters in the nematic and the isotropic phases:

$$1 + \cos \alpha = [3(q_{o_n}^2 + q_{o_i}^2) - 2(q_{o_n}^3 + q_{o_i}^3)] + 3(q_{o_n} - q_{o_i})^2(q_{o_n} + q_{o_i} - 1), \quad (5.151)$$

where q_{o_i} stands for $q_{o_i}(L)$, and g and u_o have been eliminated by using Eqs.(5.148) and (5.149). The first term in the above is the contribution from the spatial inhomogeneity of the order parameter and the second that from (roughly speaking) the solid-nematic interaction; obviously, the latter disappears when q_{o_n} coincides with q_{o_i} . Here, the nematic liquid partially wets the solid-isotropic interface. However, it should be emphasized when it happens that $q_{o_n}=q_{o_i}=0$, we have $\cos \alpha = -1$ so that the nematic liquid is completely repelled from the solid-isotropic interface; put differently, the isotropic liquid completely wets the solid-nematic interface.

Let us next proceed to the discussion of the third case.

Because of the strong ordering effect of the interface, here we have

$$q_{o_i}(H) = q_{o_n} \geq 1. \quad (5.152)$$

So that, from Eq.(5.146) and Eq.(5.147b), it follows that

$$\gamma_{si} - \gamma_{sn} = \gamma_{ni}, \quad (5.153)$$

and hence, according to Young's equation, we obtain

$$\alpha = 0. \quad (5.154)$$

This corresponds to the condition of complete wetting of the solid-isotropic interface by the nematic liquid.

The second case is the hardest to analyze among the three, as appreciable from the fact that this case is connected with such a subtle property of the interface as the prewetting transition which we have mentioned in the former section. Because of the presence of multiple local minima, the true equilibrium solution has to be determined by comparison of the interfacial tensions corresponding to the low order-parameter and the high order-parameter solutions. For the sake of calculating the contact angle, however, it is enough to note that if $q_{o_i}(L)$ is the equilibrium solution, the contact angle is given by Eq.(5.151), and if $q_{o_i}(H)$ is so, the complete wetting condition Eq.(5.154) applies. Therefore, Eqs.(5.151) and (5.154) exhaust all the possible situations.

The most remarkable feature of the contact angle in question is that it has a very clear correspondence with the degree of surface order parameter. Figure 5.19 shows the contour of equal contact angle on the plane spanned by q_{o_n} and q_{o_i} . As clearly seen, if and only if the surface order parameter in the isotropic phase exceeds the order parameter at T_c , the complete wetting condition of the nematic liquid is fulfilled. And, as already mentioned, the complete wetting by the isotropic phase ($\alpha=180$

deg) is possible only at $q_{on}=q_{oi}=0$. Finally, we would like to point out that the line of $\alpha=90$ deg, given by $q_{on}+q_{oi}=1$, also deserves a special attention as a line which demarcates the region in which the nematic order is relatively stable on the solid surface from that in which the isotropic state is more stable. The measurement of the contact angle provides us with information on the energetics of the nematic-wall interface which is supplementary to that obtainable from the wall-induced pretransitional birefringence measurements.

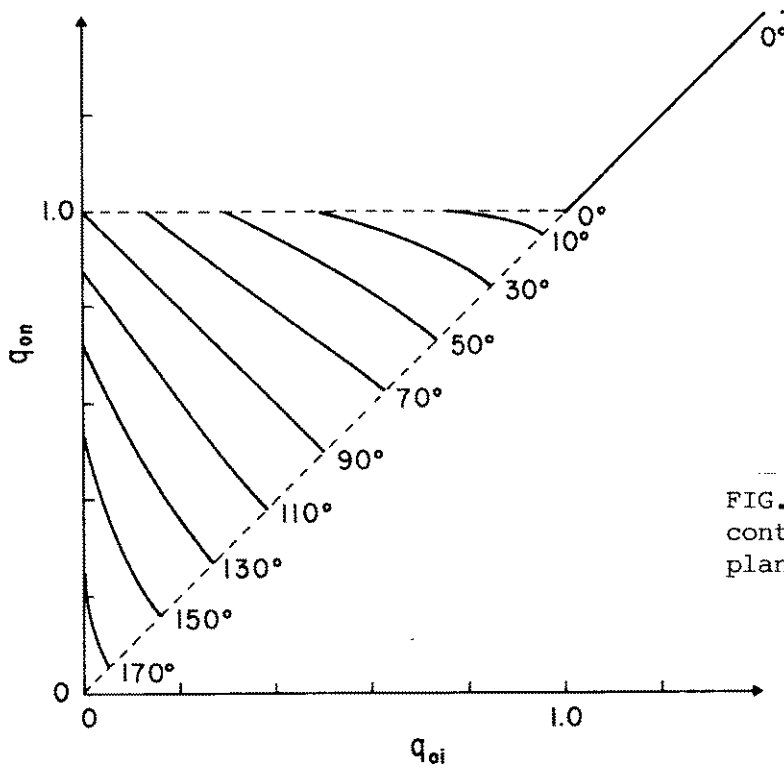


FIG.5.19. Iso-contact angle contours on the q_{on} - q_{oi} plane.

5.6 Anchoring strength in the Landau-de Gennes model[73]

Finally, we shall derive an expression for the extrapolation length based on the present phenomenological model of the nematic-wall interface. In contrast to the cases of the surface order and the contact angle, we need here to take account of the term which describes the effect of director deformations. Since the polar (out-of-plane) and the azimuthal (in-plane) anchorages can be treated in completely the same manner, we will concentrate here on the case of a polar anchorage.

5.6.1 The model

In terms of the angle between the director and the z-axis, Θ , the term in the thermodynamic potential, which is related to the curvature deformation can be written as [see Eqs.(5.114) and (5.125)] $3q^2(d\Theta/d\zeta)^2$. By multiplying it an arbitrary constant factor $K/3$, we use a slightly generalized form of thermodynamic potential than Eq.(5.125) as follows:

$$\Omega_a / (3A_s \gamma_{ni}) = \int_0^\infty \left[\eta(T)q^2 - 2q^3 + q^4 + \left(\frac{dq}{d\zeta}\right)^2 + Kq^2 \left(\frac{d\Theta}{d\zeta}\right)^2 \right] d\zeta + 2\bar{\sigma}_s(q_0). \quad (5.155)$$

In accordance with the thermodynamic route of defining the anchoring strength, we should here conceive that the nematic liquid crystal is subjected to a curvature stress in the absence of an external field. The Frank deformation energy density is now given by

$$f_d(\zeta) = 3\gamma_{ni} K q^2 \left(\frac{d\Theta}{d\zeta}\right)^2 \quad (5.156)$$

In the present model, we have neglected, for the sake of

simplicity, the coupling between the spatial variation of the order parameter and the director orientation.

To find out the anchoring strength through the thermodynamic formulas derived Chapter 4, we need to calculate the equilibrium interfacial tension (under a curvature stress) to first order in f_d . By applying the variational calculus to Eq.(5.155) with respect to $\Theta(\zeta)$, we obtain the Euler-Lagrange equation for $\Theta(\zeta)$ which reads

$$\frac{d}{d\zeta} Kq^2 \frac{d\Theta}{d\zeta} = 0, \quad (5.157)$$

with the boundary condition at the interface

$$\bar{W}_2(q_0)(\Theta - \Theta_e) = Kq_0^2 \frac{d\Theta}{d\zeta}, \quad \text{at } \zeta=0, \quad (5.158)$$

where

$$\bar{W}_2(q_0) = W_2(Q_0)/(6\gamma_{ni}),$$

and we have approximated $\sin(\Theta - \Theta_e) \sim (\Theta - \Theta_e)$, since the deviation of the director from the easy axis is assumed to be small. From Eq.(5.157), we immediately see that in the bulk nematic, where q is constant, the Frank elastic energy density becomes spatially invariant; we shall define a dimensionless elastic energy density in the bulk nematic f_n via

$$f_n = \lim_{\zeta \rightarrow \infty} f_d(\zeta)/(6\gamma_{ni} \xi_c^{-1}). \quad (5.159)$$

The Euler-Lagrange equation is an expression of the condition of mechanical equilibrium that the torque transmitted per unit area be constant throughout the nematic. Now, in terms of f_n , we can write this condition as

$$Kq^2 \frac{d\Theta}{d\zeta} = (2Kq_b^2 f_n)^{1/2}, \quad (5.160)$$

$$\bar{W}_2(q_0)(\theta_0 - \theta_e) = (2Kq_b^2 f_n)^{1/2}. \quad (5.161)$$

The equilibrium profile of the order parameter also satisfies the corresponding Euler-Lagrange equation resulting from Eq.(5.155) [see Eqs.(5.126) and (5.127)]:

$$2 \frac{d^2 q}{d\zeta^2} = \frac{d\bar{\sigma}(q)}{dq} + 2Kq \left(\frac{d\theta}{d\zeta} \right)^2, \quad (5.162)$$

and

$$\begin{aligned} \frac{dq(0)}{d\zeta} &= \frac{d\bar{\sigma}_s}{dq_0} \\ &= \frac{d\bar{W}_0(q_0)}{dq_0} + \frac{1}{2} \frac{d\bar{W}_2(q_0)}{dq_0} (\theta - \theta_e)^2, \end{aligned} \quad (5.163)$$

where $\bar{W}_0(q_0) = W_0(Q_0) / (6\gamma_{ni})$.

If we here denote the equilibrium order parameter profile in the absence of curvature stress as $q_e(\zeta)$, it is obvious from Eqs.(5.161)-(5.163) that

$$q(\zeta) = q_e(\zeta) + O(f_n). \quad (5.164)$$

where $O(f_n)$ is Landau's symbol to denote terms higher than first order in f_n . Because the thermodynamic potential in the absence of f_n is stationary with respect to the small deviation in $q(\zeta)$ from $q_e(\zeta)$, we can neglect the change of thermodynamic potential due to the variation of order parameter induced by the curvature stress. Therefore, we are allowed to replace $q(\zeta)$ by $q_e(\zeta)$ in Eq.(5.155) with an accuracy up to first order in f_n . For brevity, we shall simply write $q(\zeta)$ instead of $q_e(\zeta)$ below.

Using Eqs.(5.155), (5.160) and (5.161), the interfacial tension of the solid wall-deformed nematic interface can be written as

$$\gamma(f_n) = \gamma_0 + 6\gamma_{ni}f_n \int_0^\infty \left[\frac{1}{q^2} - \frac{1}{q_b^2} \right] d\zeta + \frac{K q_b^2}{\bar{w}_2(q_0)} 6\gamma_{ni}f_n, \quad (5.165)$$

where γ_0 is the interfacial tension in the deformation free state. Substituting the above into the thermodynamic definition of the anchoring strength Eq.(4.179b), we arrive at an expression for the extrapolation length in the present model:

$$d_e = \xi_c \int_0^\infty \frac{q_b^2 - q(\zeta)^2}{q(\zeta)^2} d\zeta + \xi_c \frac{K q_b^2}{\bar{w}_2(q_0)}; \quad (5.166)$$

Completely the same equation applies to the azimuthal anchorage.

In this equation, the second term, hereafter referred to as $d_e(2)$, is the ordinary extrapolation length representing the contribution of the direct interaction at the interface. However, the first term, $d_e(1)$, is a novel one which apparently comes from the order parameter inhomogeneity near the interface. And this term acts in such a way that if the order parameter is lower near the interface than in the bulk, this term results in an increase in the extrapolation length and hence weakens the anchoring strength. The presence of these two distinct contributions is in complete agreement with the result of the density functional theory of the anchoring strength [cf. Eq.(5.108)].

In the present formula, however, the influence of the structural inhomogeneity appears to be even more serious than in Eq.(5.108), since the local order parameter is appearing in the denominator of the integrand. Let us illustrate this point a bit more in detail by way of a simple example. If we assume the local order parameter is given by

$$q(\zeta) = q_b + (q_0 - q_b)\exp(-\zeta \xi_c / \xi), \quad (5.167)$$

we can easily carry out the integration to give

$$d_e(1) = \xi \left[\frac{q_b - q_0}{q_0} + \ln \frac{q_b}{q_0} \right]. \quad (5.168)$$

This equation clearly shows that, if the surface order parameter q_0 is small, it can make quite a substantial contribution to the anchoring strength. Indeed, if we set $q_0 = 0.1$, and $\xi = 16$ nm, which is known as a reasonable value for a coherence length near the clearing point [74,75], we find $d_e(1) = 180$ nm; this is on the same order of magnitude with the extrapolation lengths measured on real solid-nematic systems. It is therefore expected in particular that in case the surface-induced disordering transition ($q_0 \rightarrow 0$) does occur, it is expected to bring about a characteristic feature on the extrapolation length which is readily distinguishable in ordinary experimental situations. We will indeed present an experimental observation of this behavior in Chapter 7, made on an obliquely evaporated SiO film-nematic system.

It should be noted furthermore that when the surface order parameter is larger than the bulk order parameter, $d_e(1)$ gives rise to a negative contribution, which corresponds to a "super-strong anchoring condition," so to speak. Although the absolute value of this contribution is not very large, this appears to be one of the characteristics of this term in view of the fact that $d_e(2)$ should be always positive so as to assure the thermodynamic stability of the alignment. This effect is intuitively readily understandable, since the enhancement of the order parameter implies an increased rigidity of the medium, so that it will become relatively hard to deform this part in comparison with the normal region.

5.6.2 The extrapolation length as function of surface order parameter

Based on the Euler-Lagrange equation, Eq.(5.128), satisfied by the equilibrium profile of the order parameter $q(\zeta)$, it is possible to obtain an analytical expression for the extrapolation length. By a straightforward but tedious calculation, we find

$$d_e = \xi_c \frac{(q_b+3q_0)(q_b-q_0)}{q_b q_0 \{ [4-q_b^{-1}]^{1/2} q_0 + [q_0^2 + (q_b-1)(q_b+2q_0)]^{1/2} \}} + \xi_c \frac{K q_b^2}{\bar{W}_2(q_0)}. \quad (5.169)$$

This equation is obviously valid even when ξ_c is regarded as a temperature-dependent parameter.

In order to have an image of the nature of the above equation, let us shortly concern ourselves with the behavior at the clearing temperature. Since $q_b=1$ at T_c , Eq.(5.169) reduces to a very simple form:

$$d_e = \xi_c \frac{(1+3q_0)(1-q_0)}{2 q_0^2} + \frac{\xi_c K}{\bar{W}_2(q_0)}; \quad (5.170)$$

Therefore, the first term $d_e(1)$, coming from the inhomogeneity of the order parameter, is seen at this temperature to increase in proportion to q_0^{-2} as the interfacial region becomes orientationally disordered. This is in contrast with the q_0^{-1} dependence in Eq.(5.168) found by using a trial function which exponentially relaxes from q_0 to q_b . This difference can be ascribed to the fact that, at T_c , the disordered layer near the interface gradually grows to have a macroscopic thickness as q_0 diminishes, so that a complete "depinning" of the interface between the ordered (bulk) and the disordered (surface) phases can occur at last. If we take, for example, $q_0=0.1$ and $\xi_c=16$ nm as before, we now have $d_e(1)=930$ nm, which is nearly six times as

large as the value found via Eq.(5.168). This corresponds to a rather weak anchoring condition. that the influence of the order parameter inhomogeneity becomes even more significant in the vicinity of T_c , provided the surface order parameter is appreciably depressed.

In Fig.5.20, $d_e(1)$ is plotted as a function of the surface order parameter at various values of the bulk order parameter based on Eq.(5.169). As already emphasized, $d_e(1)$ increases rapidly as q_0 tends to vanish. Furthermore, it should be noted that the dependence of $d_e(1)$ on q_0 changes from the q_0^{-1} to the q_0^{-2} dependence as $q_b \rightarrow 0$. When q_0 is large, $d_e(1)$ is at around ξ_c . In this respect, the first component of the extrapolation length is seen to exclusively reflects the disordering nature of the solid-wall interface.

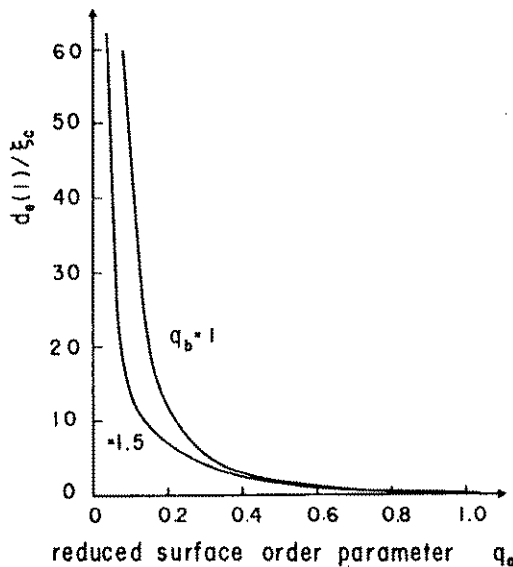


FIG.5.20. The dependence of the structural part of the extrapolation length on the surface order parameter.

5.6.3 Model calculation of the temperature dependence of $d_e(1)$: Critical behavior near T_c

In Fig.5.21, $d_e(1)$ is plotted as a function of temperature for various values of g and u_0 [see Eq.(5.124)] with a special attention on its relation to the surface-induced disordering

transition; $\bar{W}_0(q_0) = -gq_0 + u_0q_0^2/2$. The calculations have been performed by adopting the bulk order parameter which changes with temperature T as

$$q_b = \frac{1}{8} \left\{ 3 + \left[9 + 16 \left(1 + \frac{T_c - T}{T_n^* - T_c} \right)^{1/2} \right]^{1/2} \right\}. \quad (5.171)$$

This expression fits the experimental results for 4-n-pentyl-4'-cyanobiphenyl [73], when the temperature range of superheating above T_c , i.e. $T_n^* - T_c$, is assumed to be 0.24 K.

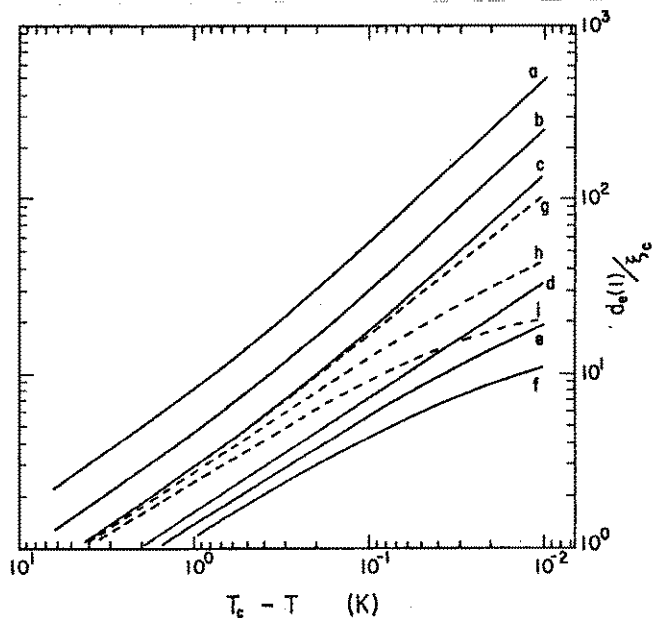


FIG.5.21. Extrapolation length $d_e(1)$ due to the interfacial inhomogeneity of the order parameter for various surface-potential parameters, u and g . The solid lines are with $g=0$ and, from upper to lower (a) $u_0 = 3$, (b) $u_0=2$ (c) $u_0=1.5$, (d) $u_0=1.0$, (e) $u_0=0.9$, (f) $u_0=0.8$. The broken lines are with $u_0=1.5$ and, from upper to lower, with (g) $g=0.01$, (h) $g=0.05$, and (i) $g=0.1$.

As clear from Eq.(5.148), when $g=0$ and $u_0 > 1$ (namely, when the disordering field is sufficiently strong in the absence of ordering field), the surface order parameter vanishes at T_c ; and, Eq.(5.143) shows that, in sufficient vicinity of T_c , q_0 decreases on heating according to $(T_c - T)^{1/2}$ [see Fig.5.22]. Concomitantly, Eq.(5.169) reveals that $d_e(1)$ should diverge as $1/(T_c - T)$, showing a critical behavior toward the clearing temperature. Since $\bar{W}_2(q_0)$ in general involves a term linear in q_0 , $d_e(2)$ is here expected to less singular than $d_e(1)$.

The calculated curves with $g=0$, however, show a slightly, yet

distinctively smaller exponent than unity even at 10^{-2} K below T_c , because of a somewhat slower decrease of Q_0 than the predicted

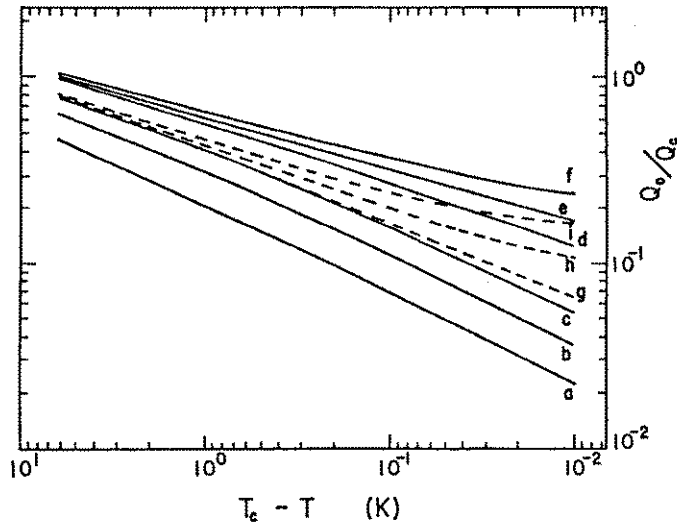


FIG.5.22. Temperature dependence of the surface order parameter for various surface potential parameters. The solid lines are with $g=0$, from lower to upper with (a) $u_0=3$, (b) $u_0=2$, (c) $u_0=1.5$, (d) $u_0=1.0$, (e) $u_0=0.9$, (f) $u_0=0.8$. The broken lines are with $u_0=1.5$ and, from lower to upper, with (g) $g=0.01$, (h) $g=0.05$, and (i) $g=0.1$.

critical behavior. And the deviation from the ideal behavior becomes quite remarkable at T_c-1 K. This shows that, even when the surface-induced disordering transition does occur, the true exponent is observable only at temperatures extremely close to T_c .

When $g=0$ but $u<1$, i.e. when the disordering surface potential is not large enough, the surface order parameter assumes a non-zero value $q_0=1-u$ even at T_c , thereby making $d_e(1)$ always finite. When $g>0$, q_0 does not vanish at T_c for any value of u , and as a result the temperature dependence of $d_e(1)$ shows a saturating behavior as the temperature gets close to T_c [Fig.5.21]. At lower temperatures, however, $d_e(1)$ is seen to approach the curve with $g=0$.

The fact that $d_e(1)$ retains a large decreasing rate even at a temperature well below T_c is a universal feature of the extrapolation length resulting from the order parameter inhomogeneity [see Eq.(5.169)]; this is due to the fact that, as the temperature is lowered, q_0 approaches q_b , thereby reducing the inhomogeneity near the interface. Consequently, this

structural contribution is expected to be important only down to a few degrees below T_c .

Chapter 6

ORDER-DISORDER PHENOMENA AT NEMATIC INTERFACES

By way of the Landau-de Gennes model of a nematic interface, we have learned in the former chapter that the orientational order near the interface is subjected to various alterations according to the anisotropic nature of the interface. And, a few experiments have been suggested, which would yield direct information on the anisotropic part responsible for those changes: (1) Wall-induced pretransitional birefringence, (2) Contact angle experiments at the temperature of the coexistence of the nematic and the isotropic phases, and (3) Measurement of the anchoring strength. In particular, the first two phenomena are connected with the term in the phenomenological expression of the interfacial tension, which does not explicitly contain the director; that is, the term solely governing the occurrence of orientational order or disorder at the nematic interface.

In this experimental chapter, we shall present the results of observations of these phenomena, focusing on the order-disorder aspects of the nematic interface; the topics concerning the director anchorage will be treated in Chapter 7.

In Section 6.1, the measurements of the contact angle at the nematic-isotropic-solid three-phase contact line, performed for various substrates, are described. First of all, the results of these observations reveal that the contact angle greatly varies from one substrate to the other, even though these substrates produce uniform alignment of good and apparently indistinguishable quality in the nematic phase. In particular, the substrates treated by the well-known "rubbing" and "oblique evaporation" techniques were found to exhibit completely opposite result as

regards the contact angle; the rubbed polyvinylalcohol surface is well wet by the nematic liquid, while the surface with an obliquely evaporated SiO film is almost completely wet by the isotropic liquid. If the prediction of the Landau-de Gennes model of the nematic interface is correct, this observation implies that the orientational order at these nematic interface should be very different from each other. It is also revealed that the contact angle experiments, more precisely the texture observations in the nematic-isotropic coexistence regime provide us with large amount of information which reflects various subtleties occurring at the interface.

In Section 6.2, we present the results of the wall-induced pretransitional birefringence experiments done on the rubbed polyvinylalcohol (PVA)-nematic and the obliquely evaporated SiO-nematic systems. These experiments unambiguously show that, as least in the isotropic phase, a dramatically enhanced orientational order does exist at a rubbed polymer-nematic interface, but at the SiO-nematic interface, the orientational order, if any, should be several orders of magnitude smaller than that at the rubbed polymer-nematic interface. In combination with the results of contact angle experiments, these observations demands (within the context of the Landau-de Gennes model) that the orientational order has to be accordingly enhanced or reduced even in the nematic phase.

Finally, in Section 6.3, the effect of layer thickness on the nematic-isotropic transition is examined by reducing the thickness of nematic layer down to below one hundred nanometers in between lens-shaped substrates. Though still highly qualitative, the results of this experiment independently confirm the above prediction by showing a correct enhancement or depression of the transition temperature with the reduction of thickness, depending on the substrate used.

All of those results show that the phenomenological description of a nematic interface, formulated in terms of the simplest orientational order parameter, gives rise to consistent picture as to various essentially distinct phenomena, at least near the phase transition point. A success of such an order parameter theory of nematic interface is expected to have a deep implication for the understanding of interfacial properties of other liquid crystalline phases, whose transition are also described by an appropriate order parameter.

6.1 Contact angle phenomena at the clearing point: Equilibrium shape of a nematic drop at the isotropic-substrate interface[1]

The contact angle we will be concerned with is the angle made by the nematic-isotropic, nematic-substrate, and isotropic-substrate interfaces when they meet together. As noted in Chapter 5, this rather exotic contact angle is expected to be quite sensitive to the anisotropic property of the interface. However, because the nematic and isotropic liquids can coexist in equilibrium only at the clearing point, the observation of such a contact angle is possible only at this unique temperature. Here we present the results of an extensive observation of the contact angle of 4-n-pentyl-4'-cyanobiphenyl (5CB) with respect various substrates including rubbed and obliquely evaporated surfaces.

6.1.1 Measurement of the contact angle

In principle, the contact angle in question can appear only at the nematic-isotropic transition point [Fig.6.1]. So, it might seem at a glance difficult to perform such an experiment in a well-controlled fashion. However, the phase transition of a real liquid crystal is by no means ideal, but due to inherent impurity in the liquid crystal, the transition is more or less broadened over a finite temperature. The 5CB we used showed a nematic-isotropic two-phase region of about 2×10^{-2} K as delivered. Hence by a careful control of temperature, it is not difficult to stay in this temperature region for indefinitely

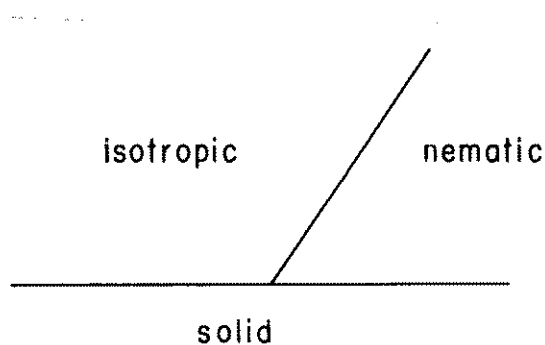


FIG.6.1. Nematic-isotropic-solid three phase line of contact.

long time, observing the true equilibrium state of the contact.

For the purpose of this observation, we have devised a precision temperature-controlled polarizing microscope in which the sample temperature can be fixed with an accuracy better than 10^{-3} K [see Appendix 1]. The contact angle was measured by a modification of the sessile drop method. Here, however, the drop of a liquid was brought about by a spontaneous heterogeneous nucleation on the surface of the substrate which occurred as the temperature was lowered (raised) from the isotropic (nematic) state [Fig.6.2]. And the temperature was fixed at an appropriate temperature during the observation.

The liquid crystal was confined in between a pair of identical substrates forming a sandwich-type cell of about $40 \mu\text{m}$ thickness. Because the drop of a nematic (or isotropic) liquid so obtained was at best $500 \mu\text{m}$ in diameter, it was not possible to use a familiar optical reflection method or such for measuring the contact angle. At present, we observed the drop under a polarizing microscope with monochromatic illumination at the wavelength of 560 nm . According to the variation of thickness over the nematic (or isotropic) drop, optical interference fringes appear, from which we can estimate the approximate shape of the drop. In order to have a maximum fringe visibility regardless of the orientation of the nematic director, we used crossed circular polarizers. The solid substrate examined and the method of surface treatments are listed in Table 6.1.

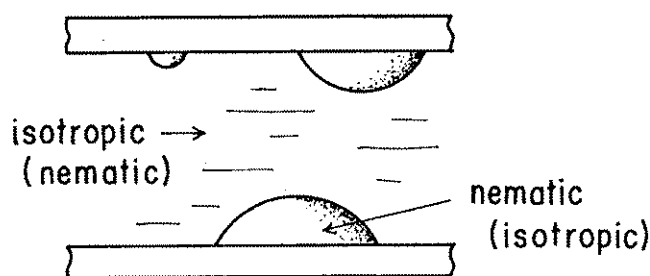


FIG.6.2. Heterogeneously nucleated drops of the nematic (isotropic) phase in the sea of the isotropic (nematic) phase.

TABLE 6.1 Substrates, methods of treatment, and the alignment.

Substrate	Method of treatment	Alignment
Rubbed PVA	Glass slides were spin-coated with 1 wt% aqueous solution of polyvinyl-alcohol(PVA), dried, and then rubbed with lens cleaning paper 100 times.	Planar
Bare PVA	Glass slides were spin-coated with 1 wt% aqueous solution of PVA and dried.	Random Planar
SiO (θ) $\theta = 0^\circ, 60^\circ, 80^\circ$	SiO was vacuum evaporated onto a glass substrate at a desired angle θ from the surface normal at the rate of 7 Å/s for 90 s.	(Random) Planar or Tilted
As cleaned Glass	Glass slides were cleaned by a hot (70°C) detergent, subjected to sonication for 5 min, rinsed with distilled water, soaked in acetone, and blown with dry nitrogen gas.	Random Planar
Rubbed Glass	Cleaned glass slides were rubbed with lens paper.	Planar
Rubbed and Cleaned Glass	Rubbed glass was re-cleaned by the same procedure as above.	Quasi Planar
CTAB film	Glass slides were dipped into a chloroform solution (0.5 %) CTAB [*] . after dried, excess CTAB was wiped out.	Homeotropic

On cooling or heating, the number density of nuclei is heavily dependent on the rate of temperature scan. In particular, if the new phase appearing in the mother phase has a small contact angle, it often happens that the small drops rapidly connect together, forming a metastable uniform layer. Once such a metastable film is formed, it is no longer possible to measure the equilibrium contact angle. So, the rate of cooling or heating has to be carefully determined so that an isolated drop could be prepared.

In order to estimate the shape of the drop from the fringe patterns, we need to have some knowledge on the configuration of the director inside the nematic. In the case of 5CB, the director is known to be tilted from the nematic-isotropic interface by an angle about 28 degrees from the interface [2,3]. Hence, for planar and homeotropic boundary condition, the director configuration which is compatible with the restriction at nematic-isotropic and nematic-solid interfaces may be drawn as something like that shown in Fig.6.3. These configurations are essentially identical with that observed in a nematic sphere suspended in its own isotropic phase [4].

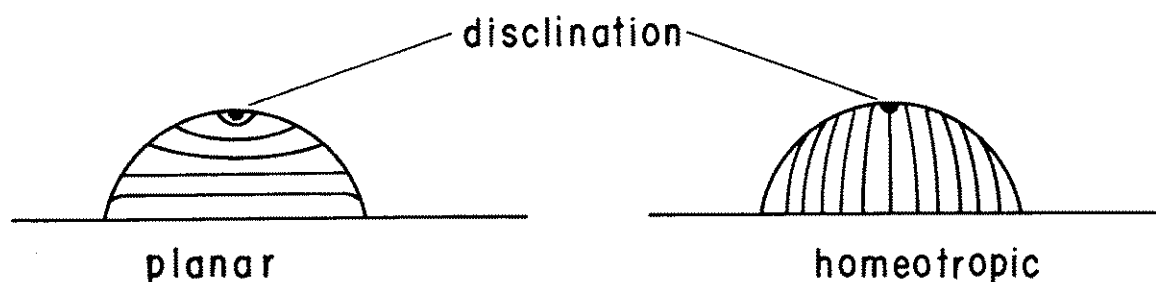


FIG.6.3. Director configuration in nematic drops with planar or homeotropic boundary condition.

In these configurations there appears a characteristic disclination on top of the drop. In particular, in the case of a planar alignment, it follows that a disclination line should

appear perpendicular to the initial alignment direction with an enhanced optical anisotropy. This is in good accord with the observation for the nematic drop as shown below. When the contact angle is small, so that the nematic drop is rather flat,

a rough estimate of the contact angle can be obtained by counting the order of fringe at the center of the drop without knowing the detailed structure of the director profile in the drop. From the value of the birefringence

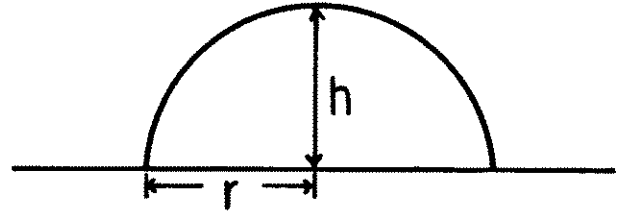


FIG.6.4. Geometry of the drop.

$\Delta n=0.11$, we see that at this wavelength of observation, one fringe corresponds to the nematic layer thickness of about $5 \mu\text{m}$. Then, knowing the depth h and radius r of the drop, and assuming that the nematic-isotropic interface is spherical [Fig.6.4], we can approximately calculate the contact angle α via

$$\cos\alpha = (r^2 - h^2)/(r^2 + h^2). \quad (6.1)$$

If the nematic drop is to assume an obtuse angle, it becomes impossible to straightforwardly apply the above mentioned procedure. But in this case, an isotropic drop brought about on heating the sample has a complementary acute angle. So that in this case too we can obtain a measure of the nematic contact angle.

6.1.2 Microscopic observation of sessile drops

For those substrates listed in Table 6.1, the equilibrium shape of nematic or isotropic drops were observed by means of the precision temperature-controlled microscope. Micrographs of the observed sessile drops are shown in Figs.6.5-6.14. And the

resulting contact angles are tabulated in Table 6.2. The scanning rate of temperature, till a first nucleus appeared, ranged from smaller than 10^{-3} K/hr up to 10^{-1} K/hr, depending on the contact angle of the new phase on the substrate.

A. General description

In actual observations, what appears most striking is the regularity of the shape of the equilibrium sessile drops; except for those cases in which the substrate surfaces are rather damaged, the drops of new phases invariably assume almost perfectly circular shape. This shape is quite stable, and, as far as the present results are concerned, there is no problem as hysteresis associated with the advancing and the receding angles [5]. When two neighboring drops coalesce, in particular, the initial dumbbell-shaped domain retains a circular shape in a few minutes. In view of the small interfacial tension (on the order of 10^{-5} J/m²) of the nematic-isotropic interface, this readiness of the drops to assume circular shape is really surprising. This, on the one hand, shows that there is not much hazard on the substrates as to pin the three-phase contact line, and on the other, indicates that the circular shape observed can indeed be regarded as an equilibrium shape of the liquid drop.

B. Specific observations

1. Rubbed and Bare PVA

At a rubbed PVA film-isotropic liquid interface, the drop of nematic 5CB adopts a very small contact angle less than 20° [Fig.6.5(a)]. This corresponds to the case of almost perfect wetting condition by the nematic liquid. And, indeed in some preparations, we observed that upon cooling from the isotropic phase, a uniform "epitaxial" nucleation of a nematic film grew to

form an almost uniform layer of the nematic [Fig.6.5(b)]. Because it is difficult to characterize and precisely reproduce the process of rubbing [6], we have not as yet succeeded in clarifying the factors affecting the variations in the contact angles. Whether the epitaxial growth mentioned above is indeed the growth of a continuous film from the beginning or as a consequence of a rapid coalescence of isolated nuclei could not be determined even at the lowest rate of cooling.

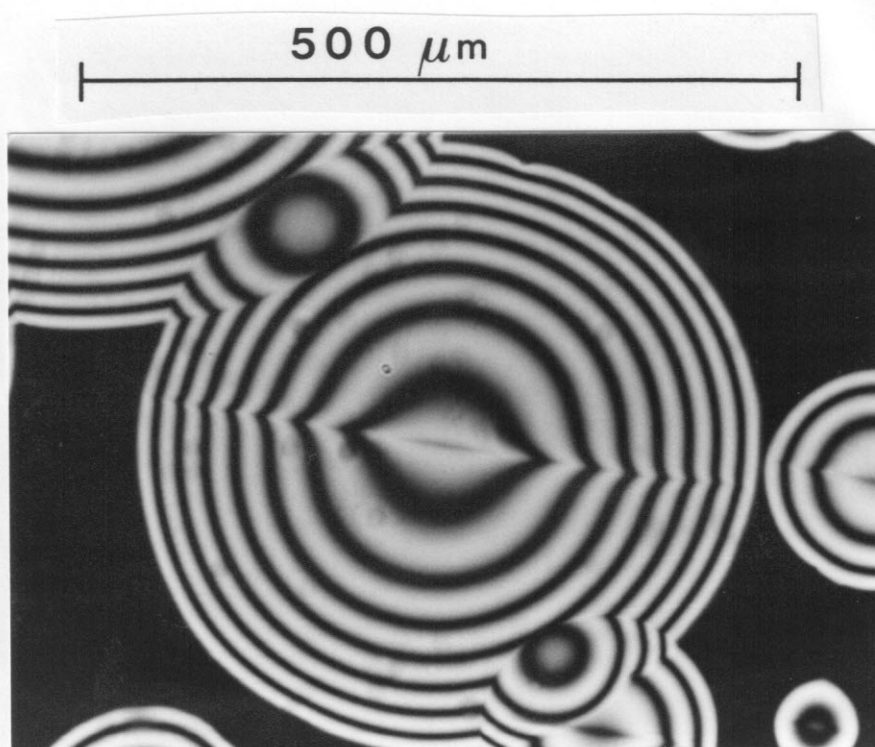


FIG.6.5(a). A drop of nematic resting at the interface between a rubbed PVA and the isotropic liquid. Note the clear disclination line on top of the drop.

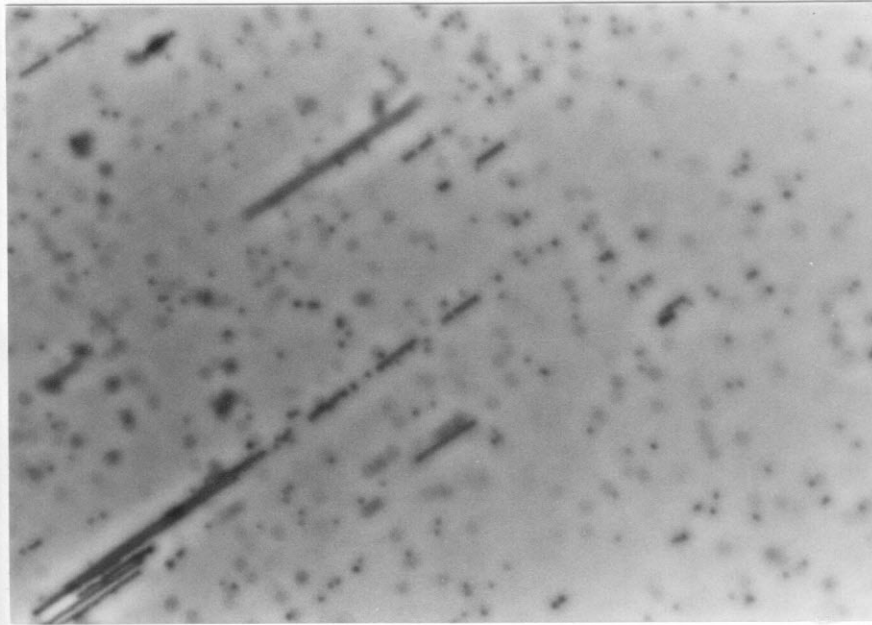


FIG.6.5(b) The "epitaxial" layer growth of nematic phase upon cooling from the isotropic phase. Substrate: rubbed PVA.

As expected from the presumed director configuration in Fig.6.3, a disclination line which is apparently bisecting the drop has been observed. Further from the distortion of the birefringence fringes by the disclination line, the optical anisotropy is seen to be larger along the disclination.

As an extreme case of a weak rubbing, we observed the sessile drop resting at the bare (unrubbed) PVA-isotropic interface [Fig.6.6]. The result in this case is dramatically different from that on the rubbed PVA, showing a nearly rectangular contact angles for both nematic and isotropic drops. In comparison with the results for the rubbed PVA, it is clearly indicated that by the very rubbing action, the PVA acquires an ability to uniformly align nematic liquid crystal as well as to be wet by the nematic liquid. Hence they may be interpreted as resulting from the same microscopic origin. As shown below this is an observation to be sharply contrasted with those for evaporated SiO surfaces.

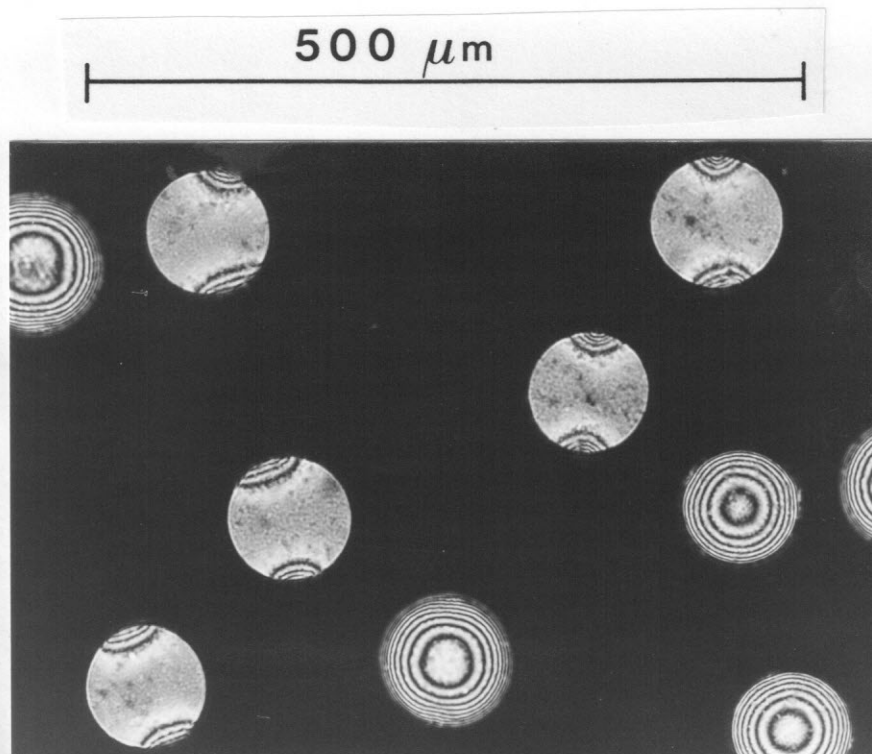


FIG.6.5(c) Drops of nematic liquid resting at the interface between the isotropic liquid and bare PVA. The regions without concentric fringes are the part where the nematic occupies the whole volume in between the two substrates.

2. Evaporated SiO

At the SiO-5CB interface, the nematic drop assumes an obtuse angle on cooling from the isotropic phase. Thus, we made an observation of the contact angle of the isotropic drop at the interface to measure the complementary angle of the nematic contact angle. In Fig.6.7 displayed are the micrographs of the isotropic drop in equilibrium with the nematic liquid on SiO films evaporated at 0° , 60° , and 80° from the substrate normal. Clearly, the isotropic liquid are now almost perfectly wetting the substrate. Though they may seem quite similar to the rubbed PVA case [Fig.6.5(a)], a characteristic difference can be readily noticed concerning the disclination line appearing at the center of the circular drops [Figs.6.7(a)&(b)]; that is, the optical anisotropy is now lower around the disclination line than

otherwise expected. This is probably because the director surrounding the isotropic drop is arranged in a complementary fashion when compared with the nematic drop.

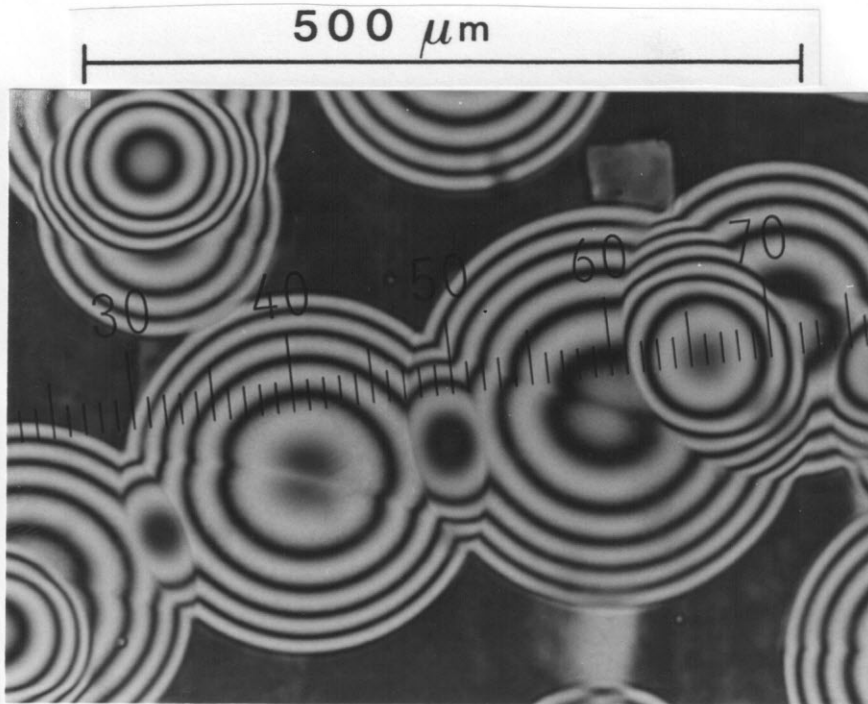


FIG.6.7(a) Isotropic drops in equilibrium with the nematic liquid at the surface of SiO(0°).

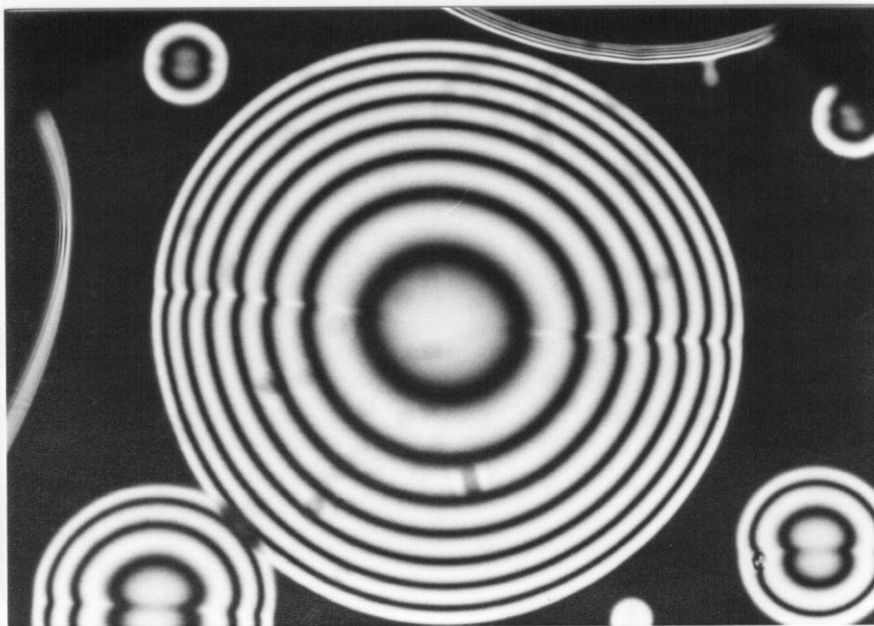


FIG.6.7(b) Isotropic drops resting at the interface between the nematic and the SiO(60°). The separation between two fringes corresponds to the thickness change of about 5 μm.

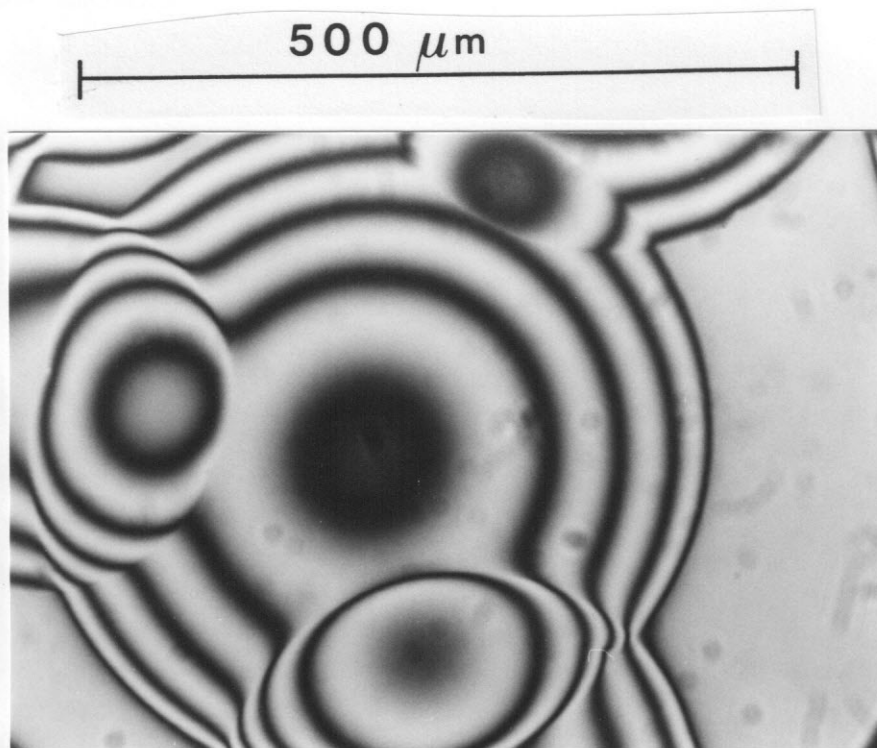


FIG.6.7(c) Sessile drops of the isotropic liquid resting on the SiO(80°).

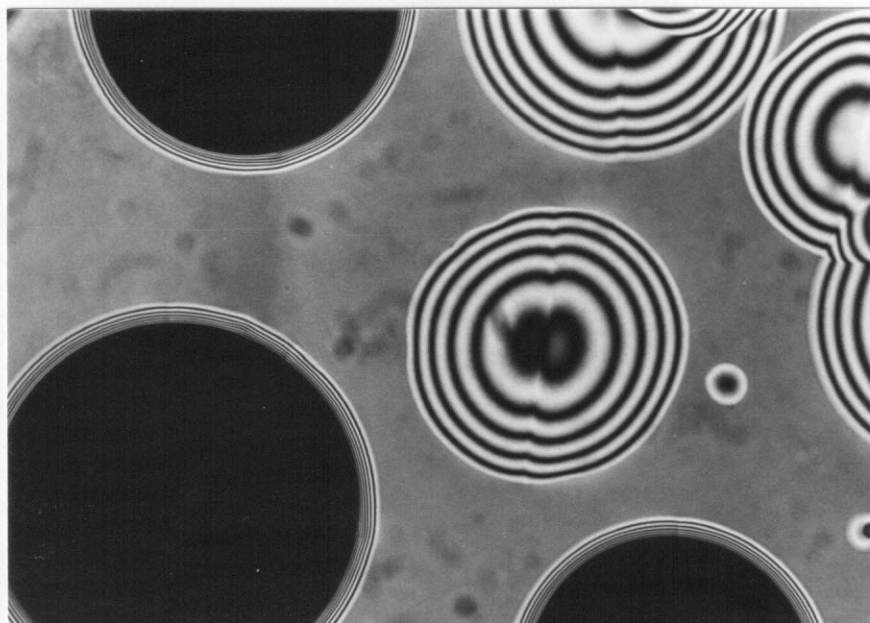
Comparison between the cases of normal evaporation and 60° evaporation shows that, in contrast to the rubbed PVA and bare PVA, the contact angles at these SiO films are almost identical with each other quite independent of whether the substrate aligns the nematic in uniform direction or not. So, it is natural to conceive that the origin of the uniform planar alignment on SiO(60°) and the nearly complete wetting by the isotropic liquid are independent aspects of the interface.

In the case of SiO(80°), however, we do not find any disclination line over the surface of the drop. As the director may be tilted on this substrate, the disclination line is expected to be repelled toward either sides of the circle to avoid the occurrence of an area with large orientational deformations. Clearly, the drop appears to be exceptionally flat judging from the separation of fringes. The contact angle of the "isotropic"

drop was estimated to be as small as 12° even after the correction of the pretilt angle was approximately taken into account. If we further take account of the contribution from the roughness [7] of the deposited SiO film as given in Ref.8, the intrinsic contact angle can be even made larger than that for the SiO(60°). However, since no reliable information on the roughness of the SiO films is available, we shall work with the apparent contact angle here.

3. As-cleaned, rubbed, and rubbed and cleaned glass

On as-cleaned glass, the alignment of liquid crystals is unstable depending on their purity and the cleaning condition of glass substrates [9,10]. Be it planar or homeotropic, the contact angle of a nematic drop was observed to assume an obtuse angle [1]. In Fig.6.8 the polarizing micrograph of a sessile isotropic drop is shown.



500 μm

FIG.6.8. Sessile isotropic liquid drops at the interface between the as-cleaned glass and the nematic phase.

Here we can see a bisecting disclination line characteristic to an isotropic drop resting on a planar-aligning substrate just as we have seen in the case of evaporated SiO films. The contact angle of this isotropic drop is as small as 28° , showing the relative stability of the isotropic phase.

When the glass surface was rubbed with the lens tissue, which was the same as that we used for PVA films, we observed a drastic change of the nematic contact angle from obtuse to acute [see Fig.6.9(a)]. In this case, however, the wetting property of the glass surface was astoundingly irregular as shown in the Figure. And we could observe the three-phase contact line to have been pinned largely along the rubbing direction [note the direction of the disclination line]. The nature of this defect is not clear.

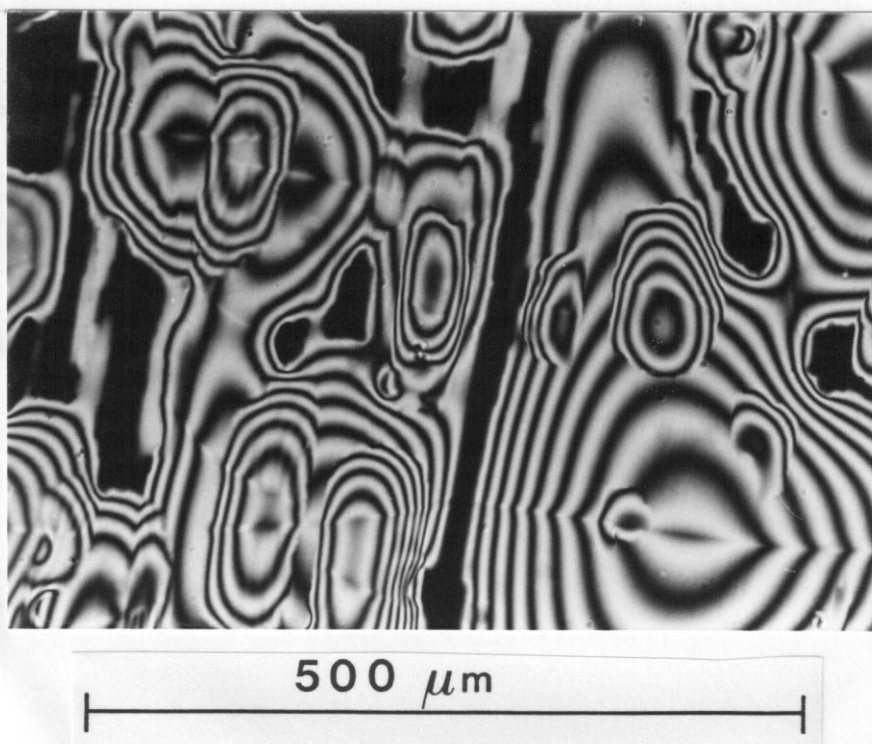
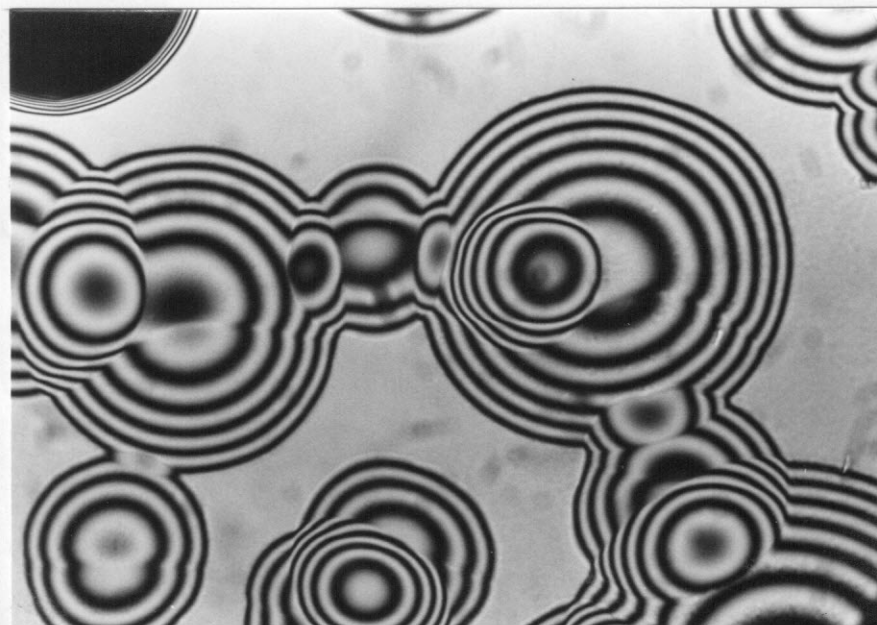


FIG.6.9(a). Nucleated irregular domains of the nematic phase on rubbed glass surface. Note, however, that the contact angle of the nematic domains is rather small.

When the rubbed glass surface was again cleaned with the standard cleaning procedure, the resulting alignment was still highly anisotropic in the direction of rubbing; but the contact angle was almost that we should obtain on as-cleaned glass [see Fig.6.9(b)]. Then, it seems likely that, by the cleaning process, some contaminant introduced by the rubbing action is removed exposing the intrinsic surface of the glass, but there remains a structural anisotropy on the part of the glass itself (groove, aligned microcrystals, etc.) which then takes action to align nematic molecules. The contaminant is obviously responsible to make the nematic contact angle that small. And, in comparison with the observations on the SiO films, it may be so much in error if we assume that the alignment mechanism of the as-cleaned and the rubbed (intrinsic) glass is essentially similar to that of the SiO films.



500 μm

FIG.6.9(b). Equilibrium shape of an isotropic liquid drop observed when the rubbed glass substrate was cleaned again by detergent, etc.

As noted in Chapter 3, the contaminant vs groove mechanisms of surface-induced alignment is a matter of long debate. The above observation seems to be of interest in the sense that it could visualize the fact that both mechanisms are indeed in action with some rough feeling of their relative importance in various situations.

4. CTAB film

This is here the only case in which homeotropic boundary condition prevails at the solid surface. Figure 6.10 shows the nematic drops resting on the CTAB film. In agreement with the prediction based on the conceived configuration of the director, we can see that at the center of the drop is a point disclination where the optical anisotropy is always absent. In this case, the estimation of contact angle is somewhat difficult because of the less significant thickness-dependence of the optical anisotropy. However, from the size of the drop which is just to touch the counter substrate, we can obtain a rough estimate of the shape of the drop based on the knowledge of the cell thickness. This way, we find the contact angle of about 70° for the nematic drop.

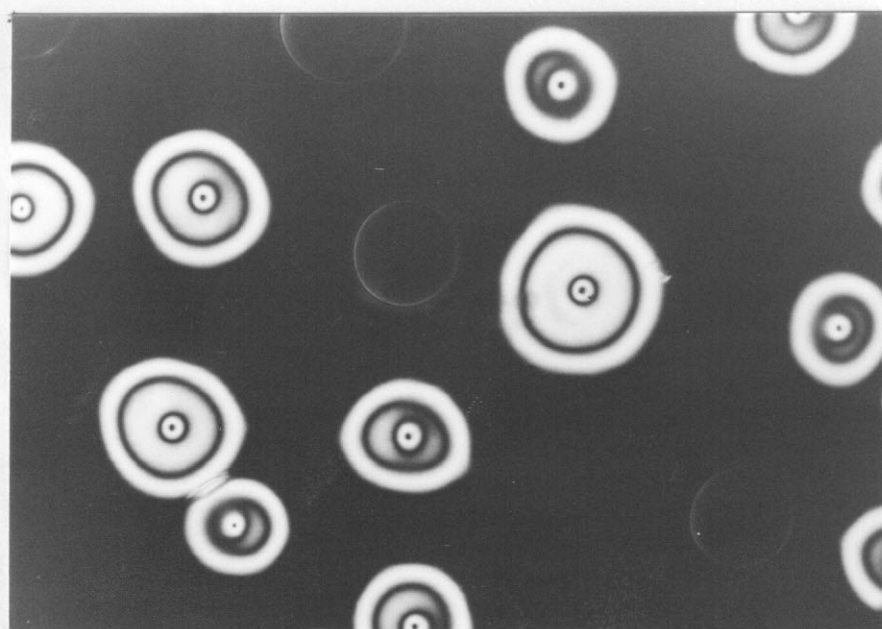


FIG.6.10. Sessile nematic drops on the CTAB-coated substrates. The dark circular regions surrounded by bright thin lines are the nematic domains in contact with both lower and upper substrates.

6.1.3 Summary of contact angle experiments

The observed contact angles of the nematic drops on various substrates are listed in Table 6.2.

TABLE 6.2. Contact angle of nematic 5CB at various solid surfaces.

Substrate	contact angle of the nematic liquid, α (degrees)
Rubbed PVA	< 20
Bare PVA	90
SiO(0°)	160 [*]
SiO(60°)	160 [*]
SiO(80°)	170 [*]
As cleaned Glass	150 [*]
Rubbed Glass	irregular but small
Rubbed and cleaned Glass	155 [*]
CTAB film	70

^{*} Values calculated from the contact angle of the isotropic liquid.

6.1.4 Relative stability of the nematic and the isotropic phases on treated surfaces

Upon plotting these results on the contact angle vs surface order-parameter space [see Fig.5.19] derived from the Landau-de Gennes theory as shown in Fig.6.11, we can clearly see the characteristic features of the present results.

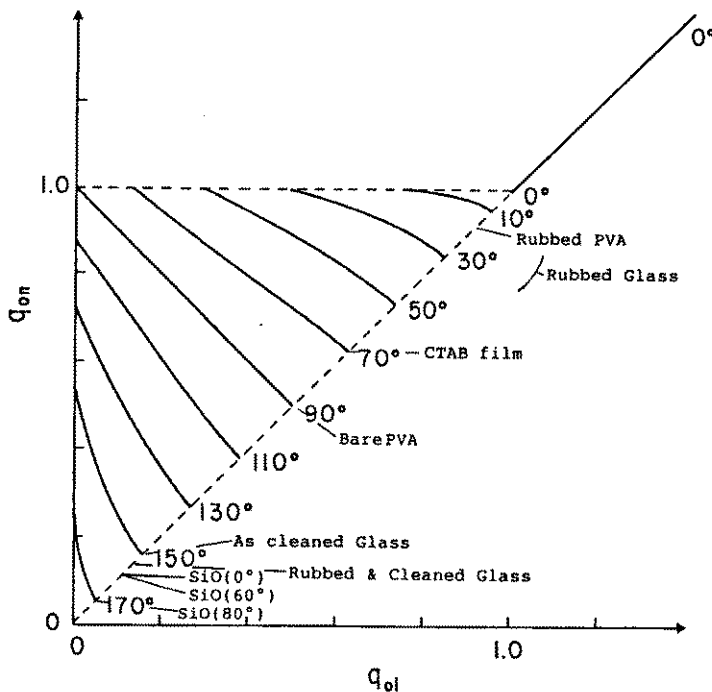


FIG.6.11. Contact angles of a nematic drop on variously treated substrates. Plotted over the iso-contact angle contours on the plane spanned by the surface order parameters q_{on} and q_{oi} , respectively, in the nematic and the isotropic phases [cf. Fig.5.19].

Namely, there exists a general tendency that rubbed or organic substrates are likely to give a small contact angle for the nematic, whereas inorganic substrates bring about an obtuse angle. Thus, based on Young's equation,

$$\gamma_{si} = \gamma_{sn} + \gamma_{ni} \cos \alpha,$$

we can conclude that on rubbed or organic substrates, the nematic state is more stable than the isotropic state ($\gamma_{sn} < \gamma_{si}$), but on inorganic substrates, the nematic state is less stable ($\gamma_{sn} > \gamma_{si}$) than the isotropic state; for more detailed discussion

of the factors determining the equilibrium shape of a nematic drop, taking account of the anisotropy of nematic liquid, see Appendix 2. Furthermore in Fig.6.11, we see that, as long as the Landau-de Gennes theory of the contact angle is correct, the surface order parameter at SiO or glass surface should be lower than the bulk order parameter, but at rubbed PVA or Glass, the surface order parameter has to always be comparable with the bulk nematic order parameter at the clearing point.

In view of the well-accepted fact that inorganic surfaces are usually of higher energy and strongly interacts with foreign substance, it might appear unreasonable that inorganic substrates are less efficient in orienting nematic molecules than organic substrates are. Although it is not the primary aim of this article to speculate on the origin of the alignment, it may be appropriate to give some words of justification for such unusual behavior as above.

The strong interaction between inorganic solid and nematic implies that nematic molecules should form themselves a strongly adsorbed layer. Circumstantial evidence for the existence of such a layer has been given by the fact that an SiO(0°) surface, which does not usually align nematics uniformly, can be made to orient nematic director by introducing the nematic liquid with a strong flow in the prescribed direction [11]; this unique axis persists even when the nematic is brought to the isotropic state.

Thus, the substrate that influences the bulk orientation is not the solid itself, but the solid covered with the nematic layer. And, the interaction between the adsorbed nematic layer and the neighboring nematics is of primary importance in determining their interfacial properties. Now, let us ask what happens when the nematic molecules in the adsorbed layer are oriented randomly rather than uniformly. On the one hand, it is clear that the effect of the adsorbed layer is to shield the field

due to solid. In this case, on the other, the mean-field felt by adjacent nematic molecules may be rather weakened in comparison with that in the bulk; this is because the large part of its neighbors are randomly oriented. Therefore, at least in the mean-field approximation, we would expect the orientational order near such a randomly adsorbed layer should be more or less deteriorated than in the bulk nematic phase. The effect of random field on the order formation [12,13] has been studied in conjunction with magnetic systems, invariably showing a certain reduction of the phase transition temperature or even a disappearance of the ordered phase itself.

6.1.4 Temporal change of the contact angle on evaporated SiO

Finally, in this section, we present an interesting observation concerning the contact angles on evaporated SiO(60°). As shown above, the contact angle of a nematic drop on the SiO(60°) is large, showing the relative instability of the nematic order. However, we observed that this contact angle was not a constant, but continuously changed from the time of preparation.

Figures 6.12 and 6.13 show the polarizing micrographs of the isotropic sessile drops 4 days and 10 days after the preparation, respectively. In the first 4 days, the sample was stored at a temperature a few degrees above the clearing point, and in the next 6 days, it was left at room temperature in the nematic phase. The micrograph just after the preparation has been shown in Fig.6.7(b).

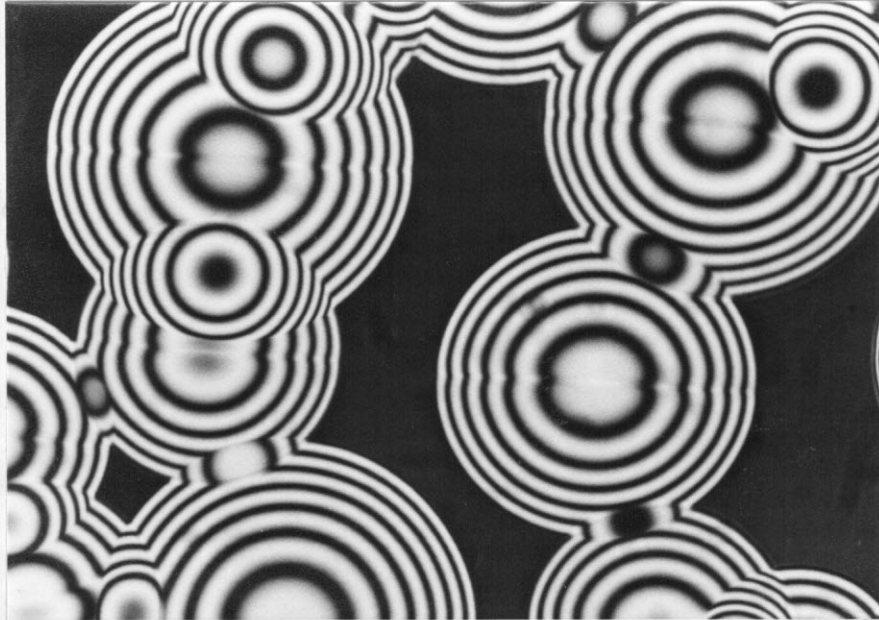


FIG.6.12. The equilibrium shape of the isotropic drops on SiO(60°) 4 days after the preparation. During this time, it was stored in the isotropic phase.

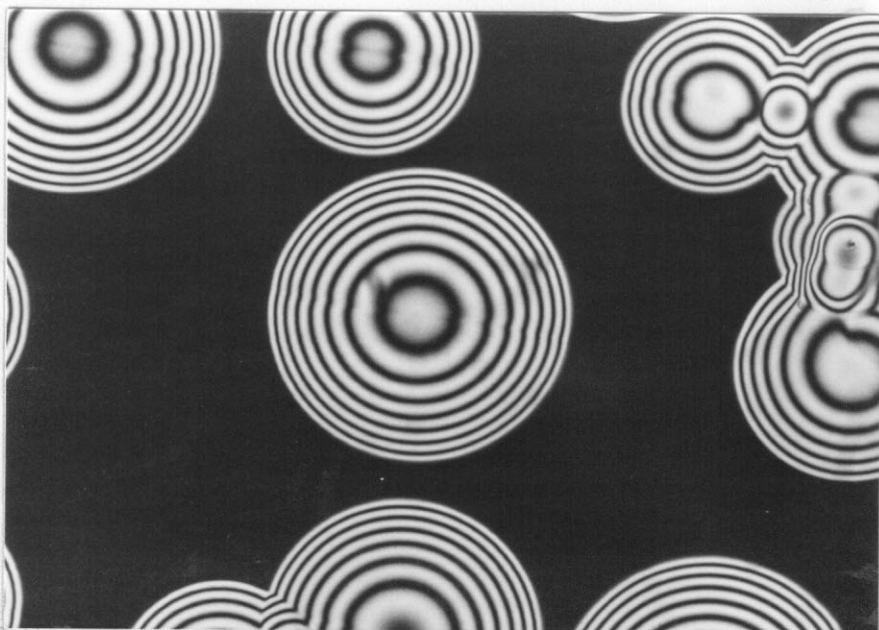
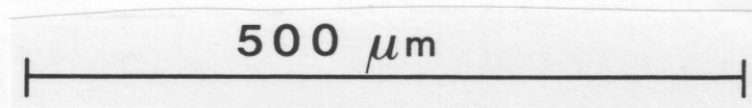


FIG.6.13. The equilibrium shape of the isotropic drops on SiO(60°) 10 days after the preparation.

As readily discernible, the contact angle of the isotropic drop has decreased steadily with time elapsed. In Fig.6.14, the contact angle of the nematic liquid is plotted as a function of time.

The contact angle may change as a result of various reasons such as impurity adsorption, rearrangement of adsorbed molecule, etc. However, the time scale of the change seems to be too long for the impurity adsorption to be dominant. It is indeed a right order of time

constant for the desorption and adsorption of strongly adsorbed molecules. Then, if it is correctly the manifestation of the spontaneous ordering process whose rate is limited by adsorption-desorption mechanism, it can indeed be considered as evidence for the existence of randomly oriented adsorbed layer.

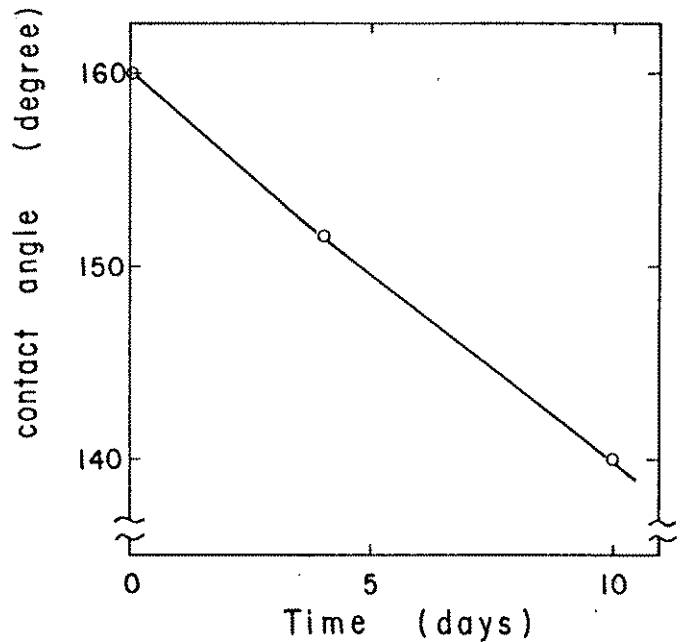


FIG.6.14. Time variation of the contact angle (for the nematic) on SiO(60°) after its preparation.

6.2 Wall-induced pretransitional birefringence

Wall-induced pretransitional birefringence yields direct information on the surface order parameter in the isotropic phase. So, it is a kind of experiment that supplements the knowledge drawn from the contact angle experiments. In view of the very different contact angles observed for the evaporated SiO films and the rubbed PVA, we have carried out the wall-induced birefringence experiments. The results of these measurements were found to be consistent with the contact angle experiments. The surface order parameter at the rubbed PVA-5CB interface is almost comparable with the order parameter in the nematic phase. However, the SiO-5CB interface exhibits only a negligible level of the pretransitional birefringence.

Birefringence measurement is the most powerful method to probe the orientational structure of liquid crystals. Since this method has been extensively employed and plays an important role in the present study as well (for thin film transition as well as anchoring strength measurement), it may be appropriate here to describe the elements of the ellipsometric birefringence measurement we have used in some detail. The results of the wall-induced pretransitional birefringence experiments follow next.

6.2.1 Measurement of a small optical phase retardation

Technically speaking, the wall-induced pretransitional birefringence experiment is nothing but a measurement of small optical anisotropy in liquid crystals. Although there are numerous methods available for measuring the refractive index of liquid crystals, the ellipsometric technique [14] may be the most sensitive one as far as the birefringence measurements are concerned; it may well be applied to the detection of a submonolayer-equivalent retardation.

Here, we shall describe the fully automated ellipsometric

system developed in our laboratory, which can detect a minute retardation down to 10^{-5} rad.

In Fig.6.15 shown is the setup of the ellipsometer system. The basic structure is identical with the ordinary ellipsometer. The light from a 2mW He-Ne laser is polarized, and is transformed to a circular polarized wave by a quarter wave plate. This light beam then passes through a stress-plate polarization modulator [15] and is led to the sample cell, which is placed in an electric oven. The strength of the transmitted light is detected by a photodiode through a quarter wave plate and a polarizer. The retardation due to the optical anisotropy of the sample can be obtained by measuring the first and the second harmonic components of the output light with respect the frequency of the polarization modulation.

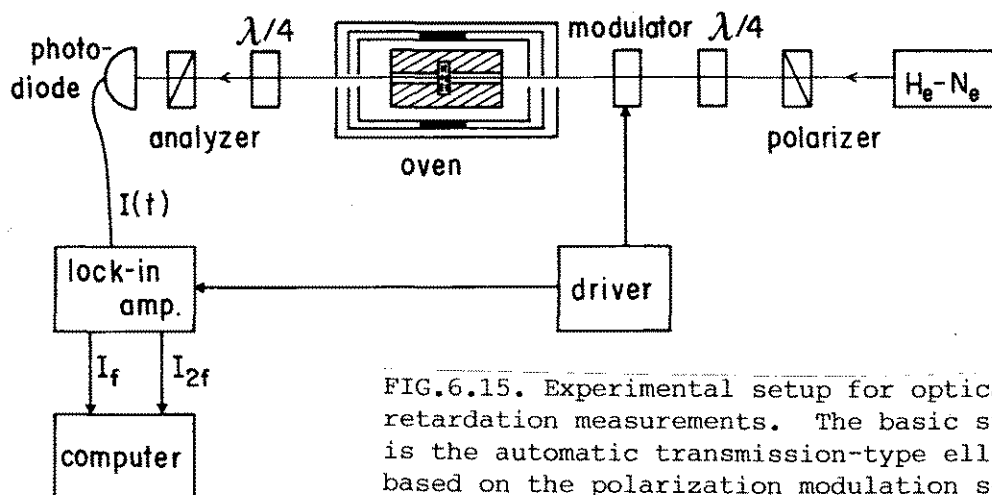


FIG.6.15. Experimental setup for optical phase retardation measurements. The basic structure is the automatic transmission-type ellipsometer based on the polarization modulation scheme. The modulator is operated at about 30 kHz, and the reference signal is fed to the lock-in amplifier.

The quantitative operation of this system can be readily analyzed when the imperfections of the optical parts can be neglected. At first, we assume that each pair of quarter wave plate and polarizer before and after the sample cell are set to form in each a circular polarizer; the optic axis of the quarter wave plate is inclined from that of the polarizer by $\pm\pi/4$.

Further, we assume the circular polarizers are set in such a way that in the absence of the sample and the modulator, the output signal vanishes.

Let $J=E(i,1)$ be the Jones vector representing the circular polarized light emitted from the first quarter wave plate with the principal axes of the stress plate modulator taken as the coordinate axis. Then, the action of the stress plate modulator is to modify its phase in a time dependent manner as follows:

$$J' = E(i, \exp i\phi(t)). \quad (6.2)$$

After passing through the optically uniaxial sample, whose optic axis is inclined by α from the axis of the modulator, J' is further transformed to

$$J'' = E(\exp(iR)[i\cos 2\alpha - \exp(i\phi)\sin 2\alpha], \\ [i\sin 2\alpha + \exp(i\phi)\cos 2\alpha]), \quad (6.3)$$

where R is the retardation due to the sample. Repeating these procedures until the end of the last polarizer, we obtain the time-dependent light intensity which impinges on the detector $I(t)$ as

$$I(t) = I_0[1 - \cos\phi\cos R - \cos 4\alpha\sin\phi\sin R]. \quad (6.4)$$

When $R=\phi=0$, it follows that $I=0$ as required from the setting. The phase modulation $\phi(t)$ induced by the modulator is generally written as

$$\phi(t) = \phi_0\sin 2\pi ft. \quad (6.5)$$

Therefore, by extracting the f - and $2f$ -components of $I(t)$, we can obtain both $\sin R$ and $\cos R$. Hence, in this method, R can be uniquely determined except for a difference of $2\pi n$. Another advantage comes from the fact that when R is small, the DC component of $I(t)$ also becomes a small quantity. So that, in

dealing with a small retardation, we can avoid the interference from shot noise which results mostly from the DC part which plays no role in the determination of R.

6.2.2 Measurement of Wall-induced pretransitional birefringence

We have measured the residual birefringence near the solid surface in the isotropic phase of 5CB by applying the above apparatus. The measurement of wall-induced birefringence has been performed by several authors [16-21] since the pioneering work of Miyano [16]. At present, it seems that, as far as a qualitative feature is concerned, a consensus has been reached as to the relationship between the wall-induced pretransitional birefringence and the nature of surface treatments. Namely, (1) rubbed substrate, be it inorganic or organic, brings about an enhanced order; (2) the surface order on an SiO film is negligibly small. Therefore, those results are seen to be, as a trend, compatible with the results of contact angle experiments described in Section 6.1. However, closer look at the problem soon reveals that there is still an inconsistency between the results of the birefringence and the contact angle experiments as pointed out by Sluckin and Poniewierski [22].

In this section, we report on a high resolution study of the wall-induced pretransitional birefringence, especially, on an SiO film-nematic interface. In contrast to the conventional studies, in which the induced birefringence has been believed not to exist on an SiO surface, we have observed a small but definitely finite surface ordering at SiO-5CB interface.

A. Pretransitional birefringence induced by a rubbed PVA surface

In Fig.6.16 shown is a typical trace of the retardation in the rubbed PVA-5CB cell as the temperature is lowered in the isotropic phase to the clearing temperature T_c (redrawn on single

substrate basis). Near T_c , we see an apparently diverging behavior in a similar manner as shown in Fig.5.15 for the surface order parameter $q_0=1.1$; however, it should be noted that it is in effect difficult to determine whether it is a true critical divergence or not, because the curve is not sensitive to the change in q_0 around $q_0=1$ as noted in Section 5.4, and the observed birefringence involves a spurious contribution from the glass substrate and the aligning PVA film, which, in some cases, amounts to 10^{-3} rad. So that, it is impossible to tell with confidence if the surface order parameter is larger or smaller than the order parameter in the nematic phase T_c . Moreover, when the retardation was observed under a very strict temperature control with the decreasing rate of 10^{-4} K/hr, the retardation showed a saturated behavior at temperatures a few 10^{-3} K above T_c . Such a behavior is inconsistent with the simple Landau-de Gennes theory of the wall-induced pretransitional birefringence [see Section 5.4], and is probably connected with the "finite size effect" which essentially gives the upper bound for the actual retardation.

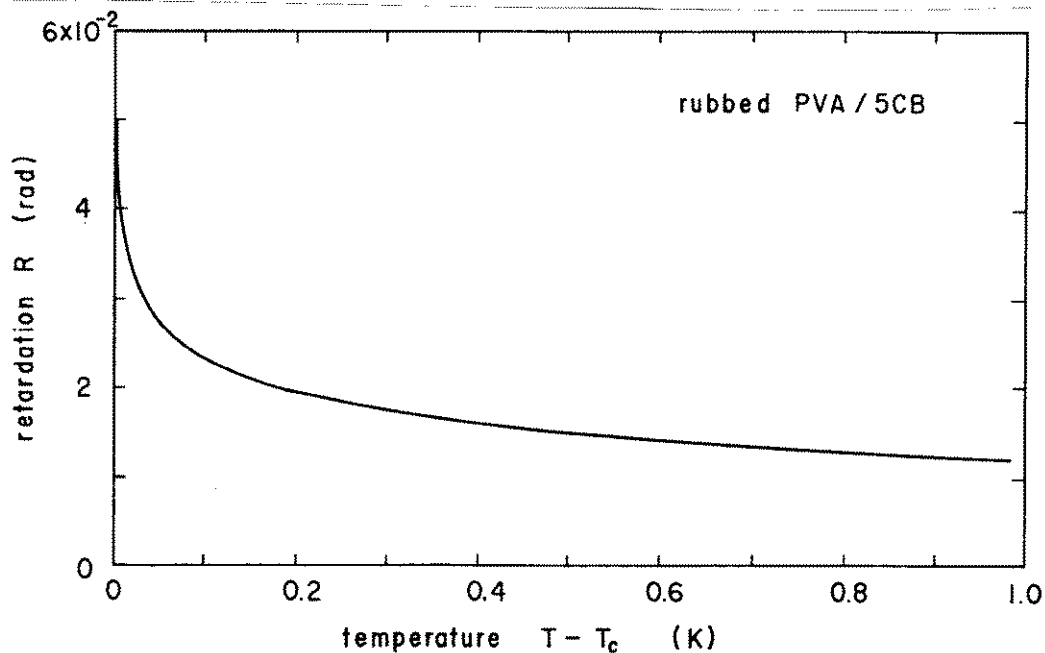


FIG.6.16. Wall-induced pretransitional birefringence at the rubbed PVA-5CB interface. The retardation shows a quasi-diverging increase as the clearing temperature ($T_c=35.3^\circ\text{C}$) is approached from the above.

Nevertheless, it is still of interest to estimate the surface order parameter. Here, we utilize Eq.(5.140). On assuming [23-25] that $T_c - T^* = 1.1$ K and $R_c = 0.011$ i.e., $\xi_c = 10$ nm, $\Delta n_c = 0.11$, we can transform the above retardation data to the temperature dependence of the reduced surface order parameter q_0 as shown in Fig.6.17. Depending on the magnitude of the spurious retardation R_s , the surface order parameter adopts a value slightly above ($R_s = 0$) and below ($R_s = 0.002$) the bulk order parameter.

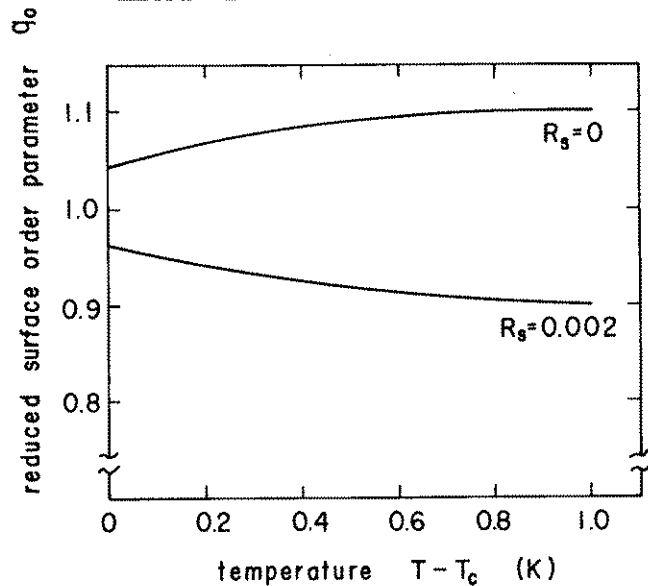


FIG.6.17. Reduced surface order parameter $q_0 = Q_0/Q_C$ as a function of temperature for the rubbed PVA/5CB interface. Whether q_0 is larger than unity or not strongly depends on the magnitude of the spurious retardation R_s .

B. Pretransitional birefringence induced by the SiO film

Figure 6.18 shows the variation of the retardation for the SiO(60°)-5CB interface.

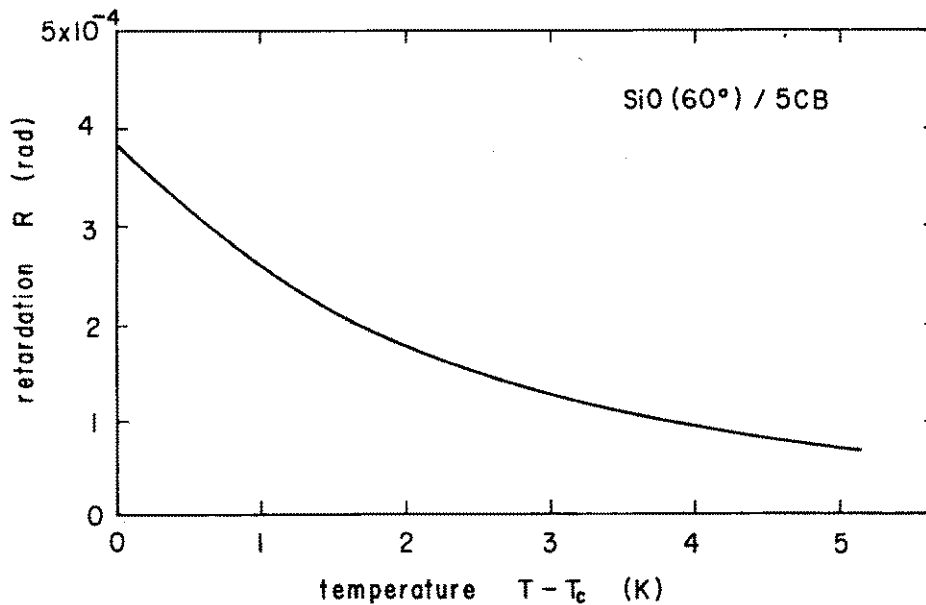


FIG.6.18. Wall-induced pretransitional birefringence at the SiO(60°)-5CB interface. Note that it is two orders of magnitude smaller than that at the rubbed PVA-5CB interface.

Obviously, the absolute value of the birefringence is nearly two-order smaller than that observed at the rubbed PVA-5CB interface, showing that the evaporated SiO is less effective in orienting nematic molecules than rubbed PVA. For a quantitative argument, however, it should be stressed that, similar to the case of rubbed PVA-5CB system, there exists a spurious contribution from the glass substrate and the SiO film, which may be as large as 10^{-3} rad and hence be comparable to the observed birefringence at present. Nevertheless, the temperature dependence of the spurious retardation was confirmed negligibly small by using a blank cell; thus, we can estimate the surface order parameter from the rate of variation of the observed birefringence. By utilizing the approximate formula Eq.(5.142), which holds for small q_0 , we obtain

$$q_0 = 0.037, \quad (6.6a)$$

for the SiO(60°)-5CB interface, where we have assumed the same values for bulk parameters as used above. Upon using $Q_c=0.27$ [23], we find for the surface order parameter in the isotropic phase,

$$Q_{oi} = 0.01. \quad (6.6b)$$

For SiO(0°), we could also measure the wall-induced pretransitional birefringence by making use of the flow-aligned uniform cell [11]. The surface order parameter was estimated to be $Q_{oi}=0.01$ in complete agreement with that we have just obtained for SiO(60°).

6.3 Nematic-isotropic transition in thin bounded films

When a thin layer of nematic liquid crystal is bounded by a couple of solid substrates to enhance the relative importance of liquid crystal-substrate interaction, a modification of the nematic-isotropic transition itself can be expected. Especially, since the nematic-isotropic transition is of weakly first order and hence the orientational order parameter is correlated over a long distance near T_c , a marked change of the transition behavior can be expected when the film thickness becomes comparable with the coherence length of the order parameter.

Sheng [26] and Schroder [27] studied the effect of a highly ordering substrate within mean field theory and showed that the transition temperature shifts upward as the nematic layer thins, and below a certain critical thickness of the order of 1000 Å, the transition becomes continuous. Sluckin and Poniewierski [22,28] also investigated the influence of a disordering substrate, and showed the occurrence of the depression of the transition temperature.

The purpose of this section is to describe the experimental results performed on thin nematic films bounded either by the oblique evaporation of SiO or by rubbed PVA. It is certainly shown that depending on the nature of the solid-nematic interfacial interaction, the nematic transition temperature shifts "upward" or "downward." Due to the semi-quantitative nature of the experiment, however, the problem concerning the turn over to a continuous transition could not be properly tackled. The present results are completely in accord with the results of the contact angle and the wall-induced pretransitional birefringence experiments, and point in the direction that the surface order is deteriorated at SiO surfaces and enhanced at rubbed PVA surfaces.

6.3.1 Experimental

Thin films of 5CB were prepared by sandwiching it in between an optical flat glass plate and a half convex lens of 1 m focal length as shown in Fig.6.19. The substrates were 30 mm in diameter and the film thickness changed from practically 0 at the center to about 200 μm at the edge of the substrate. The surface treatments tried were, as mentioned above, the oblique evaporation of SiO and the coating with PVA film followed by rubbing. Here, the treated substrates were carefully set to give a single crystalline (without twist) nematic film. The sandwiched film was placed in a brass cell, and the glass substrates were loosely fixed to the side wall with paraffine of 60° C melting point. The order-disorder transition was monitored by recording the birefringence as a function of temperature by using the experimental system described in the former section. The light beam was focused to 50 μm in diameter and impinged perpendicularly on the nematic film. The sample

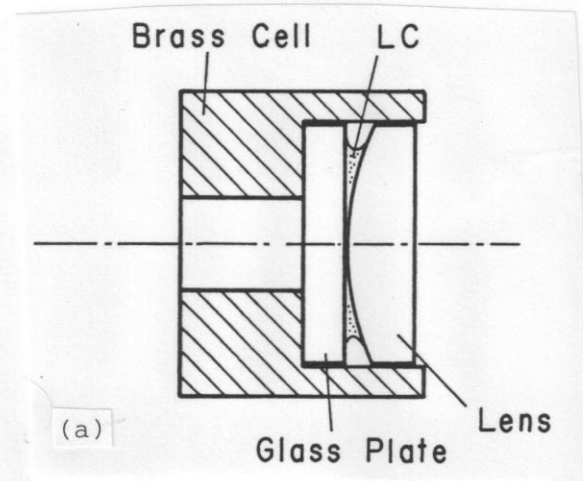
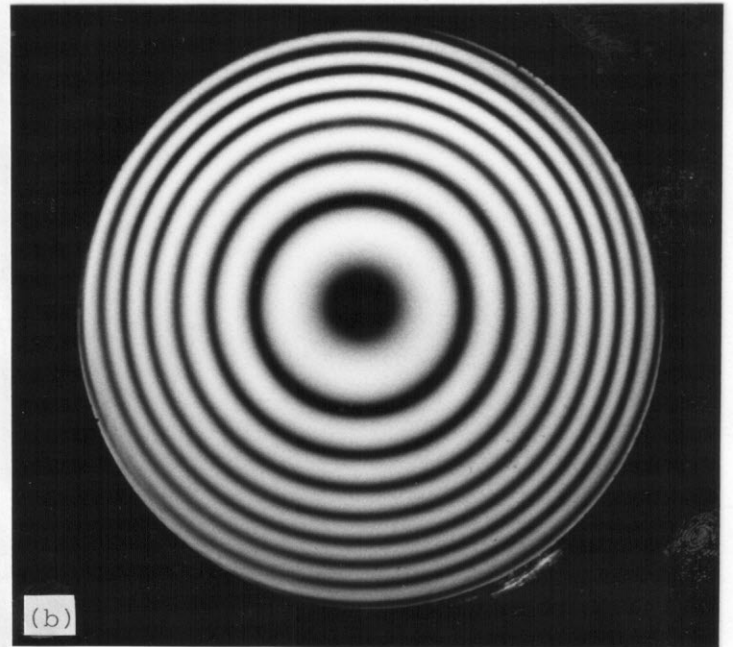


FIG.6.19. Cross-section view of the liquid crystal cell (a), and the birefringence Newton fringes observed when the cell was illuminated with a monochromatic light (540 nm) between crossed polaroids (b).

cell was placed in a precision temperature controlled oven, and the film thickness was changed by moving the oven as a whole with respect to the light path with a micrometer screw.

When studying the phase transition of a liquid thin film, we often found it difficult to insure the purity of the material, because of the large surface area-to-volume ratio. At present, however, the liquid crystal at relatively thick parts may serve as a reservoir of fresh material for thinner regions. Even if we assume the diffusion coefficient of the impurity to be as small as 10^{-7} cm²/s, the ample region of interest (within 1 mm from the center) can be virtually homogenized in a few days. For this reason, we always started the observation at least three days after the sample cell was prepared. In addition, the homogeneity was occasionally tested by confirming that the retardation varied symmetrically about the center as expected from the lens' shape.

On the other hand, the cell structure made it difficult to directly assess the actual thickness of the nematic layer, and also the film thickness itself seemed to change slightly when the temperature was varied over a relatively wide range, for example 5 K. However, since we were primarily interested in the qualitative behavior in the vicinity of the transition point, we restricted the temperature range of measurement to at most ± 0.2 K around the bulk transition temperature T_c (308.45 K), and the film thickness was roughly estimated from the retardation value at the lowest temperature by assuming the birefringence for bulk 5CB, $\Delta n = 0.11$.

6.3.2 Shift of transition temperature with the film thickness

Figure 6.19 shows the retardation as a function of temperature for thin films of 5CB sandwiched between evaporated SiO layers. For each film thickness, the retardation is normalized at $T = T_0$ to emphasize the qualitative changes occurring in the transition behavior as the nematic film thins.

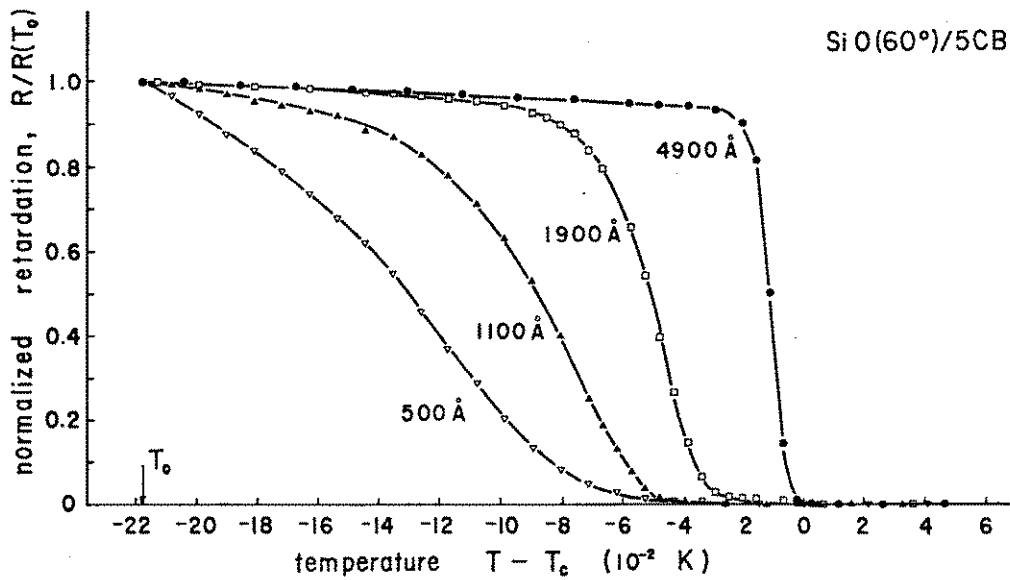


FIG.6.20. Temperature dependence of the retardation for 5CB thin films of various thicknesses sandwiched between evaporated SiO layers. For thicker films, the steepness of the transition is limited by the 10^{-2} °C-wide two phase region due to inherent impurity in the nematic. $T_c=35.3^\circ\text{C}$.

The most striking feature, here, is that the order-disorder transition changes from the virtually discontinuous one at 4900 Å to an apparently continuous one for thinner films. It must also be noted that the transition temperature, if it is identified with the inflection point, shifts downward by a few 10^{-2} K with the decrease in the film thickness. This result is consistent, qualitatively at least, with the previous observation that the ordered phase is less stable than the disordered phase on this substrate.

In macroscopic terms, the variation of the transition temperature, ΔT , with the film thickness can be related to the latent heat q and the change of the solid-liquid crystal interfacial tensions:

$$\Delta T = 2T_c(\gamma_{si} - \gamma_{sn}) / \rho q d. \quad (6.7)$$

Now, we know from the contact angle experiments that $\gamma_{si} - \gamma_{sn} \sim -\gamma_{ni}$. Then, substituting typical values $\rho=1.0 \text{ g/cm}^3$,

$q=2\times 10^3$ J/g and $\gamma_{ni}=2\times 10^{-5}$ J/m², we find $\Delta T=-0.06$ K for a 1000 at showing a reasonable agreement with the present observation.

The retardation for 5CB thin films between rubbed PVA substrates is shown in Fig.6.21.

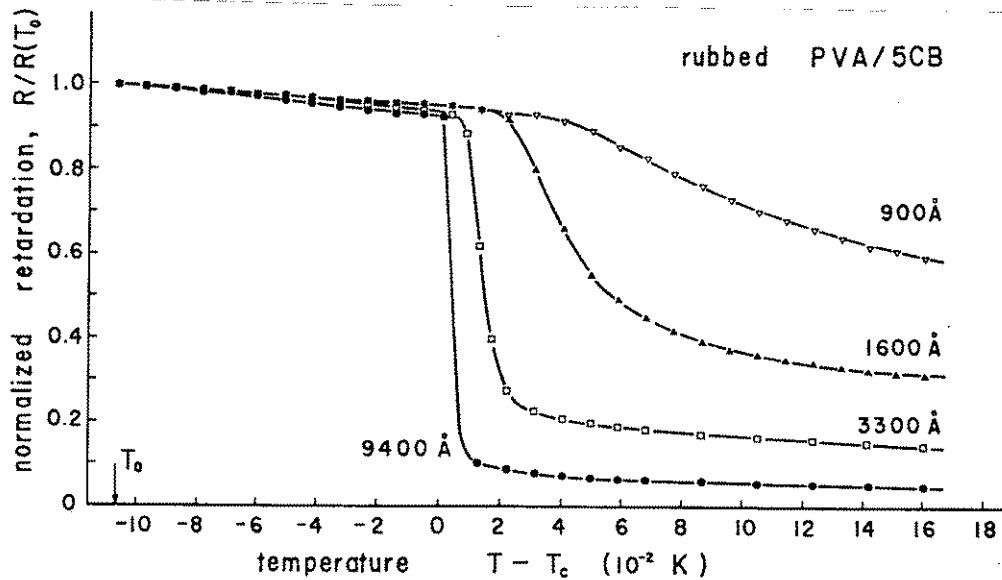


FIG.6.21. Temperature dependence of the retardation for 5CB thin films of various thicknesses sandwiched between rubbed PVA layers. In contrast to the case of SiO substrates, the transition point moves upward as the 5CB thins, and the nematic remains to be well ordered at temperatures above the clearing point ($T_c=35.3^\circ\text{C}$).

This time, the temperature dependence of the retardation below T_c is almost independent of the film thickness; but above T_c , they show a marked enhanced (averaged) order, strongly depending on the film thickness. In contrast to the case of SiO substrates, the nematic-isotropic transition temperature now shifts upward by about 4×10^{-2} K while the thickness is reduced to 900 Å. In view of the wetting property of the rubbed PVA as shown in Section 6.1, this is also in reasonable agreement with the Kelvin equation Eq.(6.7).

Chapter 7

STABILITY OF

THE SURFACE-INDUCED ALIGNMENT

The alignment of a nematic director brought about by a boundary is stabilized by some kind of "anisotropic force" that exists at the interface. It is therefore quite natural to expect that if the degree of stability, namely the anchoring strength, could be measured, one would have direct information through which the microscopic origin of the alignment might be glimpsed. Although numerous attempts [1-32] have been made in this direction so far, it is only recently that reliable measurements of the anchoring strength have become possible due to the advent of appropriate experimental techniques. Accordingly, the measurement and theoretical interpretation of the anchoring strength is still in its infancy, and there remain a number of unaddressed problems open to future investigations.

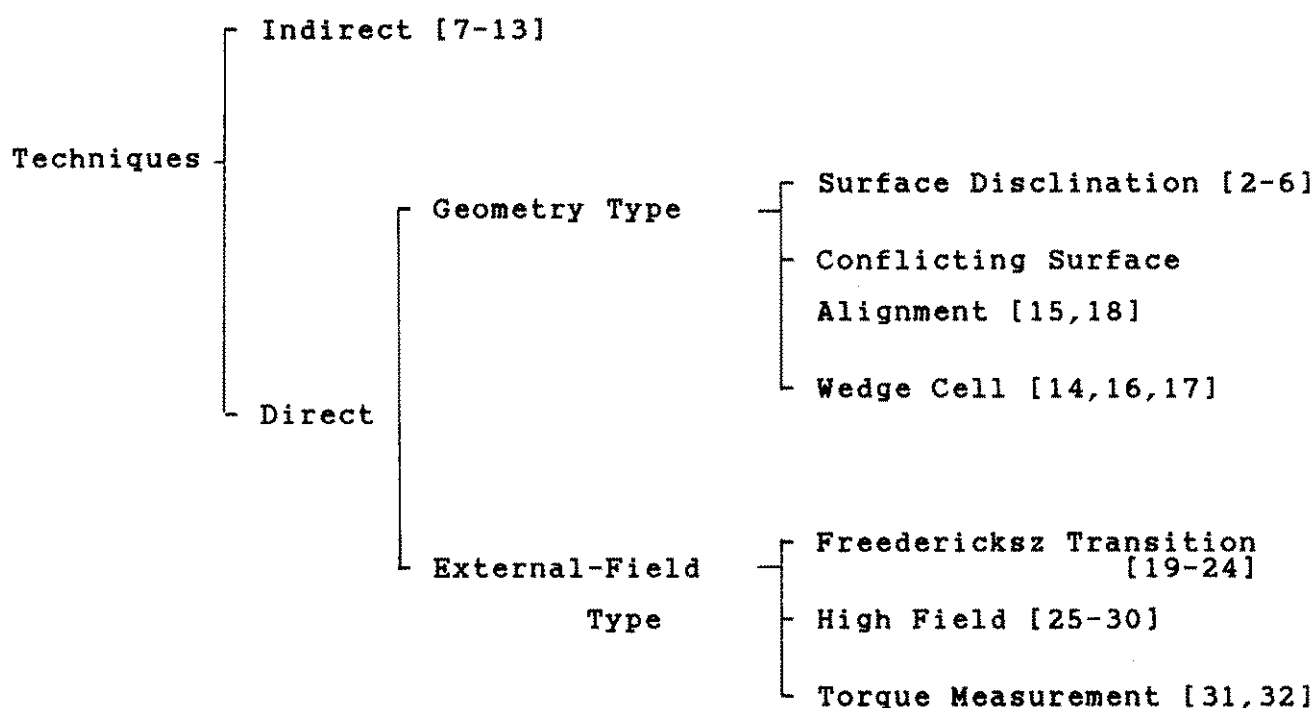
In this section, we shall describe the current status of the experimental investigations of the anchoring strength focusing on the work of the present author. In view of the crucial role played by the experimental techniques, conventional methods for measuring the anchoring strength are first reviewed with an emphasis on their reliability and precision. Next, we describe the "high electric field technique (HEFT)," developed by the present author [29,30], in detail. HEFT is an extremely simple, yet accurate method, which allows a determination of not only the extrapolation length but the entire functional form of the anisotropic part of the interfacial tension of a nematic-wall interface. The results of application of HEFT to rubbed polyvinylalcohol-nematic interface and obliquely evaporated SiO₂-nematic interface are presented, showing that the anchoring strength at the former interface is rather strong without

marked temperature dependence, while that of the latter is much smaller with a strong temperature-dependence. In particular, it is shown that the anchoring strength at the nematic-SiO interface exhibits a quasi-critical weakening toward the nematic-isotropic transition temperature. Based on the thermodynamic arguments and the Landau-de Gennes theory of the anchoring strength, it is argued that the observed behavior can be ascribed to the "surface-induced disordering transition" occurring at the nematic-SiO interface, in consistent with the contact angle and the wall-induced pretransitional birefringence experiments described in Chapter 6.

7.1 Techniques for measuring the anchoring strength

As emphasized in Chapter 4, the concept of the orientational anchoring strength has double facets, one of which is concerned with the energetics of the nematic interface and the other with its geometrical property (concerning the director profile). Furthermore, since there are several geometrical properties which are essentially connected with the nature of the interface, we can in principle conceive quite a few methods for use in measuring the anchoring strength. In Table 1, current techniques are classified according to their measurement principles.

TABLE 7.1 Classification of techniques for measuring the anchoring strength.



First, we distinguish between an "indirect" [7-13] and a "direct" [2-6,14-32] methods. The indirect method refers to a technique which rests on the physico-chemical measurements of work

of adhesion by means of, for example, traditional contact angle experiments. The direct method, on the other hand, relies, "literally," on the measurement of director configuration when the nematic is subjected in one way or another to an external curvature stress. The direct method is further categorized into several sub-groups according to how the orientational torque is brought about. For instance, the "high electric field technique (HEFT)," with which we are concerned ourselves later, belongs to the class of direct, external-field type, high field techniques.

Unfortunately, however, the applications of these techniques have been often made without paying due attention to the conditions which make these techniques really applicable. Consequently, the experimental data found in the literature often show a large scatter or inconsistency, which is so large as to force people to think that no concrete (more than an order-of-magnitude estimate) information can be drawn from measurements of the anchoring strength. One of the purposes of this chapter is to show that this is not at all the case, and if an appropriate technique is used under a controlled condition, data on the anchoring strength can be a quite significant source of information on which the nature of a nematic interface is faithfully projected as originally conceived. Below, we shall review typical methods of anchoring strength measurement with a special emphasis on the conditions which are needed to be met for these techniques to be of practical utility; for HEFT, see the following sections.

7.2.1 Indirect method

This type of technique consists in the comparison of the interfacial tension when the director is aligned parallel or perpendicular to the easy axis. As fully discussed in Chapter 4, the interfacial tension is in general dependent on the orientation

of the director at the interface, and we can express it as $\gamma(\mathbf{n})$, with \mathbf{n} being the director at the dividing surface; in the case of a planar interface between a rigid solid and a nematic liquid, the dividing surface can be taken at an arbitrary position without affecting the definition of the anchoring strength.

A. Principle

Based on the Rapini-Papoular type interfacial tension, i.e.

$$\begin{aligned}\gamma(\mathbf{n}) &= \gamma_0 + \Delta\gamma(\mathbf{n}) \\ &= \gamma_0 + \frac{1}{2} E_a [1 - (\mathbf{n} \cdot \mathbf{n}_e)^2],\end{aligned}\quad (7.1)$$

one readily obtains a formal expression of the anchoring energy:

$$E_a = 2[\gamma(\pi/2) - \gamma(0)],\quad (7.2)$$

where $\gamma(\pi/2)$ and $\gamma(0)$ denote the interfacial tension when the director is set parallel or perpendicular to the easy axis \mathbf{n}_e . Therefore, it appears that if $\gamma(\pi/2)$ and $\gamma(0)$ are known, the anchoring energy E_a is automatically calculated via Eq.(7.2).

The next step to follow is the evaluation of the relevant interfacial tensions by means of the use of the Girifalco-Good-Fowkes relation [see Section 5.1]. In order to simplify the argument, let us here consider the case in which only the dispersion force is acting between the solid and the nematic. In the literature [7-13], it is tacitly assumed that the interfacial tension $\gamma(\mathbf{n})$ can be written in the Girifalco-Good-Fowkes form,

$$\gamma(\mathbf{n}) = \gamma_S + \gamma_L(\mathbf{n}) - 2[\gamma_S \gamma_L(\mathbf{n})]^{1/2},\quad (7.3)$$

even when the director \mathbf{n} differs from the easy axis \mathbf{n}_e , where γ_S and γ_L are the "surface tensions" of the solid and the nematic, respectively, and the last term represents the work of adhesion at an arbitrary director \mathbf{n} [see the foot note on the next page].

Then, putting Eq.(7.3) into Eq.(7.2), we find

$$E_a = 2(\gamma_S^{1/2} - \gamma_L(\pi/2)^{1/2})^2 - 2(\gamma_S^{1/2} - \gamma_L(0)^{1/2})^2. \quad (7.4)$$

When there exist contributions from other types of interactions, they must be summed together to yield the anchoring energy.

This is the fundamental formula for the indirect physico-chemical technique for estimating the anchoring energy at a solid-nematic interface. The remarkable feature of this technique is that the only ingredients of the theory are the surface tensions of the solid and the nematic phases, when they exist independently. When, in particular, the anisotropy of the nematic surface tension, $\Delta\gamma_L = \gamma_L(\pi/2) - \gamma_L(0)$, is small, Eq.(7.4) approximately reduces to

$$E_a \sim 2 \frac{\gamma_L(0)^{1/2} - \gamma_S^{1/2}}{\gamma_L(0)^{1/2}} \Delta\gamma_L. \quad (7.5)$$

This equation shows that when $\gamma_L > \gamma_S$, the nematic should align at the solid surface in the same direction as at the free surface, and when $\gamma_L < \gamma_S$, it should align in the perpendicular direction. This is in its spirit similar to the Creagh and Kmetz empirical rule described in Chapter 3.

 Note: Strictly speaking, it is not allowed to regard the work of adhesion for an arbitrary alignment as a work needed to reversibly separate the solid and the nematic in which the director is uniformly aligned. This follows from the very definition of the easy axis; that is, a uniform alignment is possible (except for some metastable orientation, if any), if and only if $\mathbf{n} // \mathbf{n}_e$. So, the right-hand side of Eq.(7.3) is not an equilibrium quantity, while the left-hand side is. This pitfall results from the use of $\gamma(\mathbf{n})$, treating it as a function which can be taken independently of the bulk state. This point is often neglected in the literature.

Naemura [9,10] applied these formulas to a wide variety of surfactant-coated substrates in contact with a nematic liquid crystal, and favorably compared the resultant anchoring energies (on the order of 10^{-5} J/m²) with those directly measured with the Freedericksz technique (see below).

B. Consideration of validity and suggestions

The fundamental formula of this method, Eq.(7.4), is not a rigorous thermodynamic formula to be generally satisfied by interfacial tensions of nematics. But, as it stands, it is an approximate equation based on a number of assumptions whose validity should be carefully assessed.

One of the most serious shortcomings of this method is the use of Girifalco-Good-Fowkes semi-empirical formula, which, as mentioned in Section 5.1, can be used with certain confidence only when an error of a few 10^{-3} J/m² is permissible. As indicated above, however, the anchoring energies are usually on the order of 10^{-5} J/m². In view of these estimates, it might appear almost senseless to calculate anchoring energies by means of such physico-chemical formulas as Eqs.(7.4) and (7.5).

Nevertheless, the truth may not be this bad, because in Eq.(7.4) the anchoring energy is given as a difference between two formally similar terms. So, it is reasonable to expect that these errors (resulting from the assumption underlying the Girifalco-Good-Fowkes formalism) would cancel out to a large extent, leaving much less error in the anchoring energy. However, analogous to the interfacial tension itself, it is hardly possible to assess how perfect this cancellation will be achieved. As pointed out in Section 5.1, the Girifalco-Good-Fowkes theory neglects the variations in structure from one interface to the other. In this respect, Eq.(7.4) can be expected to in general lead to a better result, if one estimates the first and the second terms for interfaces at as similar as possible conditions. As regards

Eq.(7.5), however, this condition can be restated as that it is important to use a good value for the surface tension anisotropy for the nematic free surface; this is not at all an easy work in itself.

We should also point out another drawback of this method, which is in a sense even more serious than that mentioned above. If the director at the solid-nematic interface aligns in the same direction as that at the nematic free surface, we obtain the following inequality from Eqs.(7.4) and (7.5):

$$E_a \leq \Delta\gamma_L. \quad (7.6)$$

This indicates that the anchoring energy at any solid surface can never exceed the value at the free surface. This is physically unreasonable, as will become clear if we imagine a solid which exerts a strong torque as to enhance the alignment at the free surface. This paradox arises from the underlying assumption of the Girifalco-Good-Fowkes theory which does not properly take account of the anisotropic nature of the nematic liquid.

In view of all of these, the indirect physico-chemical technique appears to be only of qualitative or heuristic significance, as drawing an easy picture of the surface-induced alignment in terms of a language familiar to surface scientists. As a quantitative method for measuring anchoring strength, it is almost fatal that we cannot estimate the uncertainty involved in the resulting anchoring energies. On the other hand, as a theory for predicting the alignment, it is still empirical containing too many unjustifiable assumptions. This kind of technique would be useful only after the nature of the anisotropic part of the interfacial tension is fully understood.

7.2.3 Direct methods of measuring the anchoring strength

This type of techniques measure, in one way or another, the effect of solid substrate on the director profile near the interface. In this context, the wall effect manifests itself only when the director is deformed from its equilibrium configurations. Since the nematic liquid crystal can be made to deform in many ways and no liquid crystal is free from its boundary, every possible deformed configuration of nematic director contains more or less information as to the nature of the solid boundary. Thus, corresponding to all of these phenomena, there can in principle be innumerable methods for estimating the anchoring strength.

The most important characteristic of a good measurement method is that it allows for accurate, unambiguous, and easy determination of the property in question, preferably in wide variety of different systems. The development of experimental techniques for measuring the anchoring strength is actually a history of selecting director configuration that meets these requirements. And, we have now a rather large stock of such attempts as listed in Table I.

The earliest direct measurement of the anchoring energy was performed by Kleman and Williams [2] through the measurement of the width of a surface disclination line: The surface disclination line they observed was an intersection between the substrate and a wall singularity of director orientation (like a Neel wall in ferromagnets), and the region on the substrate where the director is misoriented from the easy axis is limited to inside the disclination line. The width of the surface disclination line is determined by the compromise between the bulk and the surface elastic energies; the former decreases as the disclination line becomes thicker, while the latter increases. By an approximate calculation, the optimum thickness h of the surface disclination line has been expressed as [2,4-6],

$$h \sim \pi(dK/E_a)^{1/2} = \pi(dd_e)^{1/2}, \quad (7.7)$$

where d is the cell thickness, and K the Frank elastic constant; in the case of a Neel wall, E_a and d_e are the azimuthal anchoring energy and the extrapolation length, and in the case of a Bloch wall, they corresponds to the polar anchorage. According to Eq.(7.7), the anchoring energy and hence the extrapolation length can be obtained, if the thickness of the surface disclination is known for a cell of known thickness.

Such a surface disclination is shown to be thermodynamically stable only when the cell thickness d is smaller than d_e . Hence, h is in reality not greater than the extrapolation length. Therefore, since the resolution of a polarizing microscope is at best a few micrometers, quantitatively meaningful measurements can be made, only when the anchoring energies are smaller than than 10^{-6} J/m². As the anchoring energies of solid-nematic systems of practical significance are mostly around 10^{-5} J/m², this presents a severe restriction on the applicability of this method. Furthermore, since the production of surface disclination lines cannot be satisfactorily controlled, this technique has not gained a popularity as a practical method for measuring the anchoring strength.

Other direct methods listed in Table 1 have been developed more systematically to allow measurements in uniformly aligned samples with wider range of anchoring conditions. Below, we shall focus on two prototypical techniques, (1) wedge-cell technique, and (2) Freedericksz technique as, respectively, representing the geometry-type and the external field-type techniques.

A. Characteristic lengths in a surface-aligned nematic layer under an external field [29]

In order to make a unified treatment of these techniques, it is helpful to first consider the characteristic lengths governing the director configuration in a surface-aligned nematic layer in equilibrium under an external field.

Let us consider a nematic layer confined in between a couple of solid substrates [Fig.7.1]. In view of later application to the high electric field technique (HEFT), we imagine that an external electric field is applied perpendicular to the solid-nematic interface; however, the case of magnetic field can be treated in completely the same manner. Further, we assume that the deformation is essentially planar, that is, the director is always lie in a plane determined by the easy axis and the substrate normal.

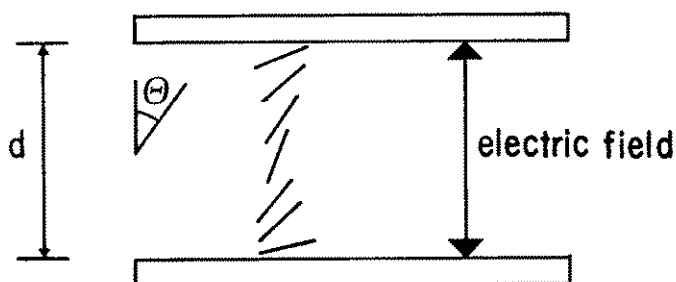


FIG.7.1. Director deformation under an electric field.

Including the effect of electric field along with the surface contribution from the lower and the upper substrates, the thermodynamic potential of the system can be written, per unit area, as

$$\Omega = \Omega_0 + \frac{1}{2} \int_0^d [(K_1 \sin^2 \theta + K_3 \cos^2 \theta)] \left(\frac{d\theta}{dz} \right)^2 + \frac{D^2}{(\epsilon_1 \cos^2 \theta + \epsilon_2 \sin^2 \theta)} dz + r_0(\theta_0) + r_d(\theta_d), \quad (7.8)$$

where K_1 and K_3 are the Frank elastic constants for splay and bend deformations, ϵ_1 and ϵ_2 are the dielectric constants for field directions parallel and perpendicular to the director, respectively, and D denotes the electrical displacement, which is shown to be constant throughout the nematic. $\gamma_0(\theta_0)$ and $\gamma_d(\theta_d)$ are the interfacial tensions for the lower and the upper solid-nematic interfaces, each regarded as a function of the polar angle of the director at the interface. Here, we consider the case of a positive dielectric anisotropy, i.e., $\Delta\epsilon = \epsilon_1 - \epsilon_2 > 0$, so that the director is forced to align along the electric field. Except for the presence of an electric field, this expression is identical with what we have studied in Section 4.6. This is a thermodynamically meaningful representation of the thermodynamic potential in Gibbs' sense, if the interface director is interpreted as the director one would have when the bulk director configuration is extrapolated to the interface.

The equilibrium configuration of the director in the "bulk" nematic is the one that minimizes the thermodynamic potential for fixed boundary conditions. Then, applying the variational calculus, we can obtain the Euler-Lagrange equation which specifies the equilibrium profile:

$$\frac{d}{dz} \left[(K_1 \sin^2 \theta + K_3 \cos^2 \theta) \frac{d\theta}{dz} \right] = \frac{d}{d\theta} \frac{D^2}{2(\epsilon_1 \cos^2 \theta + \epsilon_2 \sin^2 \theta)}. \quad (7.9)$$

and the boundary condition at $z=0$ and d ,

$$\frac{d\gamma_0(\theta_0)}{d\theta} = (K_1 \sin^2 \theta + K_3 \cos^2 \theta) \frac{d\theta}{dz} \Big|_{z=0}, \quad (7.10)$$

$$\frac{d\gamma_d(\theta_d)}{d\theta} = -(K_1 \sin^2 \theta + K_3 \cos^2 \theta) \frac{d\theta}{dz} \Big|_{z=d}. \quad (7.10)$$

These are the fundamental set of equations from which all the properties of the director configuration (in the bulk) can be deduced. A detailed analysis of these equations will be carried out in the next section in relation to HEFT.

For the purpose of qualitative discussion, let us adopt the one-constant approximation ($K_1=K_3=K$) and assume that the dielectric anisotropy is small ($\epsilon_1 \sim \epsilon_2 \sim \epsilon$). Then, Eq.(7.9) can be reduced to

$$K \frac{d^2\theta}{dz^2} = \frac{D^2 \Delta \epsilon}{2\epsilon^2} \sin 2\theta. \quad (7.11)$$

This equation clearly shows that in an electric field with D , the director tends to reorient along the field direction over the distance d_c given by

$$d_c = \epsilon (K/\Delta \epsilon)^{1/2}/D. \quad (7.12)$$

In other words, the region where the director is appreciably different from the field direction is practically localized within an interfacial layer up to d_c from the solid surface. This is the "electric coherence length" for the director. In the case of a magnetic field, a coherence length can be similarly defined as $d_c = \chi (K/\Delta \chi)^{1/2}/H$, where H denotes the magnetic field. The electric or magnetic coherence length is a characteristic length of the system which describes the response of the nematic to these external field.

In the absence of the external field, it is clear [from Eq.(7.11)] that the director rotates with a uniform gradient $[\theta_e(d) - \theta_e(0)]/d$. Here, $\theta_e(0)$ and $\theta_e(d)$ are the angles of easy axis at the lower and the upper boundaries, respectively; they are not in general different from each other. And d is a measure how strongly the system opposes to nonuniform rotations induced by, say, an external field. This is another characteristic length of

the system.

The final characteristic length of the system is the extrapolation length d_e associated with the solid-nematic interface. This is of course a measure specifying how amenable the interfacial orientation is to an external stimulus.

These three characteristic lengths exhaust all the independent parameters in the system having the dimension of length. Depending on their relative magnitudes, the behavior of the director is essentially determined. Owing to the concept of these characteristic lengths, essential connections among various techniques can be easily visualized, thereby enabling us to easily appreciate the validity condition of each method.

B. Wedge-cell technique

This is a typical example of the geometry-type methods, which introduces a necessary director deformations by means of geometry of the cell configuration or such without the aid of an external field.

Figure 7.2 shows the cell geometry used in the wedge-cell technique, which was originally proposed by Riviere et al.[14] and later refined by Barbero, et al.[17]. The principle of the method is rather simple. Imagine that we are to measure the anchoring strength at the lower interface with an easy axis $\Theta_e(0)$. In this technique, the upper substrate must be subjected to an appropriate surface treatment so that it gives the nematic an easy axis $\Theta_e(d)$ which is distinct from that

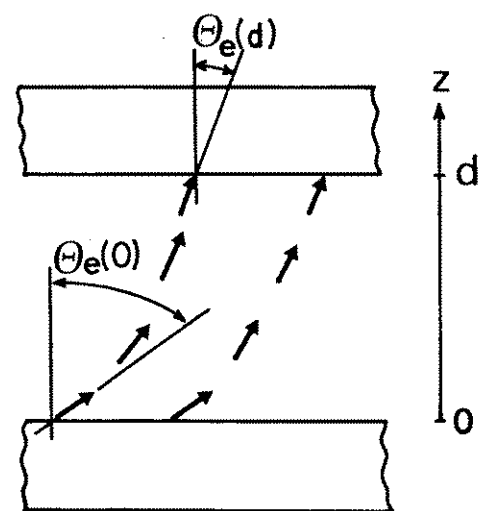


FIG.7.2. Cell geometry in the wedge-cell technique.

at the lower surface, with a sufficiently strong anchoring strength in comparison with the anchoring energy to measure. Then, both substrates are put into a "wedge" configuration subtending a very small angle (on the order of 10^{-4} rad) so that at each point, the configuration of the nematic director can be well approximated by that in a usual parallel cell.

The conflicting boundary conditions at the solid-nematic interface amounts to a so-called "hybrid" alignment in which a spontaneous deformation of the director exists. Because of the absence of an external field, the Euler-Lagrange equation (including the boundary condition) can now be interpreted as a statement of the continuity of the curvature stress along the z-axis. In the one-constant approximation, the equilibrium director profile is given by a linear function of z, as mentioned above. Therefore, based on the geometrical meaning of the extrapolation length, we can write the boundary condition at the lower interface as

$$\frac{\theta_o - \theta_e(0)}{d_e} = \frac{\theta_e(d) - \theta_o}{d}. \quad (7.13)$$

Hence, the angle of the director at the lower surface is given by

$$\theta_o = \theta_e + [\theta_e(d) - \theta_e(0)] / (1 + d/d_e). \quad (7.14)$$

This equation shows that if θ_o can be measured as a function of the cell thickness d, we can in principle obtain d_e thereof. Riviere, et al. [14] measured the angle θ_o as a function of d at an interface between an obliquely evaporated SiO and 4-hexyl-4'-cyanobiphenyl (6CB) [$\theta_e(0) \sim 30$ deg] from an optical reflectivity experiment. And, they found the anchoring energy at about 4×10^{-6} J/m².

In Eq.(7.14), it should be strictly noted that the extrapolation length and the cell thickness is appearing via

$1+d/d_e$. As a result, an appreciable degree of change in the tilt angle can be expected to occur only when d becomes as small as d_e . This fact essentially limits the accuracy of the technique. Put differently, this technique requires that the cell thickness be reduced down to

$$d \sim d_e \quad (7.15)$$

so as to assure a good accuracy. Therefore, it will be experimentally difficult to measure an extrapolation length smaller than $1 \mu\text{m}$; the upper bound for the anchoring energy would therefore be of some around 10^{-5} J/m^2 .

Measurement of the tilt angle Θ_0 from an optical reflectivity involves a rather complicated numerical fitting procedure. Barbero, et al. [17] eliminated this process by observing the "overall configuration of the director" by means of the integrated optical phase retardation experiment. As already noted in the former chapter, the phase difference R between the ordinary and the extraordinary rays after passing through a nematic sample is expressed as

$$R = \frac{2\pi}{\lambda} \int_0^d \Delta n(\Theta) dz, \quad (7.16)$$

where λ is the wavelength of light and $\Delta n(\Theta)$ is the "effective" birefringence of the nematic with the orientation angle Θ for a light beam traversing along the z -axis.

Thus, substituting Eq.(7.14) into Eq.(7.16), we can approximately express R in the following form:

$$R = A(2\pi/\lambda)[d + (1-C)d_e], \quad (7.17)$$

where A and C are constants independent of d and d_e as defined by

$$A = \int_{\Theta_e(0)}^{\Theta_e(d)} \Delta n(\Theta) [\Theta_e(d) - \Theta_e(0)]^{-1} d\Theta,$$

$$C = \Delta n[\Theta_e(0)]/A.$$

Therefore, when R is plotted against the thickness d , a straight line is obtained, from the intercept of which with the ordinate axis, we can immediately find the extrapolation length. This property provides us with a very easy and convincing method for deducing the anchoring strength. In this case, too, the validity of the technique is fundamentally governed by the relative magnitude of the cell thickness and the extrapolation length.

A modification of the Riviere method, in which the easy axis at the upper boundary is intentionally changed from one place to the other in a parallel cell geometry has been developed by Komitov and Petrov [15].

C. Freedericksz-transition technique

Another important variation of an experimental technique for anchoring measurement comes from the use of an external field as an agent to induce a desired director deformation.

As shown in Chapter 2, when the initial (uniform) orientation of the nematic layer is strictly perpendicular to the applied electric or magnetic field (we are considering the case of $\Delta\varepsilon > 0$ and $\Delta\chi > 0$), the initial alignment remains to be stable up to a well defined threshold field strength. And, above this threshold, the director begins to rotate toward the field direction.

This phenomenon called the Freedericksz transition originates from the competition between the torque exerted by the applied field and that due to the cell boundary. So, it could soon be suspected that the strength of the anchorage would have some effect on the transition. This was indeed first studied by Rapini-Papoular [19] as early as 1969 in relation to the wall-effect on the magnetic field-induced Freedericksz transition.

As understandable from its origin, the Freedericksz

transition is expected to occur (between strong anchoring substrates, i.e. $d_e \sim 0$), when the electric or magnetic coherence length becomes almost comparable with the cell thickness:

$$d_c \sim d. \quad (7.17)$$

Indeed, in combination with Eq.(7.12), this condition yields a threshold voltage $V_{th} \sim (K/\Delta\epsilon)^{1/2}$ [$H_{th} \sim (K/\Delta\chi)^{1/2}/d$]; the exact formulas for infinitely strong anchoring condition are given by $\pi(K/\Delta\epsilon)^{1/2}$ and $\pi(K/\chi)^{1/2}/d$.

Let us now imagine that both substrates are identical and such that the anchorage is of finite strength with the extrapolation length d_e . Then, in view of the obvious fact that the nematic director can be freely rotated in the absence of surface anchorage, it is naturally expected that the threshold field should be reduced, as the anchorage weakens. Rapini and Papoular [19] showed that even when the anchorage is not infinitely strong, the director exhibits a Freedericksz transition with the threshold field is given by

$$\cot\left(\frac{\pi}{2} \frac{H_{th}}{H_{th^0}}\right) = \pi \frac{d_e}{d} \frac{H_{th}}{H_{th^0}}, \quad (7.18)$$

where H_{th^0} denotes the threshold field when the condition of infinitely strong anchorage applies; the corresponding relation for the threshold voltage follows immediately from the above, when H is replaced by V . When expanded with respect to d_e/d , Eq.(7.18) can be written in a more transparent form:

$$H_{th} = \frac{H_{th^0}}{1 + 2d/d_e}, \quad (7.19)$$

Hence we see, as expected, that as the anchoring weakens and/or the cell thickness decreases, the threshold field decreases. So that, if the threshold field is measured for samples of various

thicknesses, the extrapolation length can be obtained. As in the case of the wedge-cell technique, this equation also shows that an accurate measurement is possible, only when the nematic layer thickness is reduced down to the comparable level as the extrapolation length. Then, in view of Eq.(7.17), the Freedericksz transition technique can be characterized as

$$d \sim d_c \sim d_e. \quad (7.20)$$

Naemura [20,22] observed the threshold field of the magnetic field-induced Freedericksz transition for layers of MBBA, which had been homeotropically aligned between substrates treated by various surfactants. He obtained anchoring strengths on the order of $10^{-6} \sim 10^{-5} \text{ J/m}^2$ by using sample layers with a thickness ranging from 10 μm to 100 μm . More recently, however, Yang and Rosenblatt [23], and Rosenblatt [24] realized the importance of using a thinner sample cell [to meet the condition in Eq.(7.20)] in conjunction with a high magnetic field to make an accurate measurement by means of this technique. They applied a magnetic field of up to 100 kG to a few micrometers thick layer of MBBA, homeotropically aligned between surfactant-treated substrates, and found values of the anchoring energy about one order of magnitude larger than that obtained by Naemura. The results of these studies indeed show that it is crucial to meet the requirement expressed in Eq.(7.20) for making reliable measurement of the anchoring strength.

However, it should be pointed out that the first condition of Eq.(7.20), is an auxiliary one resulting from the use of the Freedericksz transition; so that as long as one uses this technique it is automatically satisfied. On the other hand, the latter condition is the true criterion which assures the validity of this technique. Thus, it is expected that by relaxing the condition $d \sim d_c$, we can devise a more versatile method for measu-

ring the anchoring strength. Actually, there have appeared several attempts [27,28] to obtain the anchoring energy from the analysis of the director deformations in the field region well above the threshold of the Freedericksz transition. In this case, there is no restrictions on the sample thickness, and one can freely achieve the second criterion $d_c \sim d_e$ by using a sufficiently strong field. This is the idea of the high field techniques developed by Yang [27], and van Sprang and Aartsen [28]. In these techniques, however, the director deformation is expressed by a very complicated function of the field strength which implicitly involves the anchoring strength. Consequently, a laborious multi-variable numerical fitting procedures has to be performed to extract the anchoring strength.

D. Summary and comparison with HEFT

In the case of a geometry type technique, the necessary director deformation is brought about by a geometry factor characterized by the length d . In the external field type technique, it is specified by the coherence length d_c . These facts show that accurate direct measurements of the anchoring strength entail that the source of the desired director deformation should invariably have a characteristic length comparable with the extrapolation length to be determined. This condition is directly or indirectly a decisive factor for determining the performance of a particular technique.

The high electric field technique (HEFT) developed by the present author [29] is a substantial sophistication of the conventional high field techniques [27,28]. By intentionally using a very "thick" sample, with a view to completely decoupling the effect of d and d_e on the director configuration, it is made possible to measure the anchoring strength in a simple, yet unambiguous manner which does not require any numerical fitting

procedure as in the conventional techniques. This is the consequence of the fact that HEFT can be conceptually more appropriately classified as a geometry-type technique rather than as an external field-type; indeed, the reciprocal of the field strength acts like the cell thickness in the wedge cell technique. HEFT is reasonably insensitive to uncertainties both in material parameters such as the elastic constants and in the cell thickness, and is possible to determine the entire functional form of $\gamma(\Theta)$.

Finally, important characteristics of various "direct" techniques are summarized in Table 2.

TABLE 7.2 Comparison of typical "direct" techniques for measuring the anchoring strength

	Wedge-cell	Freedericksz transition	High field	HEFT
Anchorage	polar	both	polar	polar
$d_e(\text{min})$	500 nm	10 nm	10 nm	10 nm
$E_a(\text{max})$	10^{-5} J/m^2	10^{-3} J/m^2	10^{-3} J/m^2	10^{-3} J/m^2
Sample Preparation	complicated	complicated	easy	easy
Data Analysis	easy	easy	complicated	easy
Oblique Alignment	possible	in principle possible	in principle possible	possible

$E_a(\text{max})$: Largest anchoring energy measurable by the technique.

$d_e(\text{min})$: Smallest extrapolation length measurable.

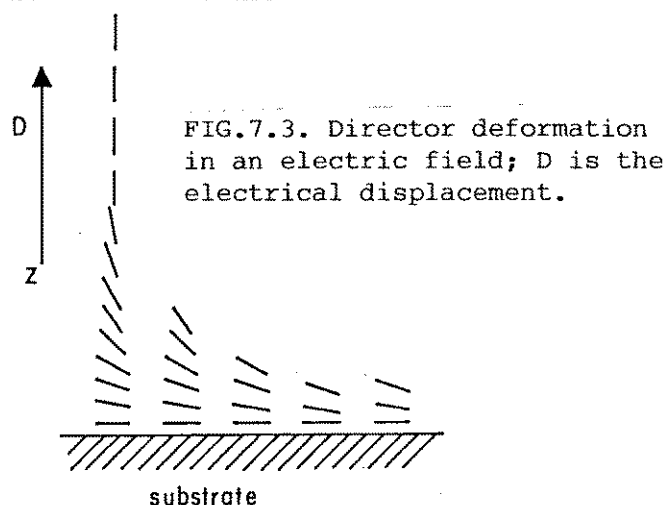
7.2 The high electric field technique

7.2.1 Intuitive account of the principle

The high electric field technique (HEFT) provides us with a means to accurate and straightforward method to measure the polar anchoring strength at a solid-nematic interface. As it is based on the very fundamental property of the Frank elastic theory, it seems appropriate here to give an intuitive comprehensible account of the measurement principle before going into the detailed mathematical analysis of HEFT.

To illustrate the point, let us first consider a semi-infinite nematic liquid crystal bounded by a substrate under an electric field applied perpendicular to the interface [see Fig.7.3]. We imagine that the nematic assumes a uniform planar alignment in the absence of the electric field.

In the presence of a finite electric field, the director tends to rotate toward the field direction as one moves from the interface into the bulk nematic. So, $\theta(z)$ is always an decreasing function of z , which (exponentially) approaches 0 as $z \rightarrow \infty$. The actual director profile is determined by the condition of minimum thermodynamic potential Ω [cf. Eq.(7.8)], which results in the Euler-Lagrange equation for $\theta(z)$ supplied with an appropriate boundary condition expressing the torque balance at the interface, Eqs.(7.9) and (7.10). For the present purpose, however, it is sufficient to note that the integral in Eq.(7.8) can be



transformed to the form $D \times J[\Theta(\zeta)]$, if $\zeta = Dz$ is regarded as a new variable of integration instead of z , where $J[\Theta(\zeta)]$ is a functional of $\Theta(\zeta)$ without an explicit dependence on D . As a consequence, a universal function of ζ , $\Xi(\zeta)$, must exist, with which we can write $\Theta(z)$ as

$$\Theta(z) = \Xi[D(z+d_e)], \quad (7.21)$$

where d_e is a parameter which determines the angle at $z=0$, i.e. Θ_0 , and may in general be a function of D ; as appreciable from the form of Eq.(7.21), d_e has a meaning of the length of extrapolation to the point where $\Theta=0$. Equation (7.21) reveals that the director profile satisfies a simple scaling property for such transformations as $D \rightarrow kD$ and $(z+d_e) \rightarrow k^{-1}(z+d_e)$. HEFT rests entirely on this property.

If the anchoring at the interface is of finite strength, Θ_0 should deviate more and more from $\Theta_e = \pi/2$ as the electric field increases, and how fast it is gives a measure of the anchoring strength. From Eq.(7.21), therefore, it is evident that the measurement of the anchoring strength essentially reduces to the determination of the extrapolation length d_e .

In HEFT, we also observe the optical phase retardation R between the ordinary and the extraordinary rays which a light beam suffers when traversing the nematic liquid crystal along the z direction. For a light with wavelength λ , R is given by

$$R = \frac{2\pi}{\lambda} \int_0^{\infty} [n_{\text{eff}}(\Theta) - n_o] dz, \quad (7.22)$$

where $n_{\text{eff}}(\Theta)$ is the effective refractive index for extraordinary light when the director is tilted by Θ from the interface normal, and n_o is the index of refraction for ordinary light. Since n_{eff} approaches n_o as $z \rightarrow \infty$, the above integral remains finite even for a semi-infinite system. Combining Eq.(7.21) with Eq.(7.22), we

obtain

$$R = \frac{1}{D} \frac{2\pi}{\lambda} \int_{\theta_0}^0 [n_{\text{eff}}(\theta) - n_o] \frac{d\Xi^{-1}}{d\theta} d\theta \quad (7.23)$$

where $\Xi^{-1}(\theta)$ is the inverse function of Ξ . This is the fundamental equation of HEFT.

The important feature of Eq.(7.23) can be seen, if the anchoring is assumed infinitely strong so that $\theta_0 = \pi/2$. In this case, the integral in Eq.(7.23) becomes a constant independent of the field strength. Hence, when R is plotted against $1/D$, a straight line passing the origin should result. On the other hand, when the anchoring is of finite strength, the increase of θ_0 with D also contributes. In order to see the behavior at such low fields as to induce only a small deviation in θ_0 , it is convenient to expand the integral in Eq.(7.23) about $D=0$:

$$R = \frac{1}{D} [(RD)_0 - D \frac{2\pi}{\lambda} (n_e - n_o) \frac{d\Xi^{-1}}{d\theta_0} \frac{d\theta_0}{dD} \Big|_{D=0} + \varepsilon], \quad (7.24)$$

where $(RD)_0 = \lim_{D \rightarrow 0} RD$, n_e the refractive index for extraordinary ray, and the residue ε is of the order of D^3 when $d(d_e)/dD$ vanishes at $D=0$ otherwise the order of D^2 . By differentiating Eq.(7.21) with respect to D , Eq.(7.24) reduces, up to 0th order in D , to

$$R = \frac{1}{D} (RD)_0 - \frac{2\pi}{\lambda} (n_e - n_o) d_e, \quad (7.25)$$

where $d_e(D=0)$ is written as d_e for simplicity. This shows that when R is plotted against $1/D$, the effect of a finite anchoring strength emerges as a downward shift of the straight line from that corresponding to the infinite anchoring strength.

In considering the realistic cases of finite thickness

samples, it is helpful to note that, even in the semi-infinite case, the essential contribution to R comes from a small region near the interface which extends over the electric coherence length d_c defined in Eq.(7.12). Therefore, a finite-thickness liquid crystal held between a pair of substrates can be expected to behave like a pair of semi-infinite systems, when the voltage across the cell is well above the threshold voltage for the Freedericksz transition, $V_{th} = \pi(K_1/\Delta\epsilon)^{1/2}$, so that the elastic deformation is well localized near the substrates. Therefore, we have

$$R(\text{finite}) = 2 \times R(\text{semi-infinite}), \quad \text{when } V \gg V_{th}.$$

Since the zero-field retardation of a planar cell with thickness d is given by $R_0 = 2\pi d(n_e - n_o)/\lambda$, and D is proportional to the product of the capacitance of the cell C and the applied voltage, we finally obtain

$$\frac{R}{R_0} = \frac{I_0}{CV} - 2 \frac{d_e}{d}, \quad \text{when } V \gg V_{th}, \quad (7.26)$$

for a sandwich-type planar cell, where I_0 is a proportional constant which depends only on the bulk parameters of the liquid crystal and the cell geometry. Thus, we can directly determine the extrapolation length d_e from the plots between R/R_0 and $1/CV$. This situation is schematically illustrated in Fig.7.4. In order that this method be of practical utility, however, the two somewhat conflicting conditions, $V \gg V_{th}$ and

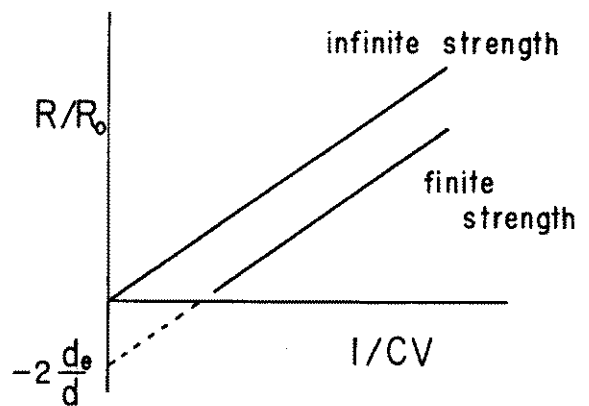


FIG.7.4. Schematic illustration of R/R_0 vs $1/CV$ plot.

$\pi/2 - \theta_o \ll 1$, must be met at the same time. This is achieved by choosing the cell thickness d in such a way that $d \gg d_e$.

As one may have noticed, we have so far made no use of the torque balance equation at the interface; that is, we have only worked with the bulk equation and have been naturally led to the concept of the extrapolation length. This is what we have experienced in Chapter 4, in developing the surface thermodynamics of a nematic interface. From a purely macroscopic view point, the extrapolation length d_e is a more fundamental concept than the anchoring energy. The primary parameter that the present method gives directly is the extrapolation length, not the anchoring energy. This situation is completely analogous to the cases of other "direct" techniques for measuring the anchoring strength.

7.2.3 Mathematical analysis of HEFT

In this section, we shall present a complete mathematical formulation of HEFT following the route drawn in the previous section. We will then examine the possible uncertainties involved in the resulting extrapolation length and anisotropic part of the interfacial tension due to errors in the material parameters and the cell thickness.

A. Formulation

We begin with the expression of the thermodynamic potential Eq.(7.8) for a nematic sample of thickness d . We assume that the lower and the upper interfaces are identical, having the common easy axis θ_e and interfacial tension $\gamma(\theta_o)$; so that, we have $\gamma(\theta_o) = \gamma_o(\theta_o) = \gamma_d(\theta_d)$ and $\theta_o = \theta_d$.

Integrating the Euler-Lagrange equation Eq.(7.8) once, we obtain

$$(K_1 \sin^2 \theta + K_3 \cos^2 \theta) \frac{d\theta}{dz} - \frac{D^2}{\epsilon_1 \cos^2 \theta + \epsilon_2 \sin^2 \theta} = \text{const.}$$

Since the system under consideration is obviously symmetrical about the mid-plane at $z=d/2$, the gradient of θ disappears at this point. Then substituting $z=d/2$ in the above, we can readily evaluate the constant of integration to give

$$\left(\frac{d\theta}{dz}\right)^2 = \frac{\Delta\varepsilon D^2}{K_1 \varepsilon_1^2} \frac{\sin^2\theta - \sin^2\theta_m}{(1+\kappa\cos^2\theta)(1-\alpha\sin^2\theta)(1-\alpha\cos^2\theta_m)}, \quad (7.27)$$

where $\alpha = \Delta\varepsilon/\varepsilon_1$ and $\kappa=(K_3-K_1)/K_1$. The angle of the director at the mid plane is denoted by θ_m .

The director deformation in the nematic layer is here optically detected by way of the measurement of the optical phase retardation R . In Eq.(7.22), where R is defined, the effective refractive index for the extraordinary ray should be specifically written as

$$n_{\text{eff}}(\theta) = n_o/(1 - \nu\sin^2\theta), \quad (7.28)$$

where

$$\nu = (n_e^2 - n_o^2)/n_e^2. \quad (7.29)$$

Then, combining Eqs.(7.22), (7.27), and (7.28), we obtain

$$\begin{aligned} \frac{R}{R_o} &= 2(K_1/\varepsilon)^{1/2} \frac{\varepsilon_1}{dD} \int_{\theta_m}^{\theta_o} \frac{1-\nu+(1-\nu)^{1/2}}{1-\nu\sin^2\theta+(1-\nu\sin^2\theta)^{1/2}} \\ &\times \frac{(1+\kappa\cos^2\theta)^{1/2}(1-\alpha\sin^2\theta)^{1/2}(1-\alpha\sin^2\theta_m)^{1/2}}{(\sin^2\theta - \sin^2\theta_m)^{1/2}} \sin^2\theta d\theta. \end{aligned} \quad (7.30)$$

Here $R_o=2\pi d(n_e-n_o)/\lambda$ is the value of the retardation of the cell when the director assumes a uniform planar alignment.

As the applied voltage V is increased above the Freedericksz threshold, the elastic deformation inside the nematic tends to localize near the liquid crystal-wall interface. We assume here that the cell thickness is chosen in such a way that there exists

a substantial range of voltage satisfying

$$d \gg d_c \gg d_e, \quad (7.31)$$

where d_c is the electric coherence length [cf. Eq.(7.12)]. The condition $d \gg d_e$ insures that the finiteness of the anchoring strength does not influence the director configuration at voltages around the threshold voltage of the Fredericksz transition V_{th} [$=\pi(K_1/\Delta\epsilon)^{1/2}$]. Furthermore, when $d \gg d_c$ holds, the nematic director behaves almost like a semi-infinite liquid crystal in contact with the substrate. Then, in this case, we can safely set $\Theta_m=0$ in Eq.(7.30). Numerical calculations of Θ_m based on Eq.(7.27) shows that when V exceeds $6V_{th}$, Θ_m becomes smaller than 10^{-3} [see Fig.7.5].

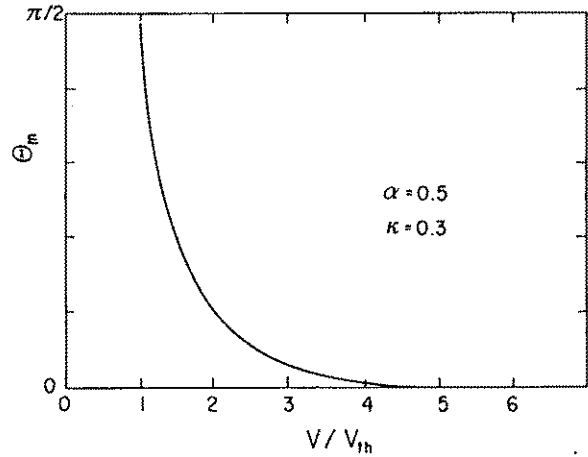


FIG.7.5. Tilt angle at the mid-plane of the cell as a function of the applied voltage.

In order to transform Eq.(7.30) to a more workable form, we should note that the electrical displacement can be related to the applied voltage by

$$D = CV/S, \quad (7.32)$$

where C and S are the capacitance and the electrode area of the nematic cell, respectively. Then with $\Theta_m=0$, we can rewrite Eq.(7.30) and the boundary condition Eq.(7.10) as follows:

$$\frac{d\gamma(\Theta_o)}{d\Theta_o} = \pi \frac{K_1}{d} \frac{CV}{\xi} \frac{(1+\kappa \cos^2 \Theta_o)^{1/2}}{(1-\alpha \sin^2 \Theta_o)^{1/2}} \sin \Theta_o, \quad (7.33)$$

where $\xi = (\epsilon_1 S/d) \times \pi(K_1/\Delta\epsilon)^{1/2}$;

$$\frac{R}{R_0} = \frac{\xi}{CV} I(\alpha, \kappa, \nu; \theta_0),$$

where

$$I(\alpha, \kappa, \nu; \theta_0) = \frac{2}{\pi} \int_0^{\theta_0} \frac{1 - \nu + (1 - \nu)^{1/2}}{1 - \nu \sin^2 \theta + (1 - \nu \sin^2 \theta)^{1/2}} \times (1 + \kappa \cos^2 \theta)^{1/2} (1 - \alpha \sin^2 \theta)^{1/2} \sin \theta \, d\theta. \quad (7.34)$$

These constitute the fundamental set of equations for HEFT.

The linear relationship between R and 1/CV as noted in the previous section can be derived by substituting

$$\gamma(\theta_0) = \frac{1}{2} E_a (\theta_0 - \theta_e)^2, \quad (7.35)$$

into Eq.(7.33), and expanding Eq.(7.34) up to first order in $(\theta - \theta_e)$:

$$\begin{aligned} \frac{R}{R(0)} &= \frac{k}{CV} - 2 \frac{K_1 \sin^2 \theta_e + K_3 \cos^2 \theta_e}{E_a d} \\ &= \frac{k}{CV} - 2 \frac{d_e}{d}, \end{aligned} \quad (7.36)$$

where R(0) denotes the retardation in the absence of the electric field [equal to R₀ if $\theta_e = \pi/2$], and k is a constant defined by

$$k = \frac{\xi I(\alpha, \kappa, \nu; \theta_e)}{\sin^2 \theta_e} \frac{1 - \nu \sin^2 \theta_e + (1 - \nu \sin^2 \theta_e)^{1/2}}{1 - \nu + (1 - \nu)^{1/2}}. \quad (7.37)$$

Equation(7.36) has just the same form as Eq.(7.26), and shows that when R/R(0) is plotted against 1/CV, a straight line results with the intercept at $-2d_e/d$. The present equation is however not restricted to the planar alignment, but equally applies to oblique alignment. This is, in fact, an analogous situation to that we encounter in the wedge cell technique in which R is linear in the cell thickness. Hence there is a good correspondence between the

cell thickness in the wedge cell technique and $1/CV$ in HEFT.

The original set of equations, Eq.(7.33) and (7.34) also provide a means to determine the functional form of $\gamma(\Theta_0)$ without assuming any a priori form as Eq.(7.35). Imagine that all the bulk parameters are known. Then, if the retardation and the capacitance are known as functions of the voltage, Eq.(7.34) uniquely defines the functional relation between Θ and V . Next, using Eq.(7.33), we can obtain $d\gamma/d\Theta_0$. Finally, we must recall that this procedure is valid only when the effect of finite cell thickness and that of finite anchoring strength are substantially decoupled by the use of a thick enough cell.

B. Estimation of systematic error

To examine how seriously the uncertainties in material parameters affect the estimate for Θ_0 and the resultant interfacial tension, we note first the following approximate formula:

$$I(\alpha, \kappa, \nu; \Theta_0) \sim \frac{1}{\pi} \frac{(2-\alpha)^{1/2}(2+\kappa)^{1/2}}{1 + 3\nu/8} (1 - \cos\Theta_0) \\ \times \left[1 + \frac{1}{3} \left(\frac{3}{8} \nu - \frac{1}{2-\alpha} + \frac{1}{2+\kappa} \right) (1 - 2\cos\Theta_0 - 2\cos^2\Theta_0) \right]. \quad (7.38)$$

Using the above equation, we can readily show that the error in Θ_0 can be written as

$$\delta\Theta_0 \sim - \frac{1}{3} \left[\frac{\delta\alpha}{(2-\alpha)^2} + \frac{\delta\kappa}{(2+\kappa)^2} - \frac{3}{8} \delta\nu \right] \sin 2\Theta_0 \\ - \delta[RCV/R(0)k] / \sin\Theta_0. \quad (7.39)$$

This indicates that the error in Θ_0 due to uncertainties in the bulk parameters becomes most serious when $\Theta_0 \sim \pi/4$. The absolute

value of the error, however, remains at most a few degrees, even when α 's involve errors as large as 0.1. In particular, since ν itself is usually smaller than 0.2, this result shows that for the present purpose, only a very crude value for ν is needed.

7.3 Experimental determination of $\gamma(\theta_0)$

The functional form of the anisotropic part of the solid-nematic interfacial tension has long been a matter of considerable debate[33,34], since Rapini and Papoular [19] postulated a sine-function dependence. However, no concrete experimental support or objection has been presented, due largely to the technical difficulty associated with directly determining the interfacial tension when the interface director is substantially deviated from the easy axis.

By applying HEFT, we have for the first time succeeded to experimentally determine the complete functional form of the interfacial tension for an interface between obliquely evaporated SiO and 5CB. The result is mostly in support of the Rapini-Papoular form, but there remains a small discrepancy which cannot necessarily be attributed to experimental error, requiring the introduction of higher order terms.

A. Experimental

The SiO film, which may also serve as an insulating layer, were vacuum deposited to 1000 Å thickness on a pair of NESAC-coated glass plates at an angle of 60 degrees from the substrate normal. The liquid crystal 5CB assumed a uniform planar alignment in between these substrates.

In HEFT, the choice of the cell thickness is crucial to assure its validity as emphasized in the previous section. If we take, for example, $K_1=5 \times 10^{-12}$ N and $E_a=10^{-5}$ J/m², the extrapolation length becomes 0.5 μm. So, in order to ensure a

substantial range of voltage satisfying $d \gg d_c \gg d_e$, the cell thickness must be larger than $50 \mu\text{m}$; too thick a sample, however, may cause an experimental difficulty in the case of a planar cell, because the director relaxation near the Freedericksz transition becomes increasingly slow with the cell thickness, thereby making it difficult to establish a uniform distortion throughout the nematic. here, we fabricated a sandwich-type cell using a $50\text{-}\mu\text{m}$ -thick polyester spacer, and the actual cell thickness was measured to be $56 \pm 1 \mu\text{m}$ from the optical interference spectrum. In order to allow for simultaneous capacitance measurements, the transparent electrodes were etched in an appropriate shape to overlap only through the nematic liquid with the area of about $7 \times 7 \text{ mm}^2$. The cell was vacuum-filled with 5CB in the nematic phase and then placed in an electric oven to maintain the temperature at $0.230 \pm 0.001 \text{ K}$ below the clearing point (308.45 K). The retardation was measured with the same transmission-type automatic ellipsometer which can resolve a retardation down to 10^{-5} rad. The block diagram of the experimental system is shown in Fig.7.6.

A sinusoidal voltage (1033 Hz) of up to $150 \text{ V}_{\text{rms}}$ was applied to the cell, and the retardation and the capacitance were measured as functions of the voltage. Since the critical slowing down was quite significant near the Freedericksz transition, the voltage was, there, scanned at a rate as low as $1 \text{ mV}/\text{min}$.

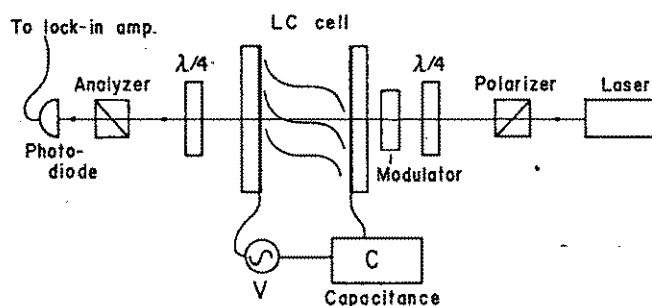


FIG.7.6. Experimental arrangement for retardation and capacitance measurement.

In order to evaluate the effect of electronic current within the nematic, the resistance of the cell was also monitored throughout

the measurement. However, we did not notice any anomalous behavior, and the resistance remained over 100 M Ω even at the highest voltage. The texture of the nematic liquid under high electric fields was also examined with a polarizing microscope; the field of view remained uniformly dark between crossed polarizers, merely suggesting a quasi-homeotropic alignment along the field direction. Because the power loss in the nematic is presently at most 0.3 mW, the concomitant rise of the sample temperature is expected to be less than 0.01 K for the present cell geometry.

B. Results

In Fig.7.7 shown are the retardation and the capacitance as functions of the applied voltage. A clear Freedericksz transition occurred at $V_{th} = 0.573 \pm 0.003$ V, and the retardation decreased steadily with the voltage. However, as shown in the inset of the figure, the retardation disappeared continuously at a finite voltage around 100 V. This indicates that at this voltage, the entire nematic including boundary layers was oriented along the field direction. This is the first experimental demonstration of the saturation transition predicted by several authors [35-37].

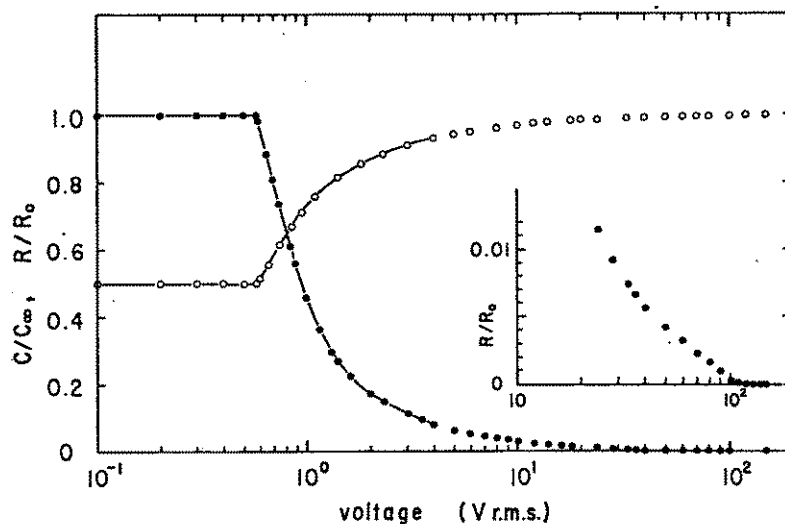


FIG.7.7. Typical changes of the retardation R and the capacitance C with the applied voltage.

The change of the retardation was always reversible, and no hysteretic behavior was observed up to saturation within the

experimental error. This implies that the anchoring energy function is monotonically increasing function from $\Theta_0 = \pi/2$ to 0.

The effect of finite anchoring strength can be clearly visualized by plotting RCV/R_0 versus the applied voltage [Fig.7.8]. Here, we see a plateau from 1.5 to 10 V, corresponding to $d \gg d_c \gg d_e$, followed by a sharp decrease at higher voltages. This shows that the finite anchoring effect sets in at around 10 V. In order to determine the extrapolation length, R/R_0 is plotted against $1/CV$ in Fig.7.9. A good linear relation can be observed as predicted by the theory. The experimental results are well reproduced by a straight line intersecting the ordinate axis at $(-2.30 \pm 0.05) \times 10^{-3}$ from which we can obtain the extrapolation length for the SiO-5CB interface as

$$d_e = 65 \pm 3 \text{ nm.}$$

By using the value of the splay constant, $K_1 = 2.4 \times 10^{-12}$ N as determined from the threshold voltage, the anchoring energy is given by

$$E_a = (3.7 \pm 0.2) \times 10^{-5} \text{ J/m}^2.$$

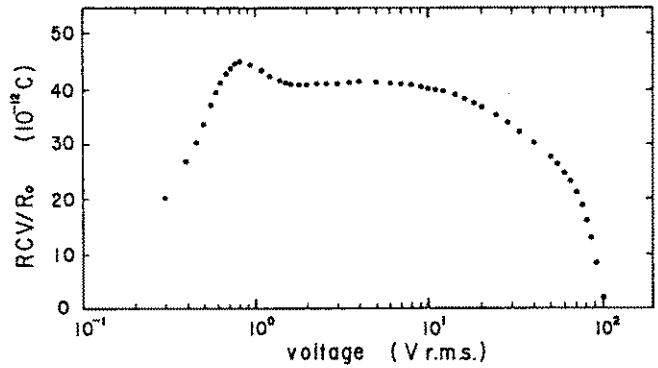


FIG.7.8. RCV/R_0 vs voltage plots showing the onset of the effect of finite anchoring strength above 10 V.

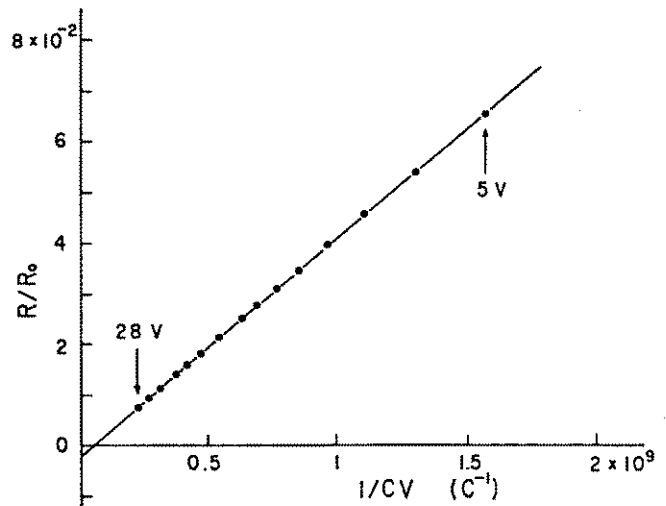


FIG.7.9. R/R_0 vs $1/CV$ plots. The intercept with the ordinate gives $-2d_e/d$. d : cell thickness.

Then, following the procedure described in the former section, we have obtained the anisotropic part of the interfacial tension as shown in Fig.7.10. The error bars around the experimental points represent possible fluctuations due to $\delta(RCV/R_0k)$, while the errors in material parameters shift all the points uniformly up or down within the region surrounded by the broken line. Fig.7.10(b) was calculated by means of a graphical integration of that shown in (a). This is also the first experimental determination of the functional form of the anisotropic interfacial tension at a solid-nematic interface. These results show that $\gamma(\Theta_0)$ as well as the anchoring energy can be determined with a reasonable accuracy, in spite of somewhat large errors involved in the material parameters.

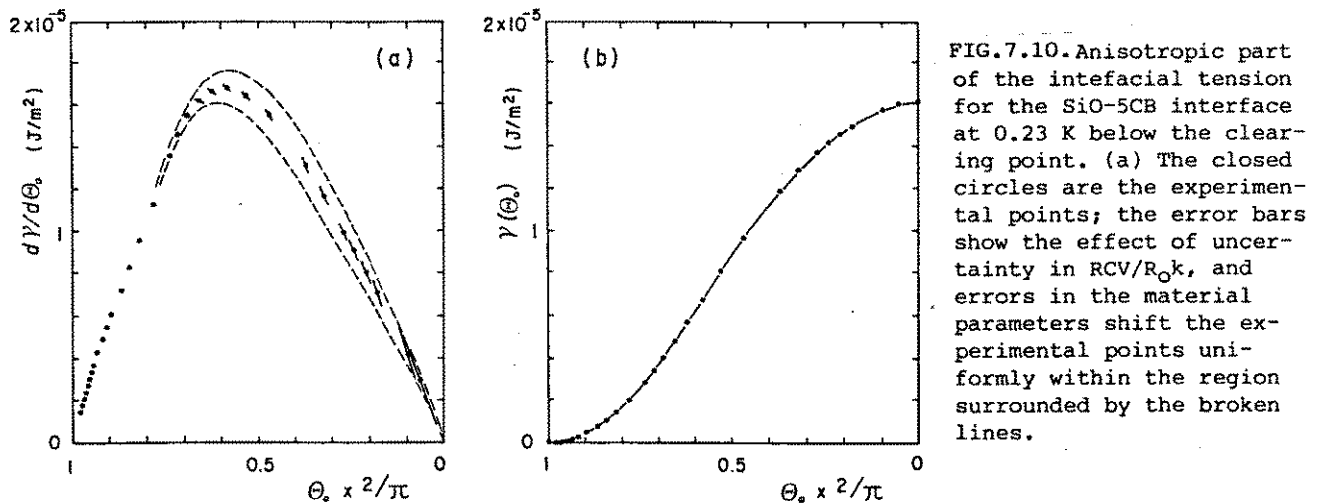


FIG.7.10. Anisotropic part of the interfacial tension for the SiO-5CB interface at 0.23 K below the clearing point. (a) The closed circles are the experimental points; the error bars show the effect of uncertainty in RCV/R_0k , and errors in the material parameters shift the experimental points uniformly within the region surrounded by the broken lines.

It is now of interest to compare $\gamma(\Theta_0)$ as determined above with the Landau-de Gennes form of the interfacial tension Eq.(5.116). For this purpose, we examined the fit of the function of the form

$$\gamma(\theta) = \frac{1}{2} E_a \sin^2 \theta + \frac{1}{4} E_1 \sin^4 \theta, \quad (7.40)$$

to the experimental result, where $\theta = \pi/2 - \Theta_0$. First, it should be noticed that, because the experimental $d\gamma(\Theta_0)/d\Theta_0$ shows a maximum at a point which is definitely different from $\pi/4$, it is

immediately clear that the first term of the above equation alone is not enough to satisfactorily reproduce the measured result. In Fig.7.11, two trial functions incorporating the second term are shown along with the experimental results. For both functions, the agreement with the experimental results seems satisfactory, except that there exists a small but definite discrepancy which cannot necessarily be attributed to experimental error. Anyway, this result indicates that, at far as the SiO-5CB interface is concerned, the Landau-de Gennes interfacial tension gives a good representation of reality.

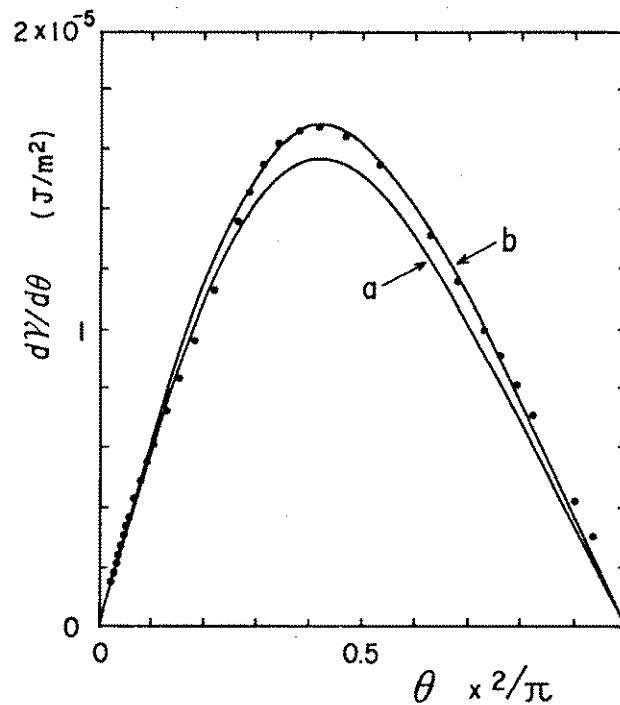


FIG.7.11. Second-order fitting of the anisotropic part of the interfacial tension by the function of the form, $\gamma(\theta)=(E_a/2)\sin^2\theta + (E_4/4)\sin^4\theta$.

(a): $E_a=3.9 \times 10^{-5} \text{J/m}^2$, $E_4=-1.8 \times 10^{-5} \text{J/m}^2$.

(b): $E_a=4.1 \times 10^{-5} \text{J/m}^2$, $E_4=-1.8 \times 10^{-5} \text{J/m}^2$.

7.3 Temperature dependence of the anchoring strength:

Rubbed PVA and Obliquely evaporated SiO

Temperature-dependence of various interfacial properties provides information that one can never reach from the measurement at a fixed temperature alone. This section is devoted to theoretical and experimental studies of the temperature-induced variation of the anchoring strength.

At first, we will discuss the implication of the temperature-dependence of the anchoring strength based on the thermodynamic theory developed in Chapter 4. We present the experimental results performed on the obliquely evaporated SiO-5CB and rubbed polyvinylalcohol-5CB systems. Here, again, we find distinctive differences between their temperature-induced behaviors; at the SiO-5CB interface, the anchoring strength is relatively small and undergoes an almost critical weakening as the clearing temperature is approached, whereas at the polyvinylalcohol-5CB interface, it is rather strong and exhibits only weak temperature dependence.

The critical exponent describing this anomalous increase near T_c does not satisfy the thermodynamic criterion derived in Chapter 4; hence, it can not be regarded as a true critical behavior, but should be understood to terminate somewhere closer to the clearing point. Based on the Landau-de Gennes model, we show that the near critical weakening is a manifestation of the surface-induced disordering transition at the SiO-5CB interface via the contribution of the order parameter inhomogeneity $d_e(1)$. This is in good accord with the results of contact angle and Wall-induced pretransitional birefringence experiments, and also reveal the utility of the Landau-de Gennes type phenomenological approach.

7.3.1 Thermodynamic consequence of a temperature-dependent anchoring strength: Energetic vs entropic alignment

The present argument consists in the comparison of the internal energy U and the entropy S of the system in the orientationally deformed and undeformed (ground) states. Let us shortly illustrate how such an argument proceeds and works by taking a bulk nematic as an example. For the present purpose, it is convenient to work with the Helmholtz free energy F instead of the thermodynamic potential. At fixed temperature, the Helmholtz free energy of a given volume containing a fixed number of molecules seeks its minimum by appropriately changing the director configuration etc. Writing the difference of a quantity G between deformed and undeformed states as ΔG , we have

$$\Delta F = \Delta U - T\Delta S. \quad (7.41)$$

Now we consider the process in which the nematic is transformed from a deformed state (II) with the Frank elastic energy density f_d to the undeformed state (I). Then, according to Eq.(4.86), we obtain, in this case, an equation for the entropy similar to Eq.(4.89) as

$$\Delta S(\text{II} \rightarrow \text{I}) = A \left(\frac{\partial K_q}{\partial T} \right)_\rho \int \left(\frac{\partial f_d}{\partial K_q} \right)_n dz, \quad (7.42)$$

where q is summed from 1 through 3; in contrast to Eq.(4.89), however, the Frank elastic constant K_q should be differentiated at constant density ρ (since the transformation is occurring at constant V and N). Because of the relation $\Theta = F - N\mu$, we have upon negligence of terms higher order than f_d ,

$$\Delta F(\text{II} \rightarrow \text{I}) = -Vf_d. \quad (7.43)$$

Putting Eqs.(7.42) and (7.43) into Eq.(7.41), we can express the internal energy of the system as

$$\Delta U(\text{II} \rightarrow \text{I}) = -Vf_d - A \left(\frac{\partial K_q}{\partial T} \right)_0 \int \left(\frac{\partial f_d}{\partial K_q} \right)_n dz. \quad (7.44)$$

Now we have all the necessary ingredients for the present discussion. An obvious statement as to the alignment in the bulk nematic is that it occurs in such a way that the Helmholtz free energy takes a minimum value at fixed temperature, volume, and orientational boundary condition. Then, according to Eq.(7.41), in attaining the equilibrium state, either one of the following four cases should happen: (1) $\Delta U < 0$ and $\Delta S > 0$, (2) $\Delta U < 0$ and $\Delta S < 0$, (3) $\Delta U < 0$ and $\Delta S > 0$, and (4) $\Delta U < 0$ and $\Delta S > 0$. It is impossible that $\Delta U < 0$ and $\Delta S < 0$. Since the Frank constants are decreasing functions of temperature (even at constant density), Eqs. (7.42) and (7.44) show that in the case of a bulk nematic, the second category of the above distinctions applies. This is an indication that the stability of the uniform alignment of the director derives from the internal energy part of the free energy, while the entropic term disfavors it. This result has a deep implication on the origin of the nematic order, and may be interestingly compared with the elasticity in other condensed media such as crystal solids and rubber materials. Furthermore, this energetistic origin of the nematic order demands that any theory which place too much emphasis on the steric repulsions between nematic molecules would fail to appropriately explain the temperature-induced behavior of the nematics.

Though much space has been spared for the discussion of bulk properties, we are now in a position to turn our argument to the interface problems. Let us consider a single component nematic in contact with a rigid solid. In conformity with the alignment at SiO(60) and at rubbed PVA in question, we assume that the alignment is planar and independent of temperature. We restrict the attention to the polar anchorage. The Helmholtz free energy

of the system may be written as

$$F = F_b + A\gamma + \Gamma\mu, \quad (7.45)$$

where Γ denotes the adsorption of the nematic liquid with respect to the dividing surface. As it is obviously impossible to rigorously separate bulk and interfacial properties from a macroscopic view point, we have to first set a basis on which the origin of the stability of the surface-induced alignment may be most appropriately discussed.

Here we chose to take the dividing surface at the point of zero adsorption for the nematic phase, i.e. $\Gamma=0$, and consider how the change of interfacial tension associated with the bulk deformation is energetic or entropic relative to the reference bulk phase. From Eq.(7.45), we have (with this choice of the dividing surface)

$$\Delta F(\text{II} \rightarrow \text{I}) = \Delta F_b(\text{II} \rightarrow \text{I}) + A\Delta\gamma^0(\text{II} \rightarrow \text{I}). \quad (7.46)$$

In terms of the surface entropy and the interfacial tension, the surface excess internal energy is written as

$$U^S = \gamma^0 + TS^S, \quad (7.47)$$

where the superscript 0 denotes the zero adsorption surface. For simplicity, we assume that the zero adsorption surface is invariant. Then, from Eq.(4.140), we have

$$\Gamma\gamma^0 = \gamma^0_0 + d_e f_d, \quad (7.48)$$

where the extrapolation length d_e is measured from the zero adsorption surface, and γ^0_0 is the interfacial tension in the absence of orientational deformation. Based on the Gibbs equation for the interface between solid and ordinary fluid [cf. Eq.(4.117)], $\Gamma\gamma^0_0$ can be shown to be a quantity of the order of f_d^2 ; hence, it can be omitted. And from Eq.(4.206a), we

readily find for the case of a rigid solid-nematic interface,

$$\Delta S^s_{\circ}(II \rightarrow I) = - K_1 f_d \left(\frac{\partial}{\partial T} \frac{d_e}{K_1} \right)_{\rho} . \quad (7.49)$$

Combination of Eqs.(7.48) and (7.49) yields

$$\Delta U^s(II \rightarrow I) = - d_e f_d - T K_1 f_d \left(\frac{\partial}{\partial T} \frac{d_e}{K_1} \right)_{\rho} . \quad (7.50)$$

Furthermore, because f_d can be written, in terms of the strain at the dividing surface C_{op} , as $f_d = K_1 (C_{op}/d_e)^2/2$ [see Eq.(4.175)], Eqs.(7.49) and (7.50) can be transformed to

$$\Delta S^s_{\circ}(II \rightarrow I) = \frac{C_{op}^2}{2} \frac{\partial}{\partial T} E_a, \quad (7.51)$$

$$\Delta U^s(II \rightarrow I) = \frac{T^2 C_{op}^2}{2} \frac{\partial}{\partial T} \frac{E_a}{T} . \quad (7.52)$$

These results show that in such an event that the anchoring energy E_a decreases with temperature, the surface entropy (relative to the zero adsorption surface) should decrease as the system is brought from an orientationally deformed to undeformed state. Similarly, the surface excess internal energy is also a function which decreases as the system is transformed to the ground state. So that, in this case, the surface alignment is stabilized by an energetistic agent.

On the other hand, if the anchoring energy increase with temperature, we can conclude from the above equations that the variation in the surface entropy should be positive, thereby contributing to decreasing the free energy of the total system. The internal energy, however, may be positive or negative, depending on the manner in which the anchoring energy increases with temperature. Anyway, the dominant factor stabilizing the

surface alignment is an entropic one in this case.

For example, if we consider the surface excluded volume effect [38], [cf. the last term in Eq.(5.19)], the anchoring energy is proportional to the absolute temperature T . Thus, Eqs.(7.51) and (7.52) show that the contribution from the entropy is positive, whereas that from the internal energy is zero. As this mechanism of alignment take account of the effect of anisotropic packing entropy, the above observation appears quite understandable. In analogy with the bulk elasticity, this case corresponds essentially to the "rubber elasticity."

As another extreme example, let us consider the macroscopic van der Waals interactions. In this case, the resulting anchoring energy is a more or less decreasing function of temperature. Hence, only the internal energy can be effective in stabilizing the surface-induced alignment.

As clear from these examples, a knowledge on the temperature dependence of the anchoring strength provides us with an essential insight into the surface process that stabilize the actual alignment. Although Eqs.(7.51) and (7.52) hold only when the anchoring energy is measured as a function temperature at constant density, experiments under a constant pressure is still expected to be a good source of information.

7.3.2 Anchoring strength at a rubbed PVA-5CB interface

In comparison with the case of evaporated SiO and 5CB, the results on which will be described below, this interface presents much less fine structure in terms of its anchoring strength. Within the experimental error, the polar anchorage at rubbed PVA-5CB interface can be termed simply as an "infinitely strong anchorage" over the temperature range very close to the nematic-isotropic transition point. Accordingly, it is impossible to find out the function form of the interfacial tension, as we have

succeeded for SiO-5CB interface. And, unfortunately, there is thus no room for the aforementioned thermodynamic relations to be applied.

The preparation and the rubbing condition of the PVA film is the same as that we used for contact angle measurement. And, in accordance with the thickness criterion resulting from the HEFT, we had fabricated a 54.4- μm -thick sandwich cell, in which nematic 5CB was vacuum-injected. The driving voltage was of sinusoidal wave with the frequency of 7.43 kHz. This rather high frequency (at least higher than that we used for the determination of $\gamma(\Theta_0)$ at the evaporated SiO-5CB interface) was chosen to avoid the transient motion of the director at high field, which has not been taken into account in the "static" theory of HEFT and becomes quite significant when the anchoring strength is large as in this case. Because this point is of crucial importance for application of HEFT to large anchoring strength, we shall add some more words below.

The theory of HEFT described in Section 7.2.3 assumes the so called "root-mean-square response" of the director to an oscillating electric field. Strictly speaking, however, it is only a caricature of reality, but there is always, however small, a component which changes in phase with the AC field. As long as the effect of oscillation to optical output is linear in the field strength, no final effect does appear resulting in the same relationship between the retardation and the voltage. However, at high field, where

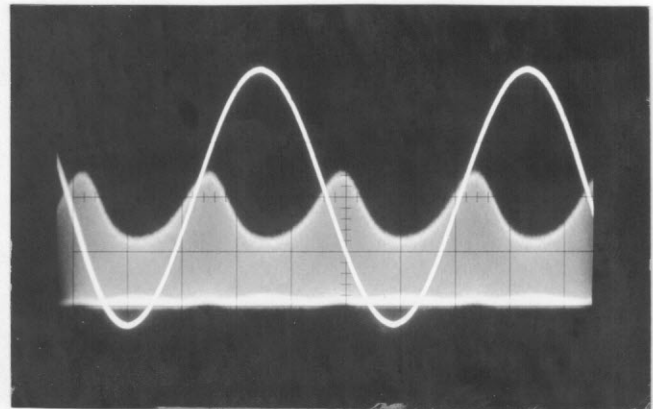


FIG.7.12. Oscilloscope traces of the driving sinusoidal voltage (1.033kHz, 80 V_{RMS}) and the optical signal. Note the asymmetry of the upper envelop of the optical signal.

almost saturation of the director configuration occurs, the oscillating director motion is no longer symmetrical about the mean-field position, but is more efficient in the rebound motion when the field crosses zero. So that, there appears a net optical effect due to this deviation from the root-mean-square field value [see Fig.7.12].

The R/R_0 vs $1/CV$ plots for the rubbed PVA-5CB system are shown in Fig.7.13 at temperatures $T_c-6.47$ K and $T_c-0.437$ K. Clearly, the plots show a good linearity as required by HEFT. The intercept of the extrapolated curve pass almost perfectly through the origin. The estimated error involved in the intercept value is $\pm 10^{-4}$. Then, the extrapolation lengths are

$$d_e = 0.0 \pm 2.7 \text{ nm}, \quad \text{at } T = T_c - 6.47 \text{ K},$$

and

$$d_e = -2.0 \pm 2.7 \text{ nm}, \quad \text{at } T = T_c - 0.437 \text{ K}.$$

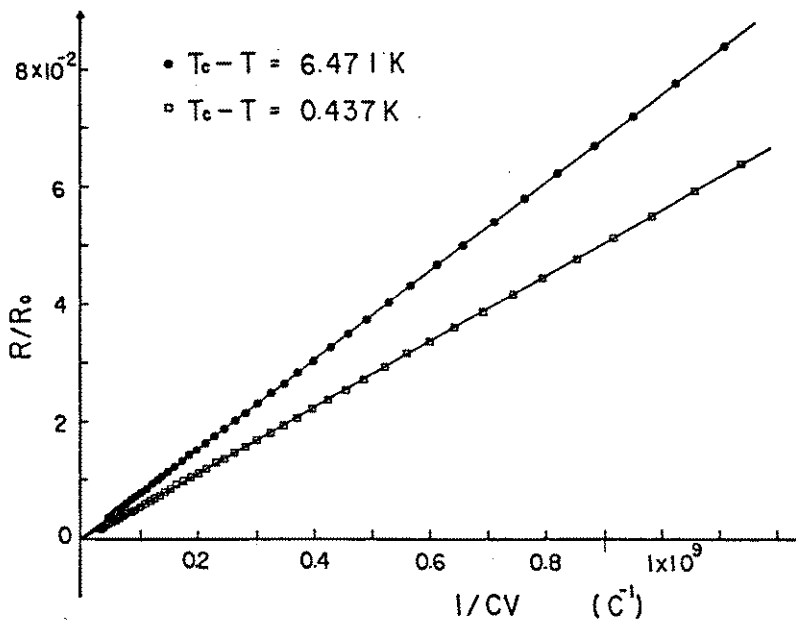


FIG.7.13. R/R_0 vs $1/CV$ plots for a rubbed PVA-5CB interface. Plots are for voltages above 4.5 V.

The anchoring energies are therefore

$$E_a > 1.8 \times 10^{-3} \text{ J/m}^2, \quad \text{at } T = T_c - 6.47 \text{ K},$$

$$E_a > 2.8 \times 10^{-3} \text{ J/m}^2, \quad \text{at } T = T_c - 0.437 \text{ K}.$$

These are the largest value ever observed for the solid-nematic interface. Although there is a systematic shift to negative side in d_e value as temperature is raised, it is not clear at present that it has something to do with the enhanced ordering at the rubbed PVA-5CB interface.

7.3.3 Obliquely evaporated SiO-5CB interface [30]

In contrast to the rather simple result observed for rubbed PVA-5CB interface, we have experienced a richer variety of phenomenon which call for serious surface-scientific interpretation. In particular, as the clearing point is approached, the extrapolation length now shows an anomalous increase, which is likely to be considered as a kind of critical phenomenon.

By means of the thermodynamic and the Landau-de Gennes theories of the nematic interface, it is actually shown not to be the case. However, this can be favorably correlated with the results of contact angle and wall-induced pretransitional birefringence experiments (Chapter 6) if it is admitted that, at the obliquely evaporated SiO-5CB interface, the surface-induced disordering transition is occurring in the nematic phase. This presents final clear evidence which corroborates the distinction between the rubbed and the obliquely evaporated surfaces.

A. Experimental

The extrapolation length was measured according to the procedure described previously, for a 5CB-SiO interface as a function of temperature from the nematic-isotropic transition point ($T_c=35.3^\circ\text{C}$) down to 5.2 K below T_c . SiO was vacuum-evaporated onto a couple of ITO-coated glass plates at an angle of 60° from the substrate normal in the vacuum of 10^{-6} Torr. The rate of deposition was about 0.9 nm/sec and the ultimate film thickness was about 60 nm. To allow for the existence of substantial voltage range satisfying the condition $d \gg d_c \gg d_e$, we prepared a rather thick sandwich-type cell by using a $50\text{-}\mu\text{m}$ -thick polyester spacer. The actual thickness of the cell was measured to be $54 \pm 1 \mu\text{m}$ from the optical interference spectrum, prior to filling the cell with the liquid crystal.

The cell was vacuum-filled with the liquid crystal in the nematic phase, and a good homogeneous alignment was confirmed with a polarizing microscope. A sinusoidal voltage (7.43kHz) of up to 150 V_{rms} was applied step by step from zero volt, and the retardation and the capacitance were measured and stored in a micro-computer. The rate of voltage scan was set carefully at each step (ranging from 1 mV/min near V_{th} to 5 V/min near the maximum voltage) to ensure quasi-equilibrium condition.

The capacitance of the liquid crystal cell is obtained directly by measuring the ratio between the applied voltage, which is being scanned, and the out-of-phase component of the current across the sample cell. The loss factor is also monitored by taking the current component in phase with the applied voltage.

B. Results and some preliminary discussion

At all temperatures examined, we observed a well-defined Freedericksz transition just as shown in Fig.7.7. Such well-defined Freedericksz transitions are an indication of the fact that the pretilt angle was always negligibly small at the 5CB -

60° evaporated SiO interface [39]. We derived the splay elastic constants at various temperatures from the threshold voltage of the Fredericksz transition. As noted before in relation to the determination of $\gamma(\theta_0)$, we observed a "continuous" saturation transition at some temperatures near T_c .

In Fig.7.14, the threshold voltage of saturation transition V_{sat} is plotted as a function of temperature. Firstly, the occurrence of the continuous saturation transition indicates, according to Sluckin and Poniewierski [37], that the Landau-de Gennes surface potential Eq.(5.116) has a negative coefficient for the fourth order term, or equivalently negative E_4 in Eq.(7.40). Secondly, the fact that the threshold voltage increases with the decrease in temperature shows that the anchoring energy is also increasing almost in proportion to V_{sat} [35].

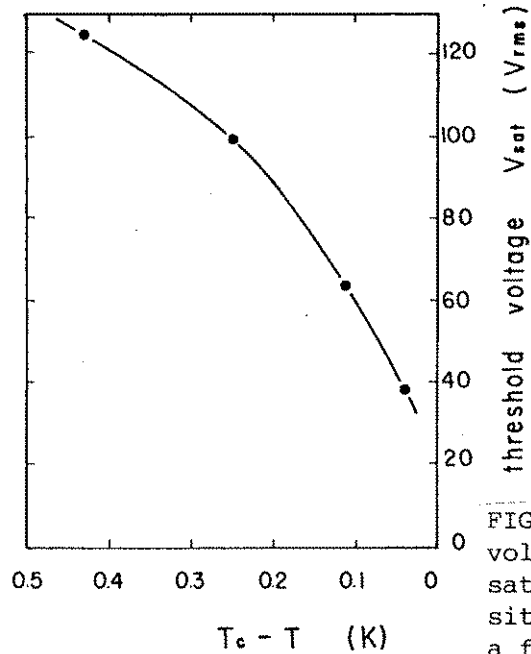


FIG.7.14. Threshold voltage for the saturation transition plotted as a function of temperature.

The extrapolation length was calculated at each temperature from R/R_0 vs $1/CV$ plots by performing a linear least-squares fitting based on Eq.(7.26). Shown in Fig.7.15 are the R/R_0 vs $1/CV$ plots ($V > 4.8 V_{rms}$) corresponding to the lowest and the highest temperatures of measurement. Clearly, the linearity of both plots is remarkably good, while we can see an inflection for

the latter plot corresponding to the saturation transition mentioned above. The solid lines represent the best-fit straight lines, and the extrapolation lengths have been deduced from their intercepts with the ordinate axis. The extrapolation lengths so obtained are depicted in Fig.7.16 against temperature and are also tabulated in Table 7.3 together with the splay elastic constant K_1 calculated from V_{th} , the birefringence $\Delta n = n_e - n_o$, and the anchoring energy $E_a = K_1/d_e$.

As discernible in Fig.7.16, the temperature dependence of the extrapolation length shows quite distinct features depending on the range of temperature. Up to $T_c - 1$ K, the extrapolation length is rather small around 30

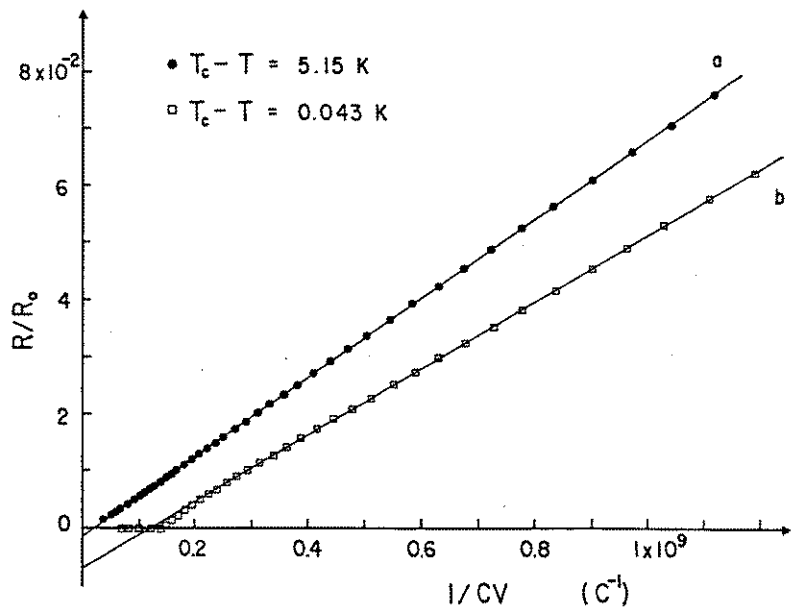


FIG.7.15. R/R_0 vs $1/CV$ plots observed at (a) 5.15 K and (b) 0.043 K below T_c . The solid lines are the best-fit straight lines determined by the least squares method applied to points above 4.8 V.

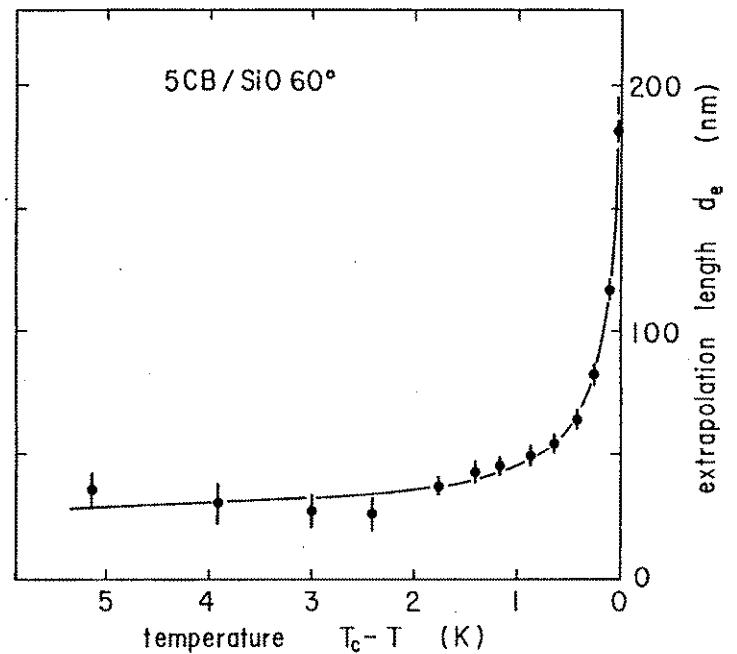


FIG.7.16. Temperature dependence of the extrapolation length d_e at the 5CB-SiO(60°) interface. The solid line is a theoretical curve based on the Landau-de Gennes type mode of the nematic interface.

nm and stays practically constant. However, at temperatures near the nematic-isotropic transition point, d_e is seen to undergo a nearly diverging increase toward T_c , and at 0.043 K below T_c it becomes six times as large as the values at lower temperatures, thereby weakening the anchoring strength.

TABLE 7.3. Results for the anchoring strength and some other bulk parameters.

$T_c - T$ (K)	Extrapolation length (nm)	Anchoring energy (10^{-5} J/m^2)	Birefringence	Splay const. (10^{-12} N)
5.15	35 ± 5	13.7 ± 2.0	0.156	4.66
3.92	31 ± 7	14.8 ± 3.6	0.149	4.28
3.00	28 ± 7	15.2 ± 3.7	0.143	3.95
2.41	27 ± 7	14.7 ± 4.1	0.139	3.71
1.77	37 ± 3	9.2 ± 0.8	0.133	3.41
1.42	42 ± 4	7.6 ± 0.7	0.130	3.23
1.17	45 ± 3	6.8 ± 0.5	0.127	3.07
0.864	49 ± 3	6.8 ± 0.4	0.123	2.88
0.645	54 ± 3	5.8 ± 0.2	0.119	2.71
0.431	63 ± 3	5.0 ± 0.2	0.115	2.53
0.245	83 ± 3	2.9 ± 0.1	0.110	2.33
0.114	117 ± 3	1.85 ± 0.005	0.106	2.17
0.043	183 ± 3	1.13 ± 0.003	0.104	2.06
0	0.102^a	1.97^a

^a Values extrapolated to T_c .

In order to show up the details near T_c , the extrapolation length is re-plotted versus the logarithm of $T_c - T$ in Fig.7.17; the solid line, also shown in the figure, represents the best-fit curve, found among the set of critical functions of the form

$$d_e = A + B[(T_c - T)/T_c]^\nu, \quad (7.53)$$

with $A=0$, $B=3.41$ nm and $\nu=-0.45$. Similarly, the anchoring energy is found to be fitted by

$$d_e/K_1 = -3.20 + 1.08[(T_c - T)/T_c]^{-0.50}, \quad (\times 10^3 \text{ m}^2/\text{J}). \quad (7.54)$$

The present results for the polar anchoring strength at the 5CB-SiO interface might be most comparable with the results of Faetti, *et al.*[32] who measured the azimuthal anchoring energy for the same interface. The anchoring energies they found, however, are nearly one order smaller than the present ones, but they also observed a nearly critical weakening of the anchoring strength toward the clearing temperature. For the sake of comparison, we have calculated the extrapolation length for the azimuthal anchorage by using the best-fit equation for the anchoring energies given in Ref.32; the absolute value of the twist constant at a temperature just below T_c has been taken from Bunning, *et al.* [40], and their values at lower temperatures were calculated following the results of Faetti, *et*

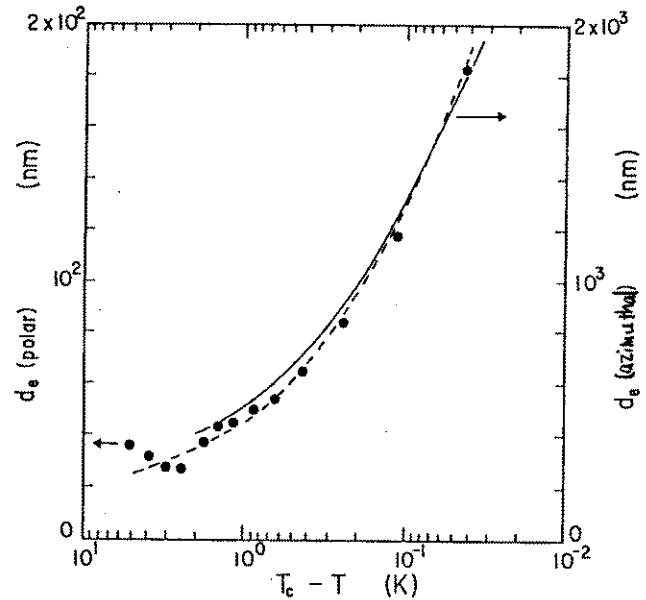


FIG.7.17. Extrapolation length for the azimuthal anchorage at the 5CB-SiO interface (solid line), calculated by using the results of Faetti *et al.*

al.[32]. In Fig.7.17, the azimuthal extrapolation length thus obtained is shown as a function of temperature together with the present result. Despite very different values of d_e 's for polar and azimuthal anchorages, we can see that the qualitative feature of the temperature dependence is quite similar for both cases. This fact strongly suggests that a single mechanism, regardless of the mode of anchorage, is indeed responsible for the temperature-induced softening of the surface alignment.

C. Insights from Thermodynamics

By substituting the fitted expression [Eq.(7.54)] into the thermodynamic relation between the surface entropy S^S and the curvature stress L_p [Eq.(4.206a) and see also Eq.(7.51)], we obtain

$$\Delta S^S(I \rightarrow II) \sim 0.88[(T_c - T)/T_c]^{-1.5} L_p^2. \quad (7.55)$$

Making use of the strain C_{op} at the interface, we can rewrite the above to give

$$\Delta S^S(I \rightarrow II) \sim 0.75 \times 10^{-6} [(T_c - T)/T_c]^{-0.5} C_{op}^2, \quad (\text{J/m}^2 \cdot \text{K}) \quad (7.56)$$

Therefore, at the temperature $T_c - T = 0.01$ K, the surface entropy increases from its ground state by $1.3 \times 10^{-4} \text{ J/m}^2 \cdot \text{K}$, when $C_{op} = 1$. In view of the magnitude of the n-i transition entropy of 5CB as estimated from the pretransitional experiments [41], i.e., $5 \times 10^3 \text{ J/m}^3 \cdot \text{K}$, the above value of the entropy increase is equivalent to a situation that a 30-nm-thick surface layer of the nematic is transformed from the nematic to the isotropic state. This is indeed a very large change, which may be readily detected in optical experiments.

Equation (7.56) shows that, as the curvature stress is applied, the ordering in the nematic liquid deteriorates faster in the interfacial region than in the bulk phase. And, moreover, the

degree of deterioration should diverge as T goes to T_c for any finite value of C_{op} . This is obviously impossible to occur in real experiments. The thermodynamic inequality derived in Section 4.9 indeed requires that, even when the extrapolation length does diverge, the critical exponent governing the divergence should be < -1 , cf. Eq.(4.215). The exponent found for the present SiO-5CB interface -0.45 does not meet this requirement. So, the observed trend cannot be regarded as a manifestation of a real critical behavior of the anchoring strength, but we should understand that the apparent critical behavior terminates somewhere closer to T_c or there is a point of cross over to a more singular behavior.

Finally, by an application of Eqs.(7.51) and (7.52), it is shown that the increase in the surface excess internal energy associated with the transformation from the ground state (I) to an excited state (II) with $C_{op} \neq 0$ is given by

$$\Delta U^S(I \rightarrow II) \sim \frac{C_{op}^2}{2} E_a + T \Delta S^S(I \rightarrow II). \quad (7.57)$$

This is positive and is an even more strongly increasing function of C_{op} than the surface excess entropy. And it also exhibits a quasi-critical increase toward T_c , in sharp contrast with $\gamma(I \rightarrow II) = (C_{op}^2/2)E_a$ which tends to vanish as T_c is approached. These results clearly indicate that the temperature-induced weakening of the anchoring strength at the 5CB-SiO interface is not occurring simply because the anisotropic surface interaction, which aligns the nematic director, reduces near T_c , but because the entropic contribution gets to compensate the internal energy part more efficiently as T_c is approached. That is, in the vicinity of T_c , the rotational barrier due to the anisotropic surface interaction is effectively lowered by the entropy increase associated with the rotation of the nematic director. This result clearly signifies the important role that the ordered structure of

the nematic interface is playing in determining the temperature dependence of the anchoring strength at this interface.

D. Calculations based on the Landau-de Gennes model

In order to make a more quantitative analysis of the above experimental result, a model calculation based on the Landau-de Gennes theory of the anchoring strength (Section 5.6) has been performed.

As shown in Eq.(5.169), the extrapolation length is comprised of two contributions of distinct origin, $d_e(1)$ and $d_e(2)$: the former is the part which comes from the spatial inhomogeneity of the order parameter near the interface, and the latter is a term connected with the direct solid-nematic interaction. Both of them are given as a function of the bulk and the surface order parameters, q_b and q_o .

In the present experiment, the reduced bulk order parameter q_b is directly given at each temperature by the birefringence normalized at the value of the clearing point:

$$q_b = \Delta n(T) / \Delta n(T_c). \quad (7.58)$$

In particular, this order parameter can be well approximated by an expression (as used already in the calculation in Section 5.6),

$$q_b = \frac{1}{8} \{ 3 + [9 + 16(1 + \frac{T_c - T}{T_n^* - T_c})^{1/2}]^{1/2} \}. \quad (7.59)$$

with $T_n^* - T_c = 0.24$ K [see Fig.7.18]. It is worth noting that this representation of the bulk order parameter follows from the assumption that the coherence length of the order parameter in the nematic phase be written as

$$\xi = \xi_o [(T_n^* - T) / T_n^*]^{-1/2}. \quad (7.60)$$

So that, it is clear that T_n^* designates a temperature where the coherence length diverge and hence the nematic order ceases to be stable. The present value of $T_n^* - T_c$ is about twice as large as that from the ordinary Landau-de Gennes theory.

In view of the very universal nature of the surface excluded volume effect and the van der Waals interaction, we have assumed

$$\bar{W}_2(q_0) = g_2 q_0, \quad (7.61)$$

for the interfacial interaction potential. As regards the order-disorder term in the interaction potential, we used the quadratic form

$$\bar{W}_0(q_0) = -g q_0 + (1/2) u_0 q_0^2$$

as before.

Figure.7.19 displays the theoretical curve for d_e fitted with the experiment. The corresponding temperature dependence of the surface order parameter is shown in Fig.7.20. Although only a curve with $u_0=1.5$ and $g=0.09$ is shown in Fig.7.19 to avoid unnecessary complication, curves with u_0 in a rather wide range including $0.9 \leq u \leq 2$ can reproduce the experimental results equally well, provided g , K/g_2 , and, among others, ξ_c are chosen appropriately; note, however, that no satisfactory fit can be attained by using a critical curve with $g=0$ and $u>1$. As understandable from Fig.5.21, as u_0 is made larger, a smaller ξ_c and a larger g have to be chosen to achieve a quantitative agreement with the experiment. However, since ξ_c is known to be

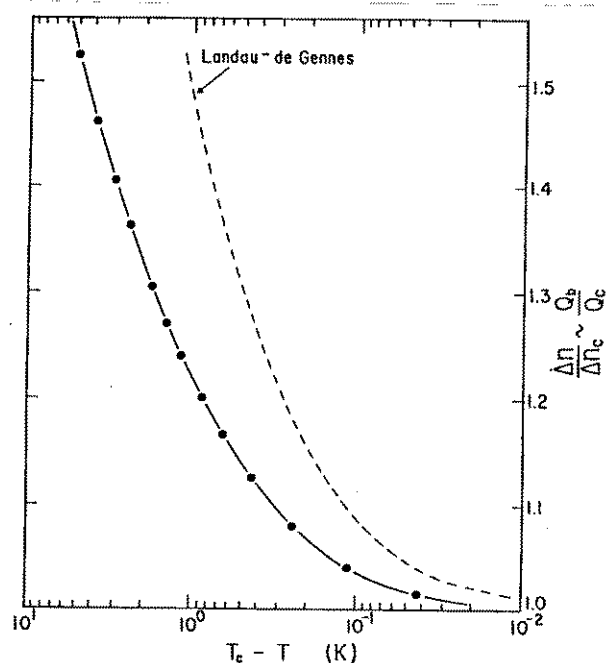


FIG.7.18. Temperature dependence of the reduced bulk-order parameter. The solid line is calculated via Eq.(7.59).

about 10 nm for 5CB [41], curves with $u_0 > 2$ can hardly be regarded realistic. The lower curve in Fig.7.19 is representing the contribution from $d_e(2)$, and shows that its effect is relatively unimportant near T_c compared with that of $d_e(1)$, though the presence of $d_e(2)$ is obviously crucial at lower temperatures. This suggests that the nearly critical weakening of the polar anchoring strength is essentially effected by the order parameter inhomogeneity coupled with the surface-induced orientational disordering at the interface.

Because of the non-critical nature of those theoretical curves which fit the experiment, the corresponding surface order parameter always remains non-zero even at the clearing tempera-

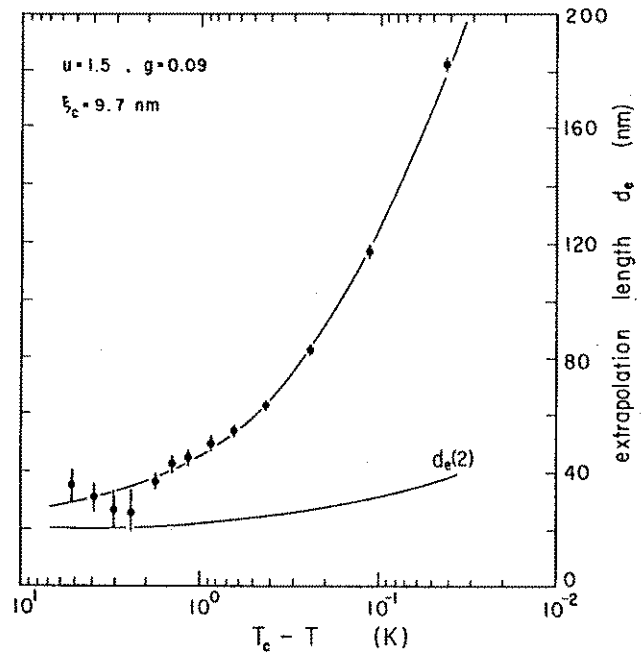


FIG.7.19. Comparison of the theory with the experiment. The upper line represents the extrapolation length d_e obtained by assuming $u_0=1.5$ $g=0.09$.

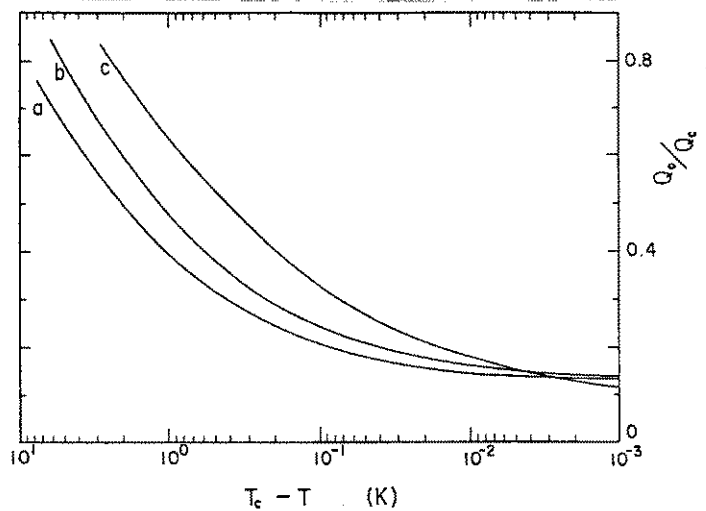


FIG.7.20. Temperature dependence of the surface order parameter for those surface potential parameters which well reproduce the experimental results of the extrapolation length: (a) $u_0=2$, $g=0.15$, (b) $u_0=1.5$, $g=0.09$, (c) $u_0=1.0$, $g=0$.

ture. This is in accord with the result of Faetti, et al. [32] and is also in qualitative agreement with the contact angle experiments [see Section 6.1]. In particular, the remarkable feature of those curves shown in Fig.7.20 is that the surface order parameter falls in a small region around 0.15 at the clearing temperature, in spite of rather large variations in u_0 and g . Furthermore, as $Q_c=0.27$ according to the literature [41], the above results indicates that $Q_0 \sim 0.04$ at T_c . And for the order parameter in the isotropic phase (just above T_c), we find $Q_{0n}=0.01$. These values are in good agreement with those predicted from the contact angle and the wall-induced pretransitional birefringence experiments in Chapter 6.

Chapter 8

CONCLUSION

In this thesis, we have made an attempt to develop a phenomenological framework for the interfacial orientational properties of nematic liquid crystals based on thermodynamic and statistical mechanical approaches. The validity of the framework was successfully tested against the results of various observations of novel orientational phenomena occurring at the interface between solid substrate and a nematic liquid crystal. As a result, it was in particular revealed that the mechanisms of surface-induced alignment of nematics on rubbed polymer surface and on obliquely evaporated SiO are dramatically different from each other, in contrast to the conventional expectations.

The interfacial phenomena we have dealt with here are extremely sensitive to the orientational properties of substrate, while allowing for quantitative analysis based on the phenomenological framework. At present, such subtle anisotropic properties of a solid surface is very difficult to probe, despite their importance in preparation of oriented organic films such as LB films. We therefore expect that the present set of the interfacial phenomena and the thermodynamic and statistical mechanical framework will serve as a unique analytical tool for solid surfaces.

Below we shall summarize the main results of the present study in detail, together with some future perspectives.

In Chapter 4, we have carried out a rigorous extension of the Gibbs thermodynamics of ordinary liquid interfaces to encompass nematic systems. The uniaxial anisotropy of nematics was fully taken into account based on the Frank theory of curvature

elasticity by adopting the director in the bulk phase as the orientational thermodynamic variable. We showed that the orientational property of the nematic interface can be completely specified by the pretilt angle and the anchoring strength. Though this is apparently the same situation as in the heuristic formalism due to Rapini and Papoular, the limitation and the physical basis of their formalism were clarified, and an alternative definition of the anchoring strength has been introduced. Based on the generalized Gibbs equation, the orientational effects on the adsorption, surface entropy, and surface energy at the nematic interface were elucidated for the first time. This shows that any phenomenological description of a nematic interface should involve the influences of the ordinary surface thermodynamic variables. So that, it is equally important and meaningful to study not only the direct orientational phenomena but such indirect surface effects. Finally, this interplay between the macroscopic orientation and the adsorption and the surface entropy has also an interesting implication into the preparation of organic thin films; that is, if a liquid crystal is used as a substrate for a spread monolayer, the pressure and the orientational as well as translational structure may be controlled by the orientation of nematic director.

In Chapter 5, rigorous statistical mechanical expressions for the interfacial tension and the anchoring strength were derived for an interface between hard solid wall and nematic, by making use of the thermodynamic definition of the anchoring strength. Though not practically useful, they apparently manifested the importance of interfacial perturbation of liquid crystalline structure. Especially, by way of a variation principle satisfied by the anchoring strength, it was shown that the anchoring strength diminishes as the orientational order degrades near the

interface. By applying a simple mean-field argument to the interfacial tension, we suggested that the contact angle of a nematic droplet resting at the interface between its isotropic phase and the substrate would be enormously sensitive to the anisotropic property of the substrate. In view of the significance of liquid structure near the interface, we developed a Landau-de Gennes type order parameter theory of the nematic interface. The interfacial tension, contact angle, and anchoring strength were obtained as an explicit function of the surface order parameter. An expression for the wall-induced pretransitional birefringence was also derived. It was especially shown that these properties are strongly dependent on the value of the surface order parameter, yet in a mutually complementary manner.

In Chapter 6, the results of the experimental observations of the contact angle at the nematic-isotropic-substrate three-phase line of contact, the wall-induced pretransitional birefringence, and the nematic-isotropic transitions in thin nematic films were presented. In particular, the contact angle was observed to drastically change according to the nature of the aligning substrate. The rubbed surfaces were found to invariably induce an acute contact angle or in some cases even complete wetting for the nematic, thereby showing that the ordered nematic state is more stable of these surfaces than the isotropic state. On the contrary, the substrates coated with an obliquely evaporated SiO tended to induce an obtuse angle for the nematic, indicating the prevalence of just the opposite situation. In terms of the Landau-de Gennes phenomenological theory, this observation demands that the order parameter at the SiO surface be appreciably smaller than in the bulk, whereas at the rubbed surface, it should be rather enhanced. These predictions were indeed confirmed (at least partially) by the pretransitional and thin film experiments.

In Chapter 7, the high electric field technique (HEFT) developed by the present author for measuring the anchoring strength was described. Next, we presented the results of the anchoring strengths measurement for 5CB on the rubbed polyvinylalcohol (PVA) and on the obliquely evaporated SiO substrates. The anchoring strength at the rubbed PVA substrate was found to be extremely large with negligible temperature dependence. However, at the SiO substrate, the anchoring strength was more than one order weaker, and furthermore showed a quasi-critical weakening as the temperature approached the nematic-isotropic transition point. Although the possibility of a true critical behavior was ruled out by thermodynamic criterion derived in Chapter 4, it could be interpreted as an indication of the thermal degradation of the surface order parameter on the basis of the Landau-de Gennes theory.

The results of the above four kinds of experiments could be consistently explained within the present phenomenological framework for both rubbed PVA and evaporated SiO substrates. The estimated phenomenological parameters qualitatively indicate that the effect of the evaporated SiO is almost exclusively to destroy the orientational order in the nematic phase, while at the rubbed PVA, strong ordering and disordering effects do coexist as manifested by the finiteness of the nematic contact angle. The SiO substrate possesses the disordering nature quite independent of whether or not the nematic is uniformly aligned. However, the strong interaction across the rubbed PVA and the nematic is always accompanied by the rubbing process. It appears quite reasonable that such a crude process as rubbing leaves both ordering and disordering structure on the rubbed film. Although the phenomenological approach based on macroscopic observation tell nothing more into the microscopic origins of these effects,

the above results may be sufficient to illuminate how far the rubbed and the obliquely evaporated substrates are from each other.

In an accepted phenomenology such as hydrodynamics or elastic continuum theory, the basic equations set a universal basis for all relevant phenomena, while the specificity of a particular system can be taken care of via a few adjustable parameters. The present phenomenological approach is still too crude to claim to reach such level. However, the origin of success, if it can be so judged, may lie in the fact that the nematic-isotropic transition is of weakly first order. In sufficient vicinity of the transition temperature, the behavior of the nematic is almost governed by the orientational order parameter, while other variables becomes less significant. So, it is essentially the same situation with the universality class associated with continuous phase transitions. In this respect, the present framework can not by pass the pitfall of the Landau theory. Then, it will lose its utility at points far from the transition point. There, we should search for another universal structure to construct an acceptable phenomenology.

Appendix I

PRECISION TEMPERATURE-CONTROLLED MICROSCOPE

As mentioned in Chapter 2, texture observations with a polarizing microscope is one of the fundamental and often decisive steps for the identification of various phases of liquid crystals and the study of their internal structures. The properties of liquid crystals are strongly temperature-dependent; in the case of 5CB, indeed, the birefringence Δn changes from 0.16 to 0.1 as the temperature is raised from 5 K below the clearing point to just beneath. And it becomes even more so near the phase transition points. Therefore, in the study of texture near the transition point and the phenomena associated with the transition itself, i.e., nucleation and growth of new phase, critical fluctuations, etc., it becomes quite important to strictly control the sample temperature.

Here described are the design and the performance of the precision temperature-controlled microscope, which has been in extensive use in my laboratory for observing wide variety of liquid crystal textures in the vicinity of the phase transition point^{*}. The temperature-controlled sample holder for ellipsometric measurements (Chapters 6 and 7) has also been designed on much the same working principles.

The present temperature-controlled microscope is a modern version of Lehmann's "oil-bath microscope," which literally means a microscope immersed in an oil bath. Here, in order to achieve a temperature fluctuations as small as 10^{-3} K with lesser

^{*} H. Yokoyama, S. Kobayashi, and H. Kamei, Rev. Sci. Instrum. 54, 611(1983).

temperature gradient over the liquid crystal cell, we have installed almost all the parts of a polarizing microscope, i.e., objective, polarizer, analyzer, etc., together with the sample cell in a multi-shielded temperature-controlled electric oven as shown in Fig.A.1. Enclosing virtually all the structure of the polarizing microscope in an oven eliminates the difficulty associated with the short working distance between the objective lens and the sample, which becomes hazardous to realize a good thermal insulation of the sample from the environment.

In Fig.A.1 shown is the cross-sectional view of the microscope, and Fig.A.2 gives the perspective view of the optics part. The oven consists of three copper enclosures and a copper block in which a sample is placed. The outer most copper enclosure is thermally insulated from the surroundings with foamed polystyrene, and is aimed to reduce the possible temperature gradient over the next copper enclosure. The two inner copper enclosures are thermally insulated from each other except at the side wall, where the temperature is sensed by a thermistor and is fed to an electric circuit for regulating the power supply to the heating wires wound around the second inner enclosure. This rather localized thermal contact between the inner most and the next enclosures is known to be very effective in reducing the temperature gradients on

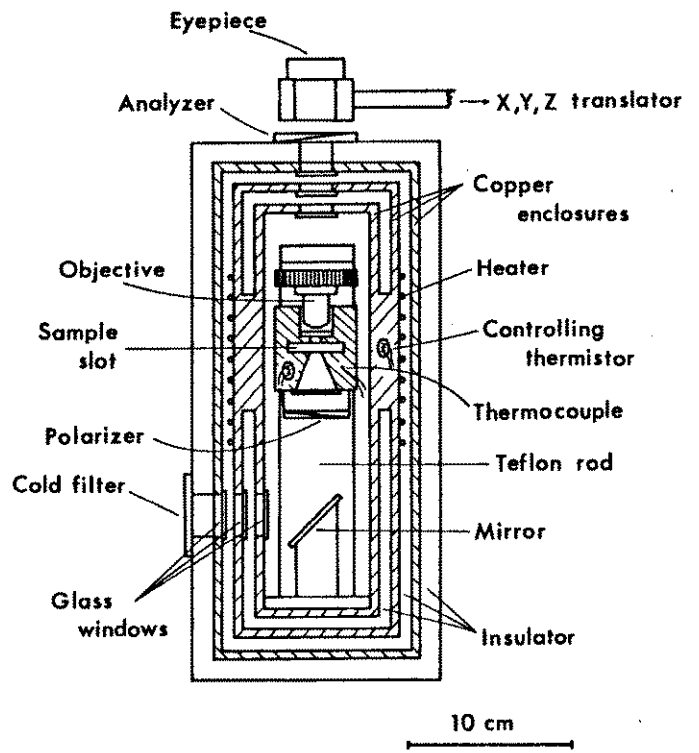


FIG.A.1. The cross-sectional view of the temperature-controlled microscope.

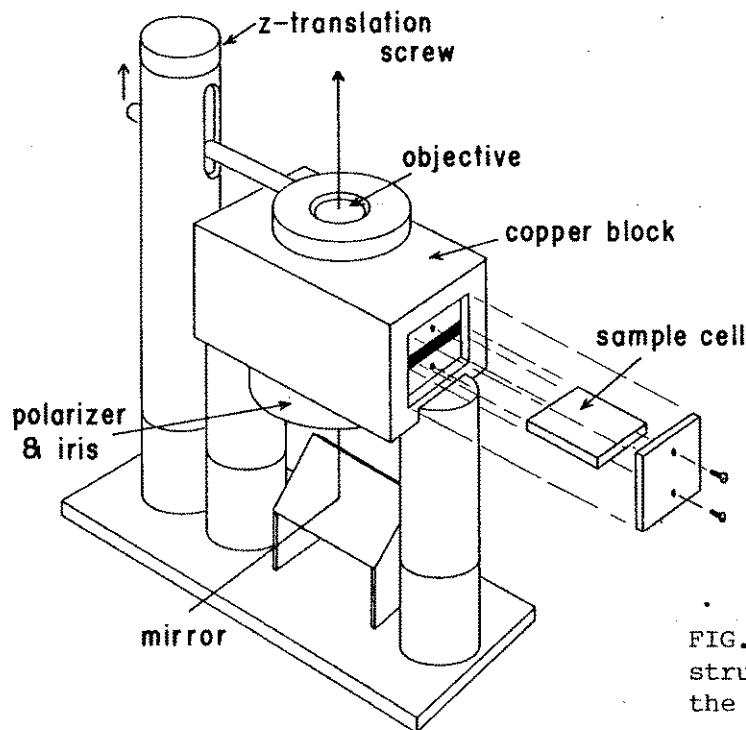


FIG.A.2. Optical structure inside the electric oven.

the inner most enclosure.* A copper block of about $200(5 \times 5 \times 8)$ cm^3 is placed inside the enclosure, while they are thermally insulated from each other by means of two Teflon rods of 3-cm diameter supporting the block. The large thermal inertia and high thermal conductivity ensure good temperature stability and homogeneity on the block. Since thermistors, though they are quite sensitive, are not suitable for absolute temperature measurements, the temperature of the copper block is simultaneously monitored with a thermistor and a copper-constantan thermocouple.

An objective, a polarizer, and a reflecting mirror were installed in the enclosure together with the copper block (Fig.A.2). The vertical position of the objective can be changed with a screw attached to the objective holder. An eyepiece was mounted in a holder which is movable in x-, y-, and z-directions. Illuminating light is introduced through a cold filter and glass windows in

* R.D. Cutkosky and B.F. Field, IEEE Trans. Instrum. Meas. 23, 295(1974).

front of the mirror, and observations are made through glass windows between the objective and the eye-piece. The cold filter cuts off the thermal radiation from the light source, thereby preventing unwanted heating of the copper block. The whole apparatus is operated in a room air-conditioned to 25 ± 1 K.

The electric circuits used in the present apparatus are similar to those employed by Grubic and Wurz^{*}, which utilized an AC-Wheatstone bridge for measuring the resistance of a thermistor. The thermistors for controlling and monitoring purposes are of bead-type (1.8 mm in diameter) having the resistance $3 \text{ k}\Omega$ at 100 C and $150 \text{ k}\Omega$ at 0 C . The AC-Wheatstone bridge was formed with the thermistor and metal film resistors with a temperature-coefficient as small as 5 ppm/K . This temperature coefficient is sufficiently small to make it meaningful to detect a millidegree difference in sample temperature, provided the resistors are thermostated to $\pm 1 \text{ K}$. The driving AC voltage is limited to 0.3 V in order for the self-heating effect in thermistors to be negligible. The temperature setting is changed by varying the resistance in the bridge circuit. And the unbalance signal from the bridge is lead to a lock-in amplifier, whose output is further fed to a proportional-integral (PI) controller driving the electric heater.

Figure A.3 shows a nematic schlieren texture observed with the present microscope at 0.01 K below the temperature (35.2 C) where the nematic phase first appeared on cooling from the isotropic phase of

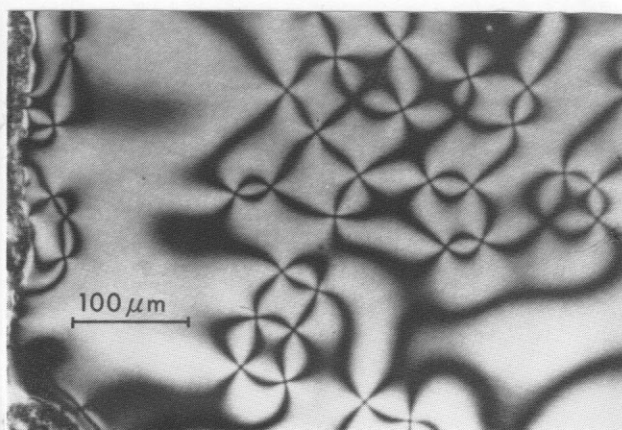


FIG.A.3. Nematic schlieren texture observed with the present microscope.

^{*} M. Grubic and U. Wurz, J. Phys. E 11, 692(1978).

5CB. It clearly shows that the performance of the present apparatus as a polarizing microscope is on the satisfactory level for, at least, qualitative observations of liquid-crystal textures.

When the temperature setting was changed, two to three hours were needed for the temperature to become almost constant. And, at a constant setting, it was observed that the readings both from the controlling and from the monitoring thermistors were stable within 10^{-3} K for indefinitely long time. It should be noted, however, that the temperature of the sample could be different from that of the block due to the opening which allows illumination and observation of the sample. So, the temperature stability at the point of liquid crystal cell was directly assessed by measuring the birefringence of the liquid crystal, 5CB, which was planar aligned by means of glass substrates coated with an obliquely deposited SiO film.

If a monochromatic light with wavelength λ is incident on the nematic cell of thickness d placed between crossed polarizers (see the inset of Fig.A.4), the output light intensity I is given by $I_0 \sin^2(\pi \Delta n d / \lambda) + I_r$, where I_0 and I_r are the intensities of the incident light and the leakage light. Since the birefringence of 5CB varies with temperature approximately following $d\Delta n/dT \sim -2 \times 10^{-2} \text{ K}^{-1}$ near the clearing point, the relative change of the output light intensity can be given by

$$\Delta I/I = -4 \times 10^{-2} (\pi d / \lambda) \tan(R/2) / [1 + I_r / I_0 \sin^2(R/2)] \Delta T.$$

where R is the retardation

$$R = 2\pi \Delta n d / \lambda.$$

So that, when $\sin(R/2) \sim (I_r / I_0)^{1/2}$, this birefringence thermometer acquires a maximum sensitivity, i.e.,

$$|\Delta I/I|_{\max} \sim 2 \times 10^{-2} (\pi d/\lambda) (I_o/I_r)^{1/2} \Delta T.$$

Hence, for a 40- μm -thick cell illuminated by a He-Ne laser ($\lambda=633 \text{ nm}$), it becomes

$$|\Delta I/I|_{\max} \sim 10^2 \Delta T$$

when the extinction coefficient I_r/I_o is assumed to be 10^{-3} . Then, it is clear that under this condition, a temperature variation on the order of 10^{-3} K can be easily resolved by this method.

Traces (a) and (b) in Fig.A.4 show the time variations of the block temperature, as measured by the thermistor, and the sample temperature evaluated from the birefringence of 5CB in 40- μm -thick cell, respectively. They clearly show that the temperature of the sample as well as that of the block can be stabilized to an accuracy better than 10^{-3} K for over several hours. It is also evident from the almost simultaneous onset of an increase near the end of those traces that the thermal contact between the sample and the copper is satisfactorily good.

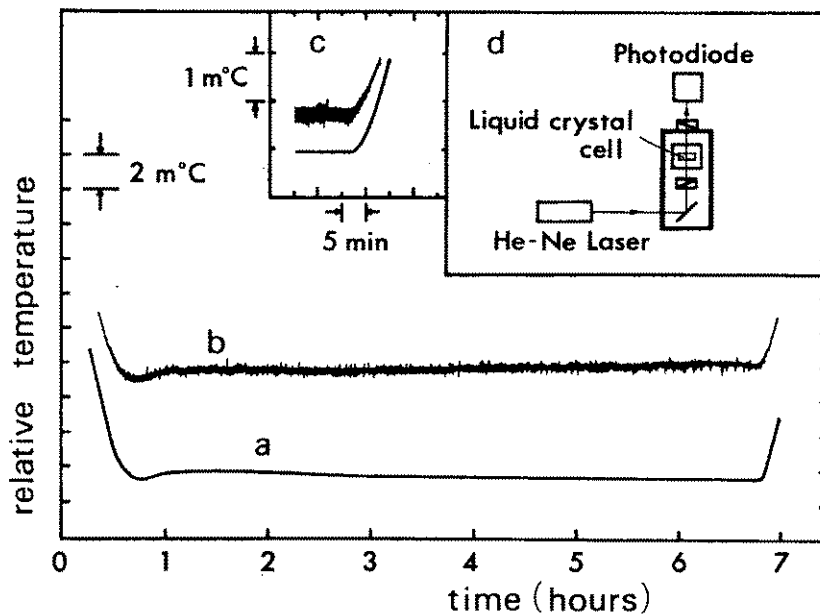


FIG.A.4. Time variations of temperatures. (a) Copper block temperature measured by a thermistor. (b) Optically measured sample temperature. (c) Details of the traces, (a) and (b), near the kinks at 6.8 h. (d) Experimental setup for optical temperature measurement.

Appendix 2

EQUILIBRIUM SHAPE OF A NEMATIC DROP

In Section 6.1, we have tacitly assumed that the equilibrium shape of a nematic drop can be determined only by the balance of interfacial tensions satisfying Young's equation just like a drop of an ordinary liquid. However, many of the surface and bulk properties of nematic liquids are anisotropic; so that, it is highly plausible that a drop of nematic, when surrounded by foreign media, would assume a characteristic form which more or less reflects the anisotropic nature of the nematic. Here, we consider the factors affecting the equilibrium shape of a nematic drop and to clarify the condition under which Young's equation can be applied as such to a nematic drop.

The equilibrium shape is the form of a liquid domain which minimizes the thermodynamic potential of the system under a given external condition. In the case of an ordinary liquid, this requirement leads to Young's equation, and in the case of a crystalline solid, it yields the well known Wulff construction^x. In both cases, the matter of finding the equilibrium shape is reduced to the problem of finding the shape with the minimum surface free energy under a given volume of the drop.

In general, however, we must take into account the superficial or volumetric elastic contributions as well, which are connected with the presence of a boundary and are thus dependent on the shape of the drop. The total thermodynamic potential of the system is expressed as a sum of (1) the usual volumetric

^x D.P. Woodruff, *The Solid-Liquid Interface*, (Cambridge, 1973), pp.9-11.

thermodynamic potential Ω_{vol} , which depends only on the volume, (2) the superficial free energy Ω_{sup} associated with the interfacial tension, and (3) the elastic energy Ω_{elas} induced by the specific boundary condition imposed at the interface of the drop as regards the orientation and/or the translation of molecules:

$$\Omega_{total} = \Omega_{vol} + \Omega_{sup} + \Omega_{elas}. \quad (A.1)$$

The second term can be specifically written as

$$\Omega_{sup} = \int \gamma(p) dA, \quad (A.2)$$

where $\gamma(p)$ denotes the interfacial free energy at the point p on the boundary, and the surface integration should be performed over the entire interfaces in the system including the boundary of the drop. Under the condition of the constant volume, Ω_{vol} is an invariant independent of the shape of the drop, and hence can be omitted in determining the equilibrium shape. The third term, however, is negligible only some special cases leading to Young's equation and the Wulff construction.

Before, considering the equilibrium shape of a nematic drop, we need to note the following property of the surface or boundary tension of a nematic liquid crystal:

The surface tension of a nematic liquid crystal is isotropic, i.e., it does not depend on the direction along which the surface tension is measured.

Proof: Consider the thermodynamic potential Ω of the region of the nematic as shown in Fig.A.5 held at fixed temperature and chemical potential. Then, for the change in L_x and L_y occurring under a fixed volume, we can write

$$d\Omega = \gamma_x L_y dL_x + \gamma_y L_x dL_y.$$

Hence, in order for the right-hand side to be integrable, we should have

$$\gamma_x = \gamma_y. \quad (\text{A.3})$$

This is essentially the surface analog of the well-known fact that in the bulk of a nematic phase, the pressure tensor is isotropic, even though the molecules are anisotropically oriented.

And, Eq.(A.3) also applies to the boundary

tension for a nematic in contact with a hard solid wall. This isotropy should not be confused with the anisotropy of the surface tension of nematics with respect to the rotation of the director at the interface.

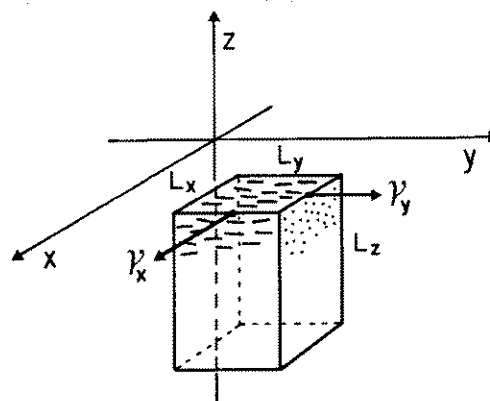


FIG.A.5. Interfacial tensions in the directions parallel (y-axis) and perpendicular to the director. The nematic liquid occupies the half space below the x-y plane.

A. Large drop

Let us first imagine that the nematic drop (resting at the isotropic-solid interface) is sufficiently large so that the volumetric elastic energy can be neglected in comparison with the superficial term; for a drop of linear dimension R , the superficial term is proportional to R^2 , whereas the elastic term is to R . In this case, the director configuration within the drop is solely determined in such a way as to minimize the anchoring energy, and is shown to take a nonuniform profile as illustrated in Fig.A.6, in which a planar alignment is assumed on the substrate surface; this configuration has also been adopted in Chapter 6 (Fig.6.3) without a detailed discussion on its validity.

Except at the disclination lines of topological origin, the director is oriented along the easy axis over the nematic-isotropic and the nematic-solid interfaces. Therefore, the superficial thermodynamic potential can be written as a sum of the free energies associated with the interfacial tensions and with the disclination lines. In particular, because of the aforementioned property of

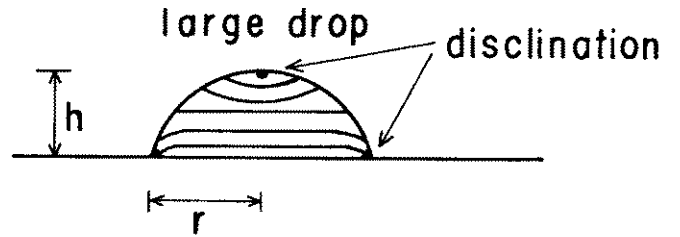


FIG.A.6. Director configuration inside a large cap-shaped drop resting on a planar aligning substrate. When the boundary condition at the nematic-isotropic interface is conical, there in general appear two kinds of disclination lines, one along the meridian and the other along the circumference.

the surface tension of nematics, the interfacial tension assumes a unique value, irrespective of the direction relative to the director, once the phases in contact, e.g. nematic and isotropic, are specified. Thus, as long as the effect of the disclination lines can be ignored, the equilibrium shape of the nematic drop can be determined in completely the same manner as that for a drop of ordinary liquid. Consequently, we obtain a circular cap-shaped drop satisfying Young's equation.

The condition under which the disclination effect is negligible can be roughly worked out by the following qualitative argument. Assuming a cap-shaped drop with a height h and a radius r ($>h$) [see Fig.A.6], we can write the contribution of the interfacial tension as

$$\Omega_{\text{sup}}(\text{tension}) = \Omega_{\text{sup}}(0) + \pi \gamma_{\text{ni}}(r^2+h^2) + 2\pi(\gamma_{\text{sn}}-\gamma_{\text{si}})r^2, \quad (\text{A.4})$$

where $\Omega_{\text{sup}}(0)$ is a constant independent of h and r . As confirmed by a direct calculation, minimization of the above under a constant drop volume $V=(\pi/6)h(3r^2+h^2)$ yields Young's equation,

$$\gamma_{si} = \gamma_{sn} + \gamma_{ni} \cos \alpha = \gamma_{sn} + \gamma_{ni} (r^2 - h^2) / (r^2 + h^2). \quad (\text{A.5})$$

In general, there appear two kinds of topological disclination lines: one along the meridian perpendicular to the substrate-induced alignment as observed in Chapter 6 [Fig.A.7(a)], and the other along the three-phase contact line resulting from the conflicting boundary conditions at the nematic-isotropic and the nematic-substrate interfaces [Fig.A.7(b)]. Denoting the free energies associated

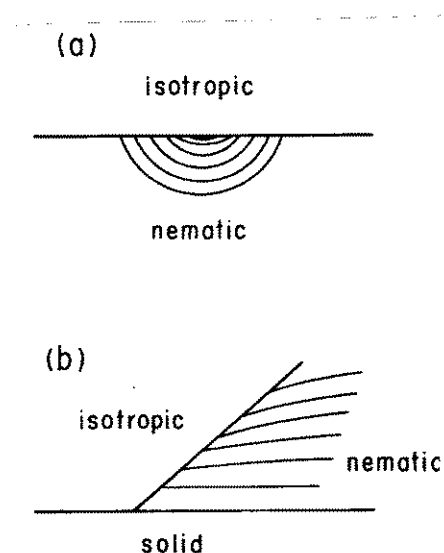


FIG.A.7. Director configuration around the disclination lines shown in Fig.A.6.

with the unit length of these disclination lines by σ_1 and σ_2 , respectively, we can write down the relevant part of the superficial thermodynamic potential as

$$\begin{aligned} \Omega(\text{disclination}) = & \sigma_1 s(r^2 + h^2) / h \cos^{-1} [(r^2 - h^2) / (r^2 + h^2)] \\ & + 2\pi \sigma_2 r. \end{aligned} \quad (\text{A.6})$$

For simplicity, we shall replace the first term by its upper bound:

$$\Omega(\text{disclination}) = 2\pi r(\sigma_1/2 + \sigma_2). \quad (\text{A.7})$$

Clearly, this contribution acts as a line tension^{*}, which modifies the equilibrium condition of the drop as expressed by Young's equation [Eq.(A.5)] to

$$\gamma_{si} = \gamma_{sn} + \gamma_{ni} \cos \alpha + (\sigma_1/2 + \sigma_2) / r. \quad (\text{A.8})$$

^{*} P. Tarazona and G. Navascues, J. Chem. Phys. 75, 3114(1981), and the references therein.

In Fig.A.7, the director configurations around the disclination lines are schematically illustrated. By following the treatment of surface disclinations due to Vitek and Kleman^{*}, we can obtain a rough estimate of the free energies σ_1 and σ_2 . For example, in the one constant approximation, we find

$$\sigma_1 \sim (\pi K/2)[\ln(R/2d_e)+1], \quad (\text{A.9})$$

where K is the Frank elastic constant, d_e the extrapolation length at the nematic-isotropic interface, and R the linear size of the nematic drop. Then, we see that for samples of a realistic size and anchoring condition, σ_1 is a quantity of the same order of magnitude as K . Similarly, we readily find that $\sigma_2 \sim K$.

Since γ_{ni} and K are on the order of 10^{-5}J/m^2 and 10^{-11}N , respectively, we can conclude from Eq.(A.8) that, only when the radius of the nematic drop is as small as $1 \mu\text{m}$, the disclination can exhibit a significant effect in determining the equilibrium shape. Otherwise, the drop is expected to assume a cap shape in agreement with the microscopic observations presented in Chapter 6.

B. Small drop

In small drops, the elastic deformations can no longer be neglected, and the director orientation at the interface is expected to be significantly deviated from the easy direction. Though it is difficult to generally treat this situation, we can formally eliminate the elastic contribution if the drop is very small. Namely, when the drop is extremely small, the elastic torque overwhelms that due to the interface, thereby making the director align almost uniformly within the drop (Fig.A.8). In this case, too, the equilibrium shape can be determined only by the consideration of the minimum condition of the superficial free energy.

^{*} V. Vitek and M. Kleman, J. Phys. (Paris) 36, 59(1975).

As clear in Fig.A.8, the interfacial tension is not constant throughout a boundary, but changes from one point to another according to how much the boundary director is distorted from the easy axis. Consequently, the equilibrium shape is not a simple cap shape as determined by Young's equation, but is more structured reflecting the anisotropy or

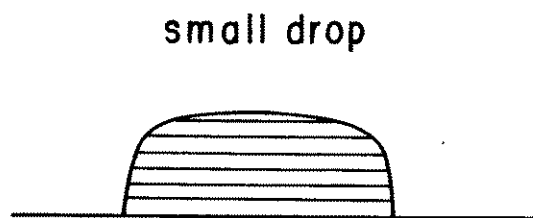


FIG.A.8. Equilibrium shape of a small nematic drop on a planar aligning substrate, and the director configuration within the drop. Due to the curvature elasticity, the director is forced to be uniformly aligned.

equivalently the inhomogeneity of the interfacial tension. Note that this case is essentially identical with the equilibrium shape problem of a crystalline solid, in which the lattice structure is preserved and the facetting which minimizes the surface free energy is searched. The optimum facetting is produced by the Wulff construction, and its extension to liquid crystal drops has been carried out by Chandrasekhar^{*}.

The distinction between the "large" and the "small" drops depends on the anchoring strength at the interface. For example, if the anchoring strength at the nematic-isotropic interface vanishes, no such a distinction exists, and the equilibrium shape of a nematic drop is always a cap shape determined by Young's equation. For an infinitely strong anchorage, however, there is no "small" drop in the above sense; this means that the director configuration is always distorted, while not entirely negligible in comparison with the interfacial tension. The onset of this intermediate situation may be characterized by the point where the

^{*} S. Chandrasekhar, in Proceedings of the International Liquid Crystal Conference, Kent State Univ., Aug. (1965).

elastic and the interfacial contributions become comparable. To find out an estimate of the size of such a drop, let us compare the interfacial free energy of a spherical drop with the radius R ,

$$F_{\text{int}} \sim \gamma_{\text{ni}}(4\pi R^2),$$

with the possible elastic deformation energy in the drop,

$$F_{\text{elas}} \sim (4\pi R^3/3)K/(2R^2) = (2\pi/3)RK.$$

Then, by equating F_{int} and F_{elas} , we find

$$R \sim K/\gamma_{\text{ni}}. \quad (\text{A.10})$$

Using $\gamma_{\text{ni}} \sim 10^{-5} \text{J/m}^2$ and $K \sim 10^{-11} \text{N}$, we see that $R \sim 1 \mu\text{m}$, showing that in nematic drop with the size much larger than $1 \mu\text{m}$, the contribution of the elastic distortion on the equilibrium shape may be neglected.

As discussed above, the equilibrium shape of a drop of liquid crystals is influenced both by the interfacial tension and by the volumetric and superficial elastic distortions. Because of the weakness of the curvature elasticity of nematics, however, the latter effect becomes significant for drops with the radius smaller than $1 \mu\text{m}$ or so, and hence the observable equilibrium shape is determined to a good approximation by Young's equation.

As the elasticity becomes stronger as in smectics, the elastic part is expected to play an important role. But, unless the medium is very hard and/or the drop is small enough, the well-known Wulff construction cannot necessarily be applied; and the equilibrium shape must be determined via the complicated compromise among the interfacial tension, the elasticity, both volumetric and superficial, and the interfacial anchorage. The wide variety of bâtonnet forms, which we observe upon appearance of smectic phase in the isotropic or nematic phase, are considered to be just of this type.

REFERNECES

Chapter 1

- [1] I. Langmuir, J. Am. Chem. Soc. 39, 1848(1917).
- [2] W.D. Harkins, J. Am. Chem. Soc. 39, 356(1917).
- [3] A.W. Adamson, Physical Chemistry of Surfaces, (Wiley, New York, 1976), pp.90-91.
- [4] M.M. Telo da Gama and K.E. Gubbins, Mol. Phys. 59, 227 (1986).
- [5] H. Kelker, Mol. Cryst. Liq. Cryst. 21, 1(1973).
- [6] F. Wallerant, Compt. Rend. 143, 605(1906).
- [7] O. Lehmann, Verh. D. Naturwiss. Vereins in Karlsruhe 19. Bd. 107(1906).
- [8] O. Lehmann, in Handbuch der Biologischen Arbeitsmethoden, Abt. III, Teil A, Heft 2, Berlin 1922, pp.123-352.
- [9] K. Hiltrop and H. Stegemeyer, Mol. Cryst. Liq. Cryst. 49, 61(1978).
- [10] C. Mauguin, Bull. Soc. Fr. Min. 34, 71(1911).
- [11] H. Zocher and Z. Coper, Phys. Chem. 132, 295(1928).
- [12] P. Chatelain, Bull. Soc. Fr. Min. 60, 300(1937);
ibid. 66, 105(1943).
- [13] J.A. Castellano, Mol. Cryst. Liq. Cryst. 94, 33(1983).
- [14] D.W. Berreman, Phys. Rev. Lett. 28, 1683(1972);
Mol. Cryst. Liq. Cryst. 23, 215(1973).
- [15] F. Grandjean, Bull. Soc. Fr. Min. 39, 164(1916).
- [16] G.H. Heilmeier, L.A. Aznoni, and L.A. Barton, Proc. IEEE 56, 1162(1968).
- [17] M. Schadt and W. Helfrich, Appl. Phys. Lett. 18, 127(1971).
- [18] for detailed description of other types of liquid crystal displays, see, for example, L.M. Blinov, Electo-optical and Magneto-optical Properties of Liquid Crystals, (Wiley, New York, 1983).

- [19] H. Yokoyama and H. Kamei, in Shinsedai Device Tansaku Gijutsu Shūsei, edited by N. Mizushima, (Realize, Tokyo, 1985), pp.38-58, [in Japanese].
- [20] J. Cognard, *Mol. Cryst. Liq. Cryst. Suppl.* 1, 1(1982).
- [21] S. Morozumi and K. Oguchi, *Mol. Cryst. Liq. Cryst.* 94, 43(1983).
- [22] B. Bahadur, *Mol. Cryst. Liq. Cryst.* 109, 1(1984).
- [23] J. Nehring, A.R. Kmetz, and T.J. Scheffer, *J. Appl. Phys.* 47, 850(1976).
- [24] K.H. Yang, *Appl. Phys. Lett.* 43, 172(1983).
- [25] K.H. Yang, *J. Appl. Phys.* 54, 6864(1983).
- [26] K.H. Yang, *Jpn. J. Appl. Phys.* 22, 389(1983).
- [27] H.L. Ong, R.B. Meyer, and A.J. Hurd, *J. Appl. Phys.* 55, 2809(1984).
- [28] M.E. Becker, J. Nehring, and T.J. Scheffer, *J. Appl. Phys.* 57, 4539(1985).
- [29] T.J. Scheffer and J. Nehering, *Appl. Phys. Lett.* 45, 1021(1984).
- [30] R.B. Meyer, *Mol. Cryst. Liq. Cryst.* 40, 33(1977).
- [31] N.A. Clark and S.T. Lagerwall, *Appl. Phys. Lett.* 36, 213(1983).
- [32] T. Hatano, K. Yamamoto, H. Takezoe, and A. Fukuda, *Jpn. J. Appl. Phys.* 25, 1762(1986).

Chapter 2

- [1] P.G. de Gennes, The Physics of Liquid Crystals, (Clarendon, Oxford, 1975).
- [2] S. Chandrasekhar, Liquid Crystals, (Cambridge Univ., London, 1977).
- [3] H. Kelker and R. Hatz, Handbook of Liquid Crystals, (Verlag Chemie, Weinheim, 1980).

- [4] M.J. Stephen and J.P. Straley, *Rev. Mod. Phys.* **46**, 617 (1974).
- [5] E.B. Priestley, P.J. Wojtowicz, and P. Sheng, Introduction to Liquid Crystals, (Penum, New York, 1975).
- [6] K. Okano and S. Kobayashi, Ekisho, (Baifukan, Tokyo, 1985) [in Japanese].
- [7] F.C. Frank, *Discuss. Faraday Soc.* **25**, 19(1958).
- [8] P.G. de Gennes, *Mol. Cryst. Liq. Cryst.* **12**, 193(1971).
- [9] D. Demus and L. Richter, Textures of Liquid Crystals, (Verlag Chemie, Weinheim, 1978).
- [10] M. Kleman, Points, Lines and Walls, (Wiley, New York, 1983).
- [11] G. Friedel, *Ann. Phys. (Paris)*, **19**, 273(1922).
- [12] P.P. Karat and N.V. Madhusudana, *Mol. Cryst. Liq. Cryst.* **36**, 51(1976).
- [13] M.F. Vuks, *Opt. Spectrosc. (USSR)*, **20**, 361(1966).
- [14] H. Zocher, *Trans. Faraday Soc.* **29**, 945(1933).
- [15] C.W. Oseen, *Trans. Faraday Soc.* **29**, 883(1933).
- [16] V.L. Podrovsky, *Adv. Phys.* **28**, 595(1979).
- [17] J. Nehring and A. Saupe, *J. Chem. Phys.* **54**, 337(1971).
- [18] J. Nehring and A. Saupe, *J. Chem. Phys.* **56**, 5527(1972).
- [19] R.G. Priest, *Phys. Rev. A* **7**, 720(1973).
- [20] D.W. Berreman and S. Meiboom, *Phys. Rev. A* **30**, 1955(1984).
- [21] H. Gruler, T.J. Scheffer, and G. Meier, *Z. Naturforsch.* **27 a**, 966(1972).
- [22] H.J. Coles, *Mol. Cryst. Liq. Cryst. Lett.* **49**, 67(1978).

Chapter 3

- [1] T.J. Scheffer and J. Nehring, *J. Appl. Phys.* **48**, 1783(1977).
- [2] A. Rapini and M. Papoular, *J. Phys. (Paris) Colloq.* **30**, C4-54(1969).

- [3] J. Cognard, *Mol. Cryst. Liq. Cryst. Suppl.* 1, 1(1982).
- [4] J.L. Janning, *Appl. Phys. Lett.* 21, 173(1972).
- [5] K. Okano and S. Kobayashi, *Ekiho*, (Baifukan, Tokyo, 1985) [in Japanese].
- [6] E. Guyon, P. Pieranski and M. Boix, *Appl. Eng. Sci. Lett.* 119(1973).
- [7] W. Urbach, M. Boix, and E. Guyon, *Appl. Phys. Lett.* 25, 479(1974).
- [8] M. Yamashita and Y. Amemiya, *Jpn. J. Appl. Phys.* 15, 2087(1976).
- [9] D.M. Buzcek, *Mol. Cryst. Liq. Cryst.* 47, 145(1978).
- [10] W.A. Crossland, J.H. Morrissy, and B. Needham, *J. Phys. D* 9, 2001(1976).
- [11] A. Toda, H. Mada, and S. Kobayashi, *Jpn. J. Appl. Phys.* 17, 261(1978).
- [12] H.A. van Sprang and R.G. Aartsen, *Appl. Phys. Lett.* 42, 669(1983).
- [13] H.A. van Sprang and R.G. Aartsen, 56, 251(1984).
- [14] D.W. Berreman, *Phys. Rev. Lett.* 26, 1683(1972).
- [15] J.M. Pollack, W.E. Haas, and J.E. Adams, *J. Appl. Phys.* 48, 831(1977).
- [16] J. Cheng, G.D. Boyd, and F.G. Storz, *Appl. Phys. Lett.* 37, 716(1980).
- [17] M. Kuwahara, H. Yayama, H. Onnagawa, and K. Miyashita, *Oyobutsuri*, 50, 1147(1981).
- [18] T. Wilson, G.D. Boyd, E.H. Westerwick, and F.G. Storz, *Mol. Cryst. Liq. Cryst.* 94, 359(1983).
- [19] Y. Levy, M. Jurcic, and J.D. Swalen, *J. Appl. Phys.* 57, 2601(1985).
- [20] H. Yokoyama, S. Kobayashi, and H. Kamei, *J. Appl. Phys.* 56, 2645(1984).
- [21] J.A. Castellano, *Mol. Cryst. Liq. Cryst.* 94, 33(1983).

- [22] P. Chatelain, Bull. Soc. Fr. Min. 60, 300(1937);
ibid. 66, 105(1943).

Chapter 4

- [1] Simplified version of this chapter has been described in H. Yokoyama, S. Kobayashi, and H. Kamei, J. Appl. Phys. 59 in press.
- [2] J.W. Gibbs, Collected works, Vol.I (Longmans, New York, 1976).
- [3] T.L. Hill, J. Phys. Chem. 56, 526(1952).
- [4] R.C. Tolman, J. Chem. Phys. 16, 758(1948).
- [5] S. Ono and S. Kondo, in Handbuch der Physik, Vol.10, edited by S. Flugge (Springer, Berlin, 1960); see also, S. Ono, Hyōmen Chōryoku (Kyōritsu, Tokyo, 1980), pp.17-45, (in Japanese).
- [6] E.A. Guggenheim, Thermodynamics, 2nd ed. (North-Holland, Amsterdam, 1966), pp.45-58.
- [7] N.K. Adam, The Physics and Chemistry of Surfaces (Oxford Univ., London, 1949), pp.106-113.
- [8] A.W. Adamson, Physical Chemistry of Surfaces (Wiley, New York, 1976), pp.46-98.
- [9] M.J. Jaycock and G.D. Parfitt, Chemistry of Interfaces, (Wiley, New York, 1981).
- [10] A.W. Adamson, loc. cit., pp.47-49.
- [11] T. Young, Philos. Trans. 95, 65(1805).
- [12] see, for example, B. Borstnik and D. Janezic, Mol. Phys. 50, 1199(1983).
- [13] D. Langevin and M.A. Bouchiat, Mol. Cryst. Liq. Cryst. 22, 317(1973).
- [14] R. Williams, Mol. Cryst. Liq. Cryst. 35, 349(1976).
- [15] S. Faetti and V. Palleschi, J. Phys. (Paris) Lett. 45, L-313(1984); Phys. Rev. A 30, 3241(1984).

- [16] G.W. Smith, Mol. Cryst. Liq. Cryst. 102(Letters), 65(1984).
- [17] H. Yokoyama, S. Kobayashi, and H. Kamei, Mol. Cryst. Liq. Cryst. 129, 109(1985).
- [18] G.W. Smith, J.L. White, and M. Buechler, Carbon, 23, 117(1985).
- [19] P.G. de Gennes, Mol. Cryst. Liq. Cryst. 12, 193(1971).
- [20] P. Sheng and E.B. Priestley, in Introduction to Liquid Crystals, edited by E.B. Priestley, et al. (Plenum, New York, 1975), pp.143-201.
- [21] P.G. de Gennes, Solid State Commun. 8, 213(1970).
- [22] P.G. de Gennes, The Physics of Liquid Crystals (Clarendon, Oxford, 1975), pp.134-136.
- [23] S. Faetti and V. Palleschi, J. Phys. (Paris), 46, 415(1985).
- [24] R.N. Thurston, J. Appl. Phys. 52, 3040(1981).
- [25] For example, see G. Navascues and M.V. Berry, Mol. Phys. 34, 649(1977).
- [26] J.J. Viecelli and H. Reiss, J. Chem. Phys. 57, 3745(1972).
- [27] M.J. Mandell and H. Reiss, J. Stat. Phys. 13, 107(1975).
- [28] F.H. Stillinger and M.A. Cotter, J. Chem. Phys. 55, 3449(1971).
- [29] A. Rapini and M. Papoular, J. Phys. (Paris) Colloq. 30, C4-54(1969).
- [30] E. Dubois-Violette and O. Parodi, J. Phys. (Paris) Colloq. 30, C-4, 57(1969).
- [31] H. Mada, Mol. Cryst. Liq. Cryst. 51, 43(1979).
- [32] J. Nehring and A. Saupe, J. Chem. Phys. 54, 337(1971).
- [33] H.P. Hinov, J. Phys. (Paris) Lett. 38, L-215(1977).
- [34] H.P. Hinov and A.I. Derzhanski, J. Phys. (Paris) Colloq. 40, C-3, 505(1979).
- [35] G. Barbero, R. Bartolino, and M. Meuti, J. Phys. (Paris) Lett. 45, L-449(1984).

- [36] C. Oldano and G. Barbero, J. Phys. (Paris) Lett. 46, L-451(1985).
- [37] C. Oldano and G. Barbero, Phys. Lett. 110A, 213(1985).
- [38] L.D. Landau and E.M. Lifshitz, Statistical Physics (Pergamon, Oxford, 1969), pp.60-63.
- [39] J.E. Proust and L. Ter-Minassian-Saraga, Solid State Commun. 11, 1227(1972).
- [40] P. Chiarelli, S. Faetti, and L. Fronzoni, J. Phys. (Paris) 44, 1061(1983).
- [41] P. Chiarelli, S. Faetti, and L. Fronzoni, Phys. Lett. 101A, 31(1984).
- [42] S. Krishnaswamy and R. Shashidhar, Mol. Cryst. Liq. Cryst. 35, 253(1976).
- [43] G. Ryschenkow and M. Kleman, J. Chem. Phys. 64, 404(1976).
- [44] H. Birecki, in Liquid Crystals and Ordered Fluids, Vol.4, edited by A.C. Giffin and J.F. Johnson (Plenum, New York, 1984), pp.852-864.
- [45] C. Rosenblatt, J. Phys. (Paris) 45, 1087(1984).
- [46] S. Faetti, M. Gatti, V. Palleschi, and T.J. Sluckin, Phys. Rev. Lett. 55, 1681(1985).
- [47] H. Yokoyama, S. Kobayashi, and H Kamei, presented at 11th International Liquid Crystal Conference, Berkeley, California, July(1986).
- [48] For example, see H.A. van Sprang and R.G. Aartsen, J. Appl. Phys. 56, 251(1984), and the references therein.

Chapter 5

- [1] T.J. Sluckin and A. Poniewierski, in Fluid Interfacial Phenomena, edited by C.A. Croxton (Wiley, New York, 1986), pp.215-253.
- [2] R. Evans, Adv. Phys. 28, 143(1979).
- [3] J.G. Kirkwood and F.R. Buff, J. Chem. Phys. 17, 338(1949).

- [4] D.G. Triezenberg and R. Zwanzig, Phys. Rev. Lett. 28, 1183(1972).
- [5] P. Schofield, Chem. Phys. Lett. 62, 413(1979).
- [6] M.H. Waldor and D.E. Wolf, J. Chem. Phys. 85, 6082(1986).
- [7] C.G. Gray and K.E. Gubbins, Mol. Phys. 30, 179(1975).
- [8] J.M. Haile, C.G. Gray, and K.E. Gubbins, J. Chem. Phys. 64, 2569(1976).
- [9] H.T. Davis, J. Chem. Phys. 62, 3412(1975).
- [10] T.J. Sluckin, Mol. Phys. 43, 817(1981).
- [11] G. Navascues and M.V. Berry, Mol. Phys. 34, 649(1977).
- [12] J.D. Parsons, J. Phys. (Paris) 37, 1187(1976).
- [13] J. Murakami, J. Phys. Soc. Jpn. 42, 210(1977).
- [14] C.A. Croxton, Mol. Cryst. Liq. Cryst. 59, 219(1980).
- [15] J.D. Parsons, Mol. Phys. 42, 951(1980).
- [16] S. Krishnaswamy and R. Shashidhar, Mol. Cryst. Liq. Cryst. 35, 253(1976).
- [17] M.G.J. Gannon and T.E. Faber, Philos. Mag. 37, 117(1978).
- [18] H. Yokoyama, S. Kobayashi, and H. Kamei, Appl. Phys. Lett. 41, 438(1982).
- [19] H. Yokoyama, S. Kobayashi, and H. Kamei, Mol. Cryst. Liq. Cryst. 99, 39(1983).
- [20] H. Yokoyama, S. Kobayashi, and H. Kamei, J. Appl. Phys. 56, 2645(1984).
- [21] K. Okano, Jpn. J. Appl. Phys. 22, L343(1983).
- [22] H. Kimura, Kobunshi Ronbunshu 43, 177(1986).
- [23] H. Kimura and H. Nakano, J. Phys. Soc. Jpn. 54, 1730(1985); see also Errata on J. Phys. Soc. Jpn. 54, 3204(1985).
- [24] H. Kimura and H. Nakano, J. Phys. Soc. Jpn. 55, 4186(1986).
- [25] M.M. Telo da Gama, Mol. Phys. 52, 585(1984).
- [26] M.M. Telo da Gama, Mol. Phys. 52, 611(1986).
- [27] D.E. Sullivan, preprint.
- [28] H.S. Green, Proc. R. Soc. A, 189, 130(1947).

- [29] R. Shuttleworth, Proc. Phys. Soc. (London), A63, 444(1950).
- [30] L.A. Girifalco and R.J. Good, J. Phys. Chem. 61, 904(1957).
- [31] R.J. Good and L.A. Girifalco, J. Phys. Chem. 64, 561(1960).
- [32] F.M. Fowkes, J. Phys. Chem. 66, 382(1962).
- [33] H. Mada, Mol. Cryst. Liq. Cryst. 53, 127(1979).
- [34] K. Okano and J. Murakami, J. Phys. (Paris), 40, C3-525 (1979).
- [35] J. Bernasconi, S. Strassler, and H.R. Zeller, Phys. Rev. A 22, 276(1980).
- [36] K. Okano, N. Matsuura, and S. Kobayashi, Jpn. J. Appl. Phys. 21, L109(1982).
- [37] H. Yokoyama, presented at 11th International Liquid Crystal Conference, Berkeley, California, July(1986).
- [38] A. Poniewierski and J. Stecki, Mol. Phys. 38, 1931(1979).
- [39] J. Stecki and A. Poniewierski, Mol. Phys. 41, 1451(1980).
- [40] Y. Singh, Phys. Rev. A 30, 583(1984).
- [41] M.D. Lipkin, S.A. Rice, and U. Mohanty, J. Chem. Phys. 82, 472(1985).
- [42] Y. Singh and K. Singh, Phys. Rev. A 33, 3481(1986);
Phys. Rev. A 34, 548(1986).
- [43] J. Nehring and A. Saupe, J. Chem. Phys. 54, 337(1971).
- [44] J. Nehring and A. Saupe, J. Chem. Phys. 56, 5527(1972).
- [45] R.G. Priest, Phys. Rev. A 7, 720(1973).
- [46] J.P. Straley, Phys. Rev. A 8, 2181(1973).
- [47] W.M. Gelbart and A. Ben-Shaul, J. Chem. Phys. 77, 916(1982).
- [48] S. Sarkar and R.J.A. Tough, J. Phys. (Paris) 43, 1543(1982).
- [49] P.G. de Gennes, Physics of Liquid Crystals, (Clarendon, Oxford, 1975).
- [50] V.L. Pokrovsky, Adv. Phys. 28, 595(1979).
- [51] G. Navascues and P. Tarazona, Mol. Phys. 37, 1077(1979).
- [52] H.T. Davis and L.E. Scriven, J. Stat. Phys. 24, 243(1981).
- [53] P.G. de Gennes, Mol. Cryst. Liq. Cryst. 12,193(1971).

- [54] P. Sheng and E.B. Priestley, in Introduction to Liquid Crystals, edited by E.B. Priestely, et al. (Plenum, New York, 1974), pp.143-201.
- [55] J.D. Parsons, *Mol. Cryst. Liq. Cryst.* 31,79(1975).
- [56] P. Sheng, *Phys. Rev. Lett.* 37, 1059(1976).
- [57] J.D. Parsons, *Phys. Rev. Lett.* 41, 877(1978).
- [58] H. Mada, *Mol. Cryst. Liq. Cryst.* 51, 43(1979).
- [59] T. Atahane and T. Tako, *Jpn. J. Appl. Phys.* 18, 19(1979).
- [60] J.C. Tarczon and K. Miyano, *J. Chem. Phys.* 73, 1994(1980).
- [61] D.W. Allender, G.L. Henderson, and D.L. Johnson, *Phys. Rev. A*, 24, 1086(1981).
- [62] C.A. Croxton, *Mol. Cryst. Liq. Cryst.* 66, 223(1981).
- [63] P. Sheng, *Phys. Rev. A*, 26, 1610(1982).
- [64] M.A. Marcus, *Mol. Cryst. Liq. Cryst.* 100, 253(1983).
- [65] A. Poniewierski and T.J. Sluckin, *Mol. Cryst. Liq. Cryst.* 111, 373(1984).
- [66] A. Poniewierski and T.J. Sluckin, *Mol. Cryst. Liq. Cryst.* 126, 143(1985).
- [67] T.J. Sluckin and A. Poniewierski, *Phys. Rev. Lett.* 55, 2907(1985).
- [68] K. Miyano, *Phys. Rev. Lett.* 43, 51(1979).
- [69] K. Miyano, *J. Chem. Phys.* 71, 4108(1979).
- [70] J.W. Cahn, *J. Chem. Phys.* 66, 3667(1977).
- [71] D.E. Sullivan and M.M. Telo da Gama, in Fluid Interfacial Phenomena, edited by C.A. Croxton, (Wiley, New York, 1986), pp. 45-134.
- [72] R. Lipowsky, *J. Appl. Phys.* 55, 2485(1984).
- [73] H. Yokoyama, S. Kobayashi, and H. Kamei, *J. Appl. Phys.* 59, in press.
- [74] B. Chu, C.S. Bak, and F.L. Lin, *Phys. Rev. Lett.* 24, 1111(1972).

[75] T.W. Stinson and J.D. Litster, Phys. Rev. Lett. 30, 688(1973).

Chapter 6

- [1] H. Yokoyama, S. Kobayashi, and H. Kamei, Mol. Cryst. Liq. Cryst. 99, 39(1983).
- [2] H. Yokoyama, S. Kobayashi, and H. Kamei, Mol. Cryst. Liq. Cryst. 107, 311(1984).
- [3] S. Faetti and V. Palleschi, Phys. Rev. A 30, 3241(1984).
- [4] N.V. Madhusudana and K.R. Sumathy, Mol. Cryst. Liq. Cryst. Lett. 92, 179(1983).
- [5] P.G. de Gennes, Rev. Mod. Phys. 57, 827(1985).
- [6] M.E. Becker, R.A. Kilian, B.B. Kosmowski, and D.A. Mlynski, Mol. Cryst. Liq. Cryst. in press.
- [7] A.W. Adamson, Physical Chemistry of Surfaces (Wiley, New York, 1976), pp.46-98.
- [8] M. Yamashita and Y. Amemiya, Jpn. J. Appl. Phys. 18, 1249(1979).
- [9] M. Ohgawara and T. Uchida, Jpn. J. Appl. Phys. 20, L237(1981).
- [10] M. Ohgawara and T. Uchida, Jpn. J. Appl. Phys. 20, L75 (1981).
- [11] H. Yokoyama, S. Kobayashi, and H. Kamei, J. Appl. Phys. 56, 2645(1984).
- [12] Y. Imry and S. Ma, Phys. Rev. Lett. 35, 1399(1975).
- [13] R.C. Dynes, J.P. Garino, and J.M. Rowell, Phys. Rev. Lett. 13, 479(1978).
- [14] R.M.A. Azzam and N.M. Bashara, Ellipsometry and Polarized Light, (North-Holland, Amsterdam, 1977), pp.1-60.
- [15] A. Fukuda and K. Kondo, Bunko Kenkyu, 29, 301(1980) [in Japanese].
- [16] K. Miyano, Phys. Rev. Lett. 51, 51(1979).

- [17] K. Miyano, J. Chem. Phys. 71, 4108(1979).
- [18] J.C. Tarczon and K. Miyano, J. Chem. Phys. 73, 1994(1980).
- [19] H. Yokoyama, S. Kobayashi, and H. Kamei, Appl. Phys. Lett. 41 438(1982).
- [20] H.A. van Sprang, J. Phys. (Paris) 44, 421(1983).
- [21] H.A. van Sprang, Mol. Cryst. Liq. Cryst. 97, 255(1983).
- [22] T.J. Sluckin and A. Poniewierski, in Fluid Interfacial Phenomena, edited by C.A. Croxton (Wiley, New York, 1986), pp.215-253.
- [23] H.J. Coles, Mol. Cryst. Liq. Cryst. 49, 67(1978).
- [24] T.W. Stinson and J.D. Litster, Phys. Rev. Lett. 30, 688(1973).
- [25] P.P. Karat and N.V. Madhusudana, Mol. Cryst. Liq. Cryst. 36, 51(1976).
- [26] P. Sheng, Phys. Rev. A26, 1610(1982); Phys. Rev. Lett. 37, 1059(1976).
- [27] H. Schroder, J. Chem. Phys. 67, 16(1977).
- [28] A. Poniewierski and T.J. Sluckin, preprint.

Chapter 7

- [1] For reviews, see H. Yokoyama, Kagaku to kogyo, 38, 857(1985)[in Japanese]; J. Cognard, Mol. Cryst. Liq. Cryst. Suppl. 1, 1(1982), and W.J.A. Goossens, Mol. Cryst. Liq. Cryst. 124, 305(1985).
- [2] M. Kleman and C. Williams, Philos. Mag. 28, 725(1973).
- [3] R.B. Meyer, Solid State Commun. 12, 585(1973).
- [4] V. Vitek and M. K. eman, J. Phys. (Paris), 36, 59(1975).
- [5] G. Ryschenkow and M. Keman, J. Chem. Phys. 64, 404(1976).
- [6] G. Porte, J. Phys. (Paris) 37, 1245(1976).
- [7] E. Perez, J.E. Proust, and L. Ter-Minassian-Saraga, Mol. Cryst. Liq. Cryst. 42, 167(1977).

- [8] E. Perez and J.E. Proust, J. Colloid Interface Sci. 68
48(1979).
- [9] S. Naemura, J. Appl. Phys. 51, 6149(1981).
- [10] S. Naemura, Mol. Cryst. Liq. Cryst. 68, 183(1981).
- [11] J. Cognard, Mol. Cryst. Liq. Cryst. 64(Letters), 331(1981).
- [12] P. Datta, G. Kaganowicz, and A.W. Levine, J. Colloid Interface
Sci. 82, 167(1981).
- [13] M. Warenghem, Mol. Cryst. Liq. Cryst. 89, 15(1982).
- [14] D. Riviere, Y. Levy, and E. Guyon, J. Phys. (Paris) Lett.
40, L-215(1979).
- [15] L. Komitov and A.G. Petrov, Phys. Stat. Sol.(a) 76, 137
(1983).
- [16] G. Barbero and R. Barberi, J. Phys. (Paris) 44, 609(1983).
- [17] G. Barbero, N.V. Madhusudana, and G. Durand, J. Phys. (Paris)
Lett. 45, L-613(1984).
- [18] B. Stryla, S. Kuczynski, and J. Malecki, Mol. Cryst. Liq.
Cryst. (Letters), 1, 33(1985).
- [19] A. Rapini and M. Papoular, J. Phys. (Paris) Colloq. 30,
C4-54(1969).
- [20] S. Naemura, Appl. Phys. Lett. 33, 1(1978).
- [21] T. Motooka, A. Fukuhara, and K. Suzuki, Appl. Phys. Lett.
34, 305(1979).
- [22] S. Naemura, J. Phys. (Paris) Colloq. 40, C3-514(1979).
- [23] K.H. Yang, Appl. Phys. Lett. 43, 62(1983).
- [24] C. Rosenblatt, J. Phys. (Paris) 45, 1087(1984).
- [25] J. Sicart, J. Phys. (Paris) 37, L-25(1976).
- [26] S. Faetti and V. Palleschi, J. Phys. (Paris) Lett. 45, L-313
(1984).
- [27] K.H. Yang, J. Appl. Phys. 53, 6742(1982).
- [28] H.A. van Sprang and R.G. Aartsen, Mol. Cryst. Liq. Cryst.
123, 355(1985).

- [29] H. Yokoyama and H.A. van Sprang, J. Appl. Phys. 57, 4520 (1985).
- [30] H. Yokoyama, S. Kobayashi, and H. Kamei, J. Appl. Phys. 59, in press.
- [31] S. Faetti, M. Gatti, and V. Palleschi, J. Phys. (Paris) Lett. 46, L-881(1985).
- [32] S. Faetti, M. Gatti, V. Palleschi, and T.J. Sluckin, Phys. Rev. Lett. 55, 1681(1985).
- [33] G. Barbero, N.V. Madhusudana, G. Durand, Z. Naturf. 39A, 1066(1983).
- [34] G. Barbero and G. Durand, J. Phys. (Paris) 47, 2129(1986).
- [35] K.H. Yang, Jpn. J. Appl. Phys. 22, 389(1983).
- [36] M.E. Becker, J. Nehring, and T.J. Scheffer, J. Appl. Phys. 57, 4539(1985).
- [37] T.J. Sluckin and A. Poniewierski, in Fluid Interfacial Phenomena, edited by C.A. Croxton (Wiley, New York, 1986), pp.215-253.
- [38] K. Okano, Jpn. J. Appl. Phys. 22, L343(1983).
- [39] D. Meyerhofer, Phys. Lett. 51A, 407(1975); S. Shimoda, H. Mada, and S. Kobayashi, Jpn. J. Appl. Phys. 17, 1359 (1978).
- [40] J.D. Bunning, T.E. Faber, and P.L. Sherrell, J. Phys. (Paris) 42, 1175(1981).
- [41] H.J. Coles, Mol. Cryst. Liq. Cryst. Lett. 49, 67(1978); C. Strazielle and H.J. Coles, J. Phys. (Paris) 40, 895 (1979).